Research and Technology

Fiscal Year 1984 Annual Report
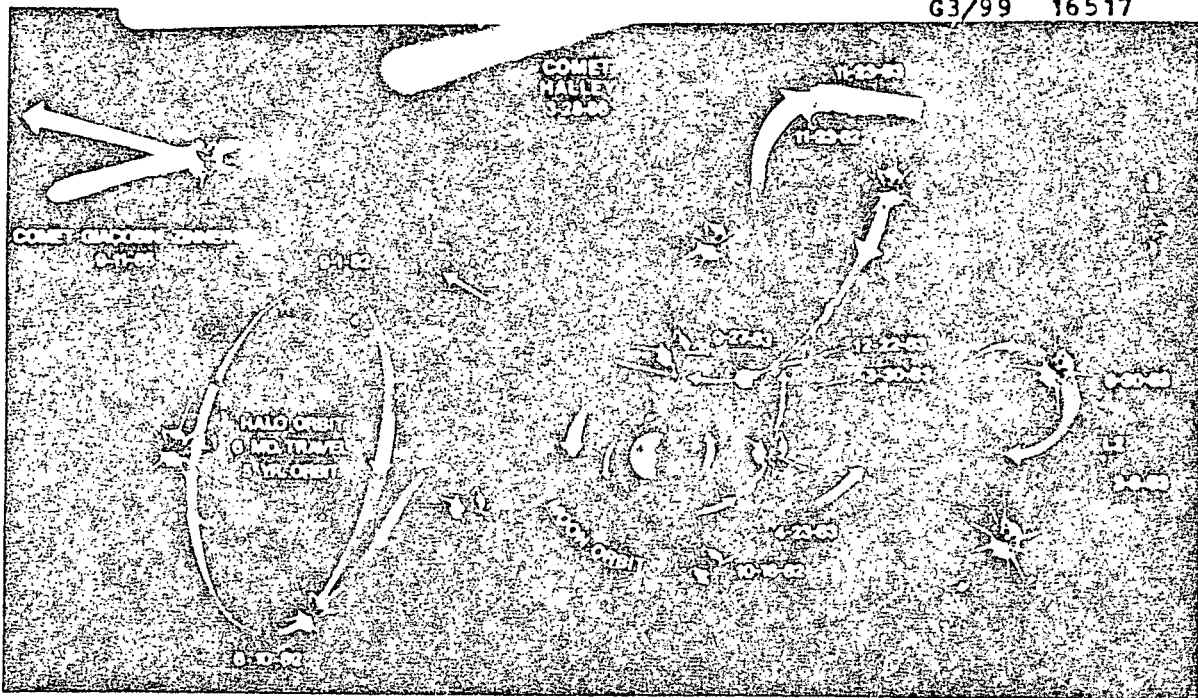
ISEE-3 MANEUVERS FROM HALO ORBIT TO COMET EXPLORATION

NASA

National Aeronautics and
Space Administration

Goddard Space Flight Center
Greenbelt, Maryland 20771

Dr. James E. Kupperian, Jr., Associate Director for User Systems in the Flight Projects Directorate at the Goddard Space Flight Center died on October 7, 1984. Dr. Kupperian was born in Milwaukee, Wisconsin, in 1925. He received his B.S. in Naval Architecture and Marine Engineering from the Webb Institute in 1946 and his Ph.D. in physics from the University of North Carolina in 1952. He was a physicist in the Optics Division at the Naval Research Laboratory from 1954-1958, where he specialized in high altitude research from rockets. His accomplishments there included the discovery of hydrogen Lyman alpha emission in the night sky, and the first measurements of ultraviolet stellar sources from outside the atmosphere.

On coming to NASA in 1959, Dr. Kupperian conceived and planned the observatory series of spacecraft that included the Orbiting Solar Observatory (OSO), the Orbiting Geophysical Observatory (OGO), and the Orbiting Astronomical Observatory (OAO). He was the founder of the Astrophysics Branch at GSFC and its chief from 1959-1970; the project scientist for the OAO from its inception, deputy project manager from 1970-1974 and project manager from 1974-75. He was project manager of the Orbiting Satellites Project until 1979. He was awarded the NASA Exceptional Achievement Medal in 1969.
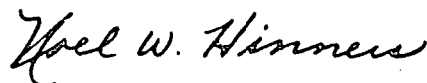
Jim Kupperian's contributions to space astronomy were truly enormous. Not only did he champion the science, but he was a leader in developing ultraviolet-sensitive photometers and spearheaded the development of precision stellar pointing systems. The vitality and vision of the early space astronomy program were given to it by Jim Kupperian. He was a giant among us. Goddard will miss him.

FOREWORD

This is the twenty fifth anniversary year of the Goddard Space Flight Center. We have had a brilliant pioneering period and have developed a remarkable ability to work together. From any perspective, the quality of Goddard work is directly related to that teamwork and fits well with a current and popular theme of our nation: the pursuit of excellence. NASA has taken pride in making that theme its hallmark.

The depth and breadth of ideas in the Center's Research and Technology Program, as reflected in this report, is impressive. Some are esoteric, such as the magnetohydrodynamic acceleration of the solar wind, and others ingeneous, such as the reshaping of the orbit of ISEE-3 so that it will encounter Comet Giacobini Zinner and approach the path of Halley's Comet. I am proud of the resourcefulness and teamwork displayed this past year by our people in the real time rescue of the Solar Maximum Repair Mission. We have some of the best minds in the country working together towards shared goals. Quoting President Reagan upon his recent visit here, "Our progress is a tribute to American teamwork and excellence."

The point of contact within the Center for this report is Dr. George F. Pieper, Code 100 (344-7301), who provided overall editorial supervision. He was assisted by an editorial committee consisting of Dr. James E. Kupperian, Code 400; Ms. Karen L. Moe, Code 522; Mr. Donald S. Friedman, Code 702; and Dr. Gerald H. Soffen, Code 600. Detailed editorial support and the production of the report were supervised by William W. Cooper, Code 251, and Brenda J. Vallette, Engineering and Economics Research, Inc., Beltsville, Maryland.

Noel W. Hinners

Noel W. Hinners
Director

CONTENTS

SPACE AND EARTH SCIENCES

The frontier of research in Space Science and Technology has pointed the way towards ideas that cross the boundaries of classical scientific disciplines. The ocean-atmosphere interface, the relation between terrestrial and planetary geology, the physics of the cosmos and the laboratory all require new perspectives. Goddard's Science and Applications Directorates have been combined into a single organization, Space and Earth Sciences, to strengthen this interdisciplinary approach. Elements of this approach will appear in a number of the following brief descriptions of our work.

EXTRATERRESTRIAL PHYSICS

### EXPLORATION OF THE MAGNETIC TAIL OF THE EARTH BY ISEE-3

The solar wind, a collisionless plasma which expands radially outward from the Sun, interacts with the Earth's polar magnetic field lines and pulls them back into a long magnetic tail similar to the ion tail of a comet. Until recently, this geomagnetic tail has been mainly studied inside of the lunar orbital distance of 60 Earth radii (Re) from the Earth. The International Sun-Earth Explorer-3 (ISEE-3) spacecraft spent a large part of 1983 in the geotail between 60 and 240 Re, greatly extending our knowledge of this region.

Before ISEE-3, the quiescent structure of the distant tail was unknown. One possibility was that the distant tail structure could be very similar to that near Earth, i.e., two distinct lobes, one in the North with solar directed field lines and one in the south with antisolar directed field lines, the two being separated by a neutral sheet embedded in a plasma sheet. Another possibility was that the distant tail might break up into multiple filaments, reminiscent of the visible structure of many ionic comet tails. In fact ISEE-3 found that the former possibility is correct. ISEE-3 has also found evidence for slow-mode shocks associated with a magnetic field line merging region located in the tail typically at 80 to 100 Re from the Earth. Detailed studies are improving our understanding of solar wind plasma transport into the tail and the composition and characteristics (and origin) of suprathermal ions in the plasma sheet. Plasma wave turbulence is much more intense at large downstream distances than had been expected.

Major new observations have been related to geomagnetic storms. The tail has been observed to increase in diameter just prior to such storms, corresponding to a buildup of stored magnetic energy derived from the solar wind. When this energy is suddenly released the plasma sheet is apparently severed close to Earth, causing the release tailward of a large plasma blob, referred to as a plasmoid (see the figure). Plasmoids typically reached ISEE-3 20 or 30 minutes after the onset of the storms as observed near the Earth. The delay in arrival is consistent with bulk flow speeds measured for the plasma of about 500 to 1000 km/sec. A plasmoid's dimensions increase substantially as it departs because it is moving through regions of decreasing magnetic pressure.

These are just some of the initial results from the exploration of the distant tail. It is expected that continued study of the data will lead to many other new results as well.

The ISEE-3 exploration of the deep geomagnetic tail was made possible in part due to the use of lunar swing-bys which considerably increased the amount of time which ISEE-3 spent in the tail. These swing-by techniques, developed by Dr. Robert Farquhar of Goddard, will also be used by the TAIL spacecraft of the International Solar Terrestrial Physics program. ISEE-3's final lunar swing-by allowed ISEE-3 to escape from the Earth's gravity and put it on a trajectory such that it will pass through the tail of comet Giacobini-Zinner in September 1985. This will be the first direct encounter of a satellite with a comet.
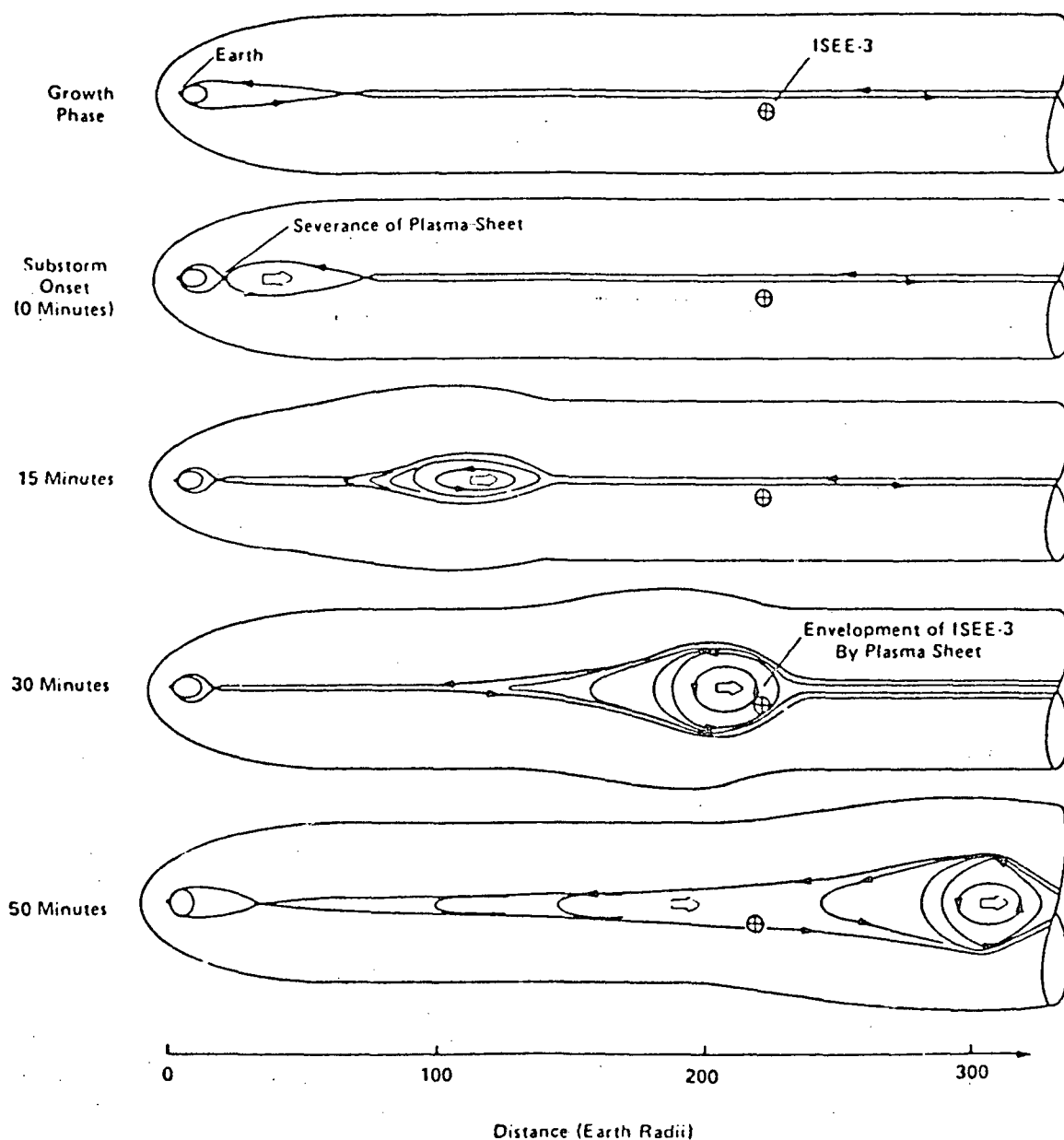
Plasma sheet severed close to Earth causing the release tailward of a large plasmoid.

Contact: Dr. Tycho von Rosenvinge
        Code 660

Sponsor: Office of Space Science and Applications

ALFVEN WAVES AND FIELD-ALIGNED CURRENT STRUCTURES

The electric currents flowing along the magnetic field lines in the magnetosphere play an important role in the electrodynamical interactions between the ionosphere and the high

altitude regions of the magnetosphere. This is because these field-aligned currents can transmit energy very rapidly over large distances. The Dynamics Explorer (DE)-1 and -2 satellites in coplanar polar orbits, the former at high and the latter at low altitudes, have revealed important characteristics about these currents. Precision measurements with high time resolution of the magnetic and electric fields and plasmas have allowed quantitative correlative investigations.

In particular, the DE-2 observations have shown that the field-aligned currents are highly structured unlike the often quoted observational features and models that present smoothly varying, simple morphological patterns. Many of the fine features of the field-aligned currents observed by the DE-2 spacecraft can be interpreted as spatial structures in the currents. This interpretation is based on the following deduction The orthogonal components of the electric and magnetic field variations are often found to be highly correlated, sometimes with the correlation coefficient greater than 0.99, indicating a near perfect correlation. Such a relationship between these two physical parameters provides the first quantitative observational proof that the field-aligned currents are equal to the divergence of the horizontal current in the ionosphere. The constant of proportionality between the electric and magnetic field variations can theoretically be shown to give the ionospheric conductance. The DE-2 observations have demonstrated that the conductance derived in this manner for the structured field-aligned current regions is just what one would expect for the upper atmosphere when it is ionized by the solar extreme ultraviolet radiation and/or precipitating charged particles.

The DE observations go one step further. In addition to these spatial fine structures, the magnetic and electric field observations on DE-1 and -2 have revealed Alfven waves (or magnetohydrodynamic waves) that propagate from the distant magnetosphere to the ionosphere. How are these waves distinguished from the stationary spatial structures discussed above? The ratio of the electric to magnetic field variations gives the speed of the Alfven wave, from which the ion density can be deduced. If the ion density so calculated agrees with the ion density actually observed on the spacecraft, then we can conclude that the observed variations are indeed Alfven waves.

Using these two techniques, we have been able to unambiguously identify Alfven waves and fine spatial structures in the field-aligned currents based on the observations from a single spacecraft. The observations of Alfven waves and field-aligned current structures provide valuable information on the plasma dynamics in the Earth's environments.

Contact: Dr. Masahisa Sugiura
Code 696

DE-2   6 SEPTEMBER 1982
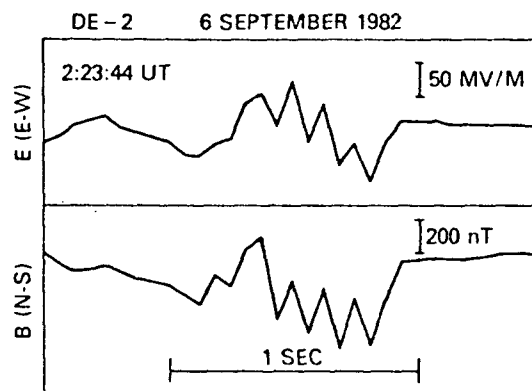
Field-aligned currents as observed by DE-2.

ACCELERATION OF CHARGED PARTICLES IN RECONNECTING MAGNETIC FIELDS

Acceleration to high energies of particles in a plasma is a familiar phenomenon in space physics, astrophysics and fusion physics. Examples include the acceleration of energetic particles in planetary magnetospheres during magnetic substorms and the production of solar and galactic cosmic rays. One approach to this problem is the possibility that strong electric fields near X-type magnetic neutral points can accelerate particles to high energies. The question of whether such electric fields exist near neutral points has led to the study of magnetohydrodynamic reconnection. Some models of magnetic reconnection in which no turbulence is present predict reconnection rates which decrease in highly conducting plasmas such as are found in space. In those models, only modest accelerations occur. However, if magnetic turbulence is present near X-points, then the reconnection rates can become elevated and significant acceleration can occur even at high conductivity. Crucial in assessing the importance of reconnection as a particle accelerator is whether particles spend much time near the X-type neutral points.

We have analyzed particle orbits in simulated fields which evolve and reconnect in the presence of finite amplitude fluctuations and found that turbulent fluctuations do appear near the reconnection zone. The fields in which the test particles propagate were produced in a two dimensional incompressible magnetohydrodynamic simulation with high conductivity. As new magnetic islands appeared due to the reconnection process, a small number of particles are accelerated to thousands of times their initial energy. These are particles that were trapped within small turbulent "magnetic bubbles" in the reconnection zone. The bubbles and particles moved

away from the reconnection zone, crossed the strong electric field region where the particles were accelerated, and then entered the reconnected island region where the reconnection electric field was weak. The simulation indicates that turbulent fluctuations in a reconnecting magnetofluid can accelerate test particles to appreciable speeds.

Contact: Dr. Melvyn L. Goldstein
        Code 692

Sponsor: Office of Space Science and Applications

THE POLAR RAIN: SOLAR WIND STRAHL IN THE MAGNETOSPHERE

International Sun-Earth Explorer-1 (ISEE-1) low energy electron measurements have revealed the frequent presence of field-aligned fluxes of a few hundred eV electrons in the geomagnetic tail lobes. These electrons are most prominent in the northern tail lobe when the interplanetary magnetic field is directed away from the Sun. This characteristic helps identify the electrons as polar rain electrons that are usually identified by their uniform precipitation pattern over the Earth's polar caps. Although tail lobe electrons have been seen previously at high altitudes, the ISEE data have provided the first demonstration of their field aligned nature, and this characteristic places a stringent constraint on their origin. By mapping the solar wind velocity distribution function into the tail lobe, we have confirmed previous suggestions that the polar rain is indeed of solar wind origin and represents the unimpeded access of electrons into whichever tail lobe is magnetically connected to the Sun. More specifically, however, we demonstrate that polar rain is composed of electrons from the solar wind "strahl" a field-aligned component of the solar wind which is difficult to measure but which is thought to be caused by collisionless transit of a hundred eV electrons from the inner solar corona to 1 AU. Furthermore, it is suggested that cases of higher energy polar rain that have been thought to require a magnetospheric field aligned acceleration mechanism may actually be due to an enhanced intensity of the solar wind strahl caused by easier access of solar corona electrons to 1 AU and the polar caps. Implications of this idea are that the polar rain holds considerable potential for studying both the Sun and the magnetosphere. Polar rain measurements may provide a good measure of the solar corona temperature and the degree to which interplanetary field lines connect with those of the Earth.

Contact: Dr. D. H. Fairfield
        Code 690

Sponsor: Office of Space Science and Applications

## PHYSICS OF THE SOLAR-PUMPED MARTIAN LASER EMISSION

Since the atmosphere of Mars is primarily carbon dioxide, its infrared spectrum shows the presence of strong lines due to the vibration-rotation spectrum of CO_2. These absorption lines are formed as the cold atmosphere absorbs infrared radiation from the relatively warm surface. In 1976, it was discovered that the cores of lines in the 10 μm band contain bright emission features. These emission features are formed as CO_2 molecules in the upper atmosphere (70 km) absorb solar radiation in the near infrared (e.g., 2.7 μm) and collisionally transfer these quanta to the $00^\circ1$ state, where they are radiated in the 10 μm band. This process proceeds at such a large rate that a population inversion is established, wherein the population of $00^\circ1$ (the upper state) exceeds that in $10^\circ0$ (the lower state). Under these conditions, the emission in the 10 μm band is laser emission, in the sense that optical amplification effects are potentially significant. Calculations indicate that the optical gain over long path lengths in the Martian mesosphere is of the order of 10 percent, similar to the single-pass gain in laboratory CO_2 lasers.

In order to better understand this emission, a theoretical model has been computed which includes the effects of pumping by 20,000 individual near infrared lines, as well as radiative exchange in the strong 4.3 μm band. The figure illustrates the processes which have been included in the model. The model predicts a value for the total flux in the emission lines which is in close agreement with the observed value. The model also predicts that the brightness of the emission should increase as the kinetic temperature of the Martian mesosphere increases. This occurs because, at higher temperatures, a larger number of ground state rotational levels can be populated, with a resultant increase in the solar pumping. Recent observations of this emission, made with the Goddard Infrared Heterodyne Spectrometer on the NASA 3-meter Infrared Telescope Facility on Mauna Kea, have confirmed this prediction. These high spectral resolution measurements show that the total energy in the emission is correlated with the kinetic temperature deduced from the frequency width of the emission profile. However, these results also show that a surprisingly large range of temperatures exists in the Martian mesosphere, with values ranging from 100 K to over 200 K. Such a large range in temperature suggests that nonradiative effects may be of major importance in determining the temperature structure of the Martian mesosphere.

Contact: Dr. Drake Deming
        Code 693.1

Sponsor: Office of Space Science and Applications

MOLECULAR PHYSICS OF NATURAL MARTIAN LASER
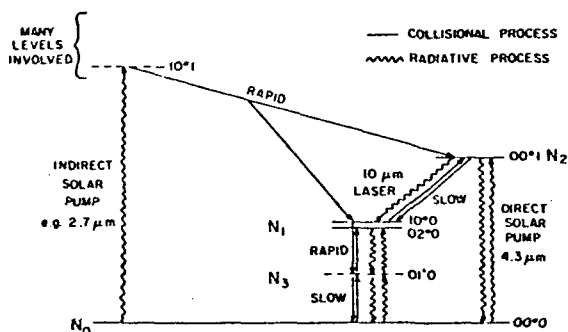
Molecular physics of natural Martian laser.

PHOTOCHEMISTRY OF DIACETYLENE AND HAZE FORMATION ON TITAN

A current proposal for the origin of the absorbing haze observed in Titan's atmosphere suggests its formation by a photochemical mechanism. It is proposed that with the existence (or formation from methane) of acetylene larger poly-enes are formed by photodecomposition of the parent molecule and subsequent reaction of the free radicals produced with the parent molecule. In this manner acetylene yields diacetylene which then yields triacetylene. This process is repeated with the larger molecule formed until solid particles are formed producing the observed haze.

The key step in this sequence of reactions is the fate of diacetylene (C_4H_2), since the reaction of acetylene leading to diacetylene has been well established in the laboratory. Consequently, we have examined the photodecomposition of diacetylene at 147, 185, 229, and 254 nm. The method involved intercepting the free radicals formed with a large excess of deuterium and subsequent chemical analysis of the deuterated products. Only at 147 nm were appreciable amounts of free radicals (i.e., C_2H and C_4H) formed. Polymer formation was the major product at all four wavelengths. Small amounts of acetylene were also found at all wavelengths studied.

Implications of these laboratory studies for the proposed polymer formation producing the absorbing haze in Titan's atmosphere are:

- Since free radicals were found in appreciable amounts only at 147 nm, the free radical mechanism leading to polymer formation can be used only at higher Titan atmospheric altitudes;

- Acetylene is produced in small amounts in the photodecomposition of diacetylene at all wavelengths studied;

- At all four wavelengths, the major product of the photolysis was a nonvolatile material presumably a polymer. Only in the 147 nm photodecomposition can the proposed free radical polymer formation be invoked with any confidence. The mechanism for polymer formation at these wavelengths is still undetermined.

Contact: Dr. S. Glicker
Code 690

Sponsor: Office of Space Science and Applications

CO₂ ON TITAN

Titan, the largest of Saturn's moons, has long been known to be the only satellite in the solar system with a substantial atmosphere. Ten times more massive than that of the Earth, this atmosphere also is composed mainly of nitrogen. Unlike the terrestrial atmosphere, however, the atmosphere of Titan additionally contains moderate amounts of many hydrocarbons (such as methane and ethane) and nitriles (such as hydrogen cyanide and cyanoacetylene).

This organic material is highly reducing and was not expected to maintain any oxygen bearing volatiles. It came as a considerable surprise, then, to discover a sharp emission feature at 667 cm^{-1} in spectra taken by the Voyager 1 infrared spectrometer that could only be attributed to carbon dioxide in Titan's stratosphere. This implied an unknown source of oxygen at these levels. The satellite's surface could not be the source because no oxygen bearing volatile could pass through the cold trap near the tropopause without condensing out in its journey to the stratosphere.

Apparently oxygen from outside the atmosphere of Titan is required. One potential source is associated with a steady state water influx from space. In addition to the water contained in chondritic meteorites, a certain amount is also available from sputtering and collisions connected with Saturn's icy satellites and ring particles.

A quantitative analysis combining photochemical and radiative transfer theory reveals the following scenario. Water enters Titan's atmosphere at a rate of about 3×10^5 molecules cm^{-2}s^{-1}; this is about 0.4 times the corresponding rate on Earth. Here the H_2O molecules are photolyzed, producing OH radicals. These radicals in turn react with carbon monoxide to produce CO_2. Some CO_2 is destroyed, principally by photolysis and by reaction with the methylene

radical, but at a combined rate that is insufficient to overcome CO_2 production. However, once the CO_2 vapor pressure reaches saturation near the tropopause, condensation and attendant precipitation occur, effectively halting a further CO_2 buildup. A stratospheric steady state CO_2 mole fraction of about 1.5×10^{-9} results.

One byproduct of the analysis is the prediction of a steady state mole fraction of $\sim 10^{-4}$ for CO (which is not a volatile at the temperature of concern). Subsequent ground-based observations in the near infrared revealed that CO is indeed present in the amount predicted. This independently confirms the identification of CO, on Titan, and opens up a new vista in the chemistry of oxygen in reducing atmospheres. A complete understanding of this chemistry may ultimately be as significant as the chemistry of reduced compounds (such as CH_4 and H_2) in the Earth's atmosphere.

Contact: Dr. Robert E. Samuelson
        Code 693.2

Sponsor: Office of Space Science and Applications

LOW-FREQUENCY WAVES AND ASSOCIATED IONS DOWNSTREAM OF SATURN

Nearly sinusoidal, long-period (1.4 to 2.8 hours) waves were observed occasionally by Voyager-2 in the solar wind during the 5 months following Saturn encounter in August 1981. These waves, seen as large amplitude oscillations of both the direction and magnitude of the magnetic field, persisted for intervals of up to 2 weeks duration. To a distance of 1300 R_S (Saturn radii; 1 R_S = 60,000 km), they were found to be accompanied by enhanced flows of 28 to 80 keV ions. These ion beams were streaming away from the direction of Saturn, most probably having been accelerated initially near Saturn's bow shock wave. As the energized ions propagated away from the vicinity of the shock, they excited the observed waves by means of an instability reaction in the ambient medium through which they passed. Such phenomena have been observed and studied extensively at Earth, but never to the large distances from the planet at which they were seen by Voyager-2 post-Saturn. At times the beam particles were not detected even though the waves were present because the beam followed the local magnetic field to large northward or southward tilt angles and could not be seen by the ion detectors, which have a 45° field-of-view in the vertical plane. This was the case for the entire wave event at 2800 R_S, the greatest distance from Saturn at which waves were observed.

Contact: Dr. K. W. Behannon
        Code 692

Sponsor: Office of Space Science and Applications

THE RADIO PLANETS AND PREDICTIONS FOR URANUS

The magnetospheres of three planets—Earth, Jupiter and Saturn—are sources of intense, nonthermal radio bursts. The emissions from these sources undergo dramatic long-term intensity fluctuations that are caused by the solar wind interacting with the planets' magnetospheres. Goddard scientists have found that the efficiency of the solar wind interaction, i.e., the ratio of the radio emission output to the solar wind energy input, is remarkably uniform from planet to planet. It appears that if the solar power impinging on a planet's magnetosphere is known, the radio emission output can be predicted.

This information relating solar wind power to radio power has been used to predict conditions at the planet Uranus, which will be visited by spacecraft (Voyager-2) for first time in January 1986. By taking a plausible range of Uranus magnetosphere sizes capable of intercepting the solar wind, predictions of radio emission energy levels are possible. Conversely, when the radio emission is first detected, probably in late 1984, early estimates of the size of the Uranus magnetosphere and its internal magnetic moment will be made.

Contact: Dr. M. D. Desch
        Code 690

Sponsor: Office of Space Science and Applications
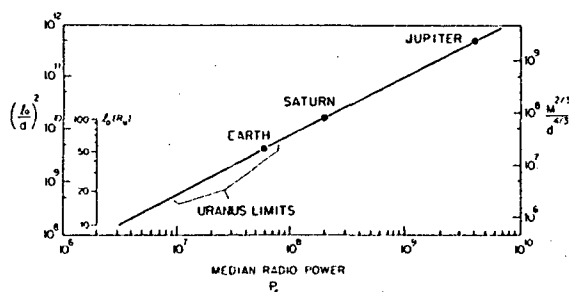
Ratio of solar wind power to radio power.

AN UNUSUALLY LARGE MAGNETIC LOOP IN THE SOLAR WIND

A magnetic configuration closely resembling one of a class of recently discovered interplanetary magnetic loops or tightly wound helices has been observed in the mid-December 1982 data of IMP-8 and ISEE-3 and is estimated to have a heliocentric radial extent $\geq \frac{1}{2}$ AU making it the largest magnetic loop yet observed at 1 AU. ISEE-3, in the solar wind about 90 R_E dawnward of Earth at the time of passage, observed the magnetic field to rotate by 170° in heliospheric latitude, as shown in the bottom 3 panels of the figure. During the rotation the field remained confined to a plane (center of figure) whose normal is radial from the Sun (R).

An interpretation of the structure is offered in the top sketch: the loop is superimposed on a "background" ecliptic plane field which reverses by 180° in heliospheric longitude during passage, returning to its initial direction (point 7) but with stronger intensity (thicker arrow) afterward. There is a suggestion that this flip in the background field and the presence of the interplanetary shock near point (6) are related to the existence of the magnetic loop.

IMP-8 in the dawn magnetosheath observed this same loop field but with shape distorted from its solar wind configuration. Ground-based instruments measured a large change in magnetic field magnitude during this time. Surprisingly there was no significant decrease in cosmic ray intensity recorded by ground-based neutron monitors: a large magnetic loop in the solar wind does not necessarily deflect cosmic rays sufficiently to cause a Forbush decrease.

Such large field configurations are of interest because of their contribution to the understanding of: (1) the large scale hydromagnetic and stability properties of the solar wind, (2) the solar atmosphere as the source of the related plasma and embedded field, and (3) the interaction of large field and plasma structures with the Earth's magnetosphere.

Contact: Dr. R. P. Lepping
         Code 690

Sponsor: Office of Space Science and Applications

MAGNETOHYDRODYNAMIC WAVES AT INTERPLANETARY SHOCKS

The Voyager-1 and -2 satellites are confirming the presence of large scale disturbances propagating through the interplanetary medium in the form of a shock wave as illustrated in the figure. This figure shows magnetic field and plasma data in the upstream and downstream
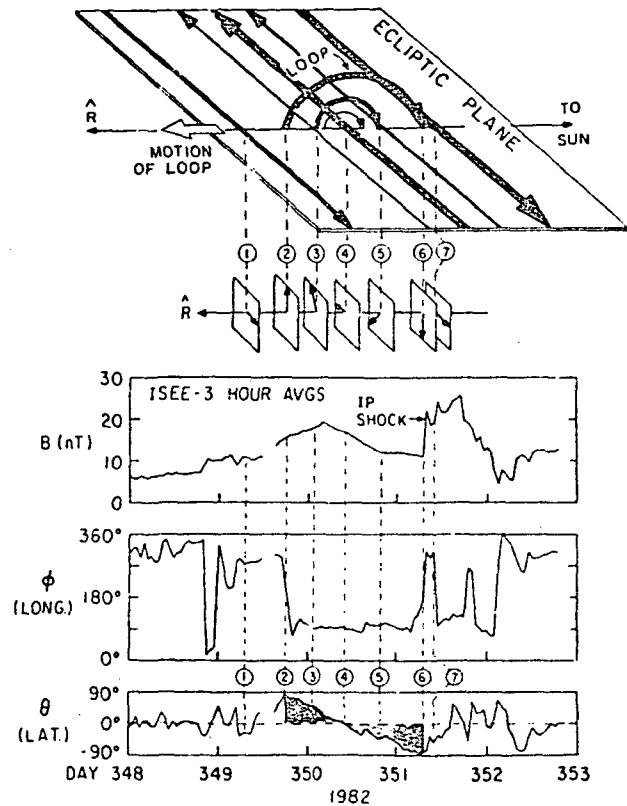

A magnetic configuration closely resembling one of a class of recently discovered interplanetary magnetic loops.

regions of an interplanetary shock that occurred at about 0918:17 UT on January 29, 1978 at about 2.16 AU.

The first four (top) panels are the interplanetary magnetic field components and magnitude obtained by the Goddard magnetometer. The other six (bottom) panels represent the solar wind velocity components, its speed and the solar wind density and temperatures, respectively, as measured by the MIT plasma instrument. These measurements have revealed the presence of MHD fluctuations near interplanetary shocks as illustrated in this figure. Properties of these waves, such as their polarization, the ellipticity, their amplitude and their propagation direction were determined by means of spectral methods together with the calculation of the reduced magnetic helicity and cross-helicity spectra.

An analysis of these waves has shown that they are generated by a resonant interaction due to the presence of a cold proton beam that seems to be associated with the shock. A theoretical investigation of the generation of these MHD
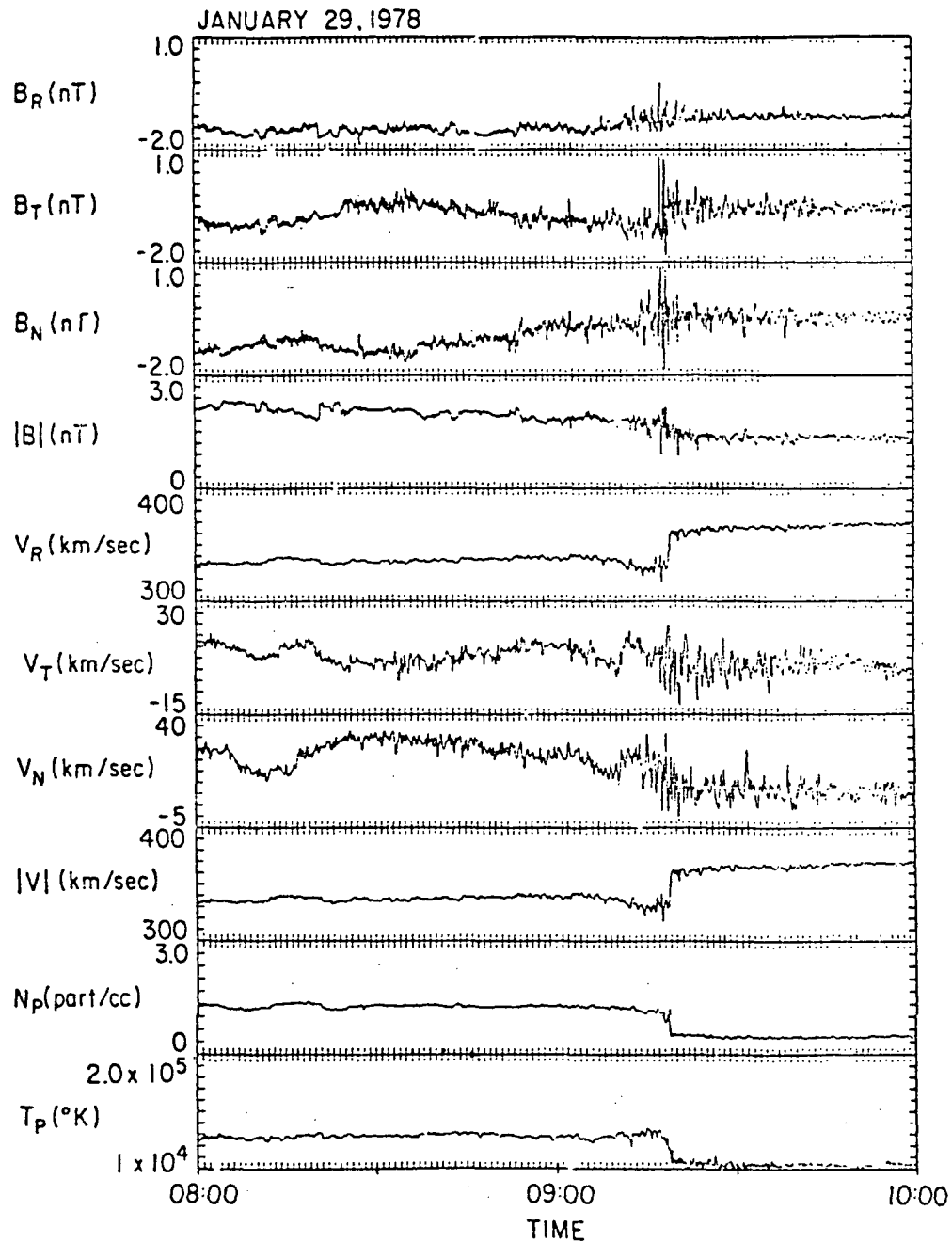
JANUARY 29, 1978

Magnetic field and plasma data in the upstream and downstream regions of an interplanetary shock that occurred at about 0918:17 UT on January 29, 1978, at about 2.16 AU.

waves by an electromagnetic ion beam instability supports our results. The presence of these cold proton beams was corroborated by an analysis of the proton distribution function measured by the MIT plasma analyzer.

Contact: Dr. A. Figueroa-Vinas
         Code 692

Sponsor: Office of Space Science and Applications

INTERACTIONS BETWEEN TYPE III BURSTS AND INTERPLANETARY SHOCKS

Many kilometer type III radio bursts observed in the solar wind show sudden intensity changes as a consequence of encountering interplanetary shocks. The trajectories of the type III bursts can be determined using the direction-finding capabilities of the ISEE-3 radio experiment. Because the cross-section of a type III electron beam is small compared to the extent of a shock, each interaction provides the approximate location of a section of the shock at a given time. The positions of a number of interactions can be used to trace the large scale geometry and motion of a shock between 10 R and 1 AU.

These interactions provide information in addition to approximate shock position. Both increases and decreases in intensity are observed; they are of varying strengths and bandwidths. These parameters are being analyzed to determine constraints on the type III emission process as well as effects due to the shock structure itself. Such features should be useful for comparison to type II bursts since they provide a well-defined frequency associated with the plasma at the shock. Consequently, they can aid in answering questions about the position and frequency of type II radio emission relative to the location of the shock.

Contact: Dr. Robert Stone
Code 690

Sponsor: Office of Space Science and Applications

IRAS OBSERVATIONS OF THE INTERPLANETARY DUST

The Infrared Astronomy Satellite (IRAS), developed and operated jointly by the Netherlands Agency for Aerospace Programs, NASA, and the United Kingdom Science and Engineering Research Council, has completed the first full sky survey in the wavelength range 10 to 100 μm. One of the unique and important characteristics of these data is that they provide information on all angular scales larger than a few arcminutes, making possible the study of diffuse astrophysical sources such as the interplanetary dust. This dust scatters sunlight at visible wavelengths, and this visible 'zodiacal light' has been extensively studied using ground-based and space-borne instruments. However, the same dust also absorbs some of the sunlight and reradiates this energy at infrared wavelengths. Measurements of this 'zodiacal emission' have long been awaited, since they can provide valuable additional information on the character, distribution, and origin of the interplanetary dust.

Initial examination of the IRAS data shows the zodiacal emission, the dominant large-scale infrared source over most of the sky at 12, 25, and 60 μm, to be surprisingly bright, implying that the grains are made of very dark material. Another surprising result is very significant zodiacal emission at wavelengths as long as 100 μm, implying a substantial component of large grains. The data also clearly show that the spatial distribution of the grains is not symmetric about the ecliptic plane, and, in fact, does not appear to have any simple symmetry plane. The implications of this for dust dynamics and origin will require further study. Perhaps the most surprising characteristic of the zodiacal emission is the apparent bands of enhanced emission located about 10 degrees on either side of the ecliptic plane. This emission has been interpreted as arising from particles in inclined orbits in the vicinity of the main asteroid belt, about 2.5 AU from the Sun. If this interpretation holds up, it will be the first strong evidence for at least 1 component of interplanetary dust which is asteroidal rather than cometary in origin.

Contact: Michael G. Hauser
Code 693.2

Sponsor: Office of Space Science and Applications

IMAGING OF THE GALACTIC CENTER WITH AN INFRARED ARRAY CAMERA

High resolution maps of the Galactic Center region at 8 to 12 microns have been made with the Infrared Array Camera system developed at NASA/Goddard Space Flight Center, revealing a complex distribution of compact and extended sources. The results are part of a study of the luminous sources and dust density in the Galactic Center region, carried out at the NASA Infrared Telescope Facility at Mauna Kea. The array camera produces diffraction limited photometric maps with extremely high relative positional accuracy; in a fraction of the observing time required with single detectors.

The observations are part of a collaborative effort, which lead to the formation of a team which was recently selected to develop the array camera as one of the three instruments for the Space Infrared Telescope Facility (SIRTF). The SIRTF Team includes the Smithsonian Astrophysical Observatory (Giovanni Fazio, Principal Investigator), Goddard Space Flight Center (Dan Gezari, Instrument Scientist), Steward Observatory, NASA/Ames Research Center, and the University of Rochester.

The Array Camera System is based on a 16 x 16 detector Aerojet Electro-Systems Co. bismuth doped silicon (Si:Bi)

Accumulation Mode Charge Injection Device (AMCID) monolithic detector array. The detector array, MOSFET preamps and CMOS signal sampling logic are operated at liquid helium temperature. Signals in each of the 16 independent channels are amplified and filtered by a warm preamplifier, read by a correlated double sampler, digitized by a 12-bit analog-to-digital converter, and tri-state latched on a data bus and routed into four first-in, first-out (FIFO) buffer memories from which they are processed in sequence by four Motorola 68000 microcomputers. Stored data are then down-loaded into an LSI 11/23 minicomputer for processing, display and storage.

A 30 x 30 arcsec (1.5 pc) region of the Galactic Center was mapped to a sensitivity of 2 Janskys in a series of 1 minute integrations. The maps were made at 8.3, 9.6 and 12.4 microns with 10 percent bandpass interference filters, and were diffraction limited. The entire array covered a 13 x 13 arcsec field of view, with each element subtending 0.8 arcsec, or about two elements per diffraction disc. Because of the array geometry, relative source positions of significantly higher precision than previously available were obtained.

Several deep exposures were made at the position of the nominal Galactic Center and the strong 2 micron source IRS-16, which is suggested to be responsible for generating a giant dust-free "bubble" at the center of the Galaxy and is a factor in local heating. IRS-16 was not detected in our observations, and the region around IRS-16 was found to be nearly void of 10 micron emitting dust, presenting itself as a minimum in 8.3 and 12.4 micron intensity, and a minimum of silicate absorption. This could be evidence of outflow around IRS-16. Maps of derived color temperature, and 9.6 micron silicate absorption, generated from the Goddard image data show that IRS-16 region is a local minimum in temperature and silicate absorption. Our color temperature map suggests that the sources are heated from outside, with the possibility that primary luminosity sources appear both within and outside the ring-like structure observed at radio wavelengths.

However, the deep integrations at 12.4 microns do reveal an enhancement at the position of the nearby radio source "21", on the ridge of emission midway between IRS-1 and IRS-2. Previously this source has only been detected at radio wavelengths. These data are the first evidence of a compact infrared source at the position of radio source 21. IRS-21 is unique in that it is the only infrared source on the ridge of emission which is common to all of the 'paths of infall" of gas towards the Galactic Center determined by 6-cm VLA observations. These results will bear upon the broader question of the energetics of the Galactic Center region: whether the observed emission can be attributed to the process of star formation, or the presence of a superluminous compact object at the Galactic Center.

Contact: Dr. Dan Gezari
            Code 693.2

Sponsor: Office of Space Science and Applications
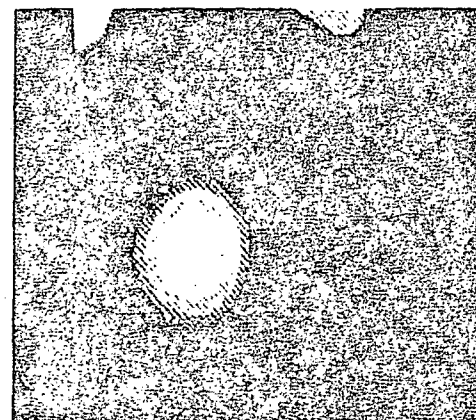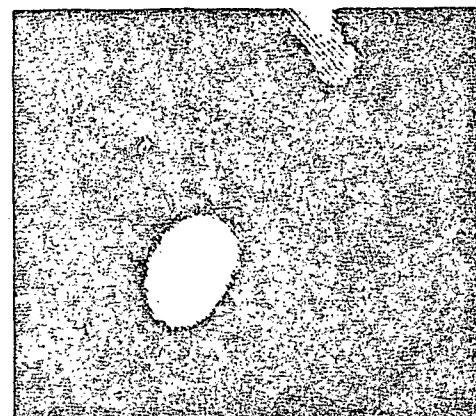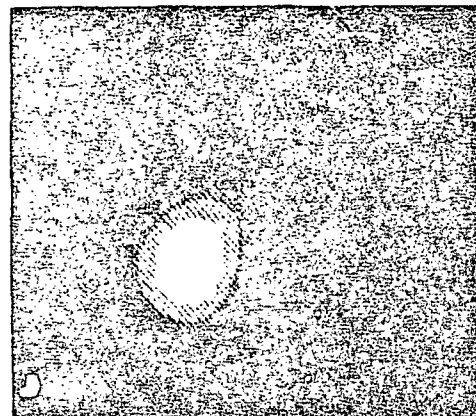
Images of the Galactic Center with an Infrared Array Camera.

DEVELOPMENT OF SENSITIVE THERMAL SENSORS FOR RADIATION DETECTION

During the past year, we have made substantial progress in the development of sensitive thermal detectors for use as far infrared and submillimeter detectors from orbiting telescopes. We have also made initial tests of a new concept, a thermal detector as an X-ray spectrometer. The performance of the device is in good agreement with predictions of theory for thermal X-ray spectrometers developed by the Goddard Space Flight Center (GSFC). Devices under development at GSFC offer the prospect of high (<5 eV) resolution with high efficiency.

Devices have been constructed and tested down to 0.1 K. High sensitivity in thermal detectors used as either power or energy detectors is achieved by the minimization of its heat capacity and operating temperature. The heat capacity is minimized by constructing the detector from dielectrics and superconductors which have low heat capacities at low temperatures. Some devices tested employed ion implanted thermistors and superconducting aluminum leads. The performance of the devices tested shows that the sensitivity of detectors tested at 0.3 K is set by fundamental limits, the thermodynamic statistical fluctuations in the temperature of the detector itself.

The noise equivalent power of a 0.1 K detector built and tested at GSFC is 2×10^{-17} W/Hz with a 1 ms time constant. This is an excellent detector suitable for many infrared applications. Preliminary tests of a moderate heat capacity detector at 0.3 K used as an X-ray spectrometer yield a resolution of 130 eV FWHM at 6 KeV, somewhat better than a state-of-the-art solid-state detector and in agreement with predictions of our theory.

Theoretical studies have proceeded in parallel with experimental work, so that accurate modeling of results and predictions of performance are possible. Fabrication techniques and test procedures are well developed and should result in excellent progress in the future.

Contact: Dr. Harvey Moseley
          Code 693.2

Sponsor: Office of Space Science and Applications

## INTERSTELLAR MOLECULES: DISCOVERY OF SiCC IN SPACE

One of the most peculiar molecules ever to be detected either in space or in the laboratory, and the first ring compound to be identified beyond the solar system, has been discovered by the GISS Astrophysics group in the expanding shell surrounding a bright infrared star. This molecule is SiCC, shown in the accompanying energy level diagram, a very compact three membered ring that can be considered a small, highly reactive fragment of the common abrasive silicone carbide (carborundum). The identification is based on spectra obtained with the GISS millimeter wave telescope.

Nine SiCC rotational transitions (arrows in figure) lying in wavelengths between 3 and 1.7 mm have been clearly observed toward IRC + 10216, a fairly nearby evolved carbon star that is one of the brightest objects in the sky at 2 microns in the near infrared. Although these transitions have never been observed in the laboratory, there is no doubt that they are produced by SiCC, since they lie at exactly the frequencies expected for a symmetric 3-membered ring, and the bond lengths derived from the astronomical frequencies are in good agreement with those recently derived at Rice University from a laser two-photon ionization experiment on SiCC in a supersonic molecular beam.

The C-C bond length in SiCC, 1.268 A, is almost exactly that of the C_2 ion, suggesting that the ring is highly ionic, i.e., C_2-Si+. A theoretical *ab initio* quantum calculation of the SiCC structure by S. Green at GISS confirms this suspicion: the dipole moment is large, as expected for an ionic bond. If this is indeed the nature of the bond, the attachment of metals like Si—elements with low ionization potential such as Mg, Al, Ca, Fe, etc.—to conjugated carbon chains may be fairly common, suggesting a whole family of "nonterrestrial" molecules which may be detected in carbon rich stellar atmospheres and circumstellar shells. This in turn suggests a possible solution to a classical puzzle: the fate of metals of carbon-rich atmospheres. In normal oxygen-rich stellar atmospheres, metals exist at low temperatures mainly as oxides; the discovery of SiCC suggests that in carbon atmospheres they may be systematically attached to organic molecules of a peculiar sort—straight conjugated carbon chains, of which C-C is the simplest member.

Contact: Dr. Patrick Thaddeus
          Code 610

Sponsor: Office of Space Science and Applications
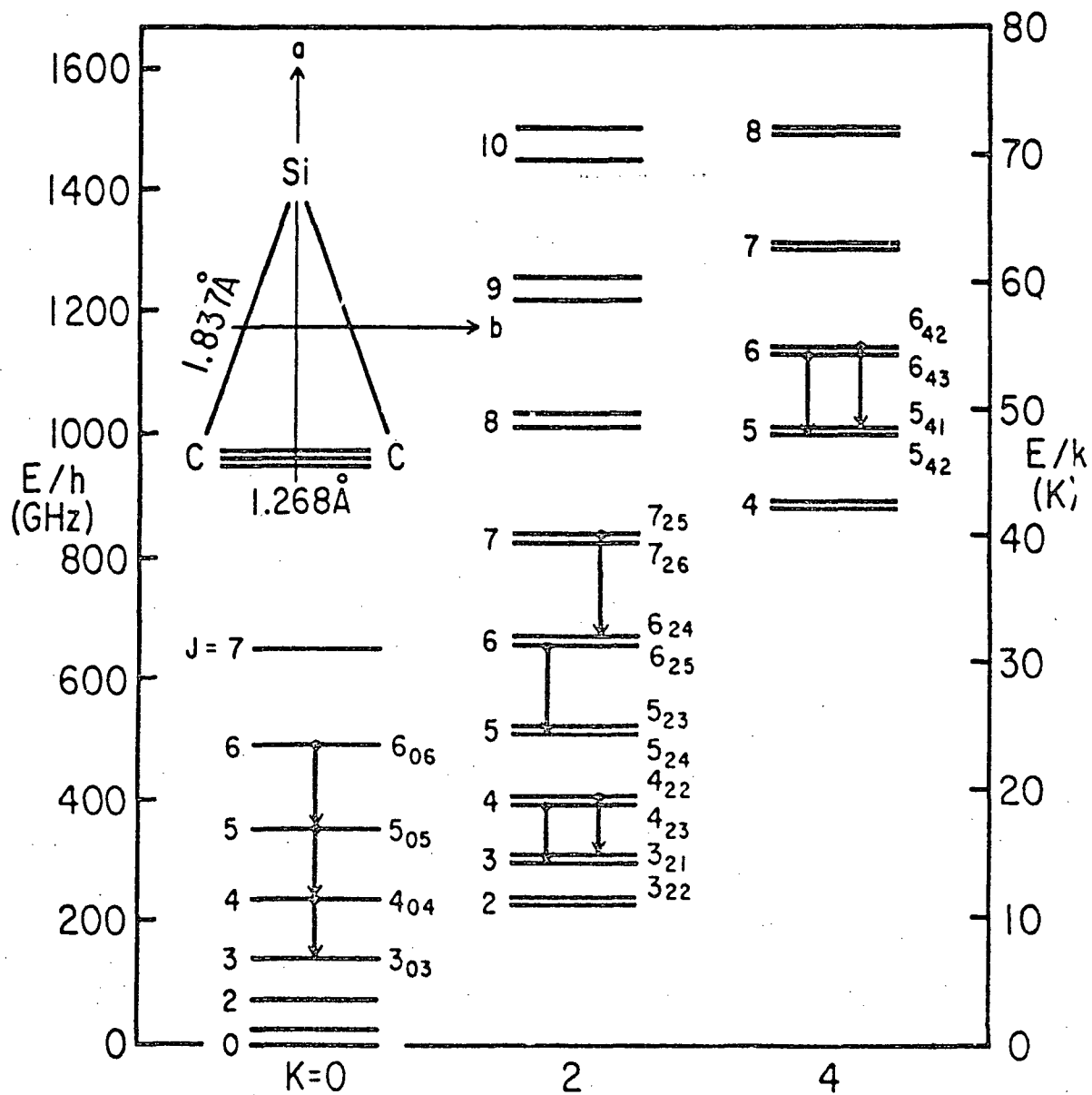
Energy levels of the SiCC molecules.

HIGH ENERGY ASTROPHYSICS

LOW-ENERGY GAMMA-RAY ASTROPHYSICS SPECTROSCOPY AND IMAGING OF LOW-ENERGY GAMMA-RAY SOURCES

The present generation of high-resolution gamma-ray spectrometers has recently discovered a number of narrow lines in the spectra of several astrophysical sources. Three examples are the 511-keV position annihilation line from the center of our galaxy, the 1.5 MeV line from SS433 which is probably produced by nuclear excitation in the jets of the source, and the 1.8 MeV line from the region of the galactic plane due to the decay of ^{26}Al accumulated over the last million years from explosive nucleosynthesis in supernovae and novae.

In all three cases the statistical significance of the detection was small. Also, the instruments that made the observations all had large fields of view ($\sim 10°$FWHM) and no imaging capabilities, so that the exact location and extent of each source of gamma-ray emission is not known. However, the results are tantalizing and suggest that nuclear and annihilation gamma-ray lines are a common feature of many astrophysical objects.

The 511-keV line from the Galactic Center region is a particularly interesting feature. It is very narrow (~ 2 keV FWHM) which implies that the positions are annihilating in a relatively cool region, and yet the line is intense and variable indicating that the positrons are being produced in a small, hot region. One theoretical interpretation is that the positrons are created in the vicinity of a massive black hole that is thought to exist at the dynamic center of the galaxy, and then escape that region and annihilate in cooler clouds that spiral around the black hole at a distance of approximately 1 light year. A major observational goal in the field of gamma-ray spectroscopy is to map the 511-keV emission.

We are currently building a new-generation balloon-borne instrument called the Gamma Ray Imaging Spectrometer (GRIS) that will have a factor of 4 to 8 better sensitivity than current spectrometers, and will be the first instrument in this energy range (20 keV to 10 MeV) that is capable of imaging sources. In order to achieve these objectives, two new concepts are being developed and incorporated in the instrument. The first is a coded aperture imaging system that includes a moving mask with active NaI elements. The goal is to be able to localize sources such as the galactic center 511-keV source to better than a degree. The second new concept is segmented germanium detectors. By dividing the outer contact of a germanium detector into horizontal segments and applying different coincidence conditions between the seg-

ment signals in different energy ranges, the background in the detectors can be reduced by a factor of >7 between 20 keV and 2 MeV.

The GRIS flight program is scheduled to begin in the Fall of 1986. The observing plan calls for detailed spectroscopic and imaging studies of known line sources, and an extensive search of new candidate objects such as the nuclei of active galaxies, X-ray pulsars, supernova remnants, and recent novae.

Contacts: Dr. Neil Gehrels
          Code 661

Sponsor: Office of Space Science and Applications

GALACTIC GAMMA RAY ASTRONOMY

Studies of the galactic diffuse matter distribution, the galactic photon density distribution, and the cosmic ray scale height strongly support a concept that, not only is the diffuse galactic gamma radiation predominately from cosmic ray interactions with photons and matter, but the galactic cosmic rays in the plane are correlated with the matter density on the broad scale of galactic arms.

Although the large majority of the diffuse galactic gamma radiation results from cosmic ray interactions with matter, the Compton contribution to the diffuse gamma radiation over most regions of the Galaxy is calculated to be 10 to 20 percent depending on latitude and longitude. In the inner galaxy, the contribution is smaller due to the effect of the Compton radiation itself on the parent cosmic ray electron spectrum.

The correlation of the cosmic rays with the arms, as shown in this work, and the associated general increase of the cosmic ray density from the outer galaxy to the inner part are very strong arguments that the bulk of the cosmic rays are galactic and not extragalactic. The correlation of the cosmic rays with matter also means that galactic gamma rays provide a relatively high contrast picture of the structure of the galaxy. Future high sensitivity studies of the galactic gamma radiation, such as those with the Gamma Ray Observatory, will provide new insight into the structure and dynamic evolution of the Galaxy.

Contact: Dr. Carl E. Fichtel
        Code 660

Sponsor: Office of Space Science and Applications

WHAT IS THE COSMIC X-RAY BACKGROUND TELLING US ABOUT THE QUASARS MISSING AT HIGH REDSHIFTS?

There is now strong evidence that the increase in the space density of high luminosity quasars with redshift ($z = \Delta\lambda/\lambda$, from spectral lines) does not persist beyond $z = 3.5$. On the other hand, the observation of some quasars at $z = 3.5$ indicates that "seeing" effects (e.g., due to obscuration by intergalactic dust) cannot readily explain the paucity of these objects at such high redshifts. However, recent analysis of GSFC HEAO data shows that the power-law X-ray spectra of bright quasars cannot be similar to the spectrum characteristic of those faint unresolved sources that dominate the extragalactic thermal X-ray background. If these thermal type sources of the cosmic X-ray background are indeed quasar-like objects at z ~3.5, then they would have to be extremely weak in most of the atomic emissions usually associated with typical quasars. This would suggest a pronounced spectral evolution whereby young quasars with thermal X-ray emission and relatively weak optical lines eventually become canonical quasars with nonthermal X-ray emission and strong optical lines.

A model that we have used for characterizing the line emitting regions associated with active galactic nuclei has been applied to this problem. Considering the thermal type spectrum of the X-ray background as that appropriate for the central source of ionizing radiation in this model, it has now been shown that young quasars could very well be extremely weak in most of the optical emissions usually associated with typical quasars. Correlation of data from future observations made with the Hubble Space Telescope and broadband X-ray telescopes (such as the observatory we are planning for the OSS-2 mission) should provide the information required for tracking the early stages of quasar evolution and thereby help distinguish such spectral transitions from changes in space density and/or luminosity alone.

Contact: Dr. Elihu Boldt
        Code 661

Sponsor: Office of Space Science and Applications

X-RAY SPECTROSCOPY OF SUPERNOVA REMNANTS

At the end of their lifetimes, some stars die in the massive explosion of a supernova. The material surrounding the star, as well as debris from the star itself are heated to X-ray temperatures. Study of the X-ray emission provides information about the temperature, density, and composition of the hot material.

In a young remnant such as observed by Tycho Brahe, before the shockwave from the explosion has heated much interstellar material, the emission serves mainly as a probe of the matter from the star. Processed material spewed out in these explosions is believed to be one of the principal contributions to the enrichment of the interstellar medium. Determination of the quantity of each element released in a supernova places important constraints on how much of the material in the galaxy has been processed through exploding stars. Study of these products also supplies information as to which of several plausible scenarios could explain the supernova.

We have been studying spectra taken with the GSFC Solid-State Spectrometer on the HEAO-2 satellite from several young remnants. Those known, or suspected, to contain pulsars show spectra with the smooth, power-law forms as predicted to arise from relativistic particles such as a pulsar would produce. Other remnants, whose shape does not indicate the presence of a central object, have lines in their spectra corresponding to atomic transitions in elements of moderate atomic number. The pattern of line strengths indicates that the plasma is tenuous and has not been shocked long enough to have attained ionization equilibrium. To fit our data, we have obtained calculations of spectra that result
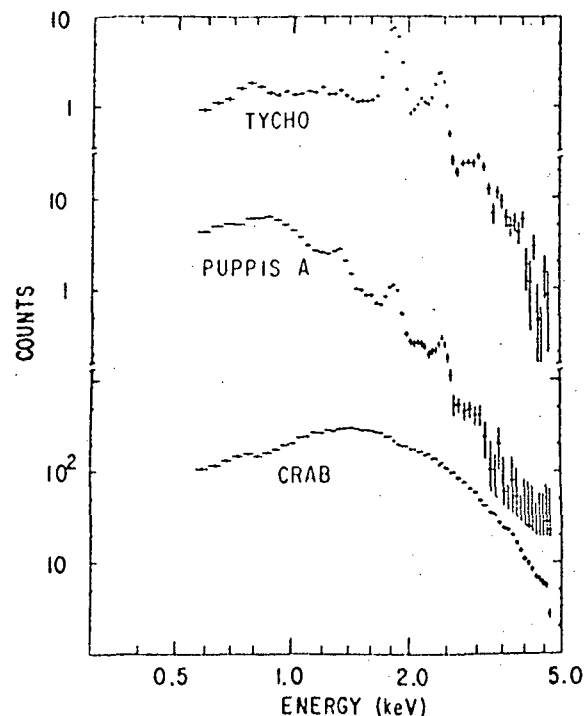
Sample pulse height spectra from three types of remnants.

when the effects of this time-dependent ionization are included. Even allowing for the enhancement in some line strengths which arises in the nonequilibrium models, the measurements of several young remnants still require substantial abundance enhancements. The composition inferred for two well studied remnants agrees with that predicted for the outer layers of a carbon deflagration supernova, a popular scenario for one type of outburst.

In an older remnant, X-rays arise principally from shocked interstellar material. Spectra from the remnant Puppis A show it to have emission consistent with a circa 10.000 year old shock which has encountered a variety of densities in the surrounding material. One region, which appears as a cloud in X-ray images of the remnant, appears to be at least ten times more dense than the bulk of the plasma.

Contact: Dr. Andrew Szymkowiak
         Code 661

Sponsor: Office of Space Science and Applications

GAMMA RAY EMISSION FROM SS433

Gamma-ray spectral lines have recently been discovered from SS433, a galactic compact object known from optical and radio observations to emit relativistic jets. The gamma-ray observations, performed with the high resolution Ge detector on High Energy Astronomical Observatory-3 (HEAO-3) (R.C. Lamb et al. Nature 305, 37, 1983), detected several lines. The line with the strongest intensity and highest statistical significance, seen during a radio and X-ray flare at 1.495 MeV, has been interpreted either as a blueshifted ^{24}Mg line of rest energy 1.369 MeV or as a blueshifted 1.380 MeV line following p—^{14}N fusion in the CNO cycle. The latter interpretation is due to R.C. Boyd (Ap.J. Letters 276, L9, 1984).

For both interpretations, the implied blueshifts are consistent with the optical blueshift at the time of the flare. But the fusion model predicts several other lines whose intensities are in conflict with HEAO-3 observations. In particular, it predicts a line with rest energy 6.175 MeV with intensity equal to that at 1.380 MeV. While a line at about 6.7 MeV was seen from SS433, the fact that its intensity is much weaker than that of the 1.495 MeV line is a strong argument against the fusion model.

If the observed line at 1.495 MeV is due to ^{24}Mg excited by interactions of fast Mg nuclei with ambient gas, an explanation is needed for its very narrow observed width (recoil would broaden the line to a width about 3 times larger than

observed), and for the fact that stronger lines from C, O and Ne deexcitations are not seen. Such an explanation has been provided by R. Ramaty, B. Kozlovsky and R. E. Lingenfelter who suggest (Ap. J. Letters 285, L 13 1984) that the gamma-ray emitting Mg nuclei in SS433 are imbedded in grains moving at the velocity of the jets. Grains would narrow the lines by stopping the recoil nuclei faster than they can emit gamma rays. In addition, the depletion of O and Ne in the grains relative to cosmic abundances would account for the absence of strong very narrow lines from these elements. The much weaker very narrow ^{16}O line could be identified with the observed 6.7 MeV line and several other lines predicted by the grain model could be detected by future observations.

Contact: Dr. Reuven Ramaty
         Code 665

Sponsor: Office of Space Science and Applications
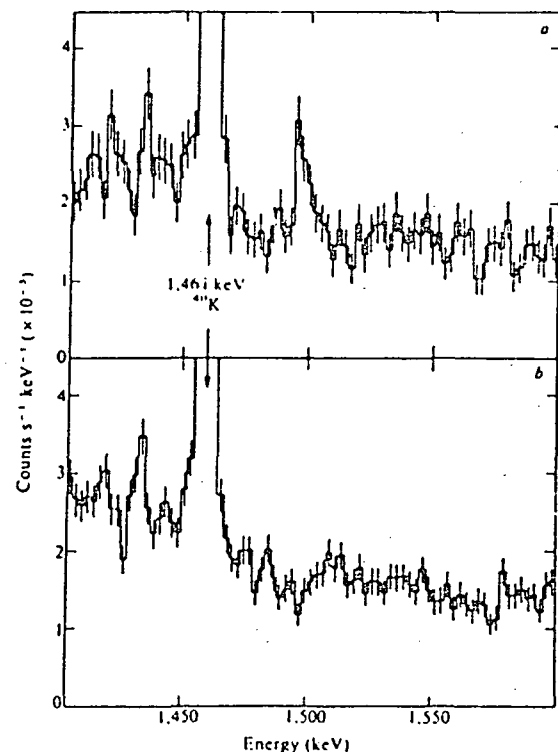
Count rate spectra: a—from a 30°-wide region centered on SS433; and b—from a 78°-wide nearby background region (from Nature, 305(37), 1983).

RECREATION OF THE EARLY UNIVERSE CONDITIONS IN COSMIC RAY INTERACTIONS

One of the great recent successes of particle physics has been the unification of the weak (W) and electromagnetic (EM)

interactions, which as been experimentally verified with the discovery of W± and Z particles at CERN. According to the theory W and EM forces unify at high temperatures (10^{14} °K) and become distinct at lower ones due to spontaneous symmetry breaking. This symmetry breaking (of paramount importance for the theory to work) is a phase transition very similar to the phase transition in a super conductor, which occurs when the temperature drops below a critical value. The mathematical description of the phenomenon is made in terms of a field, the Cooper pair field, which below the critical temperature acquires mass, thereby breaking the gauge invariance principle (very much in the same way that a finite mass for the photon would break the gauge invariance of electrodynamics). The equivalent quantity in particle physics is the Higgs field which also acquires mass as the Universe cools thereby breaking the gauge symmetry unifying the W and EM forces.

In high energy collisions it is possible to recreate the conditions prevailing in the Early Universe prior to the decoupling of W and EM interactions. Such high energy collisions could take place in cosmic ray interactions in the atmosphere and may soon be achieved in proton-antiproton collisions at CERN. There is indeed a certain class of cosmic ray events of very high energy (1000 TeV), the so-called Centauro events, with properties which defy any conventional explanation. These properties include high multiplicity, deep penetration in the atmosphere and absence of pions which are, in general, abundantly produced in all normal nuclear collisions. However, it was shown, that these properties can find a natural explanation in terms of the decay modes of a coherent Higgs field state (i.e., a particle consisting of self contained Higgs field). Such a configuration can indeed be formed if the conditions of the early Universe prior to the symmetry breaking were created in those high energy collisions. The mere observation of the Centauro events, therefore, provides evidence that such an extreme state of matter can be achieved in nuclear collisions.

Contact: Dr. Demosthenes Kazanas
        Code 665

Sponsor: Office of Space Science and Applications

SOLAR FLARE PARTICLES

During the last several years ^{3}He-rich events have been observed to occur, at energies of ~ 1 MeV/nucleon, once every 3 weeks on the average. In these events, the ratio ^{3}He/^{4}He is observed to increase several thousandfold over the normal photospheric value. Typically, heavier elements are also enhanced in their abundance. Associa-

tions of these events with low energy electrons (2 to 100 keV) are now making it possible to pinpoint the time of release from the Sun to within 2 minutes, offering for the first time the possibility of relating direct observations of the Sun to these bizarre events.

We have also studied the relationship of energetic particle intensities near Earth to coronal mass ejections (observed by coronagraph) and to emissions of gamma rays by solar flares. It is found that interplanetary particle events are almost always associated with coronal mass ejections, while the particle intensity is poorly correlated with the gamma-ray intensity in the energy range 4 to 8 MeV. The latter is surprising since these gamma rays are known to be produced by energetic particles. One possible interpretation is that coronal mass ejections facilitate the escape of particles from the flare site into interplanetary space. Gamma-ray production, then, may be increased when most of the particles are unable to escape from the flare site and instead remain to produce gamma rays. An alternate interpretation is that the particles we observe near Earth are not from the same population responsible for the gamma rays, but instead are a separate population accelerated by shock waves which are generated by coronal mass ejections.

Contact: Dr. Tycho von Rosenvinge
        Code 661

Sponsor: Office of Space Science and Applications
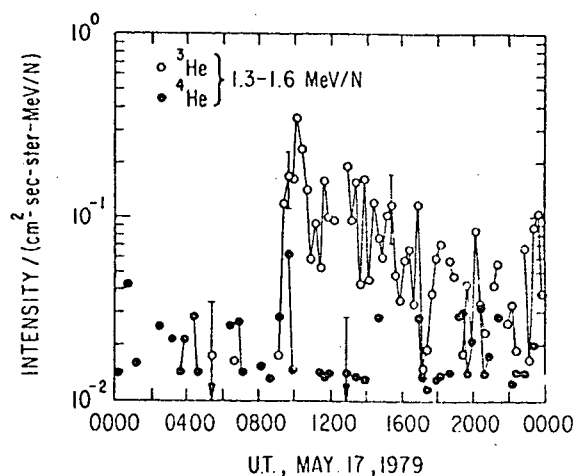
A time history plot of the intensities of ^{3}He Open circles) and ^{4}He (closed circles) for a ^{3}He-rich event.

DEVELOPMENT OF A QUANTUM X-RAY CALORIMETER

The study of the spectra of astronomical objects is the fundamental way in which astronomers can determine the composition, temperature, degree of ionization, and sometimes even the kinematics of emitting objects. In X-ray astronomy, with gas temperatures of 10^6 to 10^8 K, the spectra are expected to exhibit highly complex line structures due to the myriad of atomic transitions that exist in the high-Z elements. These line complexes serve as a diagnostic probe into the environment of the emitting region.

The satellite experiments that were flown throughout the late 1970's and early 1980's demonstrated that X-ray line emission is very pronounced in many types of X-ray sources, but the energy resolution that is required to separate the lines from neighboring ionic states and other atomic species has not been available, except for some o. the brighter X-ray sources. The reason is that although dispersive spectrometers are capable of yielding a high spectral resolution, they sample only a small interval of the spectrum, or have relatively low detection efficiency. Nondispersive spectrometers (such as proportional counters or solid-state detectors) have a higher throughput, but with only moderate energy resolution. The ideal spectrometer for use in X-ray astronomy would have an energy resolution of the order of an electron-volt, and nearly 100 percent detection efficiency over the energy range 0.1 to 10 keV.

An entirely different and novel X-ray spectrometer that should have these 'ideal' properties is being developed at Goddard. Whereas all previously used X-ray detectors convert an incident X-ray into electric charge (through photoelectric processes in a gas or solid), a detector that actually measures the heat that an X-ray produces when it is absorbed in a solid has been devised. A small chip of Si (0.25 mm cube) is doped with impurities that cause it to function as a highly temperature-sensitive electrical resistor (thermistor).

When an X-ray is absorbed the temperature of the chip rises by a small amount, and the resulting resistance change in the thermistor is sensed. Individual X-ray events will deposit typically $10-^{17}$ calories. However, the precision to which the energy of the incident X-ray can be determined is limited by the thermal fluctuations in the absorbing solid. To minimize these fluctuations it is necessary to use a low heat capacity material at very low temperature. A detailed analysis indicates that a small volume of Si at 0.1 K can achieve an energy resolution of 1 eV, or $E/\Delta E \, 10^3$ to 10^4 in the 0.1 to 10 keV energy band. This performance would actually be superior to a dispersive spectrometer, and with nearly 100 percent detection efficiency over the 0.1 to 10 keV energy range.

Several such "X-ray calorimeters" have been fabricated and tested, and the results indicate that the X-ray calorimeter does indeed detect individual X-rays with an energy resolution that is consistent with the thermodynamic properties of the Si chips used. Future tests will focus on optimum detector geometry and impurity concentration, and the development of repeatable production techniques.

Ultimately, it is planned that a complete detector, including X-ray absorber, thermistor, and electrical and thermal leads be etched from a single piece of Si, just as microelectronic circuits are made.

If this new detector technology is successful, it could allow the high resolution spectra of thousands of celestial X-ray sources to be measured in a fraction of the time required by previous techniques.

Contact: Dr. Richard L. Kelley
Code 661

Sponsor: Office of Space Science and Applications

ASTRONOMY AND SOLAR PHYSICS

SOLAR MAXIMUM MISSION FLARE STUDIES

The Solar Maximum Mission (SMM) spacecraft was repaired in space by the crew of the Space Shuttle *Challenger* on April 11, 1984. Following the repair, it was possible to resume observations with fine-pointed instruments aboard the SMM

that had been inactive since November 1980, when the spacecraft attitude control system was partially disabled.

The newly active instrument made observations complementary to those of other onboard experiments that do not require fine pointing and that took useful data during the

3½-year interval from November 1980 to the successful repair. Among the latter is the Hard X-Ray Burst Spectrometer (HXRBS), which recorded the strongest X-ray burst of the current sunspot cycle during the great solar flare of April 24th, leading ground controllers to interrupt the post-repair engineering checkout of the SMM spacecraft to facilitate observations of the active region that gave rise to the flare.

Also after the repair in space, the fine-pointed Ultraviolet Spectrometer and Polarimeter on SMM was used to make a survey of ultraviolet continuum emissions from flares. Continuum flares were found to be more common at ultraviolet wavelengths than in visible light. Indications of possible pulsation effects in flare continua were noted. On May 20, 1984, impulsive phase bursts in the ultraviolet continuum were seen to vary simultaneously (to within 0.2 second) with hard X-ray bursts that were observed with the HXRBS. (The impulsive phase is a stage of major, rapid energy release that occurs near the start of a solar flare.) These observations should help to explain the physical phenomena associated with the penetration of the solar atmosphere by energetic particle beams generated in solar flares. On May 21st, X-ray bursts observed with the HXRBS were found by a radio telescope in Brazil to be accompanied by radio bursts, simultaneous with the X-ray bursts to a precision of 0.1 second, and occurring at the high radio frequency of 90 GHz, which implies that very strong magnetic fields were present at the source on the Sun.

Contact: Dr. Stephen P. Maran
        Code 680

Sponsor: Office of Space Science and Applications

A LEAKY WAVEGUIDE SOLAR WIND THEORY

Twenty years ago, the existence of the solar wind was confirmed by the direct observation of the flow from Earth orbiting spacecraft. This discovery was one of the major scientific achievements of NASA's then fledgling space exploration program. Today, studies of the solar wind continue, but the emphasis has changed considerably.

The most important observational result in recent years has been the discovery that high speed solar wind streams originate in coronal holes. Coronal holes are large regions on the surface of the Sun where the magnetic field connects directly to the interplanetary magnetic field. The recognition of this association has had two important consequences for solar wind theory: (1) it has narrowed the range of acceptable solar wind models by providing

realistic estimates of the plasma properties in both the interplanetary medium and in the region where the wind is accelerated, and (2) it has emphasized the fact that at least one major component of the solar wind originates in a discrete magnetic structure within the solar corona.

Recent theoretical efforts have dealt almost exclusively with the implications of these two additional constraints for the various mechanisms proposed for acceleration of the flow. These studies have demonstrated that traditional sources of acceleration cannot account for the properties of the high speed flow and that additional acceleration mechanisms must be sought. At this point, the most likely source of additional acceleration seems to be magnetohydrodynamic (MHD) waves propagating up from the solar surface. Although theories for acceleration of the solar wind by MHD waves exist, they are not yet completely selfconsistent. They account for flow tube geometry in the equations for the large scale flow, but ignore the effect of flow tube geometry on the propagation of the waves assumed responsible for the acceleration.

Physicists at Goddard Space Flight Center have been developing a theory for acceleration of the solar wind which overcomes the shortcomings of the more traditional approach. The theory that is beginning now to emerge is best described as a leaky waveguide theory. Results so far show that coronal holes can act as leaky waveguides for MHD waves in the solar corona. Wave flux which enters at the base of the corona is guided by the magnetic structure of the coronal hole from the photosphere out into the interplanetary medium. But unlike typical metallic waveguides, the boundaries of the coronal hole are not rigid, and a significant amount of wave energy can be radiated from the walls into the surrounding medium.

The energy which leaks out of the coronal hole is transported across magnetic field lines by compressing the plasma in a direction transverse to the background magnetic field. As one might expect, the force on the solar wind plasma which results from the propagation of these waves is different than the force predicted by traditional theory. More detailed models are being constructed to begin to quantify these differences with sufficient precision to allow observational tests of the theory. There is every reason to believe that this strong interaction between observation and theory will lead to an increased understanding of the processes which result in the acceleration of the solar wind.

Contact: Dr. Joseph M. Davila
        Code 682

Sponsor: Office of Space Science and Applications

SYMBIOTIC STARS

The nature of the high energy source that is responsible for the peculiar emission properties of a class of astronomical objects known as symbiotic stars has recently been revealed by space observatories. Symbiotic stars have long bewildered astronomers because of the dual nature of their emission. This has led astronomical spectroscopists to believe they are an unusual class of binary star system.

Generally, symbiotic star systems include a highly evolved voluminous red giant star, whose surface temperature around 2500 degrees is nearly half that measured at the Sun's surface. As such, its emission is seen predominantly at visible and infrared wavelengths. However, the continuous spectrum at visible wavelengths attributed to the cool giant is interrupted by sharp emission lines that arise from a variety of atomic species. The presence of these emission lines in symbiotic spectra suggest a very tenuous ionized gas is present in the systems, which is heated by a hot ionizing source of energy. Because the emission from the red giant is not sufficiently energetic to explain the presence of these atomic species, astronomers have postulated the existence of a subluminous hot star, similar to white dwarfs or compact stars that are found at the center of planetary nebulae which have characteristic surface temperatures between 25,000 and 100,000 degrees.

Space observatories such as the International Ultraviolet Explorer (IUE) afford astronomers an opportunity to study the hot ionizing source of energy in these systems in a unique manner that is not possible from ground-based observatories. This follows because the cool red star in the system, which dominates the integrated light at visible wavelengths, makes essentially no contribution in the ultraviolet, where the hot star emits most of its energy.

Recent observations obtained with the Very Large Array radio telescope at Socorro, New Mexico (see accompanying figure) of one symbiotic star suggests mass is being expelled from the system in a manner reminiscent of mass explosion in active galaxies. It is believed that the cool red giant in the R Aquarii system tidally exchanges material with the compact hot star in the system. At particular phases of the binary orbit, mass flowing from the cool star onto the compact hot star forms a disk around the hot secondary. If the mass flow between the component stars is sufficiently great, material contained within the accretion disk can be expelled perpendiclar to the axis of the disk in the form of a jet or collimated stream. A hot jet material or ionized column of gas was unexpectedly detected in R Aquarii; it subsequently has become an object of increased interest in the astronomical community, having been observed ex-tensively from the ground with optical and radio telescopes and from space with IUE.

Evidence for mass expulsion from symbiotic systems suggests that this class of tidally interacting binary may be in a rapid evolutionary phase, where mass lost by the cool giant to the hot secondary determines the evolutionary endpoint of the system. The details of symbiotic systems are not understood but potentially could be very important. This follows because nearly 40 percent of the stars in the galaxy are binaries; the symbiotic phase may reflect a crucial evolutionary phase of gravitationally bound stars, in which the physical properties of the stellar component stars change very rapidly on timescales which are short compared to the lifetime of the Sun. Work with ground-based radio and optical telescopes and with space observatories is continuing in order to better understand the temporal nature of these unique astronomical objects.

Contact: A. G. Michalitsianos
         Code 680

Sponsor: Office of Space Science and Applications
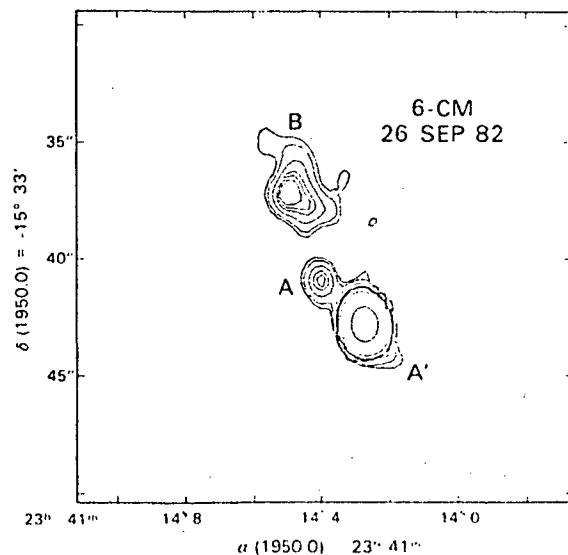
Images of the galactic center region taken with the Goddard 16 x 16 array camera at the IRTF in August 1983.

WOLF-RAYET STARS: A POSSIBLE SOLUTION TO A 117-YEAR OLD PROBLEM

In 1867 the French astronomers Wolf and Rayet discovered a rare type of star which had an extraordinary spectrum for a star. The spectrum consisted of broad, strong emission lines

crossing a faint continuum. For over 100 years the character of these stars remained a mystery. In the last 15 years observations made from the ground and from space have shown that Wolf-Rayet stars are hot stars having masses about 15 times the mass of the Sun. In addition, Wolf-Rayet stars have readily detected winds. The question has been, and is still, why are the spectra of Wolf-Rayet stars so different from those of the normal stars of the same mass and luminosity with which Wolf-Rayet stars are associated.

In the last 5 years some astronomers have put the pieces of the puzzle together to suggest that Wolf-Rayet stars are the remnants of very massive stars which have lost more than half their mass because their winds have blown the outer layers of the star away. This explanation is unsatisfactory because no mechanism based on physics is suggested for starting the massive wind which is required and for keeping the wind blowing strongly for one million years.

Studies by astronomers and physicists at the Goddard Space Flight Center suggest another explanation for what is seen.

Work is progressing to confirm key factors in the explanation. The new hypothesis is that Wolf-Rayet stars differ from the normal stars of the same mass and luminosity with which they are associated by having greater than normal, but still small, surface magnetic fields. Observations of the Sun and theoretical studies have shown that interactions between the magnetic fields in the atmosphere and the motions on the surface of the Sun can generate spectra like that seen for Wolf-Rayet stars, and these interactions can generate winds. Evidence is accumulating that the same sort of thing occurs for hot stars. Soon the 117-year old puzzle of the Wolf-Rayet stars may yield to improved knowledge of atomic physics coupled with key observations made with the IUE satellite, and complex computations done with the NASA computers.

Contact: Dr. Anne B. Underhill
Code 680

Sponsor: Office of Space Science and Applications

ATMOSPHERES

VENUS: CLIMATOLOGY OF CLOUDS AND WINDS

As the Pioneer Venus Orbiter completes its sixth year in orbit about Venus, images and polarimetry data returned by our cloud photopolarimeter experiment permit an increasingly valuable characterization of both the cloud climatology and the long-term behavior of the general circulation patterns at Venus cloudtop altitudes.

We can infer information on the aerosol particle properties and on the vertical cloud structure by analyzing the intensity and polarization of scattered sunlight at several wavelengths. Polarimetry data at the beginning of the mission revealed an abnormally large amount of submicron-sized haze mixed with and extending above the main Venus cloud, which is composed of concentrated sulfuric acid droplets 1 μm in radius. The refractive index we deduce for the haze is consistent with that for sulfuric acid as well, although such an identification remains tentative. While the haze is evident at all latitudes, it is most prominent in both polar regions, where it has frequently been so thick that the base cloud is barely discernible and the polar regions are abnormally brightened.

Monitoring of the quantitative amount of haze over the polar regions reveals significant variations in thickness on both short and long time scales. As the accompanying figure illustrates, increases or decreases in the optical thickness can

exceed an order of magnitude over a period of several weeks. There also is a long-term decrease in thickness from orbit insertion to about orbit 1000, but the magnitude of the short-term variations somewhat masks this trend. Observations by the University of Colorado ultraviolet spectrometer experiment, also on board the Pioneer Venus Orbiter, indicate that temporal variations seen in the sulfur dioxide mixing ratio at cloudtops may be correlated with variations in haze amount, lending support to the identification of the haze particles as sulfuric acid. These temporal variations in the amount of haze can play a significant role in determining the nature of the solar energy deposition in the atmosphere of Venus.

We can deduce wind vectors for many locations on Venus by comparing the locations of small-scale cloud features in image pairs made by the cloud photopolarimeter at near-ultraviolet wave-lengths, where there is good feature contrast. These cloud-tracked wind determinations indicate significant long-term variability in the dynamical state of the atmosphere. We find that the so-called "4-day rotation" of the Venus cloud features is highly variable and generally closer to being a 5-day rotation. Specifically, over 5 years of observations the equatorial rotation period has increased from 4.7 to 5.2 days (equivalent to about a 10 m/s decrease in wind speed). The trend appears to have leveled off or reversed in 1983. Zonal winds are fastest at the equator, with jets appearing and disappearing at all latitudes. At times, the

latitudinal profile approximates solid body rotation with lit-
tle change over several months (such as the spring of 1980).
In at least one instance, though, the profile has changed
markedly on a time scale of weeks (spring of 1982). Zonal
winds appear to be about 10 m/s faster in the afternoon than
in the morning.

The observed decrease in winds may be caused by transport
of momentum in the atmosphere by propagating waves.
Fourier analysis of UV brightness patterns in cloud
photopolarimeter images implies the presence of two
planetary-scale waves with periods near 4 and 5 days,
associated with the well-known dark 'Y'' feature and bright
polar bands, respectively. The 4-day oscillation was present
early in the mission but disappeared in 1982, when the winds
were at a minimum in strength, before reappearing in 1983.
The 5-day wave has been observed unambiguously only dur-
ing the first 8 months of the mission, although there is ten-
tative evidence of its return in 1983 da.... Comparison of
simultaneous zonal wind and UV brightness fluctuations sug-
gests that zonal winds are strongest near the vertex of the
"Y" and that dark regions in the UV images are colder than
bright regions by 5° to 10°K.

Contact: Dr. Larry Travis
         Code 640

Sponsor: Office of Space Science and Applications
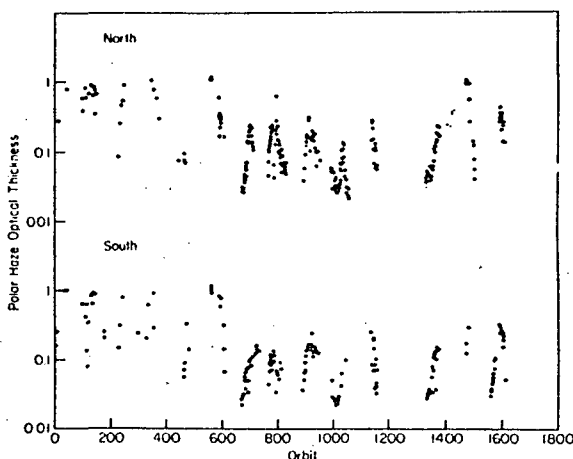
*Variation of optical thickness (wavelength 935 nm) of the
submicron-sized haze laying above the main Venus cloud
for the North and South polar regions. The orbital period
of the Pioneer Venus Orbiter is approximately 24 hours.*

INTERANNUAL VARIATIONS OF NEUTRAL
HYDROGEN IN THE VENUS THERMOSPHERE

A series of studies of the aeronomy of the atmosphere of
Venus have been stimulated from the in-situ observations of
instruments on the Pioneer Venus Orbiter. After encounter
in December 1978, the Orbiter has made daily passes through
the lower atmosphere orbits about the planet. For the first
600 days, on-board propulsion was used to maintain the
satellite periapsis height at relatively low altitudes, between
about 141 and 180 kilometers. In this interval, which ex-
tended from December 1978 to mid-1980, the Orbiter made
three excursions through the midnight-dawn local time region
of the planet. In this local time sector, the light ions and
neutrals are observed to pile up the nightside, forming a
midnight-dawn bulge. This asymmetry is believed to result
from the combined effects of atmospheric corotation plus
superrotation.

Within the nightside bulge, the concentrations of neutral
hydrogen and helium have been studied in earlier work to
identify the characteristics of the diurnal distributions dur-
ing the first Venus year. During the past year, the initial in-
vestigation has been extended to determine the presence of
possible interannual variations in the hydrogen bulge distribu-
tions. Concentrations of H, derived from in-situ ion and
neutral mass spectrometer measurements of $O+$, $H+$,
O, and CO_2, show the diurnal bulge persists for the first
three Venus years.

Peak levels of n(H) near 2 to 5 x 10^7/cm^3 are identified, with
a night to day concentration ratio of about 200/1. The
presence of short-term fluctuations of as much as a factor
of three from day to day reflects the variability in the ion
and neutral concentrations often detected on the nightside.
Allowing for this superimposed variability, little difference
in the magnitude of n(H) between 1979 and 1980 is indicated,
which appears to be consistent with the fact that the solar
euv flux level changed very little between successive tran-
sits of the bulge. On the other hand, there is some sugges-
tion in the modulation observed in n(H) that short term varia-
tion in the euv flux due to solar rotation may influence the
bulge characteristics. Although the ion and neutral variability
complicates the identification of chemical equilibrium, rather
similar behavior in the distributions of n(He), which is
measured directly, lends confidence to the n(H) results.
Overall, the attempt to understand the hydrogen and helium
variability provides a stimulus for more detailed analysis of
the nightside aeronomy and its relationship to both solar and
solar wind inputs.

Contact: H. A. Taylor, Jr.
         Code 610

Sponsor: Office of Space Science and Applications

CLOUDS AND CLIMATE: INITIATION OF THE INTERNATIONAL SATELLITE CLOUD CLIMATOLOGY PROJECT

Cloud-radiative feedback on the climate has been identified as a major focus of study in both the National and World Climate Programs. Our research on this subject is comprised of three elements: cloud and convection parameterization studies in climate models, development of satellite remote sensing techniques to deduce cloud radiative properties, and participation in the International Satellite Cloud Climatology Project (ISCCP) as the Global Processing Center.

The heart of this research is development of a set of consistent radiative models to calculate the effects of clouds on atmospheric radiative forcing and on satellite-measured radiances. We have used a detailed 1-D radiative-convective model to examine climate sensitivity to various postulated cloud feedbacks and to diagnose the behavior of our full global 3-D climate model (GCM) with predicted clouds. The same radiative model used in the GCM has also been adapted to analyze satellite-measured radiances; in particular, models of spectral radiances measured by all AVHRR channels have been completed. Use of the same radiative model in data analysis results in derived cloud parameters consistent with those in the GCM.

The figure shows July results from a preliminary 4-month climatology obtained for 1977 from NOAA 5 scanning radiometer data as a pilot project for the ISCCP. The three panels show cloud cover fraction, cloud optical thickness and cloud top temperature—a complete set of radiation parameters. The process of examining these results and comparing them with other cloud information has led to improvements in the analysis used for ISCCP.

The ISCCP will be based on a more comprehensive satellite data set; collection was initiated on July 1, 1983 from five satellites providing 3-hr, 30-km coverage of the whole globe (except for the Indian sector). The Goddard Institute for Space Studies as the Global Processing Center for ISCCP, produces the two primary data products: a normalized global radiance data set with associated conventional weather report data and a climatology of global cloud radiative properties. Intercomparison of six alternative cloud analysis methods, including derivations of preliminary cloud climatologies, has been performed and development of the ISCCP algorithm is nearly complete. This cloud analysis is the most systematic analysis of global satellite imagery attempted to date.

Contact: Dr. William B. Rossow
Code 640

Sponsor: Office of Space Science and Applications
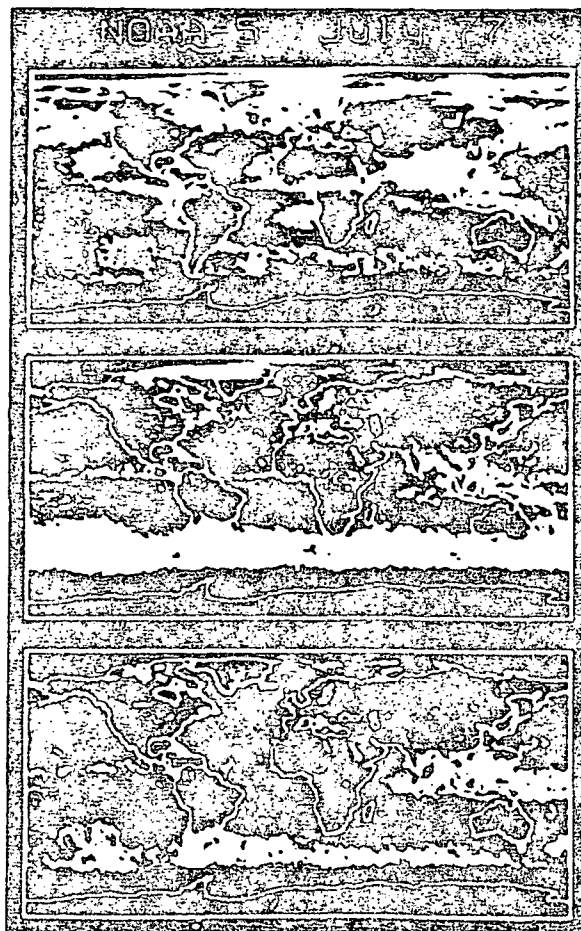
Monthly mean cloud cover fraction (a), cloud optical thickness (b), and cloud top temperature (c) for July 1977 obtained from NOAA-5 scanning radiometer measurements once per day.

TROPOSPHERE/STRATOSPHERE CLIMATE MODELING

Climate changes induced by increasing concentrations of greenhouse gases will likely affect the dynamics and stability of the atmosphere, which in turn affect the transfer of trace gases between the troposphere and stratosphere, and the wind and temperature distribution in the stratosphere itself. Such changes must be factored into any assessment of the impact of freons or other anthropogenic releases on stratospheric ozone; and, since the distribution of ozone will itself influence the surface temperature, they should be included in projections of climate change.

We have developed a 21-layer troposphere-stratosphere model to investigate the interaction between climate perturbations and the stratosphere. The model contains all the physics included in our standard 9-layer climate model, but

with its well resolved stratosphere it is more appropriate for investigating the potential stratospheric alternations associated with climate change.

The model has been run for 15 months and its output compared with climatology. The model successfully reproduces many of the observed stratospheric features, including the winter stratospheric jet, summer stratospheric easterlies and long wave forcing. The accompanying figure shows the model-generated temperature field in the mid-troposphere and in the upper stratosphere during January. As is evident from the figure, the mid-troposphere distribution results from a mixture of waves with different longitudinal wave numbers, while in the upper stratosphere the winter hemisphere is dominated by wave number 1. This feature also occurs in observations, resulting from progressive reflection of waves with higher wave numbers by the strong west winds in the winter stratosphere.

Principal model deficiencies appear to arise from the need for improvement in its treatment of radiation above 45 km and in its condensation of water vapor in the lower stratosphere.

As noted above, the long wave dominance of the winter stratosphere arises from the propagation of long waves from the troposphere. As climate changes, this long wave forcing of the stratosphere is also likely to change. The expected tropospheric warming will probably alter the latitudinal temperature gradient in the troposphere, with greater warming at high latitudes, and this will affect tropospheric energetics. In the doubled CO_2 experiment performed with our standard 9-level model, wave number 1 at mid-latitudes was reduced by 20 percent in winter and spring, compared with the control run for the current climate. One planned utilization of the 21-layer troposphere-stratosphere climate model is to investigate how the stratosphere changes in the doubled CO_2 climate.

Contact: Dr. David Rind
Code 640

Sponsor: Office of Space Science and Applications

CLIMATE SENSITIVITY: MODELS AND EMPIRICAL DATA

The fundamental issue in long range climate, time scales of 10 to 100 years or longer, is the sensitivity of climate to a change in 'boundary conditions'. For example, how much will increasing atmospheric CO_2 alter the Earth's surface temperature? If the 'greenhouse' warming of CO_2 is only 1 °C, the effects may not be much greater than those due to natural climate variability. On the other hand, a warming
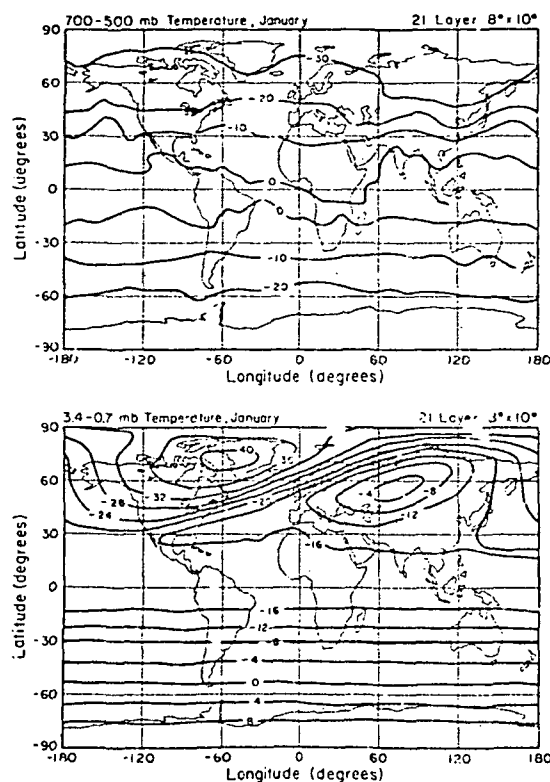
Figure 1. Twenty-one model-generated temperature field for the midtroposphere (top) and upper stratosphere (bottom) for January (14th month of the integration).

of 3 °C or more would transform our climate to a condition far outside that previously experienced by mankind.

The objective of our long-range climate studies is to obtain improved understanding of climate sensitivity, and thus to help chart the course of the Earth's climate during the next several decades. These studies of climate sensitivity are pursued both with global climate models and on the basis of empirical evidence from past climate changes.

The geographical distribution of surface air warming computed in our global climate model with doubled atmospheric CO_2 is shown in the figure. The high latitude enhancement of the warming is due to the positive ice/snow albedo feedback and the stability of the atmosphere at high latitudes, which tends to concentrate the warming near the ground.

The physical processes contributing to the 4 °C global mean warming in the model can be analyzed by inserting the changes in the 3-D model one-by-one into a diagnostic energy balance climate model. The net effect of the changes in atmospheric water vapor is a large positive feedback (Figure

1, lower part); the water vapor changes correspond to a feedback factor $f_w \sim 1.6$. Decreases in ground albedo as a result of reduced ice and snow cover yield a feedback factor $f_i \sim 1.1$, while changes in the clouds yield $f_c \sim 1.3$.

These analyses help identify physical processes which contribute most to uncertainty about true climate sensitivity. For example, clouds are a major reason for the uncertainty in climate sensitivity, because present information on clouds is inadequate to permit evaluation of cloud prediction schemes. It is expected that the International Satellite Cloud Climatology Project, discussed below, will improve understanding of the influence of clouds on climate sensitivity.

The pure model results for climate sensitivity can be tested quantitatively on the basis of empirical data from climate changes in the past. A valuable test is provided by the data from the CLIMAP project, which reconstructed the climatic boundary conditions, such as ice coverage and ocean surface temperature, for the Wisconsin ice age (18,000 years ago). Although the basic mechanisms for glacial to interglacial climate changes are probably subtle, it is not necessary to unravel the sequence of cause and effect of the ice ages to obtain an estimate of climate sensitivity from the known boundary conditions. In particular, the feedback factor for fast processes, such as changes of atmospheric water vapor, clouds and sea ice, can be estimated by comparing the total cooling 18,000 years ago to the direct (no feedback) temperature change that would be caused by slowly changing boundary conditions (land ice cover, vegetation cover, atmospheric CO_2).

Because of uncertainties in each of these boundary conditions, we obtain a range of values for the climate sensitivity to doubled $CO_2$2.

$$\Delta T_{eq}(2^*CO_2) = 2.5\text{-}5°C, \qquad (1)$$

in good agreement with the 3-D model estimate of $4°C$. This paleoclimate approach can be expected to yield improved evaluation of climate sensitivity. As knowledge of paleoclimate boundary conditions improves, the climate models become increasingly realistic.

Another empirical test of climate sensitivity is provided by the temperature change in the past century, since CO_2 increased substantially during that time. This test differs from that above, because it does not involve a comparison of equilibrium climate states. Thus the response time of the climate system, due principally to the ocean's large heat capacity, must be taken into account. If we do this by using a simple model, which assumes that uptake of heat by the

ocean is similar to that of passive transient tracers, the observed global warming of $0.5°C$ in the past century implies an estimate of climate sensitivity similar to that of equation (1).

The climate sensitivity inferred from recent climate trends is limited in precision by uncertainties in past atmospheric composition, the true global temperature change and its cause, and the rate at which the ocean takes up heat. However, as knowledge of these factors improves, this technique for investigating climate sensitivity will become more powerful.

Contact: Dr. James E. Hansen
          Code 640

Sponsor: Office of Space Science and Applications
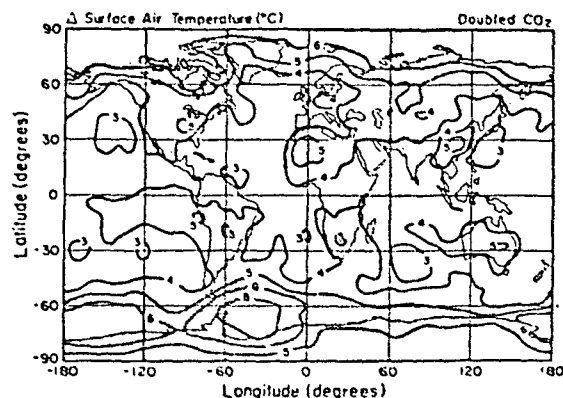
Global warming in three-dimensional model for doubled CO_2.
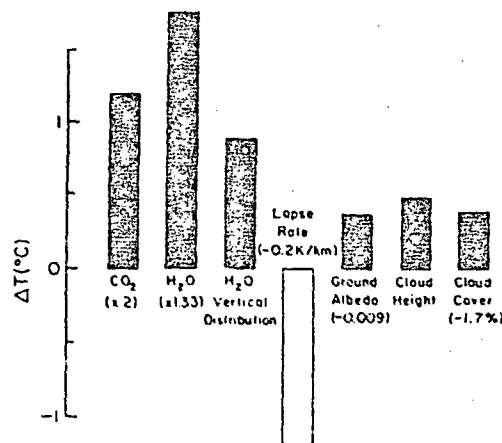
Contributions to global warming in model.

USE OF SATELLITE DATA IN NUMERICAL WEATHER PREDICTION

Real data impact studies conducted at Goddard have shown that the use of the First GARP Global Experiment Satellite Observing System (including operational TIROS-N temperature soundings, cloud tracked winds and drifting buoys) have a small positive impact in the forecast skill in the Northern Hemisphere. In the Southern Hemisphere the impact is much larger, adding about 2 days of forecast skill to that obtained from the conventional observing system. Temperature soundings are most important in the extratropics and cloud tracked winds in the tropics. Drifting buoys contribute to the accuracy of the sea level pressure forecast in the Southern Hemisphere especially during the first day.

A series of simulation experiments is being conducted as a cooperative effort between the European Centre for Medium Range Weather Forecasts, the National Meteorological Center and the Goddard Laboratory for Atmospheric Sciences, to provide a quantitative assessment of the potential impact of proposed observing systems on large scale numerical weather prediction. For these studies, an advanced analysis/forecast simulation system has been developed which provides for a more realistic assessment of the potential impact of proposed observing systems than was possible in earlier studies. This system has been calibrated using a real data impact experiment and has been used to assess the relative impact of TIROS-N temperature soundings and LIDAR wind profile data. Results from these experiments indicate that 3-dimensional wind profile data are more effective than temperature data in controlling analysis errors. If the proposed accuracies and coverage for LIDAR wind profiles can be achieved, the experiments show that a very significant improvement in Southern Hemisphere forecast skill will result. In the Northern Hemisphere, the impact is smaller but still significant. A case study showed a major improvement in the prediction of a storm over the United States which was poorly forecasted with the simulated current system. The use of either accurate temperature soundings representing an advanced passive sounder, or wind profile data resulted in the improved cyclone forecast.

Contact: Drs. Robert Atlas and Eugenia Kalnay
Code 610

Sponsor: Office of Space Science and Applications

NATURE

CONTROL

CONTROL + TIROS

CONTROL + PERFECT T

CONTROL + WINDS
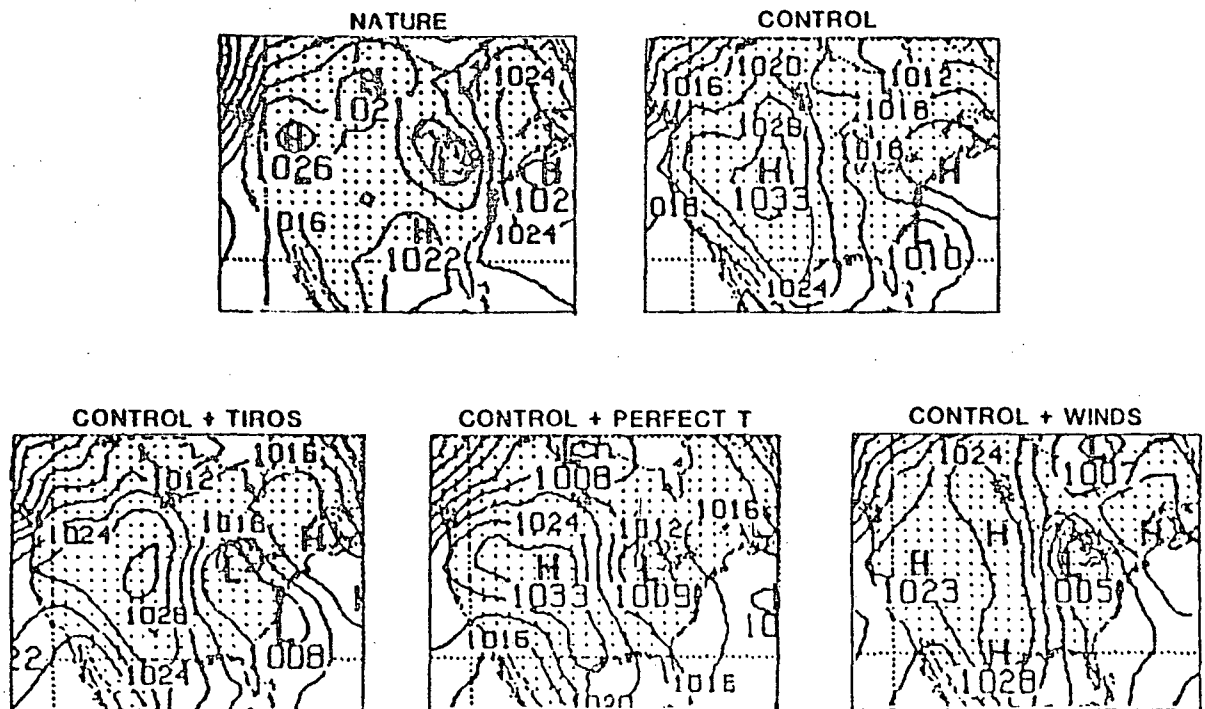
Simulated nature (verification) and 5-day simulated forecasts illustrating the effect of currently available temperature sounding data, perfect temperature soundings, and wind profile observations on the prediction of a low-pressure system near the Great Lakes.

SOUTHERN HEMISPHERE
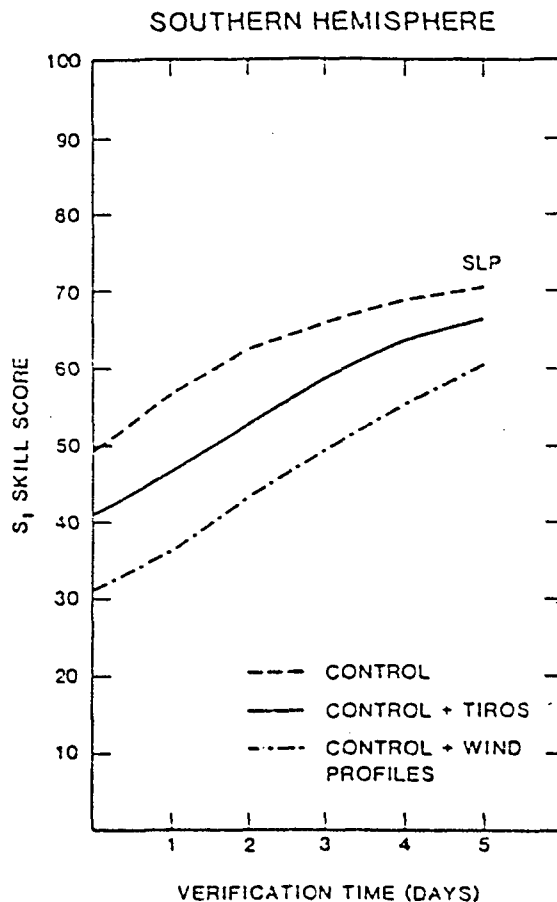
Impact of simulated TIROS-N temperature soundings and simulated wind profile data on numerical sea level pressure forecasts for the Southern Hemisphere. (Low values of S_1 skill score indicated high forecast accuracy).

REMOTE SENSING OF WEATHER AND CLIMATE PARAMETERS FROM TIROS-N SATELLITES

HIRS2 and MSU are the 20-channel infrared and 4-channel microwave passive sounders on the operational low-Earth orbiting satellites. They monitor emission arising primarily from the Earth's surface and the atmosphere up to the mid-stratosphere. These, together with the SSU, a three-channel pressure modulated infrared radiometer, which monitors emission from the mid and upper stratosphere, comprise the TIROS Operational Vertical Sounder (TOVS) system. The TOVS data are analyzed operationally by NOAA NESDIS to produce vertical temperature-humidity profiles using a method based primarily on statistical regression relationships between observed radiances and atmospheric parameters.

The approach used by GSFC is fundamentally different from the current operational approach. Rather than rely on empirical relationships between observations and meteorological conditions, we attempt to find surface and atmospheric parameters which, when substituted in the radiative transfer equations describing the dependence of the observations on the meteorological conditions, match the observations to a specified amount. We believe a physically based retrieval scheme has an important advantage over a statistically based scheme. This is the ability to include the effect of secondary but important factors such as surface temperature, surface emissivity, surface elevation, reflected solar radiation, satellite zenith angle, and most significant of all, clouds, on the observations. All of these parameters, together with the atmospheric temperature profiles, are either solved for, or directly accounted for, in this iterative scheme. As a result, the analysis of radiance data produces not only global fields of atmospheric temperature profiles necessary for initialization of numerical weather prediction models, but also provides several other weather and climate parameters. These parameters include sea and land surface temperature and their day-night differences which, over land, are related to soil moisture; fractional cloud cover, cloud top temperature, and pressure, and their day-night differences; and ice and snow cover which are derived from the retrieved emissivity of the surface at 50.3 GHz and the ground temperature.

Global retrievals (50,000 retrievals per day) have been run at 125 km resolution for January and July 1979 and March and July 1982. Research with the fields has shown the following:

1) Forecast assimilation cycles for January 1979, substituting our HIRS2/MSU temperature profiles for operational retrievals, resulted in significant improvement in satellite forecast impact over North America and Europe.

2) Monthly mean sea surface temperature fields derived by us from HIRS2/MSU data were compared with those derived from ships, AVHRR, and SMMR in a NASA sea surface temperature intercomparison workshop. The results showed HIRS/MSU to be the most accurate, both in RMS error and anomaly patterns.

3) Monthly mean day-night ground temperature difference fields were computed from the HIRS2/MSU retrievals for a number of months, from which monthly mean soil moisture and evapotranspiration fields were derived. These fields were consistent both with climatological values of soil moisture and with the cloud fields derived from HIRS2/MSU data.

4) Global monthly mean fields of cloud fraction (high/middle/low) and their day-night differences were generated from HIRS2/MSU data. The results were consistent with

climatology as well as model-generated rainfall. Cloudiness in highly convective regions was found to be more prevalent at night over land and during the day over ocean. Low clouds showed the reverse behavior in both cases.

5) Monthly mean ice and snow fields were derived from HIRS2/MSU data for a number of months. Weekly fields showed reasonable consistency and variations.

Contact: Dr. Joel Susskind
          Code 610

Sponsor: Office of Space Science and Applications

THE INFLUENCE OF LAND-SURFACE CONDITIONS ON DESERTIFICATION

It is generally well known that land surface roughness, on scales that interact with a turbulent eddy (~2 km or less), greatly affects the turbulent exchange of heat moisture and momentum between the Earth and the Planetary Boundary Layer (PBL). In nature, such surface roughness is produced by vegetation and small-scale orography. Of these two, the tall vegetation, i.e., forests, is perhaps a major contributor.

Recently, we have conducted several simulations with the Goddard General Circulation Model to determine how low surface roughness of deserts affects the circulation and rainfall. Specifically, in our July simulations, it was found that a low surface roughness of deserts led to a reduction of the cross-isobaric component of circulation (Fig. 1). This reduction on the cross-isobaric component of circulation reduced rainfall in the Sahara Desert. In particular, the ITCZ over the Sahara Desert was pushed southward in better agreement with observations (Fig. 2). Another influence of low surface roughness was due to its effect on the surface energy balance; inefficient turbulent transport of heat and moisture produced warmer ground (20 °C) during the middle of the day for the smoother Sahara Desert. This warming increased the longwave cooling of the ground while correspondingly reducing the surface sensible heat flux.

In order to clearly understand the role of surface roughness in bringing about changes in the rainfall, further simulation studies were carried out in which the surface roughness over all land was reduced to that of a smooth desert. These simulations clearly identified the underlying mechanisms. The changes in the rainfall for the smoother land were again largely produced by (1) a reduction in the cross-isobaric component of flow in the subtropics and extratropics and (2) a corresponding increase in the PBL wind speed in the regions near the equator where the Coriolis force is vanishingly small. These changes significantly altered the rainfall magnitude and distribution.

In our previous studies we found a strong influence of surface albedo and soil moisture in the tropical desert border regions. We hypothesized a significant role of vegetation over the Indian subcontinent on the Indian monsoon. Deforestation, which produces higher surface albedo and low surface roughness, was expected to weaken the monsoon whereas the lack of evapotranspiration was expected to have a negative feedback effect on the Northern Indian monsoon. Our studies indeed bore out the soundness of this hypothesis. Figure 3a shows the changes in the July monsoon rainfall as a result of increasing the albedo from 0.14 to 0.20 over the Indian continent; Figure 3b shows the corresponding change in rainfall due to the combined effect of higher albedo and low surface roughness; and Figure 3c shows the changes in rainfall due to the combined effect of high surface albedo, low surface roughness and no evapotranspiration. Obviously, highest reduction in the monsoon rainfall over India was produced by higher albedo and low surface roughness.

We have clearly established that vegetation on the Earth increases the land surface radiation balance which increases fluxes of sensible heat and moisture into the PBL. The vegetation enhances evaporation through its effect on evapotranspiration and modification of ground hydrology. It also provides surface roughness that causes moisture convergence through the surface drag force. All of these yield positive feedback effects on the rainfall. In an otherwise uniform atmosphere, roughness of tall vegetation induces turbulence that causes the PBL to deepen; the cumulus clouds are more likely to emerge from the region of a deep PBL. From these results we can infer that the vegetation on the surface of the Earth is an important sustainer and probably a very significant determinant of the climate on Earth.

Contact: Dr. Yogesh Sud
          Code 610
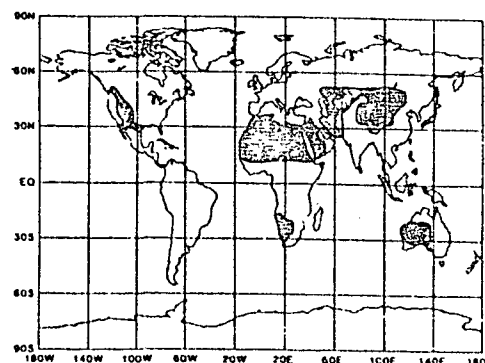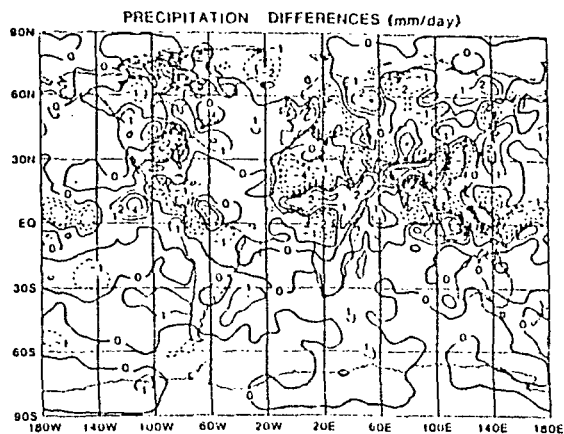
Sponsor: Office of Space Science and Applications

Figure 1.   Desert regions which were prescribed with low surface roughness in the experiment.

PRECIPITATION DIFFERENCES (mm/day)

Change in precipitation (experiment—control) as a result of low surface roughness. Solid lines represent increase and dashed lines represent reduction.

SIMULATION OF GLOBAL CLOUDINESS

Rapid progress continues in attempts to simulate the observed pattern of global cloudiness, using an advanced atmospheric general circulation model. Cloudiness simulations are necessary for successful climate forecasting, because the clouds reflect solar radiation that would otherwise warm the Earth, and at the same time they act as a blanket that traps outgoing infrared radiation emitted by the Earth. The balance of the outgoing and incoming radiation streams determines the mean global temperature. During the past year, a 3-year simulation and many shorter runs have produced a wealth of simulated cloudiness statistics. The results are being analyzed by comparison with cloudiness retrievals based on HIRS/MSU data, and with NIMBUS 7 Earth radiation budget observations. Successful aspects of the simulation include realistic simulation of low-level cloudiness over the subtropical oceans in summer and off the east coast of the U.S. in winter, greater cloudiness on the night side of the Earth in both the observations and the simulations, and a generally realistic model depiction of the seasonal changes of cloudiness and radiation.

A significant problem is that the model tends to underpredict tropical cirrus clouds. Stimulated by these and other findings, several improvements have been developed for the model, and are currently being tested.

Contact: Dr. David Randall
             Code 610

Sponsor: Office of Space Science and Applications
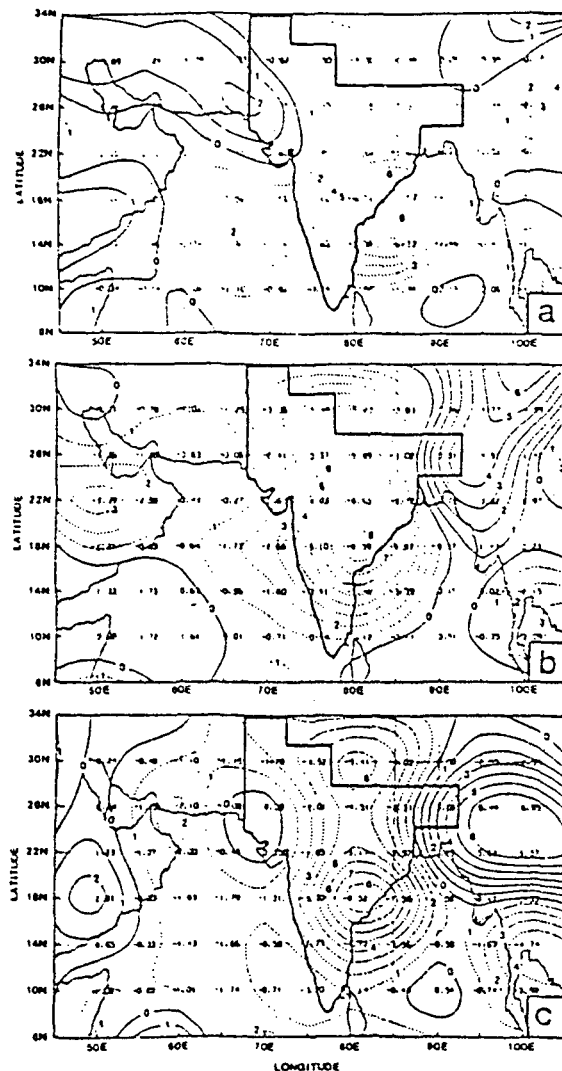
Influence of land surface parameters on the July rainfall: (a) surface albedo increase, (b) surface albedo increase and surface roughness decrease, and (c) surface albedo increase, surface roughness decrease with no evapotranspiration. (Dashed lines represent a decrease.)

SEVERE STORM RESEARCH

Storm Scale Research

Satellite observations combined with numerical cloud simulations have shown that troposphere/stratosphere interaction

is vital to understand the cold-warm couplet seen on infrared satellite imagery over regions of intense thunderstorms (see Fig. 1 on attached sheet).

Cold upwelling features in aircraft microwave image data at 90 GHz and 180 GHz have been related to radar reflectivity maxima for strong thunderstorm cells, indicating a layer of large ice particles in the clouds. This inference is supported by numerical cloud modeling.

An infrared-based rainfall estimation scheme has been developed that detects rain centers in systems of cumulus clouds.

The potential and limitations of satellite and IR-based soil moisture estimates have been further established and preliminary determinations as to the importance of soil moisture in initiation of intense convection has been made.

It has been determined from conventional composites that VAS-based parameters are keys to tropical cyclone dynamics and these parameters have been derived for specific case studies.

Three-dimensional cloud model simulations for a tropical, waterspout-producing cumulus indicate that superimposed vortex pairs reaching below cloud base down to the ocean surface were produced by cumulus drafts tilting the vortex tubes in an environment with the observed wind profile. Waterspout occurrence has been related to interaction of cold outflows from cumulus clouds, suggesting their similarity to many tornadic situations in the subtropics.

A multi-cumulus model on the NASA CYBER 205 documents for the first time how the dynamics of cloud merging occur and the role played therein by gust front outflows. Merged systems are virtually always involved in the production of heavy rain and severe weather.

Mesoscale Analysis and Modeling

Numerous numerical simulations of various severe weather events have accurate processes which lead to severe storms. The cases include the April 10, 1979, disastrous Wichita Falls tornado case, the Grand Island tornado outbreak on June 3-4, 1980, and the notorious Presidents' Day snowstorm on February 18-19, 1979.

The VAS (Visible Infrared Spin Scan Radiometer (VISSR) Atmospheric Sounder) Assessment has been completed, which shows the utility of VAS moisture imagery and sounding profiles for the mesoscale analysis of a prestorm environment, especially in depicting the moisture structure prior to the outbreak of severe weather, which conventional networks are too sparse to specify.

The sensitivity of the mesoscale forecasts to adiabatic processes (heat input from boundaries and clouds) and initial divergence in the air flow has been assessed. Cases have been isolated in which incorporation of these processes into the initial state of the atmospheric system has significantly improved the 0-12 hour weather forecast. Numerical experiments have also been completed which suggest that the insertion of VAS data will have greater impact if done on a "time-continuous" basis, rather than in a static mode (several insertions vs. one insertion).

An independent evaluation of near-time numerical forecasts using the Mesoscale Atmospheric Simulation System (MASS) model has been completed with results indicating that mesoscale numerical predictor models have great potential in the forecasting of severe storms.

The analysis of the Presidents' Day snowstorm indicates the importance of upper- and lower-level jet streaks in the prestorm environment. The results also point to the mesoscale nature of the factors causing storm deepening and to the role of a stratospheric-tropo-spheric exchange in the rapid development of the cyclone.

Contact: J. Simpson
          Code 610

Sponsor: Office of Space Science and Applications

STUDIES WITH A GLOBAL ENERGY BALANCE CLIMATE MODEL

A climate model resolving the seasonal cycle and the two horizontal dimensions has been developed at GSFC over the last few years and applied to several problems of current interest. Models of this type are useful when for various reasons a general circulation model experiment is not warranted or not feasible. For example, in cases where the signal to natural variability is small it may be advantageous to first consider such a statistical dynamical model because extremely long runs may be necessary in the application. In this case the simpler statistical dynamical model serves as a pilot study device.

The model developed at GSFC is a thermo-dynamic model whose solution yields the equilibrium seasonal cycle for the surface temperature field over the globe. The model is essentially a statement of the conservation of heat energy for individual columns of the Earth atmosphere system. Various terms such as the infrared radiation flux to space are parameterized with Earth radiation budget data from satellites such as Nimbus-6. The primary agent modulating the seasonal
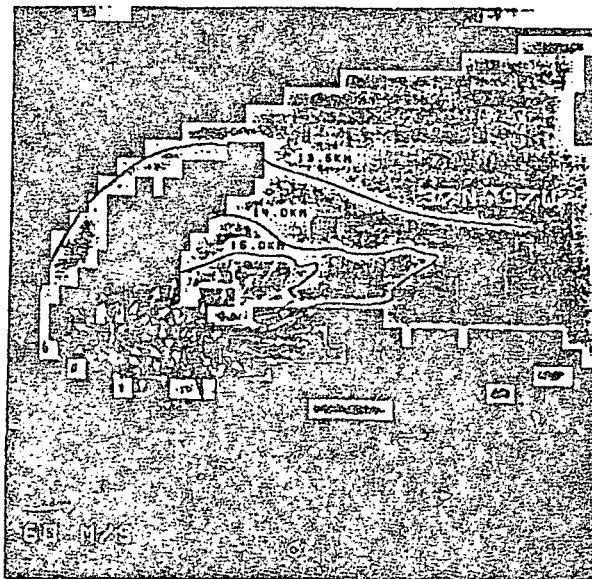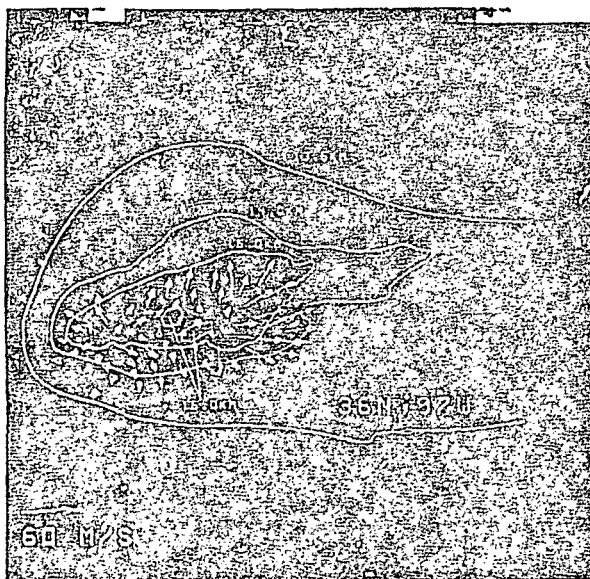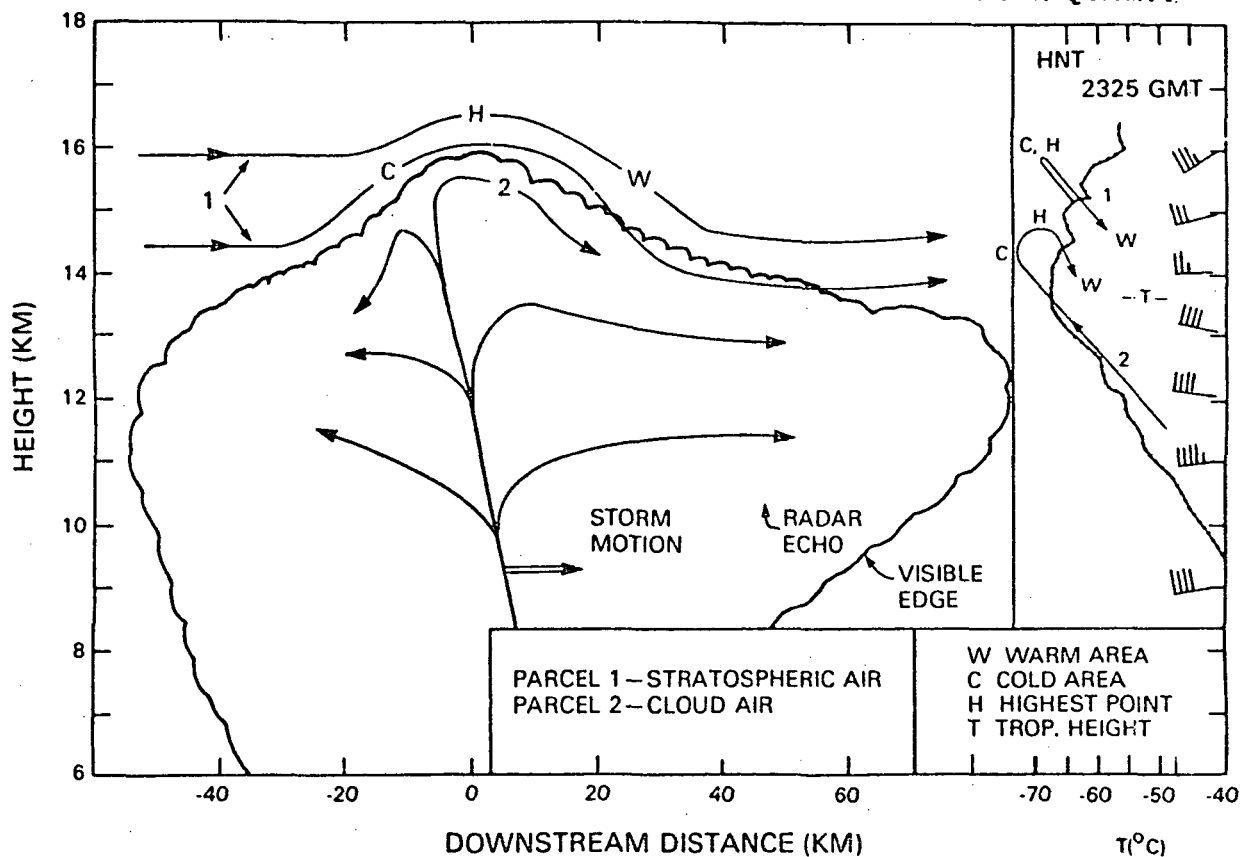
Cold/warm couplet on severe tornadic thunderstorm system over Oklahoma on May 2, 1979. Visible (left) and infrared (right) GOES images with stereo height contours (labeled in km) and storm-relative Doppler radar-determined winds (arrows) superimposed for the 11.9-km level, showing outflow.

cycle amplitude is the heat capacity per unit area which is a strong function of surface type—ocean surface can store 60 times more heat per unit time than land. By adjusting its few empirical parameters the model can be brought into remarkable agreement with the observed seasonal cycle.

The model is then very useful for looking at the dependence of the seasonal cycle of the temperature on such externally defined variables as the Earth's orbital elements (eccentricity, tilt, precession of equinoxes) or the configuration of land-sea geography which can be changed by continental drift. Geological observations imply that the first effect appears to be the cause of the major periodic glaciations which have occurred over the last few million years. Studies with the GSFC energy balance model support this hypothesis further by suggesting the growth of large continental ice sheets especially in North America when orbital elements favor cooler summers which was the case about 125,000 years ago when the last great glaciation began.

Similarly, the model can be used to investigate the seasonal cycle tens of millions of years ago. This study suggests that the configuration of land-sea distribution was such as to not favor ice sheets until about 30 or 40 million years ago, at about which time Greenland and Antarctica became glaciated. Even later the conditions became favorable for the periodic glaciations induced by the tiny periodic orbital changes.

The model can also be used to understand the climatic response to time varying forcings, especially in the frequency range around one cycle per year. In particular one can study the geographical patterns of the responses to a time varying solar constant. For example, the figure shows the pattern of the response to a time varying solar constant whose frequency is ten cycles per year. This frequency was chosen because recent measurements of the solar constant indicate fluctuations in this range. The figure shows a strong preference for the amplitude to be large over land. Further studies have shown that as the frequency is lowered the patterns wash out so that at zero frequency the pattern is uniform. Studies of this type can also be used to estimate the geographical response patterns due to other transient forcing agents such as the carbon dioxide concentration in the atmosphere. These latter experiments suggest that very little difference will be expected in the response over land versus that over ocean surfaces for the kinds of time scales expected in carbon dioxide change scenarios. The aforementioned caveats naturally apply to these conclusions.

Contact: Gerald R. North
          Code 610

Sponsor: Office of Space Science and Applications
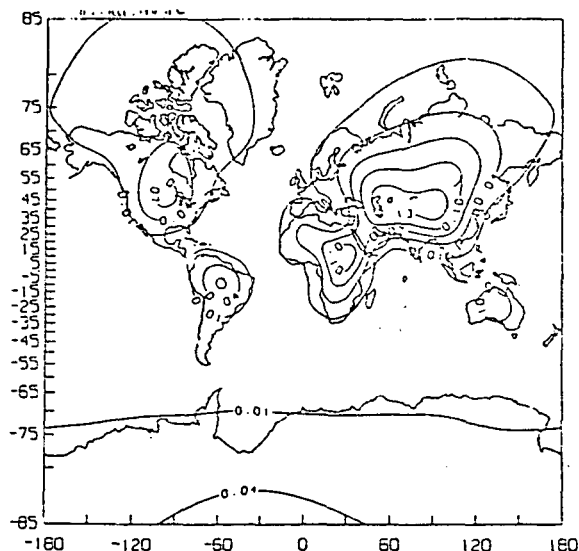
Model amplitude of the sinusoidal response in surface temperature to a similar change in solar constant whose amplitude is 0.8 percent. The frequency of the variation is ten per year. (From Weather and Climate Responses to Solar Variations, Colorado Associated Universities Press, Boulder, Colorado, 1985.)

TROPICAL DISTURBANCES AND MIDLATITUDE CLIMATE

The major climate anomalies associated with the 1982-83 El Nino/Southern Oscillation (ENSO) have created enormous worldwide weather-related socio-economic hardships and have brought into sharp focus the need for a better understanding of the short-term climate variability of the Earth-atmosphere-ocean system. Central to the scientific problems associated with ENSO is the possible connections between tropical convection and the extratropical circulation system. Satellite-derived information is extremely useful for estimating convection and precipitation because of its global coverage in an otherwise inadequate ground-based observation system, especially over the tropical oceans.

Data from the National Meteorological Center (NMC) provide adequate coverage in the extratropics for conventional meteorological parameters such as wind, temperature, and geopotential height, which are derived from ground-based and satellite observations. Thus, the tropical/mid-latitude connections are best studied by a combination of satellite-derived estimates of convection, rainfall, etc., in the tropics, and the standard NMC data.

This approach takes advantage of the rich sources of satellite data presently available at NASA/GSFC and NOAA. To aid in the interpretation of results from the observational studies, theoretical and modeling efforts are being carried out in parallel. For the past several years, we have followed the above strategy.

A key to the basic understanding of the mechanisms of climate fluctuation during ENSO appears to lie in the variability of the tropical heat source/sink distribution. Excitation of intrinsic modes driven by adiabatic heating is found occasionally to lead to ENSO-like large climate anomalies. One of the most important components of intraseasonal variation in tropical convection is found over the western part of the Pacific. During the northern winter, convection over the maritime continent of Borneo/Indonesia and the equatorial central Pacific is dominated by a 40- to 50-day oscillation, which possesses a dipole-like spatial patter linking the above regions. Eastward propagating signals, appearing as outbursts of convective cloud clusters originating from the Indian Ocean, appear periodically to feed energy into this dipole oscillation. Extratropical circulation climate anomalies are found to be strongly correlated with the tropical 40- to 50-day oscillation. An upstream wavetrain-like anomaly over Eurasia is found to precede convection over Indonesia.

The orientation and evolution of the anomaly suggest a predominantly midlatitude-to-tropics energy propagation. Subsequently, wavetrain signals are found downstream over the Pacific-North American region, where a poleward energy flux from the tropics is indicated. Such an observation has a profound implication for long-range weather prediction over the continental United States, as it suggests that short-term climate anomalies (or persistent weather, such as prolonged cold or heat spells) may have their origins far upstream, over East Asia and in the tropical western Pacific.

Satellite observations of non-conventional meteorological parameters have confirmed and added an extra dimension to the above picture. Using 9 years of satellite outgoing longwave flux to infer cloud fluctuations associated with the above phenomena, we find that the above teleconnections seem to be associated with two intrinsic modes of tropical-extratropical interactions: (1) a coupling between the tropical dipole convection anomaly with polar air outbreak over East Asia and (2) a blocking over the eastern North Pacific, respectively (see figure). During the phase of the 40- to 50-day oscillation, when Indonesian convection is strong, the tropical-extratropical interaction takes place via the Hadley circulation over Southeast Asia. During the opposite phase of the oscillation, an amplified Rossby wave occurs over the eastern North Pacific in a blocking-like formation, forced in part by strong convection over the equatorial central Pacific.

Because the intrinsic modes described above are in some aspects similar to the more long-lived and more intense climate anomalies observed during ENSO, we hypothesize that the above intraseasonal variability of the tropical ocean-atmosphere and the ENSO phenomenon are governed by the same underlying physics. In a recent theoretical study, we have shown that the 40- to 50-day oscillation may, under certain conditions, trigger an inherent instability in the tropical ocean-atmosphere system that is responsible for the onset of the ENSO. This interpretation brings to light a potential mechanism for the occurrence of the ENSO and poses a challenging problem in climate dynamic research.

Contact: William K. M. Lau
        Code 610

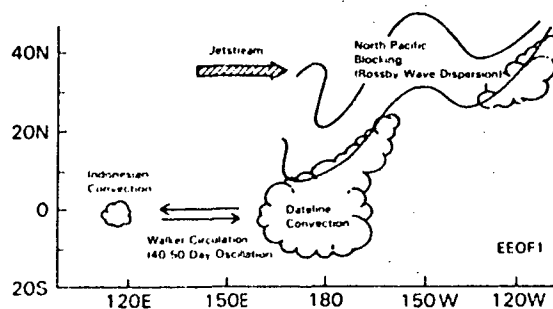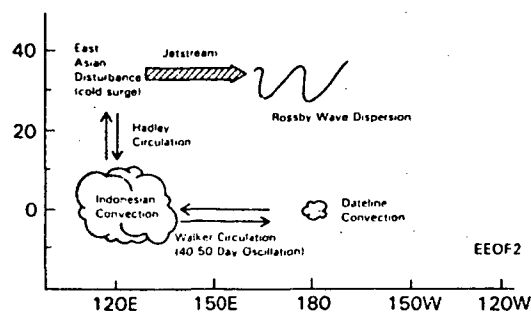Sponsor: Office of Space Science and Applications

Figure 1. Schematics of the two normal modes of midlatitude-tropical interaction associated with the 40-50 day oscillation in tropical convection over the Pacific.

IS EL CHICHON IMPACTING OUR CLIMATE?

Variations of the mean surface air temperature in the Northern Hemisphere over the past few hundred years have to some extent been correlated with the occurrence of major volcanic eruptions. The causal connection between volcanic eruptions and climate is provided by the radiative effects of aerosols that develop in the stratosphere in the aftermath of an eruption, a product of the released sulfur dioxide gas. Other factors affecting mean Northern Hemisphere temperatures include increasing levels of CO_2 and potential changes in the solar constant, but they are not as well correlated, probably because these changes are too small for the effects to be detected (CO_2) or we are lacking a historic record (solar constant). Internally caused variations, such as those associated with the El Nino/Southern Oscillation, can mask the expected effect. In any event, the eruptions of El Chichon in Mexico in March-April, 1982 provide a unique opportunity to observe the effects first hand and to try to understand the dynamics of climate change associated with such radiative perturbations.

The data gathered up to now—from satellite, aircraft, balloon, and ground observations—are unprecedented in their detail and scope. They provide a fairly complete picture of the chemical and microphysical properties of the stratospheric aerosol layer, its spatial distribution, and its evolution in time. At our present level of understanding, and at a time when climate models with detailed treatment of radiative transfer are readily available, nature has given us one of those rare chances to test our models in a real-world climate sensitivity experiment.

The stratospheric aerosol layer affects both the incoming solar radiation (by increasing the Earth's albedo, thus reducing the heating of the Earth by solar radiation) and the outgoing terrestrial infrared radiation (by increasing the infrared opacity of the atmosphere, thus reducing the cooling of the Earth by terrestrial emission to space). The two competing effects do not cancel each other; the solar radiation effect dominates, leading to a net cooling of the Earth-atmosphere system.

Radiative transfer methods developed over the last 5 or 6 years were utilized to develop and model the radiative properties of the stratospheric aerosol layer across the entire spectrum, exhibiting a variation in space and time within the bounds of the measurements. The stratospheric aerosol layer model was then imbedded into the Multi-Layer Energy Balance Model (MLEBM), a 2-dimensional model of the Northern Hemisphere climate, which is ideally suited to studying the effects of radiative perturbations on the Earth-atmosphere system. The results are shown in Figure 1. They reveal a decrease in the model mean Northern Hemisphere temperature which reaches a maximum of approximately 0.6°C, occurring between 1 and 2 years after the eruption. Analysis of surface air temperature measurements over the Northern Hemisphere by Angell and Korshaver (NOAA/ERL Air Resources Laboratory) do not as yet show that the real world is following the model. Their results (Figure 2) indicate that in the first year following the eruption the Northern Hemisphere temperature (especially in the temperature zone) was reaching record highs, having moved opposite to the expected direction. The problem, of course, was the occurrence of the strongest el Nino event ever recorded, which became clearly evident in the late spring of 1982, shortly after the El Chichon eruption. (As far as we know, the proximity in time of the two events is a coincidence.) The El Nino, which is characterized by massive, large changes in tropical Pacific sea surface temperatures and a sudden change in the tropical winds (from the usual strong easterlies to winds predominantly from the westerly direction) is known to have a strong impact on the extratropical climate, and had no doubt led to the sharp increase in surface temperatures throughout the Northern Hemisphere, which began in the winter following the eruption. Temperatures up to the spring of 1984, 2 years after the eruption, are still well above normal, although abated somewhat from the extreme high in the winter of 1982-83.

It will require several more years before conclusions can be drawn concerning the impact of El Chichon on climate. It is worth noting that there is still some residual ambiguity concerning the effects of the Mt. Agung eruption in the spring of 1963. Most students of the subject agree that the lower than normal temperatures in the years 1964-65 are related to the effects of Mt. Agung, although it is recognized that there was an ongoing general decline beginning in the mid-forties that continued until around 1970 (see Figure 2).

What this study tells us about major volcanic eruptions is that, barring the effects of internally caused changes (such as those associated with an El Nino), the perturbation on the climate system is quite strong. It supports the observed statistical relationship between climate and volcanic eruptions that have taken place over the past few hundred years. By varying the parameters characterizing the stratospheric aerosol layer in the model, we have learned which parameters are climatically important and the extent of climate sensitivity to those parameters.

Because there are a number of physical processes influencing climate, it is difficult to isolate the effects of one event in the real world. To extract information from observations, it is necessary to unravel the intertwined effects of many processes. Models, on the other hand, permit us to isolate an individual process, and individual components of that process, in order to understand the underlying physics. By moving

back and forth between model and observations, we can improve our understanding of those processes and thereby improve our capability for modeling climate.

Contact: Dr. Albert Arking
         Code 610

Sponsor: Office of Space Science and Applications
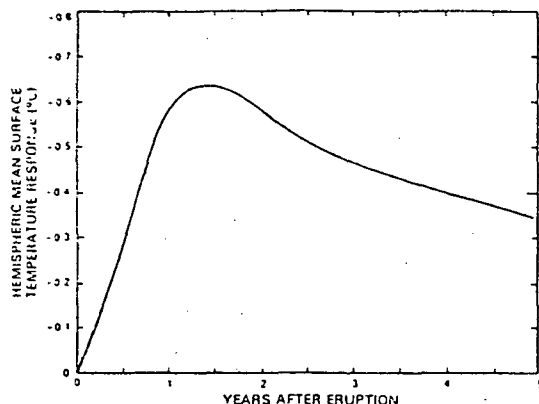
Effect of the El Chichon stratospheric aerosol layer on mean Northern Hemisphere surface air temperatures, based on the GSFC/MLEBM climate model and neglecting internally caused changes, such as those associated with the El Nino event that began about the same time.

TROPOSPHERIC PHOTOCHEMISTRY

Research on tropospheric photochemistry is directed towards improving our understanding of the relationships between observed trace species concentrations and the physical, chemical, and biological sources and sinks which influence these concentrations. This program consists primarily of the development and use of mathematical models. Heterogeneous chemistry and Monte Carlo techniques are currently being developed and will be incorporated into tropospheric models. Present emphasis is on the use of one and two-dimensional models to investigate the general features of the global distributions of selected trace species.

Recent results of these model studies include the following:

(1) Observed concentrations of carbon monoxide were used in conjunction with a one-dimensional latitude-dependent model to show that large biospheric sources of CO must be present in the tropics.

(2) The variation of ozone with latitude in the global troposphere was successfully replicated using a relatively complete photochemistry and coupled transport model.

(3) A one-dimensional, latitude-dependent model was coupled with an energy balance climate model having the same geometry. This permits interactive studies of tropospheric chemical processes and climate change.
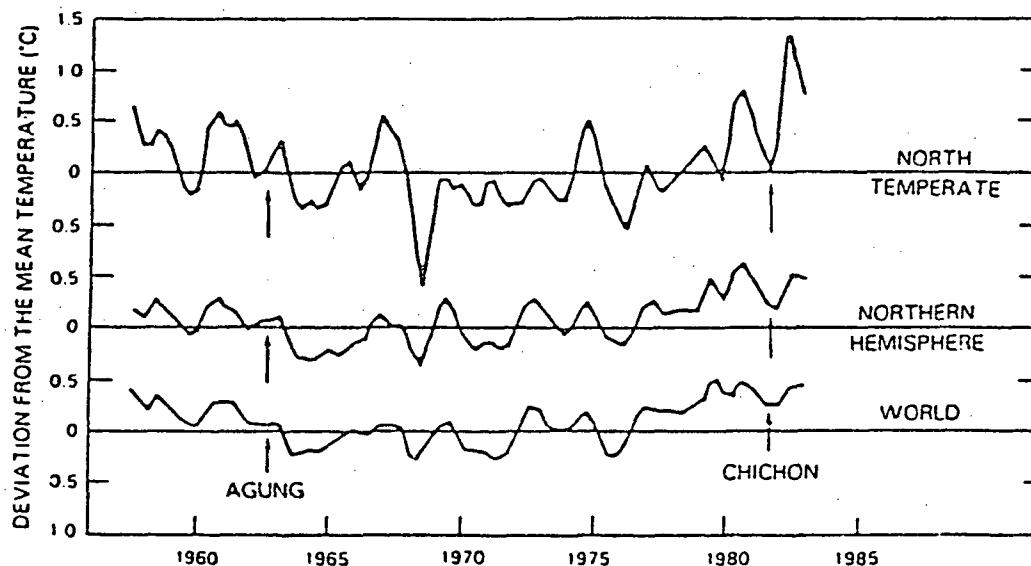
Record of surface air temperature deviations from the seasonal mean after twice applying a 1-2-1 smoothing to successive seasonal values. Tick marks at the bottom correspond to the northern summer of the indicated year. (From Angell and Korshover, Monthly Weather Review, June 1984.)

(4) A box model was developed to study the effect of intermittent loss due to washout on odd nitrogen concentrations in the lower troposphere. In addition to illustrating the range of variability to be expected for nitric acid concentrations, this model showed that a seemingly appropriate and widely used averaging procedure for obtaining mean loss coefficients may lead to large errors in model results.

Emphasis in current research is on the following areas: extension of the annually-averaged models employed in previous studies to study seasonally-dependent phenomena; extension of the heterogeneous loss (box) model to consideration of additional species, such as sulphur dioxide, and additional processes, such as cloud chemistry; the development of Monte Carlo techniques for study of trace species distributions. To develop seasonal models, monthly data on the latitude dependence of relevant physical parameters such as percent cloud cover, rainfall amount, and cyclonic activity are presently being incorporated. Source variations are poorly known for most trace species, but may be investigated using observed concentrations. Theoretical scavenging coefficients for nitric acid derived as part of the heterogeneous loss study mentioned above are presently being compared with coefficients derived from 6 years of precipitation data obtained at Brookhaven National Laboratories in Long Island, NY. Initial results are encouraging and indicate that the techniques used in that study may be applied in more general and comprehensive models. Vertical tropospheric profiles of odd-nitrogen components, NO, NO_2, and HNO_3, were obtained from an initial application of the Monte Carlo method and were in reasonable agreement with observed values. One result from this model was that stratospheric injections of odd-nitrogen alone cannot account for observed concentrations in the remote troposphere. Data on wind variance and Lagrangian correlation times, required for the Monte Carlo model, are inadequate for the upper troposphere, hence present emphasis is on development of a two-dimensional boundary layer model for which more generally accepted values of these quantities are available.

Contact: Dr. Richard W. Stewart
            Code 610

Sponsor: Office of Space Science and Applications

BALLOON-BORNE LIDAR MEASUREMENTS OF STRATOSPHERIC TRACE CONSTITUENTS

The principal question of stratospheric chemistry remains the degree to which the ozone layer will be depleted by various anthropogenic emissions, principally chlorofluorocarbons and oxides of nitrogen. Considerable effort has been expended to test the atmospheric models which predict col-

umn ozone decreases. This is done by comparing model results with simultaneous measurements of chemically related species. Hydroxyl radical (OH) has remained one of the most difficult species to measure because of its very low concentration in the parts-per-trillion range. In spite of its scarcity OH is one of the most important species in the stratosphere. Hydroxyl participates in a number of catalytic cycles which regulate ozone concentration in some regions of the stratosphere. Examples of these cycles are the following reactions:

$$OH + O_3 \rightarrow HO_2 + O_2$$

$$HO_2 + O \rightarrow OH + O_2$$

net $\qquad O + O_3 \rightarrow O_2 + O_2$

$$OH + O_3 \rightarrow HO_2 + O_2$$

$$HO_2 + O_3 \rightarrow OH + 2O_2$$

net $\qquad O_3 + O_3 \rightarrow 3O_2 \qquad 3O_2$
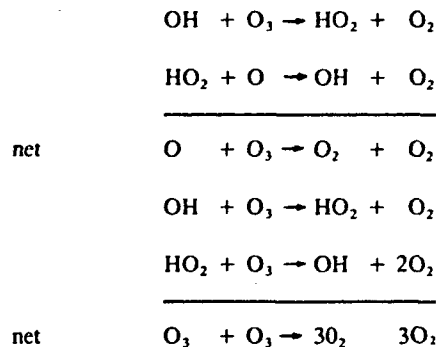
Atomic chlorine (Cl) arising from the photodecomposition of chlorofluorocarbons and nitrogen oxide (NO) from a variety of natural and man-made sources participate in similar catalytic cycles which destroy ozone. Hydroxyl radical influences the chlorine and nitrogen oxide cycles by its reactions with hydrochloric acid (HCl) and nitrogen dioxide (NO_2). HCl serves as a "reservoir" molecule for chlorine species removing chlorine from the active catalytic cycle. Hydroxyl reacts readily with hydrochloric acid as shown

$$OH + HCl \rightarrow H_2O + Cl$$
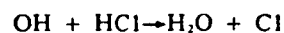
which releases atomic chlorine to destroy more ozone. On the other hand, hydroxyl removes catalytically active nitrogen oxides from their cycle by the following reaction:

$$OH + NO_3 \rightarrow HNO_3$$

which forms nitric acid a reservoir for nitrogen oxides.

The balloon-borne lidar system measures the concentration of hydroxyl in the stratosphere by the process of remote laser-induced fluorescence. In this technique a precisely tuned laser beam is transmitted into the atmosphere and is absorbed by the hydroxyl radical. Following the absorption the hydroxyl re-emits light at other specific wave-lengths. The lidar detects these emissions. By relating the emission strength to the amount of energy transmitted the hydroxyl concentration can be inferred. Our lidar uses a frequency doubled tuneable dye laser pumped by a doubled neodymiumyag laser to generate the required wavelength (282 nm). The hydroxyl fluorescence in the wavelength range 306 to 315 nm is collected

by a 12" diameter telescope and spectrally resolved by a
double monochromator. A gated photon counting system
records the strength of the fluorescence signal as a function
of range from the instrument by measuring the time interval
between the laser pulse and the return signal. An onboard
computer controls the entire data collection procedure and
processes the information collected for transmission to the
ground. The instrument is housed in a pressurized, thermally
regulated vessel. Figure 1 shows the instrument just before
its launch in October 1984. The foam insulated pressure
vessel and large radiator panels for eliminating waste heat
are readily visible.

A profile of hydroxyl radical concentration versus altitude
obtained from the October 1984 launch is shown in Figure 2.
The error bars shown represent one standard deviation of
uncertainty due to photon counting statistics. There is an addi-
tional uncertainty of ± 50 percent arising from calibration
of the instrument. Each data point represents an average of
1000 laser shots representing a temporal average of about
4 minutes. The balloon altitude range during this period is
represented by the vertical bar. The hydroxyl concentration
values represented here are 2 to 3 times lower than predicted
by current one-dimensional stratospheric models. However,
the model uncertainty plus the instrument uncertainty are
large enough that no sharp disagreement between theory and
experiment can be asserted from these results alone. Addi-
tional flights are scheduled for the fall of 1984 and spring
of 1985. Efforts are underway to increase the signal-to-noise
ratio, decrease the calibration uncertainty, and expand the
measurement capability to include additional stratospheric
species—in particular nitrogen dioxide and water vapor.

Balloon-borne lidar system.

Contact: Dr. William S. Heaps
              Code 610

Sponsor: Office of Space Science and Applications

MEASUREMENTS OF STRATOSPHERIC AND MESOSPHERIC OZONE BASED ON SATELLITE-BORNE SPECTROSCOPIC INSTRUMENTS

Investigations of the long term variability of the Earth's ozone
layer occupy a prominent place in atmospheric science both
because of practical concerns related to the impact of ultra-
violet solar radiation on the biosphere and the important role
of ozone in determining the structure and dynamics of the
upper atmosphere. The Goddard Backscattered Ultraviolet
(BUV) and Solar Backscattered Ultraviolet (SBUV) spectral
radiometers on Nimbus-4 and Nimbus-7, respectively, have
been extremely successful in defining the seasonal latitudinal
behavior of upper stratospheric ozone over the period from
1970 to the present. With our increasing understanding of
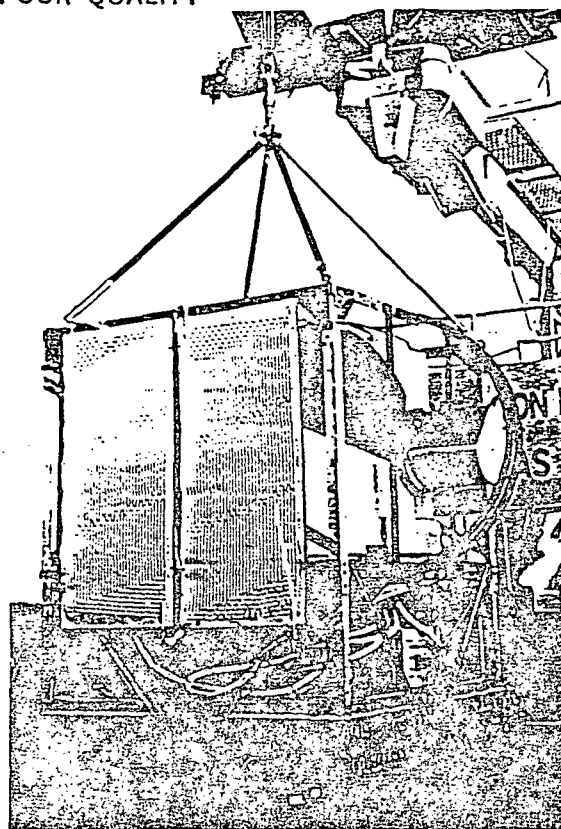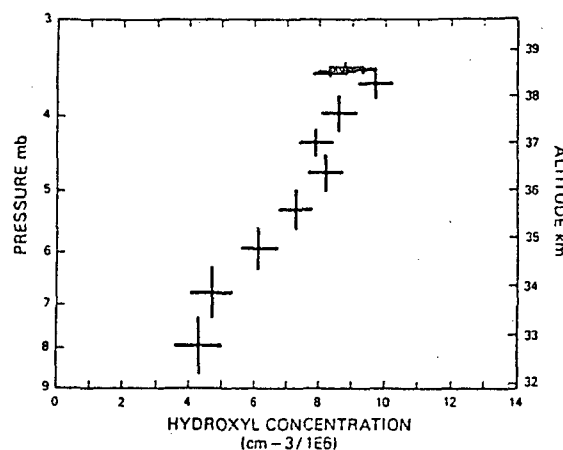
Hydroxly profile (October 27, 1983).

these topics, the focus of new satellite-based ozone measurements is shif*** to the detection and scientific interpretation of lor ** .. changes in the ozone layer and their driving mechanisms.

Of particular interest are decreases in upper stratospheric ozone such as predicted to result from industrial release of chlorofluorocarbons (CFC's) and variations driven by changes in the ultraviolet solar irradiance over the Sun's 11-year activity cycle. Current theoretical models indicate that both solar variability and CFC's lead percentage in ozone that maximize near an altitude of 40 km and have similar rates of change, with the 11-year effect alternating in sign while the CFC-related decrease is approximated by a linear trend over time. These results imply that a long-term data base, covering at least one solar cycle, is required to separate the anthropogenic and Sun-driven effects.

In addition, the ozone measurements must be accompanied by high quality data on the ultraviolet solar irradiance if we are to unambiguously isolate ozone changes related to the Sun from other perturbations. Quantitative analysis shows that we require an ozone base over at least the altitude region 30 to 50 km which is essentially free of instrumental artifacts, the tolerable uncorrected drifts being on the order of 1 percent over a 10-year period.

For the purpose of detecting long-term changes in stratospheric ozone and the incident ultraviolet solar irradiance, NASA and NOAA are cooperating in the flight of three optically identical SBUV/2 instruments on the TIROS operational satellites during the 1980's. A fourth instrument is scheduled for launch on the Upper Atmosphere Research Satellite (UARS) in 1989.

Past experience has exposed two problem areas related to the detection of long-term changes in ozone and the solar irradiance. The first concerns the the selectivity changes experienced by optical instruments over long periods of Earth orbit. The second centers on the necessity of comparing measurements obtained by different, though optically identical, instruments. The comparability of different prelaunch radiometric calibrations is the key issue here. To address these problems Goddard scientists are now modifying the SBUV/2 engineering model for regular flights on the Space Shuttle.

In a related effort, the Tanberg-Hansen ultraviolet spectrometer on the SMM solar observatory is being utilized to measure ozone and other constituents by recording the solar ultraviolet occultation profiles at local sunset as the spacecraft view of the Sun is eclipsed by the Earth. Observations at wavelengths between 280 and 240 nm provide profiles of ozone concentration versus altitude for 50 to 70 km region.

For small separations in longitude and short time spans, the measured profiles are very reproducible, but logitudinal and temporal differences are evident in the overall data set.

The distribution of mesospheric ozone is very sensitive to the amount of water vapor present. This occurs because photochemical dissociation of water leads to hydrogen compounds which remove ozone. SMM ozone profiles have been used in conjunction with photochemical calculations to estimate the mesospheric water vapor mixing ratio. Such analyses imply a water vapor mixing ratio which decreases from 6 ppm (parts per million) near 50 km, where it is consistent with satellite water measurements, to a mixing ratio of only 2 ppm at 70 km. This result is consistent with recent ground-based microwave measurements of water. The decrease of the water vapor mixing ratio with altitude requires that the time for vertical mixing of water from the stratosphere be an order of magnitude longer than usually assumed.

Contact: Dr. John E. Frederick
Code 610

Sponsor: Office of Space Science and Applications

STRATOSPHERIC DATA ANALYSIS

Atmospheric data, to be useful, must be analyzed in terms of the concepts or theories as to how our atmospheric system works. Satellites present a significant opportunity to obtain a global view of the elements making up the atmospheric system but also present the problem of dealing with very large data sets which have more information than a single investigator can effectively use. We thus have a broad ranging program for satellite data analysis which is using not only the data on solar flux and ozone from our SBUV instruments but also temperature data from the National Meteorological Center and temperature and constituent data from the LIMS instrument on Nimbus-7. The studies involved in this program include:

- investigation of ozone-temperature correlations and their relationship to wave propagation in the stratosphere

- investigation of possible correlations of solar activity and upper stratospheric ozone

- determination of the response of upper stratospheric ozone to solar proton events

- derivation of stratospheric wind fields from temperature data and evaluation of interannual variability

- determination of ozone flux divergences from ozone and derived wind data

- derivation of the photochemical production and loss rates for ozone from measured constituent data and derived information on unmeasured constituents

- derivation of SO_2 and aerosol concentrations from the TOMS and SBUV data after the El Chichon volcanic eruption

- derivation of NO concentrations from measured SBUV radiances. These and other studies are now producing the first global view of stratospheric processes.

The existing data provides a first test of our ability to use our transport models to forecast the evolution of stratospheric constituent fields. Large uncertainties still remain in such experiments because of the unmeasured constituents. The forthcoming UARS data should remove the major uncertainties.

An example of recently derived information is shown in the figure. The SBUV was designed to measure ozone but contamination from the El Chichon volcano was used to derive a measure of the aerosol content.

Contact: Dr. R. S. Stolarski
           Code 610

Sponsor: Office of Space Science and Applications

AEROSOLS MAY 1-15, 1982
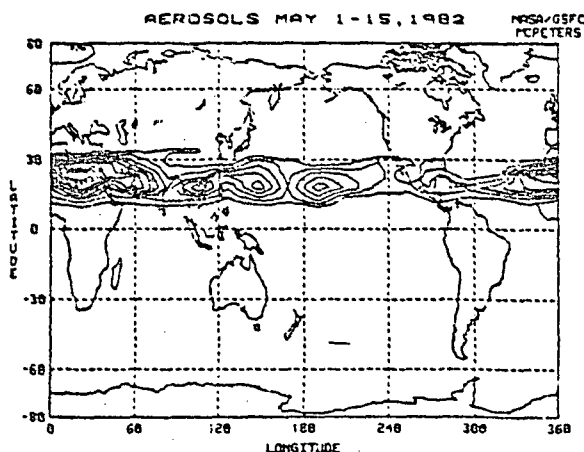
The eruption of El Chicon (17.3 N, 93.2 W) on April 4, 1982, injected large amounts of material into the stratosphere that formed a persistent layer of mostly H_2SO_4 aerosol between 20 and 30 km.

STRATOSPHERIC TRANSPORT MODELS

Both two-dimensional and three-dimensional models are being used to investigate how the interplay of dynamics and photochemistry determines the distribution of ozone and other constituents in the stratosphere. In the two-dimensional model, the focus is on how seasonal variations in the stratospheric winds give rise to the observed large-scale latitudinal and seasonal variations in stratospheric trace species. A relatively recent concept, that of the residual mean circulation, has been used to formulate the meridional and vertical transport circulation to transport long-lived source gases such as N_2O, methane, and the chlorofluorocarbons. Figure 1 shows the modeled N_2O distribution in August as a function of latitude and pressure altitude. Note the bulge of high N_2O amounts extending out of the tropical troposphere toward the lower stratosphere. This feature is seen in both satellite and in situ measurements of N_2O.

A three-dimensional model is being used to look at day-to-day changes in the distribution of stratospheric constituents. We have calculated air trajectories from two general circulation model forecast experiments that we have run for these periods. We have superimposed some trajectories over the 10 mb geopotential height field that was derived from NOAA/NMC data and ozone mixing ratio fields that were measured by the SBUV to illustrate the role of dynamical processes in determining the ozone distribution. Figure 2 shows the 10 mb geopotential height field for January 23, 1979, along with the superimposed trajectories beginning on January 19, 1979, and ending on January 29, 1979. Note that the air parcel trajectories curve counterclockwise around the polar vortex from the North Atlantic region over Northern Europe and Asia and are directed over the polar regions between the high and low geopotential height centers. The air then travels clockwise around the high geopotential height region. Figure 3 shows the ozone mixing ratio field at 10 mb for January 23, 1979, along with the superimposed air trajectories beginning on January 19, 1979, and ending on January 29, 1979. Note that the overall pattern of ozone mixing ratio at 10 mb is of high ozone amounts at low latitudes and low ozone amounts at high latitudes. The measured ozone amounts are found to be enhanced over Northern Asia where the trajectories turn poleward, and the ozone amounts are diminished over the northwestern United States where the trajectories turn southward. Also, note that the north-south ozone gradients are strongest where the trajectories are zonal and weakest where the trajectories are meridional.

Contact: Dr. Marvin A. Geller
           Code 610

Sponsor: Office of Space Science and Applications
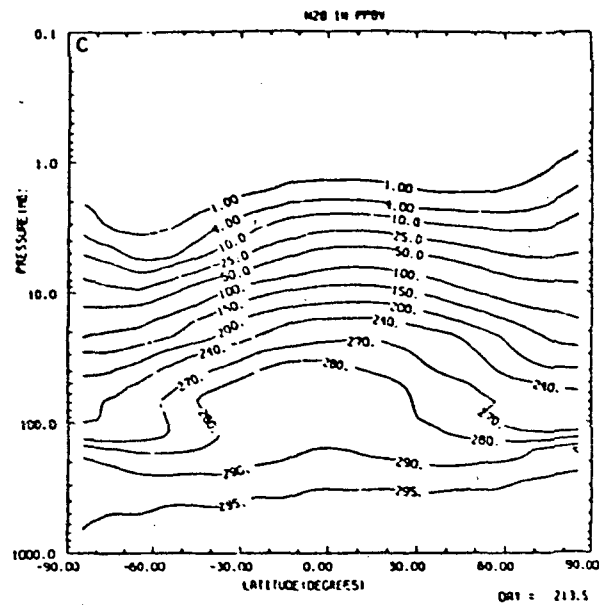
*Figure 1.   Zonally averaged N₂O mixing ratio
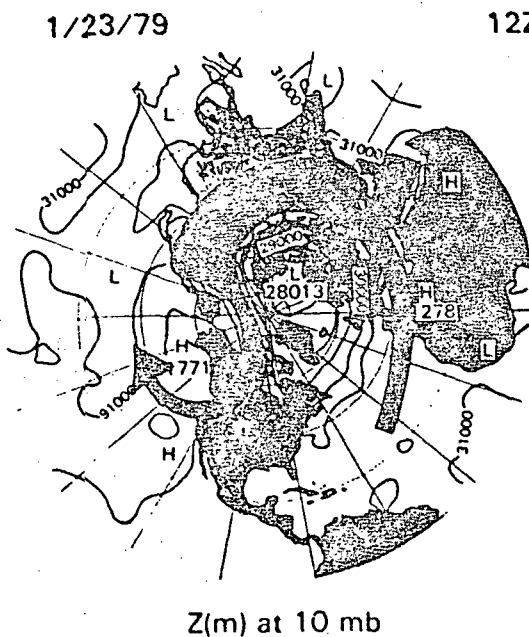distribution for August from the 2-D model.*

1/23/79   12Z   1/23/79

Z(m) at 10 mb

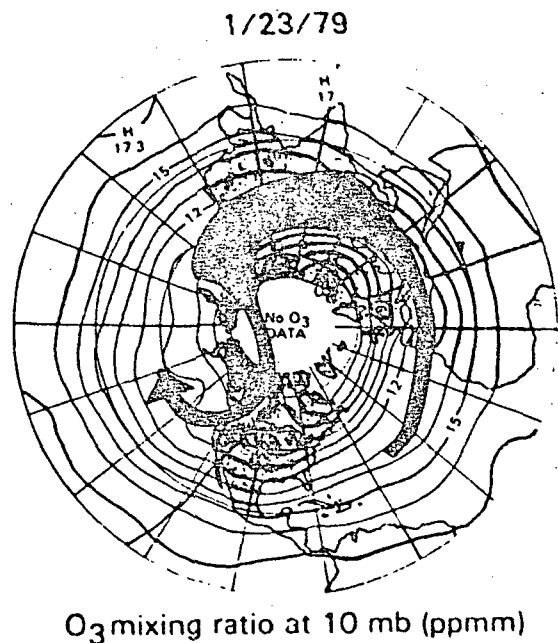*Figure 2.   10 mb geopotential height field.*

O₃ mixing ratio at 10 mb (ppmm)

Figure 3.   Ozone mixing ratio field at 10 mb.

WAVE DUCTING IN THE LOWER ATMOSPHERE

Gravity waves and associated travelling ionospheric disturbances (TID's) are common features of the thermosphere, observed all around the globe with ground-based and satellite-borne instruments. The principal excitation sources are believed to be in the auroral zones and polar caps, where energetic particles precipitate magnetosphere and solar wind-induced electric fields are effective. Strong correlations are found between wave activity and the occurrence of magnetic substorms.

Based on classical gravity wave theory and numerical simulations, significant progress has been made toward an understanding of these phenomena. One particular class of waves, however, the so called medium-scale perturbations with horizontal wavelengths typically less than 400 km will pose a major problem. In the viscous medium of the thermosphere, these perturbations should be dissipated over horizontal distances comparable to their wavelengths; yet in reality they seem to propagate, virtually unattenuated from the auroral zones all the way down to equatorial latitudes.

Considering the auroral energization process due to Joule heating, a realistic spectral model has now been developed which describes the transient response of the atmosphere from the Earth's surface up to 700 km. In this model, a wave mode has been identified which has the right properties to explain the observations. Due to total reflection from the surface and partial reflection or refraction near the mesopause temperature minimum (at 80 km), a wave duct forms in the nondissipative lower atmosphere. Gravity waves originating in the auroral zones at higher altitudes enter the wave duct from above, and within it, they can travel large horizontal distances without being dissipated. From this duct, the gravity waves then leak back into the thermosphere. Taking a "detour" through the nondissipative lower atmosphere, thermospheric perturbations can propagate with velocities of about 200 m/sec across the globe, which is consistent with observations.

Contact: Dr. H. G. Mayr
             Code 610

Sponsor: Office of Space Science and Applications

NIMBUS-7 CLIMATE DATA SET DEVELOPMENT

Now in its sixth year of operation, the Nimbus-7 satellite is producing several long-term climate related data sets. In fact, Nimbus-7 is the single most significant source of experimental data from Earth orbit, relating to atmospheric and oceanic processes. Nimbus-7 data sets, once validated, are made available from Federal archives. These data sets are in various stages of development, and their status is presented below.

Data from the Coastal Zone Color Scanner (CZCS) consisting of radiance, chlorophyll, sediment, and sea surface temperature, and covering 4 years, have been archived. Data production and validation continue.

Solar and Earth radiation data covering 4 years from the Earth Radiation Budget (ERB) Experiment have been produced and archived. Production of the fourth year of data has begun.

Limb Infrared Monitor of the Stratosphere (LIMS) Experiment data covering 7 months (LIMS cryogenic lifetime), and containing stratospheric temperature, ozone, water vapor, nitric acid, and nitrogen dioxide profiles, have been produced and archived.

A 4-year data set of stratospheric aerosols in the polar regions from the Stratospheric Aerosol Measurement (SAM II) Experiment has been produced. Data production and validation continues.

Five years of global ozone data, consisting of vertical concentration profiles and total burden concentrations from the Solar Backscatter Ultraviolet (SBUV) and Total Ozone Mapping Spectrometer (TOMS) Experiment, have been archived. The production of the sixth year of data is underway, with archiving scheduled for 1985.

The production of the Scanning Multi-channel Microwave Radiometer (SMMR) Experiment data continues and now extends into the fifth year of orbital data. The data consist of brightness temperatures and the following derived products: sea ice (multiyear ice fraction and sea ice concentration), total atmospheric water vapor over ocean, sea surface temperature, and sea surface wind speed. The first 3½ years of data have been archived.

Contact: Dr. Edward J. Hurley
             Code 630

Sponsor: Office of Space Science and Applications

OCEANS

DYNAMICS OF OCEAN-ATMOSPHERE INTERACTIONS

Until recently, numerical models of the atmosphere treated the ocean surface properties as unaffected by atmospheric changes, while numerical models of the ocean treated the atmospheric conditions as specified and unaffected by oceanic dynamic response. This way of handling the oceanic boundary conditions was imposed by computer limitations, and because the scales of atmospheric and oceanic motion dominated by the rotation of the Earth are so different, Oceanic models require much finer grid sizes than atmospheric models.

The computers now becoming available are making it possible to model the dynamics of both media. We have started to explore how the dynamics of the joint ocean-atmosphere system behaves when neither medium is locked into a fixed state. Both the ocean and the atmosphere are permitted to respond to fluxes from the other medium as it reacts as an active participant in joint dynamics.

The importance of taking account of the joint dynamics has been demonstrated in recent work on modeling of the air-sea interaction processes that underlie the El Nino Phenomenon. This is a temperature anomaly in the Eastern Pacific Ocean that appears to be related to weather and oceanic anomalies on a worldwide scale.

The mutual influence of atmospheric and oceanic dynamics was demonstrated in a joint oceanic-atmospheric model. The model showed that the atmospheric response to evaporation and heat transfer from the ocean modifies and enhances the anomalous behavior of the upper ocean. It was found that an event such as the warming in the tropical Pacific Ocean is not readily explained without considerations that include ocean currents, atmospheric reactions to evaporation and heat, and the oceanic reactions to the atmospheric changes.

This work is done by specially designed numerical experiments to illustrate the importance of local joint dynamical air-sea couplings on global atmospheric and oceanic processes.

Contact: Dr. Paul Schopf
          Code 671

Sponsor: Office of Space Science and Applications

SST anomalies generated from numerical model of the tropical upper ocean.

RECENT RESULTS OF SEA ICE RESEARCH

Sea ice is a vital component in the climate system. For instance, it serves as a strong insulator, restricting exchanges of heat, mass, and momentum between ocean and atmosphere; it lessens the amount of solar radiation absorbed at the ocean's surface, due to its very high albedo relative to that of ice-free oceanic mixed layer, due to the salt rejection which occurs as the water freezes. This mixed-layer deepening sometimes further leads to bottom water formation, thereby influencing the deep circulation of the entire world ocean.

Satellite data and numerical modeling have, in recent years, greatly increased our knowledge and understanding of the global distribution of sea ice and its seasonal and interannual variations. Microwave imagery from the Electrically Scanning Microwave Radiometer (ESMR) and the Scanning Multifrequency Microwave Radiometer (SMMR) on the Nimbus-5 and -7 satellites has provided global sea ice information at a resolution of about 30 km. Visible and infrared imagery from Landsat, NOAA, and Tiros-N satellites provide more detailed information, using a much higher resolution, although for smaller regions of the globe and at lesser frequency. Such higher-resolution imagery proves valuable for studying the dynamics and morphology of individual sea ice floes.

It is with the microwave data, however, that the large-scale distribution of the ice is easily observed. The value of microwave observations for sea ice studies derives from the sharp contrast between the microwave emissivities of sea ice and open water and the fact that the microwave radiances are not obscured either by overlying cloud cover or by

darkness. This allows calculation of sea ice concentrations within the individual fields of view imaged by the satellite instrument (these fields of view being roughly 30 x 30 km), and integration to the total areal coverage of sea ice in any chosen region.

Analysis of compiled data from several satellite sensors over the nine-year period 1973 to 1981 has revealed that the sea ice of the southern hemisphere experienced a marked reduction in its wintertime areal extent during the mid-1970s, from 20 million square kilometers in 1973 to 17 million square kilometers in 1977, but that this reduction was reversed in subsequent years (see figure). Hence the mid-1970s phenomenon, initially interpreted by some as a possible geophysical reflection of a carbon dioxide-induced warming of the atmosphere, was more likely part of the natural year-to-year fluctuations of the ice cover and not indicative of a long term trend. The satellite data base remains too short to reveal whether the southern hemisphere sea ice tends to undergo multiyear cyclical variations of some near-constant period.

Satellite data have also revealed unexpected phenomena in the sea ice cover, particularly the occurrence and recurring nature of certain polynyas, or sizeable, nonlinear open water regions in the midst of the sea ice cover, in both the northern and southern hemispheres. The largest such polynya is the Weddell Polynya off the coast of Queen Maud Land in the Antarctic. This polynya, covering 200,000 square kilometers, existed throughout the 1974, 1975, and 1976 winters, but not in any other winter of the 1973 to 1983 decade. Its size and westward movement over time have led to several speculations on its cause and its relationship to oceanic and atmospheric circulations. The observational information on this polynya is based almost exclusively on the microwave data of the Nimbus-5 ESMR.

The multi-channel nature of the SMMR instrument has allowed calculation of other variables in addition to sea ice concentrations. SMMR data have been used to determine sea ice temperatures and multiyear ice fractions, multiyear ice being sea ice which has survived a summer melt season. The SMMR results suggest that the fraction of multiyear ice in the central Arctic may be less than had been assumed based on early thermodynamic sea ice models and that the multiyear ice pack undergoes substantial interannual variations.

Recent interest in marginal ice zones has resulted in a major international experiment using coordinated observations from ship, aircraft, and satellites. This Marginal Ice Zone Experiment (MIZEX) consists of two field programs, the first centered in the Bering Sea (MIZEX-West) and the second centered in the Greenland Sea (MIZEX – East). Preliminary results from MIZEX-West have provided a means for

distinguishing among new, young, and first-year sea ice types through the utilization of polarization differences observed with multichannel passive microwave radiometers. Results from both programs are expected to substantially improve our understanding of air-sea-ice interactions and to improve and extend our capability to utilize space observations for sea ice research.

Contact: Dr. Claire L. Parkinson
         Code 671

Sponsor: Office of Space Science and Applications
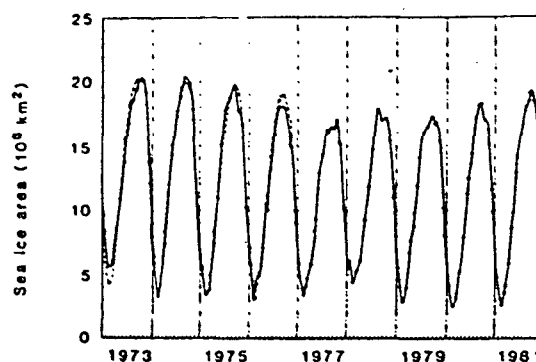
Areal sea ice extent in the southern ocean as a function of time, 1973-1981, derived from satellite observations.

SEA SURFACE MICROSCALE DYNAMICS

The deeper layers of the ocean are largely inaccessible to present remote sensing techniques; interpretation of sea surface remote sensing data to infer the dynamic process in the deeper layer is, therefore, crucial to applications of satellite data in oceanography and air-sea interaction. The dynamics of waves and the air and water boundary layers all involve complicated nonlinear interactions between surface and subsurface dynamic processes that challenge our understanding.

An important recent result is the finding that the effect of wind on surface gravity waves changes their nonlinear behavior. Nonlinear effects become very important when surface gravity waves travel over many wave periods and wavelengths; one effect of the nonlinearity is that wave modulations, to the lowest order of approximation, are governed by a nonlinear Schrodinger equation, so that wave packets have quantum properties. Laboratory experiments in the Wind-Wave tank at the Wallops Flight Facility have revealed that wind stress inhibits wave packet formation. The

initial stage of packet formation in a periodic wave train is the occurrence of sideband modulations.

The laboratory results shown in the figures demonstrate that under zero wind, the spectrum of an initially periodic wave train develops sidelobes (Figure 1), while at a wind velocity of 7 m/s the sidelobes fail to develop (Figure 2). This agrees with the general understanding of wind and damping on surface wave propagation, and represents a satisfying confirmation of our ideas and justifies further theoretical and experimental work on sea surface fluxes and wave propagation.

Contact: Dr. Norden E. Huang
        Code 671

Sponsor: Office of Space Science and Applications

SURFACE CONTOUR RADAR MEASUREMENTS

Recent analysis of data from the GSFC Surface Contour Radar (SCR) indicates that it is superior to pitch-and-roll buoys (PRB) for the measurement of many aspects of the sea surface directional wave spectrum (DWS). The SCR operates at 36 GHz and is mounted in the GSFC P-3 aircraft. Its oscillating mirror scans a pencil-beam laterally to measure the elevations at 51 evenly spaced points on the surface below the aircraft. At each of the points, the SCR measures the slant range to the surface and corrects in real-time for the off-nadir angle of the beam (including the effect of aircraft roll angle) to produce the elevation of the point in question with respect to the horizontal reference. The elevation measurements are false-color coded and displayed on the SCR color TV monitor so that real-time estimates of significant wave height, dominant wavelength, and direction of propagation can be made. The real-time display allows optimal selection of aircraft altitude and flight line direction even during a flight over a visibility obscured sea without prior knowledge of the wave conditions.

Comparisons of DWS from the SCR and PRB are made through the use of Fourier coefficients and spreading factors. In 1973, an extensive set of DWS observations were made using the University of Hamburg meteorological buoy and an Institute of Ocean Sciences PRB during the Joint North Sea Wave Project (JON-SWAP). In analyzing the consistence of the magnitudes of the Fourier coefficients, [1]Hasselmann et al. (1980), plotted S_2 versus S^1 where each is an independently arrived at estimate of the spreading factor for the azimuthal distribution of energy in the DWS. Ideally, all of the data points should fall on a 45° line. The data from Hasselmann et al. 1980) is reproduced at the top of the figure. It is apparent that there is a large scatter in the data. For comparison, the SCR data points for a similar data set have been replotted in the same format in the middle (200 m aircraft altitude) and bottom (400 m) of the figure. There is virtually no scatter in the SCR data compared to the PRB data. The slope of the SCR data points appear to be slightly greater than unity and the dotted straight lines in the figure have been least squares fitted to the data. It is interesting that the right side asymptote of the PRB data also has a slope which exceeds unity, but the scatter in the data was apparently so large that Hasselmann et al. did not consider it noteworthy.

In general, the radar system determines the Fourier coefficients with significantly less noise and bias than PRB. The high spatial resolution and rapid mapping capability over extensive areas makes the SCR ideal for the study of fetch-limited wave spectra, diffraction and refraction wave patterns in coastal areas, and wave phenomena associated with hurricanes and other highly mobile events.

Contact: Dr. Edward Walsh
        Code 672

Sponsor: Office of Space Science and Applications
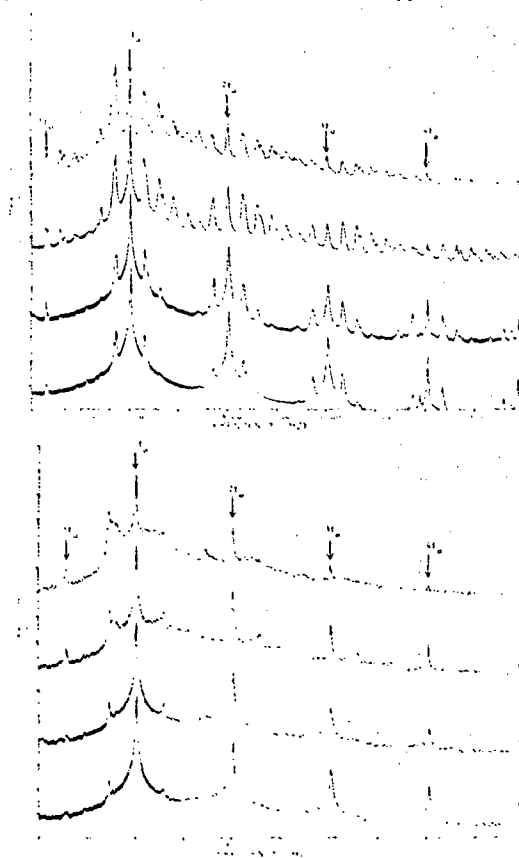
Under zero wind, the spectrum of an initially periodic wave train develops sidelobes, whereas at a wind velocity of 7 m/s, the sidelobes fail to develop.
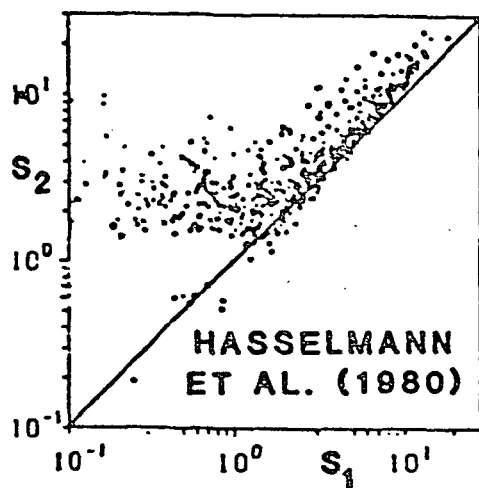
Data from Hasselmann et al.
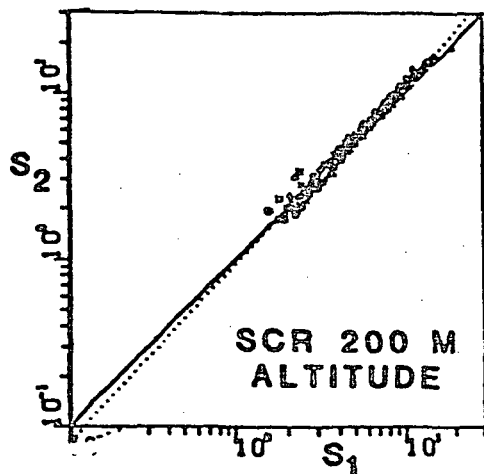
SCR data points (200 m).
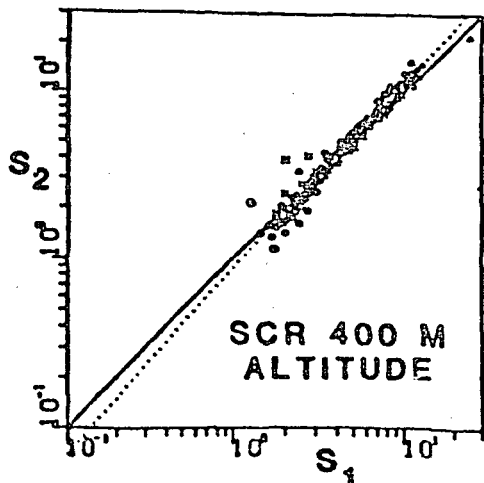
SCR data points (400 m).

NIMBUS-7 COASTAL ZONE COLOR SCANNER OBSERVATIONS OF OCEANIC BIOLOGICAL PROCESSES

The Nimbus-7 Coastal Zone Color Scanner (CZCS) is the first satellite-borne sensor designed to infer surface layer concentrations of photosynthetic pigments in the ocean. Since these pigments (e.g., chlorophyll-a) preferentially absorb blue light, a reduction in the relative intensity of upwelled blue light from the ocean compared to green light can be used as a measure of the pigment concentration.

During the past year, the operational CZCS atmospheric correction and bio-optical algorithms have been implemented on the Goddard Atmosphere-Ocean Image Processing System (AOIPS), thus allowing oceanographers to interactively work with ocean color data sets. This new capability has already lead to a number of important contributions to our understanding of dynamical and biological processes in the regions currently being studied at GSFC. These sites include the southeastern continental shelf of the United States, the northwest coast of Spain, the Adriatic Sea and the eastern Pacific Ocean (Peru and the Galapagos Islands). In all cases, the derived concentrations have compared quite closely to the shipboard observations.

Examples of CZCS pigment images from the Galacian coast of Spain are provided in the accompanying figure. Within the rias (bays) are some of the most productive aquacultures (mussels) in the world, while major sardine and hake fisheries are found offshore. The nutrient source which supports the productivity of these populations has been recently identified to be the upwelling of nutrient rich oceanic waters into the coastal zone and not terrestrial runoff. Primarily, the upwelling is a result of wind forcing, but the coastline and bathymetry strongly influence the strength of the upwelling in ways that are not well understood. Satellite imagery is invaluable for studying these regions because massive phytoplankton (e.g., algae) blooms can develop quite rapidly making observation by traditional shipboard techniques difficult. For example, the two images indicate a ten-fold increase in concentration around Cape Finistere in less than 6 days.

Contact: Dr. Charles R. McClain
        Code 671

Sponsor: Office of Space Science and Applications
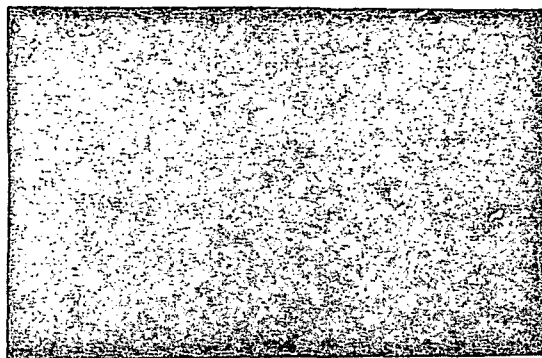
Coastal Zone Color Scanner Images of surface layer chlorophyll concentration. The color code ranges from dark blue to brown, indicating concentrations of less than 0.1 to greater than 4.0 mg/m³.

AIRBORNE ACTIVE-PASSIVE OCEAN CHLOROPHYLL MEASUREMENTS

Field research activities with the Air-borne Oceanographic Lidar (AOL) focused on (1) the evaluation of the new Passive Ocean Color Subsystem (POCS), (2) the application of this improved instrument to a major oceanographic experiment denoted as the Shelf Edge Exchange Processes (SEEP) program, and (3) the development of all new techniques to calibrate the POCS simultaneously with the usual pulsed lidar fluorosensor.

To accommodate passive detection (and thus implement the POCS) the NASA AOL fluorosensor was modified to electronically integrate the previously ignored, solar induced direct current output available from all the photomultiplier detectors viewing the focal plane of the transmission diffraction grating lidar spectrometer. The resulting simultaneous narrow/wide bandwidth operation of the spectrometer photomultiplier detectors allows important new studies related to (1) calibration of active multichannel lidar systems, (2) effect of sea state on passive and active ocean color measurements, (3) active lidar validation of passive ocean color in-water algorithms, (4) subsequent improvements of satellite-borne ocean color scanners, and (5) chlorophyll *a* fluorescence quantum yield variability.

The AOL/POCS was calibrated for the SEEP flights using an internally illuminated hemisphere (GSFC/Sensor Evaluation Branch). In order to compare ocean color data, the NASA Langley Research Center flew the Multichannel

Ocean Color Sensor together with the AOL. The AOL laser-induced chlorophyll *a* fluorescence, obtained simultaneously, was used as the independent data source to which the passive instrument could be compared.

The accompanying figures (a and b) show data from a typical flight line executed in the New York bight during the SEEP field experiment. In (a), the calibrated AOL passive ocean color data were processed (without atmospheric and reflected sky radiance correction) using a 3-band curvature algorithm. The agreement with the laser induced chlorophyll *a* fluorescence is exceptionally good. To further validate the AOL/POCS, the data from the Multichannel Ocean Color Sensor (MOCS) was similarily processed with the curvature algorithm and also compared to the laser data [see (b)]. From these data, it can be seen that the AOL/POCS can acquire very high quality data simultaneously with the laser fluorosensor.

The data were taken during the SEEP experiments in the spring of 1984.

Contact: Dr. Frank E. Hoge
Code 672

Sponsor: Office of Space Science and Applications
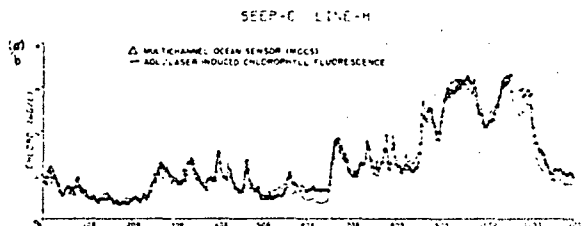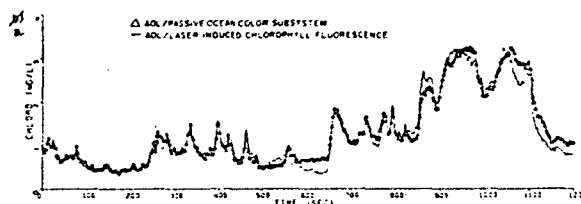
Data from a typical flight line executed in the New York Bight during the SEEP field experiment.

TERRESTRIAL PHYSICS

LENGTH OF DAY AND THE SOUTHERN OSCILLATION/EL NINO

The Southern Oscillation (SO) is the single most prominent signal in interannual, global-scale atmospheric fl~~~ :ations. It is characterized by an irregular see-s; v exchange of air mass between eastern and western hemispheres in the tropical and subtropical Pacific-Indian Ocean region. For some unknown reasons, every once in a few years the SO wind field will collapse and, through ocean-atmosphere interactions, cause extensive meteorological disruptions—a phenomenon known as an El Nino (EN) event. A most dramatic example of such an SO/EN event happened during the year 1982-83.

Since the SO/EN represents an extensive mass transport in the atmosphere/ocean, and since the angular momentum of the whole Earth is conserved, there must be exchanges of angular momentum between the atmosphere/ocean and the solid Earth. The changes in the angular momentum of the solid Earth is reflected in, among other things, the variations of the Earth's rotational speed, which in turn changes the length-of-day (LOD). The question to be addressed is whether the SO/EN effect on the LOD is strong enough to be detected and, if so, how important is it?

It is customary to measure the overall intensity of the SO in terms of the so-called SO Index (SOI), usually defined as the difference in the normalized monthly sea-level (air) pressure between Tahiti and Darwin, Australia. The occurrence of an El Nino condition is invariably indicated by a prolonged drop in the SOI values (see Figure 1). We constructed the SOI time series for the period 1957–1983 and shall compare it with the LOD observations.

The ΔLOD has been constantly and accurately monitored since the advent of atomic clocks in the late 1950's and its variations, denoted by ΔLOD, published regularly. The ΔLOD time series we shall use is acquired from the Bureau International de l'Heure, also for the period 1957-1983. Since the SO/EN is an interannual fluctuation with time scale of 1 to, say, 10 years, it is necessary to remove from the ΔLOD time series the dominant seasonal components with periods no longer than 1 year (which is known to be caused by seasonal changes in the atmospheric circulation system) as well as the "decade fluctuations" with time scale longer than, say, 10 years (which is suspected to be caused by core-mantle interactions within the Earth). We do this by least-squares fitting, and subsequently subtracting two harmonic components (with annual and semiannual periods, respective-

ly, representing seasonal ΔLOD variations) and a 4th-order polynomial (representing the decade ΔLOD fluctuations). The resultant time series is thus duly called the interannual ΔLOD.

Figure 1 shows the two time series, SOI(t) and interannual ΔLOD(t) for the period 1957-1983. The qualitative correlation is rather encouraging, in particular with respect to the El Nino events over the years, each of which is indicated by an arrow whose length corresponds to the intensity. The most dramatic example is, again, the 1982-1983 episode. The quantitative linear correlation coefficient is found to be 0.55, and the amount of angular momentum exchange associated with one SOI unit is 7.7 x 10^{24} kg m^2 sec^{-1}. In conclusion, it is believed that much, if not most, interannual LOD variation is caused by the Southern Oscillation/El Nino, and the true correlation is considerably higher than its apparent value considering the fact that the SOI is merely an indicator derived from two local atmosphere measurements.

Contact: Dr. B. F. Chao
        Code 620

Sponsor: Office of Space Science and Applications
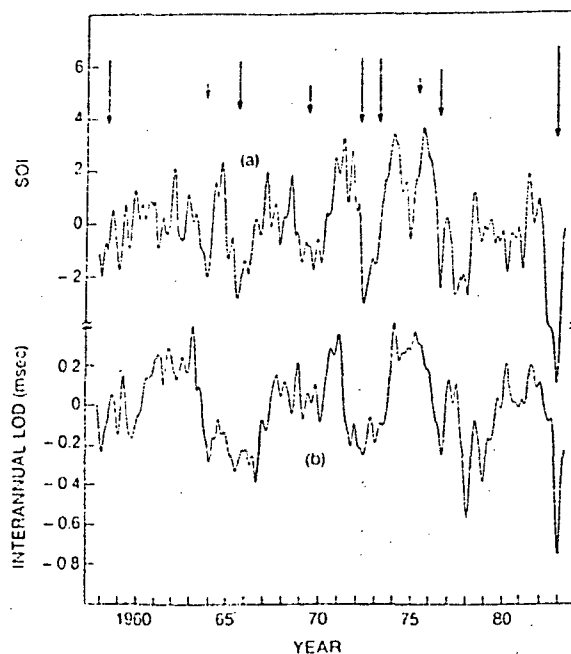
Comparison of the Southern Oscillation Index (SOI) and the interannual length-of-day (LOD) variation. Arrows indicate El Nino events.

INTERPRETATION OF SATELLITE LASER RANGING MEASUREMENTS IN CALIFORNIA

Satellite Laser Ranging (SLR) measurements of a baseline between Quincy and San Diego, CA across the boundary between the North American and Pacific Plates have shown a steady contraction over the last decade. The current estimate of the contraction rate is about 6.4 cm/yr with an uncertainty of 1 or 2 cm/yr. While it is apparent that this motion is associated with the north-westerly motion of the Pacific with respect to North America the distribution of the crustal deformation over 900 km length of the baseline has not been studied in detail up until now.

A study has been initiated to resolve the likely locations and mechanisms for the crustal distortion responsible for the baseline changes. Several tectonic regions are being studied. In southern California the SLR baseline crosses the Garlock, San Andreas, Cucamonga (or eastern section of the San Gabriel), and Elsinor Faults. North of the Garlock Fault the baseline lies within the Sierra Nevada province. An analysis of the strain field in the vicinity of the major southern California faults suggests that fault crossing dislocations can account for only about 3 cm/yr contraction at the azimuth of the SLR baseline.

It appears, however, that the strain field in southern California is a broad scale feature extending well beyond the expected range of an elastic dislocation.

Uniform straining between the Mexican border and the Garlock Fault results in a contraction rate of 4.5 cm/yr in fairly good agreement with the SLR results and geologic records. The broad scale deformation is consistent either with distributed yielding at depth or an elastic flow below a brittle surface layer of the lithosphere. North of the Garlock Fault small microfaulting appears to be a pervasive feature of the Sierra Nevada mountains. However, the magnitude and orientation of the faulting results in only a small effect on the SLR baseline—an extension of less than 1 mm/yr.

Several other potential sources of motion are also being investigated to determine whether they have a significant impact on the observed contraction. These include the tilting of the Sierra Nevadas (in particular the eastward tilting of the northern Sierras not far from the terminus of the SLR baseline), deformations due to either the ancient Kern Canyon Fault (crossed by the SLR baseline at Lake Isabella) or an eastward extension of the White Wolf Fault, and local motion.

Contact: Dr. S. C. Cohen
         Code 620

GLOBAL MEAN SEA SURFACE BASED ON SEASAT ALTIMETER DATA

Satellite altimeter data have provided an important new basis for the mapping of the global sea surface topography. The altimeter system provides a measurement of the satellite height above the sea surface. When these measurements are combined with satellite height information calculated from precision tracking data, the topography of the ocean surface can be mapped. The 70-day global set of SEASAT altimeter data have recently been used to compute a global mean sea surface on a 0.5° x 0.5° grid. The figure presents a contour map of this mean sea surface.

The mean sea surface map is a very good approximation of the geoid over the ocean areas and is dominated by the gravity field of the Earth. As shown in Figure 1 the height of the sea surface above (or below) the reference computational ellipsoid ranges from -100 meters south of India to -80 meters north of Australia. The map shows long-wavelength gravitational features such as the maxima over the western boundary of the Pacific Plate, the mid-Atlantic Ridge south of Iceland and in the southwestern Indian Ocean. Long-wavelength gravitational depressions are noted south of India, off the coast of Baja, California, and in the Caribbean. The map clearly shows the island chains and the trench systems in the Pacific and Caribbean, the south-eastern boundary of the African plate and numerous other short-wavelength features.

The accuracy of the SEASAT altimeter data is on the order of 5 cm, however a comparable accuracy could not be achieved for the mean sea surface because of radial spacecraft ephemeris errors, tidal model errors and ionospheric and tropospheric refraction model errors. The rms accuracy of the mean sea surface presented in the figure is on the order of 70 cm. This surface is a more accurate representation of the geoid over the ocean areas than has been provided by the previous analyses of surface gravity data and satellite orbit perturbations. In some southern ocean regions an order of magnitude improvement in the accuracy of the geoid has been realized.

One of the most important applications of satellite altimetry is in the area of satellite oceanography. The geostrophic ocean currents produce a deviation on the order of a meter in the ocean surface from the geoid. Thus, if an accurate geoid is available, the altimeter data can be used to map the

large-scale oceanic flow. The present long-wavelength accuracy of the GSFC satellite-derived geoids is sufficient to permit detection of the major ocean basin gyres. The time varying circulation can be measured with the technique of satellite altimetry independent of the geoid. The measurement of the time variability is an important quantity for further development of ocean circulation models.

NASA is currently developing the Ocean Topography Experiment (TOPEX) Satellite in order to measure the time variable and mean ocean circulation beginning in the late 1980s. The proposed satellite will provide altimeter data with a precision of 2 cm and an absolute accuracy of about 14 cm over a period of at least 3 years. These data in combination with satellite measurements of the wind speed and direction and in-situ oceanographic measurements will be extremely valuable for the modeling and long range prediction of global atmospheric and oceanic anomalies such as the El Nino/Southern Oscillation and other processes on a global basis.

Contact: Mr. J. G. Marsh
           Code 620

Sponsor: Office of Space Science and Applications

0.5° GRID. 1 M CONTOUR
$A_e - 6378137m$, $1.f = 298.257$
REF. NO. 83402
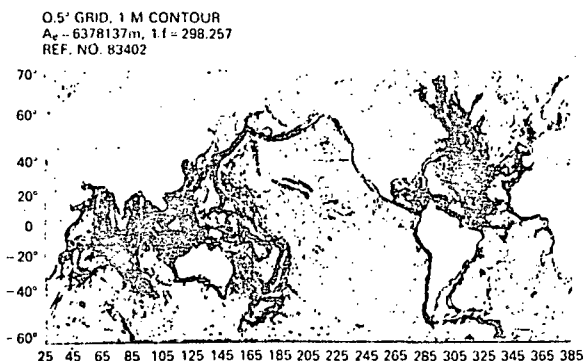
Mean sea surface based on Seasat altimeter data.

THE ORBIT OF LAGEOS AND SOLAR ECLIPSES

On May 4, 1976 a Delta rocket lofted the Laser Geodynamics Satellite (Lageos), into a high-altitude orbit. This satellite, circling 5900 km above the Earth's surface, aids in geophysical studies. Stations scattered across the globe bounce laser beams off Lageos' many retroreflectors. Measurement of the station-Lageos distance with the beams allows Lageos to monitor continental drift, polar motion, and Earth rotation. In effect the laser system carries out long-

distance surveying, with the lasers replacing the familiar surveyor's telescope and the satellite his leveling rod.

One needs to know Lageo's orbit accurately for the satellite to perform its mission. To know the orbit, one needs to know the forces acting on Lageos.

A well-known force is that due to solar radiation pressure. The slight pressure of sunlight on Lageos, as well as its interruption when the satellite plunges into the Earth's shadow, are accurately known and included in programs which compute Lageos' orbit.

However, one force overlooked until now is the diminution of solar radiation pressure due to solar eclipses. Here the Moon obscures part (or perhaps all) of the Sun's disk, causing sunlight to weaken and solar radiation pressure to diminish. The reduced force obviously alters Lageos' trajectory differently from that due to full sunlight.

Examination of Sun, Moon, and Lageos position reveals that Lageos suffered 30 solar eclipses between launch and the end of 1983, an average of about four per year. Most of the eclipses had little effect on the orbit. For instance, 23 of the 30 eclipses changed the orbital semimajor axis by less than 2 mm. But the eclipse on December 15, 1982 increased the semimajor axis by 11.2 mm, and the one on March 27, 1979 gave the biggest effect of all, an increase of 17.6 mm. This last eclipse caused an error in Lageos' along-track position to build up at the rate of 1 meter per day, which is significant for Lageos' mission of high-precision measurements. Thus the solar eclipse effect, though small and infrequent, is important enough to include in programs which compute the orbit.

Contact: Dr. D. P. Rubincam
           Code 620

Sponsor: Office of Space Science and Applications

CONSIDERATIONS IN SATELLITE MAGNETIC ANOMALY MODELING OF OCEAN CRUSTAL MAGNETIZATION

Approximately 20 years of very intensive research has been directed toward a quantitative definition of the Thermo-Remanent Magnetization (TRM)—magnetization acquired by certain minerals as they are cooled through their Curie temperature, the temperature above which thermal agitation prevents spontaneous magnetic ordering, and which is frozen in the direction of the ambient main magnetic field) of alternating normally and reversely magnetized blocks of rock paralled to spreading ocean ridges. The outcome of this effort is a global reversal time scale which serves as a basis

for the Continental Drift-Sea Floor spreading hypothesis. Generally, it was thought that TRM was the only coherent magnetization in the ocean crust with all other types of magnetization treated as "noise."

In the late 1960's, however, samples actually drilled from the crystalline basement of the oceanic crust were found to have a different character than previously analyzed rocks which had been dredged from the ocean floor. One of the major surprises and one that is of particular interest in modeling the satellite anomaly field was that some of the rocks had very high intensities of Viscous Remanent Magnetization (VRM)—magnetization acquired or lost by some minerals as a function of the length of time of exposure to an ambient magnetic field at temperatures substantially below their Curie temperature; this magnetization is not as stable as TRM and increases, decreases or changes direction in response to variations in the ambient main magnetic field.

As a result of this observation, a new approach to interpreting and modeling the satellite magnetic anomaly field over oceans is suggested. It appears that the upper 0.5 km extrusive basaltic layer, 2A, is largely and perhaps exclusively responsible for the TRM mentioned above in relation to the magnetic reversal time scale. This magnetization is generally invisible at satellite altitudes because the width of individual magnetic blocks is small, tens of kilometers, relative to the resolution of the data, hundreds of kilometers, so that the normal and reverse magnetizations cancel each other. An exception to the above probably occurs when field reversal activity is low for long periods of time. Massive basalts (diabases), rocks characteristic of the 1- to 2-km thick layer, 2B, are the rocks which were found to have the very high levels of VRM. This layer may provide a general background magnetization in normal ocean crust and anomalous magnetization where it thickens and thins as in oceanic structures such as plateaus. Crustal layer 3, consisting of gabbros (the intrusive equivalent of basalt) and cumulate gabbros and peridotites as well as the layer 4, upper mantle, although not presently sampled, are thought on petrologic grounds to be much less magnetic than layer 2.

Some success has been recently achieved using this scheme in the modeling of oceanic plateaus as well as oceanic crustal plates which are forced under continental plates (subduction zones). In addition, aspects of this approach will be used in modeling the magnetization contrast, or lack thereof, at continent/ocean margins, which lack subduction zones, where the continental crustal thickness is greater than three times that of the ocean crust.
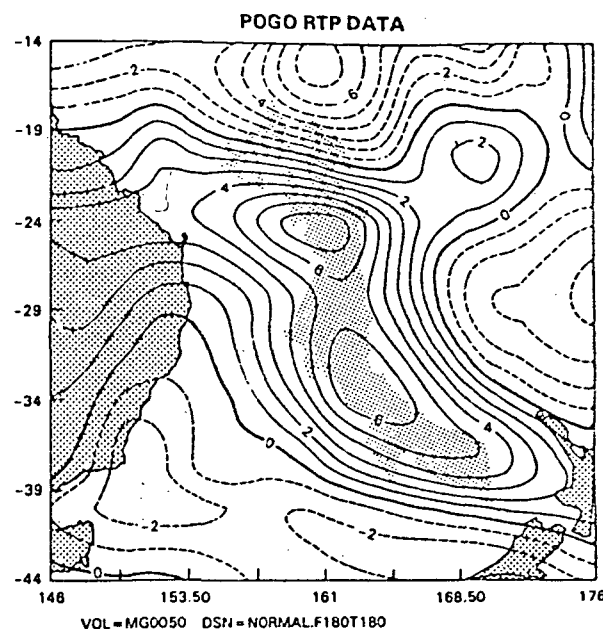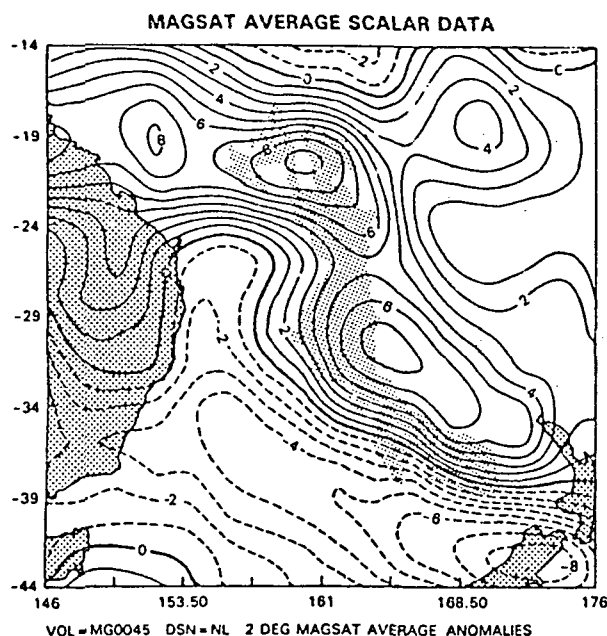
Contact: H. Thomas
        Code 620

Sponsor: Office of Space Science and Applications

OCEANIC STRUCTURES AND MAGSAT ANOMALIES

One of the most enigmatic types of structures on the ocean floor are submarine plateaus, which rise several kilometers above the ocean basins. Several dozen such features are known in the Atlantic, Indian, and western Pacific Oceans. Their origins are sometimes unclear, but two major types seem to exist: submerged slivers broken off from continents and thickened piles of ordinary oceanic crust. Many of these plateaus have satellite elevation crustal magnetic anomalies over them, which are due to changes in the composition and structure of the crust. The Magsat and POGO (Polar Orbiting Geophysical Observatory) data can be used to help clarify the nature of these features. We previously showed that in general plateaus made of thickened oceanic crust should produce relatively strong positive magnetic anomalies at satellite elevation. By contrast, continental fragments in general will produce negative or only weakly positive magnetic anomalies. A general comparison with the dozen best known plateaus showed that most fit the expected pattern, but that there were several interesting exceptions that demanded more detailed study. Such studies have now been completed for the continental Lord Howe Rise and the Ontong-Java Plateau, whose nature is controversial.

The Lord Howe Rise (see the figure) is a known continental fragment broken off from the Australian continent when the Tasman Sea opened. Despite its continental nature, both Magsat and POGO data show a strong positive crustal magnetic anomaly lying over the plateau. Numerical modeling has shown the observed anomaly can be explained if the lowest crustal layer of the plateau has a magnetization which is much higher than ordinary for continental crust. It seems likely the lowest crustal layer was either altered or replaced by denser, more mafic rocks, and this may well be related to the submergence of this continental sliver. By contrast, the strong positive anomaly which overlies the 40 km thick Ontong-Java Plateau is best fit by a model of thickened oceanic crust. This large feature near the Solomon Islands northeast of Australia is probably *not* a continental fragment, despite its great thickness, but represents an accumulation of volcanic material during a period of interrupted sea floor spreading. In this example the satellite magnetic anomaly data provide a clear choice between alternative theories of the origin of the submarine plateau.

Positive satellite magnetic anomalies are also found over many oceanic trenches where the sea floor is being consumed by subduction. We previously showed that the subducted oceanic crust, which remains cold by comparison with the surrounding mantle for tens of millions of years, can produce the observed anomalies at satellite elevation. Using seismic data to constrain the volume and geometry of the

MAGSAT AVERAGE SCALAR DATA	POGO RTP DATA
VOL=MG0045 DSN=NL 2 DEG MAGSAT AVERAGE ANOMALIES	VOL=MG0050 DSN=NORMAL.F180T180

Magsat and POGO data over the Lord Howe Rise.

subducted slab, we have recently successfully reproduced the observed magnetic anomalies over the Aleutian, Middle America and Kuril Trenches. In the Aleutian arc, south of Alaska, the present-day subduction is the cause of the main east-west trending anomaly seen in the Magsat data. A northwest trending spur in the anomaly pattern may be due to a relic slab from a previous period of subduction along what is now the continental margin, prior to 60 million years ago. The Middle America Trench anomaly is well-reproduced by a model incorporating only the present-day subducted slab, although minor improvements in the agreement between observation and model do occur if the effects of surface features in central America are included. The success in accounting for the observed anomalies through models of subducted slabs means the satellite data may be useful in determining the thermal structure of the slab. In particular, if the magnetization of the oceanic crust is known, it should be possible to use the satellite data to determine how far down the slab the temperatures remain low enough for the rocks to still be magnetic. This would help us understand the evolution of the slab during the subduction process.

Contact: H. Frey
        Code 620

Sponsor: Office of Space Science and Applications

MARTIAN VOLCANIC AND TECTONIC FEATURES

Previous studies of the properties of the smallest recognized volcanic cones on Mars showed that these subkilometer features may be similar to a peculiar type of terrestrial volcano found in Iceland called "pseudocraters." Pseudo-craters on the Earth are formed where lava flows out over water or water-saturated ground. The hot lava vaporizes the water and the resulting steam explosion produces the small pitted cone. On Mars no surface water exists, but calculations have shown that surface or near surface ice will produce the same effect. If the small martian cones are ice-volcano products, then their abundant distribution in the northern plains of Mars is an important clue to the past distribution of surface or near-surface volatiles on that planet. We have extended this work to look at the relationship between cone properties (dimensions, distribution) and background terrain, in order to better understand the origin and history of these features.

In the Acidalia region of Mars, volcanic cones with diameters less than 1000 m are found on six different types of plains. Using superimposed impact craters to determine the relative ages of the plains-forming units, we see systematic trends in the properties of cones with age of the background terrain. Cones on the older, fractured plains are generally larger and more widely distributed, and have on average a larger crater/cone diameter ratio than cones on the younger,

smoother plains. The details of these trends appear to be due to a combination of age-dependent erosion and deposition of dust on the martian surface. Over time the smallest cones are preferrentially removed, increasing the mean cone diameter and decreasing the density of cones. Inward erosion of the central crater widens the pit and increases the crater/cone diameter ratio. On one group of fractured plains the cones seem to have been affected by wide-blown dust, which has further reduced their density, raised their mean diameter and altered the crater/cone diameter ratio. These studies provide constraints on the martian climate in the regions where the cones exist which would not be available otherwise.

A fundamental problem in martian geologic evolution is the presence of a major dichotomy between the cratered southern highlands and the sparsely cratered northern lowlands. The boundary between these two major crustal units is as fundamental as that between the continents and ocean basins on the Earth. On Mars it is a complex, sometimes scarp-like feature where tectonic fracturing, mass-wasting, aeolian deposition and stripping, and perhaps volcanism have occurred. Understanding the nature and origin of this boundary is basic to martian crustal evolution. Our photogeologic mapping of specific structures which appear to be characteristic of this scarp has revealed important variations in the nature of this boundary. Broken and detached plateaus, presumably pieces of the ancient highland plateau, occur along some parts of the boundary but are totally absent elsewhere. In some regions these plateaus appear as isolated fragments hundreds to thousands of kilometers north of the apparent scarp.

Knobby terrain, which consists of remnant hills and peaks with perhaps some volcanic features, shows highly variable occurrences along the northward of the boundary. In some regions topography appears to exert control on the distribution of these and other features, but elsewhere where the topogbraphic characteristics are the same, the distribution of these features shows no obvious relation to elevation. Furthermore, many of these "scarp-related" structures are found in other isolated locations around Mars, suggesting that the processes responsible for their development are not confined to the highlands/lowlands boundary.

Contact: H. Frey
         Code 620

Sponsor: Office of Space Science and Applications

DETERMINING SOIL CHEMICAL ANOMALIES FROM PLANT REFLECTANCE

Geobotanical investigations are concerned with the use of plants as indicators of underlying geochemistry of geologic structure. It is felt that satellite remote sensing of terrestrial geology must consider geobotanical phenomena, since two-thirds of the Earth's landmass is covered by some form of higher plant life, and one-third is covered by a continuous canopy of vegetation. A recent investigation has shown some specific effects of anomalously high concentrations of heavy metals in the bedrock on the physiology of plants growing on the overlying soils. Additional investigations have monitored the manifestations of physiological change on the level of the plant community. The changes in plant community dynamics are detectable as changes in the signal received with a remote sensing detector.

A recent field investigation examined the effects of heavy metals on active growing fungal root tips. Tip structures are formed when young roots are invaded by fungi, creating a symbiotic association between the fungi and the living cells of roots known as mycorrhizae. These associations are enormously important to tree species as they greatly increase the root's water and mineral absorption capabilities in addition to potentially preventing further invasion of less desirable fungi. Results of a field study found a significant decrease in the number of active mycorrhizal in soil samples collected within forested areas associated with above-normal concentrations of soil heavy metals, when compared to similar sites with background levels of soil metals. The results suggest that above-normal concentrations of heavy metals adversely affect plant roots and fungal associations, which may then evoke a plant stress response. Since root vitality regulates the vitality of the shoots, metal stress on plant roots may play a fundamental role in the geobotanical responses observed in plant canopies.

One of the canopy responses associated with the presence of soil metal enrichment is the early onset of fall leaf coloration in deciduous trees. Previous results from ground-based leaf collections indicated that premature leaf color changes could be used as an indicator of soil mineralization. Black-and-white aerial photographs filtered for the red band corroborated the previous investigations. Observations in the red part of the spectrum were employed for this study because spectro-photometric measurements suggested that a band from 600 to 700 nm captures the rise in red reflectance characteristic of any leaf undergoing fall color change. The aerial photographs were used to identify two sites characterized by a premature fall color change in an area suspected of containing anomalous concentrations of soil copper. Soil

samples were collected from these two sites and from two additional sites in which the leaf canopy was still green. Geochemical analysis revealed that the sites characterized by premature fall coloration has a significantly higher median soil copper concentration than the other two sites.

A similar study, conducted in the spring of 1983, was designed to test the effects of soil heavy metal concentration on bud break and leaf emergence. In this study bud break and leaf emergence were monitored for three species of oak (*Quercus alba* L., white oak; *Q. rubra* L., red oak; and *Q. prinus* L., chestnut oak) and one maple species (*Acer rubrum* L., red maple). Two locations within a mixed hardwood forest region in the Mineral, Virginia, area were chosen as study sites. The two sites were homologous with the exception that the soil at one location (the mineralized site) contained anomalously high levels of Pb, Cu and Zn with respect to the background site. A delayed bud break of approximately 7 to 10 days, and a concomitant offset in leaf emergence were observed in the oaks (see the figure).

The results of these investigations have contributed to the repertoire of geobotanical techniques and to a deeper understanding of plant-soil interactions. It appears that anomalous concentrations of soil heavy metals impair plant processes at least on the level of tip associations in the plant roots.

Furthermore, the disturbance of physiological processes is expressed on the level of the plant canopy in a retardation of leaf emergence in the spring and a premature leaf senescence in the fall. Research is continuing in the effort to exploit these physiological and morphological effects as remote sensing indicators for geobotanical investigations.

Contact: R. Bell
                Code 620

Sponsor: Office of Space Science and Applications
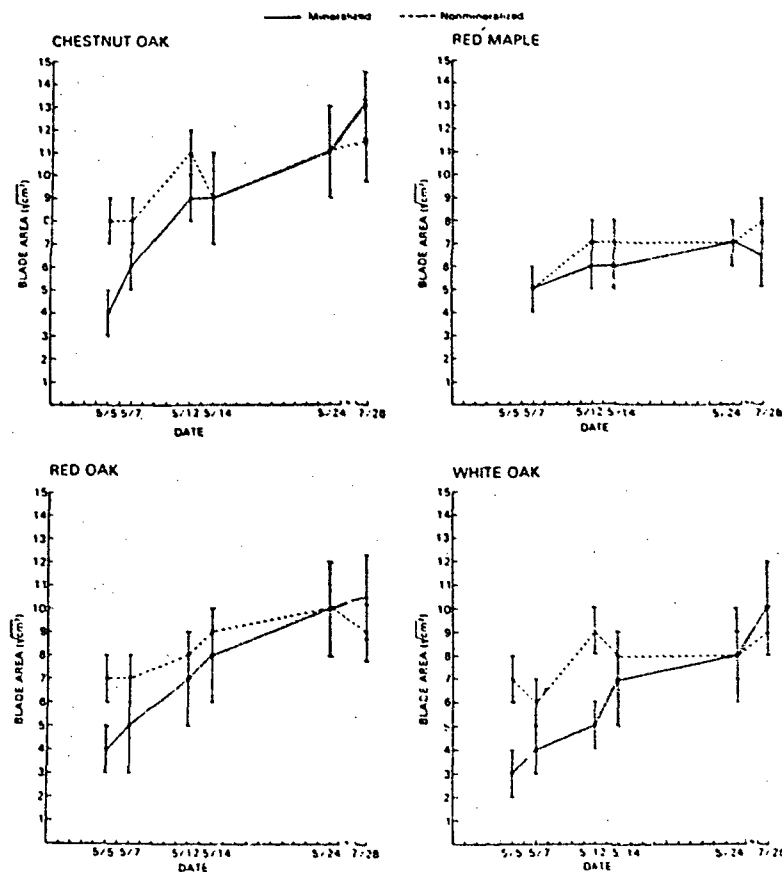
Transformed leaf area versus time.

FIELD STUDIES OF SURFACE COVER REFLEC-
TANCE PROPERTIES

Recently, several studies have clearly indicated that plant canopies do not reflect the incident solar radiation in an isotropic manner (i.e., Lambertian or scattering radiant energy equally in all directions). However, virtually all applications of remotely sensed data (for example, satellite multispectral scanner data) of the Earth's surface make the assumption that such surfaces are Lambertian. This can lead to inaccuracies in the computation of the Earth Radiation Budget from satellite, errors in climate model and plant canopy model computations, etc.

A specialized portable field instrument has recently been designed and built, and field measurements studies have been initiated to begin to better understand the nature of the bidirectional reflectance properties of a variety of vegetation and other surface cover types. This information will eventually enable the accurate computation of Earth surface and planetary albedos using satellite data and make possible corrections to reflectance measurements of Earth features whether measured from a nadir-looking or an off-nadir pointing sensor. This capability and understanding will lead to improved assessments of Earth surface features from spaceborne sensors using off-nadir, multiple angle measurements, such as the French SPOT system or the planned pointable Multi Linear Array sensor to be flown by the U.S. on the Space Shuttle.

The new field instrument is a unique two-axis scanning-head, three-channel (visible, near-infrared, and shortwave infrared; 0.66, 0.83, 1.66 m, respectively) radiometer called the PARABOLA that has been designed, along with a collapsible support boom, to be self-contained and easily transportable to remote sites. The motor-driven instrument enables the acquisition of radiance data for almost the complete (4π) sky- and ground-looking hemispheres in 15° instantaneous field-of-view sectors for all three channels in only 11 seconds.

The initial field measurement studies were performed on several different surface types including bare soil and cultural vegetation, such as tame pasture grass, soybeans, wheat, and corn. Recently, the PARABOLA instrument was flown on a hot air balloon to acquire measurements over forest canopy. The field measurements were taken to encompass a range of atmospheric conditions and Sun elevation. Hemispherical surface albedo computations from these data reveal that when using unidirectional nadir reflectance to estimate the albedo, the error can be as high as 40 percent because of the anisotropic characteristics of the surface. Markedly different and spectral wavelength dependent bidirectional reflectance distribution characteristics were observed for the different types of surface covers.

In addition, different cover types were observed to exhibit quite different bidirectional reflectance characteristics under different atmospheric (haze) conditions. For example, a soybean canopy exhibited a reduced reflectance and an orchardgrass canopy exhibited an increased reflectance in the visible region with an increase in the diffuse/direct ratio of irradiance. Plant canopy architecture, biomass, leaf optical properties, and plant spatial arrangement over the soil background are all important factors in determining the bidirectional reflectance from the vegetative cover. Natural plant communities in various environments representative of the variety of global ecosystems must now be measured to gain the understanding required to adequately interpret and use spaceborne sensor data for global studies.

Contact: Dr. Donald W. Deering
　　　　　Code 620

Sponsor: Office of Space Science and Applications

REMOTE IDENTIFICATION OF PLANT TYPES BY
USE OF LASER-INDUCED FLUORESCENCE
SPECTRA

While current solar reflectance measurements have application to field and remote assessment of vegetational parameters such as total green biomass and canopy cover and have been used with some degree of success for the prediction of crop yield, the technique has difficulty in the detection of plant stress and plant class differentiation. This problem stems from the insensitivity of reflectance measurements to those biochemical and physiological changes (1) resulting from stress and (2) due to species differences. With the exception of reflectance changes due to changes in chlorophyll concentration, the reflectance technique has to rely upon nonspecific factors such as morphology, leaf geometry, vegetation-soil background relationship, relative temporal changes, leaf water, and canopy temperature for indications of stress and plant type.

A technique, amenable to remote sensing use, which could detect changes in the biochemical status of plants subject to various stress conditions and also differentiate plant species on the basis of inherent biochemical differences, exploits the relationship of the mechanism of photosynthesis to the fluorescence yield of the chlorophyll, i.e., the light emission intensity when chlorophyll is excited by light of a shorter wave-length. Measurements of fluorescence due to other plant constituents are also utilized in the technique.

The rationale for the use of fluorescence measurements for determination of photosynthetic efficiency is based primarily upon the mechanism of energy transfer in photosynthesis, i.e., the manner in which light energy is transferred from

the accessory pigments to chlorophyll a and from chlorophyll a to the primary electron acceptors which in conjunction with certain enzymes mediate the synthesis of carbohydrates. The efficiency of this sequence of energy transfer reaction governs the amount of absorbed light dissipated as fluorescence. Thus for a given concentration, the chlorophyll fluorescence is an inverse function of photosynthetic efficiency. The fluorescence intensity of the nonphotosynthetic pigments is a direct function of concentration. Our experiments are based upon the assumption that genetic differences between plant species, and metabolic changes caused by environmental stress should be manifested by changes in the fluorescent intensity due to the various plant pigments. Our studies make use of laser radiation as a fluorescence exitation source — laser-induced fluorescence (LIF).

LIF emission by green plants is being investigated as a possible technique for the remote identification of plant types and species. The technique has been successfully used to identify five major plant types in the laboratory. These included herbaceous dicots, e.g., soybeans, herbaceous monocots, e.g., corn, conifers, hardwoods, and algae. Each of these plant types exhibited a characteristic LIF spectra when excited by a pulsed N=2 laser emitting at 337 nm. Monocots and dicots while possessing common fluorescence maxima at 440 nm, 685 nm, and 740 nm can be differentiated from one another on the basis of the monocot spectra having a much higher intensity at 440 nm relative to that at 685 nm than is observed in the dicot spectra. Conifers have fluorescence maxima at 440 nm, 525 nm, and 740 nm, but none at 685 nm. Hardwoods exhibited fluorescence at 440 nm, 525 nm, 685 nm and 740 nm.

Algae had a very low fluorescence maxima at 440 nm, no fluorescence at 525 nm, a relative very high fluorescence maxima at 685 nm and a maximum at 740 nm. Also in algae, the ratio of the fluorescence intensity at 685 nm to that at 740 nm was much greater than that for monocots, dicots, and hardwoods.

The LIF technique offers potential use for individual species identification.

Contact: Emmett W. Chappelle
　　　　　Code 620

Sponsor: Office of Space Science and Applications

LANDSAT THEMATIC MAPPER: PROVEN PERFORMER

With the launch of Landsat-5 in March, 1984 and the earlier operation of the Landsat-4 instruments, analyses have continued into the characteristics and scientific utility of the sen-
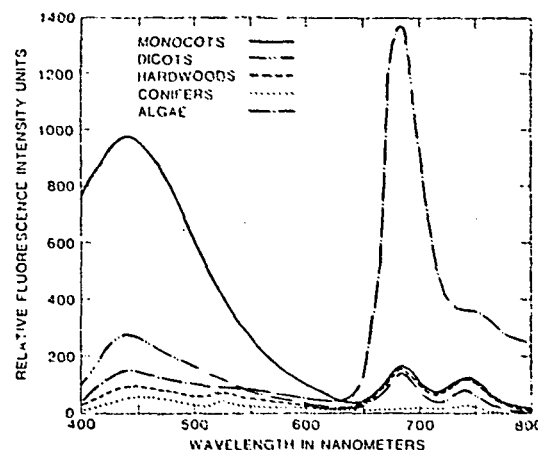
Changes in LIF characteristics of plants following exposure to stress conditions.

sors and their data products. Landsat-5 is essentially identical to Landsat-4, carrying both the advanced Thematic Mapper (TM) as well as the Multispectral Scanner (MSS). A large effort was undertaken to characterize and compare the TM instruments on Landsats-4 and -5 in terms of their spectral, radiometric and geometric characteristics based on both prelaunch and in-orbit data. Analyses have indicated the TM sensors to be excellent radiometers in terms of stability, calibration and overall image quality. Several small sources of radiometric noise have been identified and characterized. Methodologies to reduce the noise are being developed to produce the cleanest possible data for investigators. In general, radiometric noise levels are one percent or less of the full dynamic range of the sensor (i.e., less than two digital counts out of a range of 256 digital counts).

In the science area, the utility of three TM sensor advancements, relative to the MSS sensors, was evaluated. The evaluation was based on land surface feature ('thematic') mapping accuracies (i.e., classification accuracies where land feature classes are urban, agriculture, water, etc.) obtained using TM data acquired over two geographic areas: (1) the vicinity of Washington, D.C.; and (2) western Pennsylvania. The sensor characteristics under study were spectral band configuration (seven TM bands compared to four MSS bands), data quantization (8-bit TM data compared to 6-bit MSS data), and spatial resolution (30 m TM resolution compared to 80 m MSS resolution). For the Washington, D.C. data, the TM band configuration and TM data quantization were responsible for a 9.5 percentage point increase in classification accuracy when results obtained with TM data were compared to results obtained with simulated MSS data. The TM spatial resolution did not contribute to this increase.

For the Pennsylvania data, the TM spatial resolution was responsible for a 16.3 percentage point increase in classification accuracy when results obtained with TM data were compared to results obtained with simulated MSS data. In contrast to the Washington, D.C., data, TM spectral band configuration and data quantization did not contribute to the improved accuracy obtained with Pennsylvania TM data.

These contrasting results indicate that the utility of a particular TM sensor characteristic is highly dependent on the geographic area viewed by the sensor. In Pennsylvania, the land feature classes of interest were spectrally distinct in the four MSS visible and near infrared spectral bands. The new TM spectral bands and increased data quantization were not necessary to achieve class separation. The classes, however, occurred in small fields and TM data were required to effectively resolve these fields. In Washington, D.C., the land feature classes occurred in larger areas which could be well resolved by the MSS. The TM spatial resolution may have actually increased confusion between classes resolving class components (e.g., the grass lawns, asphalt and cement streets, and rooftops of a suburban class). The MSS resolution simplified the situation by integrating the reflected radiance from class components to generate a less variable spectral representation of each class. The Washington, D.C.,

classes, however, were not spectrally distinct within the MSS spectral bands. The new TM spectral bands, particularly the two middle-infrared bands, and the increased data quantization were needed to increase the spectral contrast between classes. The research with the TM data from these two areas indicates that TM data are generally more useful than MSS data for thematic mapping. The source of the utility, in terms of sensor characteristics, depends on the spectral and spatial attributes of the land surface feature categories within a particular geographic area.

The research also indicates that the prevalent methodologies for thematic mapping do not fully exploit the advantages Lof the TM spatial resolution. The increased resolution clarifies shapes, sharpens boundaries, and accentuates the textural appearance of categories. These advantages are visually apparent in a comparison of MSS and TM imagery of Washington, D.C. (see the figure). Alternate approaches to thematic mapping which exploit these image characteristics are currently under development and evaluation.

Contact: Brian Markham
        Code 620

Sponsor: Office of Space Science and Applications

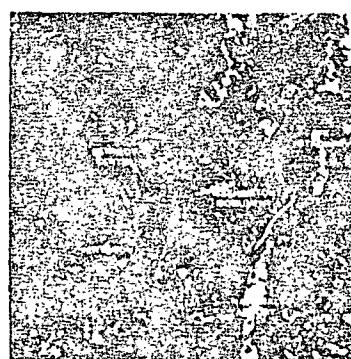## COMPARISON OF SIMULTANEOUSLY COLLECTED LANDSAT-4 TM AND MSS DATA OF WASHINGTON, D.C. (11/2/82)

THEMATIC MAPPER SUBIMAGE

MULTISPECTRAL SCANNER SUBIMAGE

512 BY 512 PIXELS

256 BY 256 PIXELS

NOTE: EACH IMAGE REPRESENTS AN AREA APPROXIMATELY 9 MILES BY 9 MILES.

Comparison of simultaneously collected Landsat-4 TM and MSS data of Washington, D.C. (11/2/82)

RADIANT SCATTERING BEHAVIOR OF VEGETATION

Fundamental research efforts have improved our physical understanding of radiant scattering in vegetation canopies. This has been accomplished through the analysis of both model simulation data and field directional reflectance data in the visible and near infrared wave-lengths. The directional scattering behavior of vegetation has been described and explained for various solar zenith angles, and various canopies with different densities, leaf orientation distributions, and optical properties. The work has been in response to providing an intelligent basis for defining specifications of Earth observing sensor systems and for inferring important aspects of physical and biological processes of the plant system.

During the past year hand-held radiometers have been used to measure the directional reflectance characteristics of natural vegetation canopies ranging from bare soils to complete canopies with 100 percent ground cover. Bands similar to the NOAA Advanced Very High Resolution Radiometer (AVHRR) Band 1 (0.58 to 0.68 μm) and Band 2 (0.73 to 1.1 μm) were used in data collection. The cover types reported were a plowed field, annual grassland, steppe grassland, hard wheat, salt plain, and irrigated wheat. The annual grassland, steppe grassland, and salt plain had unique geometric structures (plant clumping and leaf orientation distributions) that were extreme as compared to the vegetation types reported in the literature. Strong anisotropic trends were documented. The largest variations in reflectance with changing view angle occurred at large solar zenith angles for bare soils and grasslands with very low vegetation covers. As vegetation densities increased and the solar zenith angle decreased, reflectance variations decreased. The dynamics of the directional reflectance distributions were analyzed and physical principles responsible for the observed dynamics were proposed. Past studies have demonstrated that the normalized difference transformation [AVHRR (Band 2—Band 1)/(Band 1 + Band 2)] is useful in monitoring green vegetation biomass. A difficulty in utilizing AVHRR data that scans out to 56° is that the signal for any particular target can change significantly with various view angles. It was demonstrated, however, that this transformation generally decreased the directional variation of the signal. However, there were exceptions. For each remote sensing application the user should be aware of these variations for the specific cover types being studied, solar zenith angle and scanning direction of the sensor with respect to the solar azimuth.

A three-dimensional radiative transfer model was developed and is unique in that it predicts (1) the directional spectral reflectance factors as a function of the sensor's azimuth and zenith angles and the sensor's position above the canopy, (2) the spectral absorption as a function of location within the scene, and (3) the directional spectral radiance as a function of the sensor's location within the scene. It is one of two existing models with such general three-dimensional capabilities. This 3-D model was expanded to include the antisotropic scattering properties of leaves as a function of the leaf orientation distribution in both the zenith and azimuth angle modes. The model was applied to complete vegetation canopies of various leaf orientations—erectophile (mostly erect leaves), planophile (mostly horizontal leaves), spherical (equal probability of all leaf orientations), and heliotropic (Sun-tracking leaves). It was found that these canopies had unique reflectance distribution characteristics which were supported by the field measurements. The dynamics of these distributions were physically explained by directional scattering effects of two mechanisms. The first mechanism causes the characteristic "bowl" shape of complete canopies that is—increasing reflectance with increasing off-nadir view angle for azimuth directions. It is caused by shadowing gradients and view projection gradients within the canopy. The second mechanism is the primary directional scattering of the leaves (phase function) due to leaf orientation, source direction, and leaf transmittance and reflectance values. The combination of these two mechanisms in the various canopies are responsible for the dynamics of the overall shape of the directional reflectance distributions.

Fundamental knowledge of the physics of the scattering behavior as gained in this study is important. This growing body of knowledge will ultimately serve the remote sensing and Earth science community in many ways. For example, it will provide (1) insight and guidance in developing new extraction techniques or evaluating the robustness of existing extraction techniques of canopy characteristics, (2) a basis for better interpretation of off-nadir satellite and aircraft data, (3) a basis for defining specifications for future Earth observing sensor systems, and (4) a basis for defining important aspects of physical and biological processes of the plant system. Such fundamental knowledge is very important to the long-term advancement of remote sensing and Earth science programs.

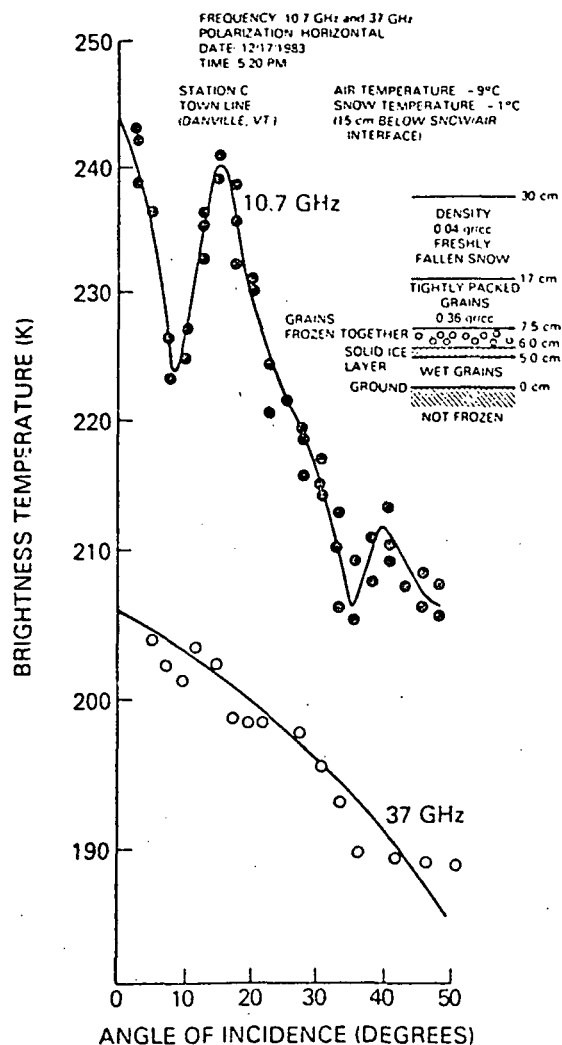Contact: Dr. Daniel S. Kimes
            Code 620

Sponsor: Office of Space Science and Applications

MICROWAVE FIELD MEASUREMENTS OF SNOWPACK PROPERTIES

The ever-increasing demand for water throughout the world imposes a challenging problem for water resources managers. A conservative estimate of future needs indicates an increase

of 3 to 5 times the present demand by the year 2000. Since snow represents an important source of the water supply, improved knowledge of snow water storage over large regions should improve the estimate of spring runoff and lead to better management of the water resources.

Microwave measurements have the capability to penetrate the snowpack and respond to variations in subsurface properties. They provide the only means to sense the snow depth or water equivalent information under nearly all weather conditions.

FREQUENCY 10.7 GHz and 37 GHz
POLARIZATION HORIZONTAL
DATE 12-17-1983
TIME 5.20 PM

STATION C
TOWN LINE
(DANVILLE, VT)

AIR TEMPERATURE -9°C
SNOW TEMPERATURE -1°C
(15 cm BELOW SNOW/AIR INTERFACE)

Microwave brightness for snowpack with embeded ice layers

Microwave radiation emitted from the ground beneath a snowpack is attenuated and scattered by the snow crystals. The effect of scattering is proportional to the size of snow crystals which is dependent on the age of snow. The emanating radiation measured by radiometers is used to infer internal snowpack properties. Observations from spaceborne radiometers have been used for areas with uniform snow cover such as the Great Plains of the U.S. with some success. A significant regression relationship (at 95 percent confidence level) has been achieved for retrieving snow depth over homogeneous areas. One of the challenging aspects in retrieving snow parameters is to understand the inhomogeneity of the snowpack caused by the different phases of metamorphism of the snow. This process normally produces vertical variations in the snow density and ice layers. To study this problem microwave brightness temperatures of snow at frequencies of 10.7, 18 and 37 GHz were measured by truck-mounted radiometers in Vermont last winter. Preliminary results indicate that the brightness measured at different incidence angles reveal the interference effect between ice layers. This effect is clearly displayed at the 10.7 GHz observations. However, at 37 GHz the interference is not very distinguishable due to strong scattering of snow crystals (see figure). By using multifrequency techniques, it is possible to study the age and evolution of the snowpack due to different weather conditions, as well as the snow depth. This is important in extending our understanding on the interaction of snow covered surface with the Earth climate system.

Contact: A. T. C. Chang
         Code 620

Office: Office of Space Science and Applications

CANOPY TEMPERATURE AND TRANSPIRATION MODELING

A soil-plant-atmosphere model (see figure) for calculating canopy temperature and transpiration was developed which is usable in conjunction with remotely sensed infrared radiometric observations to understand spatial and temporal variabilities of transpiration and surface temperature. Remotely sensed surface temperatures can also be used to understand and quantify plant stress resulting from soil water shortage. The model is semi-dynamic, in that the dynamics of soil and plant tissue water are predicted but the plant is assumed to be in steady state with respect to its water balance and energy balance. Soil evaporation and drainage are included, and also the atmospheric stability corrections for the aerodynamic resistance. Input data for the model are hourly meteorological data,

soil hydraulic properties, and plant characteristics (albedo, extinction coefficient for net radiation, plant height and stomatal diffusion resistance). It is a physically based model and it explicitly recognizes the plant physiologic control in water extraction from soil by the roots and water transpiration from leaf stomata. Plant-to-plant differences in soil water extraction and transpiration are predicted by the model.

The model has been tested extensively against published data and empirical results. Empirical results for the dependence of canopy temperature on air vapor pressure deficit are predicted well by the model, and so, also the observed diurnal variation of leaf water potential (which is the force exerted by the leaves to extract soil water). Under clear sky conditions the canopy-air temperature difference is largely determined by the relative humidity: the effects of wind speed and radiation are comparatively weak. Different plants react to humidity quite differently.

The model was used to study the sensitivity of transpiration to plant root distribution, since it was realized that concur-

rent to any remotely sensed canopy temperature, the information about the root distribution may not be available. The study showed that the rooting depth was the most important rooting characteristic for its affect on transpiration and canopy temperature. Quantitatively, a 10 percent error in rooting depth could lead to 20 to 30 percent error in estimating daily transpiration. Further sensitivity study using the model is in progress.

A simplified version of the soil-plant-atmosphere model is also being studied for simulating evapotranspiration of large areas on a global basis as part of an atmospheric general circulation model.

Contact: Bhaskar Choudhury
         Code 620

Office: Office of Space Science and Applications
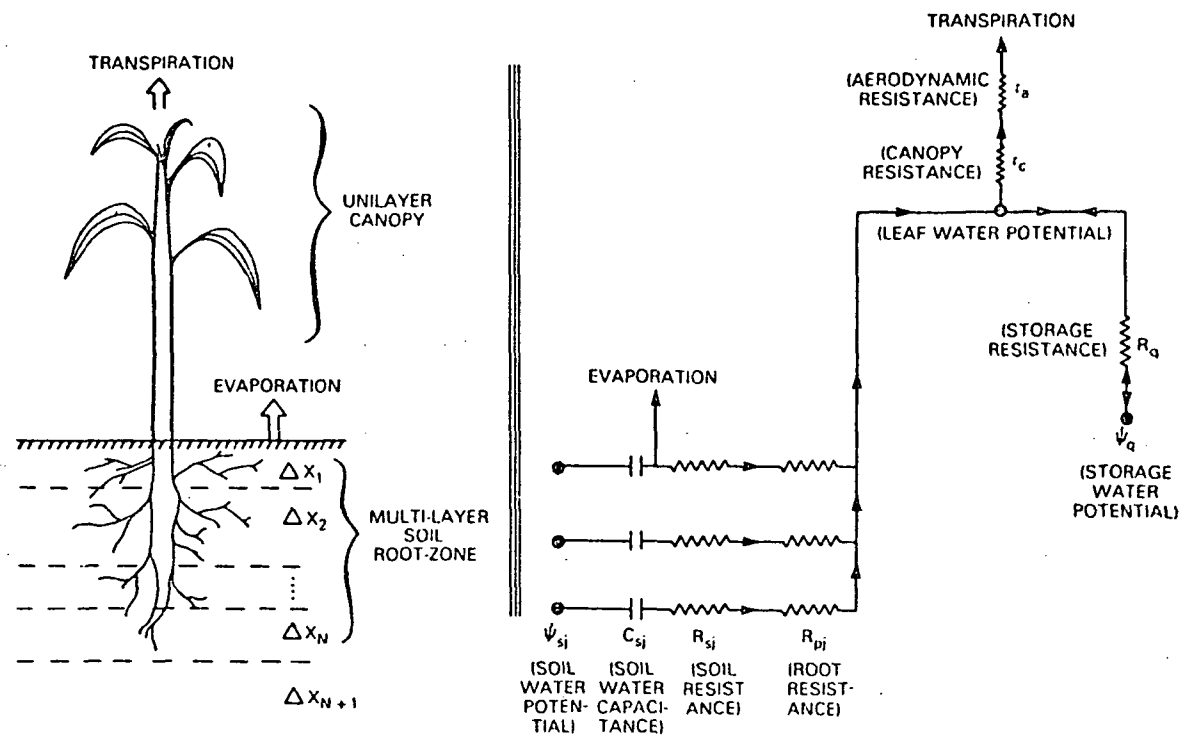
Schematic illustration of the model.   The flow of water is indicated by arrows and it is represented via Ohm's law as an electrical current.   The model solves for the leaf water potential which satisfies a water balance equation for the canopy.

VEGETATION ANOMALIES AS OBSERVED BY RADAR

Previous studies of Seasat Synthetic Aperture Radar and, more recently, Shuttle Imaging Radar-A images have indicated a significantly higher L-band (23.5 cm wavelength) radar return from mature corn whether standing or recently cut (Figure 1a) and from certain forest areas. In the case of corn, this high return diminishes over a period of one month following combining, a form of harvesting, which leaves the stalks randomly scattered over the soil surface. From the data available a correlation was found between the wavelength of the radar and the stalk's nodal separation. Detailed measurement of both moisture and density in different portions of the corn stalk at various stages of growth indicates relatively uniform water distribution during the growing stage. At maturity, flow diminishes rapidly causing the stalk to dry while the water content remains high in the nodes. At the time of cutting, volumetric water in the nodes is three times the water in the intervening stalk. Thirty days after being cut the ratio reduces to one. The enhanced radar response is thought to be due to the nonuniform concentration of water acting like a dipole antenna which creates a high return which diminishes as the stalks dry.

Generally, radar response from taller vegetation (e.g., trees) is bright due to scattering from woody trunks and branches. In forested areas, with standing water beneath the forest canopy, the radar return is brighter. This is due to the forward scattering from the vertical trunks being specularly reflected at the water surface. Figure 1b is a SEASAT SAR image of Cedar Island in Pamlico sound on the North Carolina coast. The brighter areas on the right and left sides are forests. The less bright area in between is flooded marsh on wind roughened open water. Normally the flooded marsh would be dark due to the grass keeping the water surface smooth. The increased backscatter from the marsh area may be due to water on the vegetation resulting from rain within an hour of the overpass.

There is also an SIR-A image of this area available in which these backscatter differences are more pronounced, i.e., the marsh area is very dark and the forest area on the right is very bright due to flooding at high tide. Much more documented imagery must be collected, at various wavelengths, to determine if other frequencies would respond the same way over selected vegetation. These additional data would help resolve the numerous and interesting questions raised by these observations.

Contact: Bruce J. Blanchard
Code 620

Office: Office of Space Science and Applications
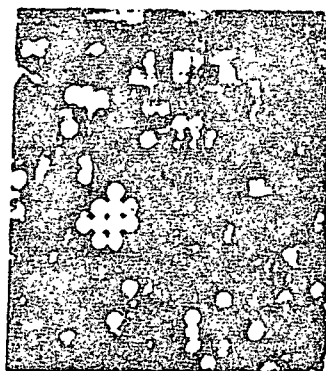
A

SIR-A

REV 17 11/13/1981
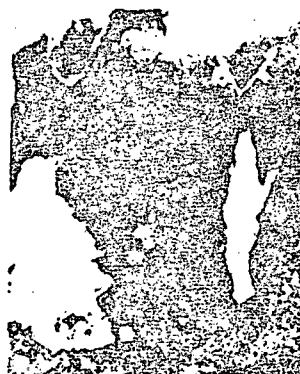
B

SEASAT SAR

REV 400 7/25/1978

Figure 1. A. All bright circular areas coincide with mature or recently combined corn. As time after combining increased the radar response decreased. B. Vegetated areas appear brighter following a recent rain. The forested areas are brightest and might be interpreted as flooded while marsh vegetation in the lower center might be interpreted as dry forest. Unless one knows about recent meteorological events misinterpretation can easily occur.

TECHNOLOGY

Technology programs at GSFC are directed toward providing advanced technology for the development of new sensors, for spacecraft subsystems, and for the extraction of information from the data obtained in space missions. Efficient and reliable tracking, communications, and data acquisition are essential for NASA flight operations if they are to meet their mission objectives. GSFC is pursuing several programs to develop new techniques for the tracking, acquisition, and handling of data from future flight programs.

SPACE TECHNOLOGY

TECHNOLOGY FOR FORECASTING PERFORMANCE OF HIGH VOLTAGE INSULATION

High voltage (many kilovolts) power supplies are required for a wide range of scientific and application payloads on NASA missions. During the past several years, work at the Goddard Space Flight Center has focused on the development of nondestructive test techniques of high voltage components and assemblies to enhance performance and reliability of kilovolt level power supplies for space application. The techniques make use of the partial discharge (P.D.) phenomena associated with high voltage breakdown.

A stepwise ramp technique has been used successfully in D.C. partial discharge testing on high voltage components and on resin-packaged high voltage devices. Data is acquired during a 10 second ramp to ¼ rated voltage (V_r) followed by a 2 minute pause; then data is acquired for 100 seconds at the ¼ V_r plateau. This is followed by ramping to ½, V_r, and so on, and so forth, to V_r. For test specimen intended for D.C. service, this ramp method gives more information about insulation integrity then purely quiescent D.C. measurements. This is especially true for specimen of high resistivity which causes the discharge frequency to be deceptively low at constant D.C. By contrast during ramping upwards, the spacecharge has not yet been established, the voltage distribution is capacitive, and the P.D. behavior resembles that of an A.C. test. This gives many more pulses in the voids, and without the undesirable heat produced if 60 hz A.C. were applied.

The equipment used consists of a commercially available P.D. detection system and corona-free high voltage power supply to 60 KV D.C., into which the test specimen is hard wired. The output P.D. pulses are coupled via buffer amplifier to a multichannel analyzer which counts the pulses acquired over the desired time span, sorts them out as to charge content in picocoulombs (pc), and also integrates the total charge stored. Measurements are carried out in an electrically shielded room, and the samples can be immersed in electronic insulating liquid or high vacuum during test. Figure 1 shows the facility and also the types of parts and passive assemblies to which this technique is applicable.

Extended studies were conducted on potting materials with different resistivities. With resistivity of 10^{16} ohm-cm (perfect) samples no pulses appeared on ramping until about 20 KV/mm (500 volts/mil) field strength, but low resistivity resins (10^{11} ohm-cm) had many pulses even on the rise to 5 KV/mm (125 volts/mil). Material samples containing intentionally placed gaseous voids had high charge content P.D.'s of several hundred to several thousand pc's. Thus one could interpret P.D. signatures of resin-potted image tubes such as the Faint Object Camera (FOC) tube: the better electrical potting resin could be chosen, the test applied at progressive stages of potting and some large voids could be demonstrated in a front-end witness sample.

Many types of commercial high voltage capacitors used in kilovolt power supplies were tested using the ramp P.D. technique. Figure 2 shows two contrasting P.D. histograms obtained with this method. The one with many discharges

up to and above 400 pc comes from a mylar foil, hollow air-filled capacitor which is unsuitable in the vacuum of space. The capacitor with very few low level discharges is a solid, resin impregnated mica unit which has flown successfully.

Life tests at 85°C and rated voltage on several types of capacitors and on material samples have been completed and subjected to the P.D. test before and after. These tests demonstrated a good correlation between samples that showed a high initial P.D. activity and samples that failed during life tests. It was noted that some capacitors with high level of P.D. activity also would have been rejected by a rigorous screening test consisting of visual inspection, dielectric withstand voltage (DWV), capacitance and dissipation factor measurements.

The P.D. test technique has proven to be a more sensitive measurement for determining the insulation integrity of a component or assembly. Adding this technique offers an acceptance/rejection criteria improvement of several fold over that currently available. Work is continuing on coils and transformers to determine if the P.D. technique is equally applicable to these devices.

Contact: R. Bever
            Code 711

Sponsor: Office of Aeronautics and Space Technology

BAD CAPACITOR

TOTAL NUMBER OF PULSES = 47624

$\Sigma n_i q_i$ = 537,127 PC

MYLAR FOIL, HOLLOW
MAN G, CYLINDER
10,000 PF, 8 KV
CALIB 2 5 - 400 PC
0 -- 8 KV
IN 40 SEC

NUMBER OF PULSES (N)

0   400

INCREASING CHARGE CONTENT OF PULSES → PC

GOOD CAPACITOR

TOTAL NUMBER OF PULSES = 44

$\Sigma n_i q_i$ = 434 PC

RESIN-IMPREGNATED MICA
MAN U
C = 10,000 PF, 8 KV
CALIB 2 5 - 400 PC
0 -- 8 KV
IN 40 SEC

NUMBER OF PULSES (N)

0   320 PC

INCREASING CHARGE CONTENT OF PULSES - PC
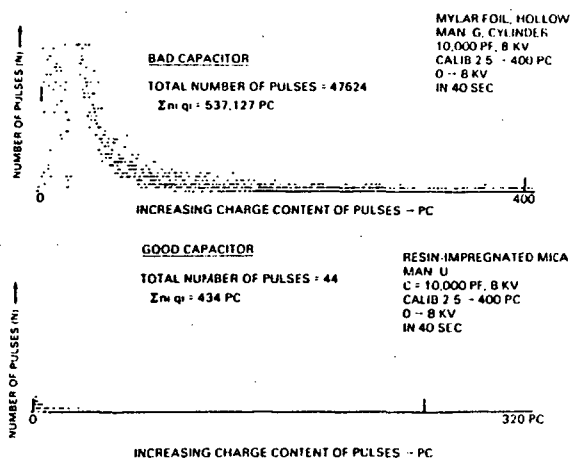
TECHNOLOGY FOR FORECASTING PERFORMANCE OF HIGH (KV) VOLTAGE FLIGHT EQUIPMENT

PARTS

MATERIALS

ASSEMBLIES

ENCAPSULATING &
POTTING POLYMERS

CAPACITORS
CABLES
CONNECTORS

POTTED IMAGE
TUBES AND
IMAGE TUBE STAGES

COILS
TRANSFORMERS
(10 WAY A C - JPAY P C)

HIGH VOLTAGE
D C. PARTIAL DISCHARGE
TEST FACILITY
(TO 60 KV DC IN AIR
DIELECTRIC LIQUID OR VACUUM)

POTTED
ELECTRONIC
ASSEMBLIES
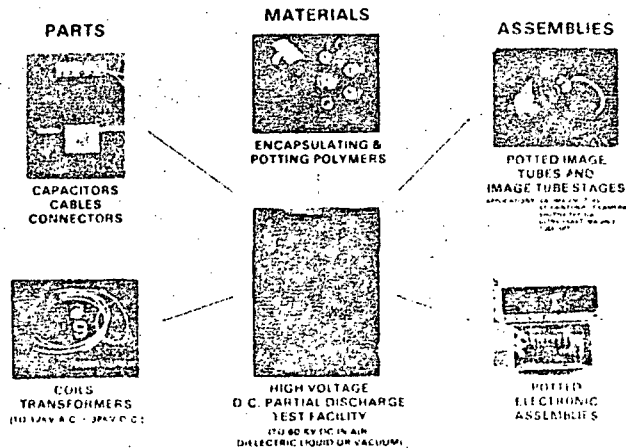
Technology for forecasting performance of high-voltage (kV) flight equipment.

SUPERFLUID HELIUM-POROUS PLUG TESTS

A large number of present and future space missions (IRAS, COBE, SIRTF, SPACE-LAB 2's IRT, GP-B, LDR) require cooling detectors or entire instruments with superfluid helium (temperature < 2.17 Kelvin). To maintain a relatively constant low temperature, evaporating helium must be vented to space, but at the same time the liquid must be contained within a dewar without the aid of gravity. The porous plug accomplishes these objectives by acting as a phase separator between superfluid helium and helium gas. We have tested the porous plug to be used in COBE as well as similar plugs in carefully controlled environments to simulate their behavior under various conditions. From this testing and concurrently developed theory derived from the two-fluid model of superfluid helium, we have been able to better understand the behavior of the porous plug.

The phase separating ability of the porous plug derives from the unique properties of superfluid helium. To understand these properties, the two-fluid model has long been used. The model considers liquid helium below the lambda point to be made up of two interpenetrating fluids; one normal having nonzero viscosity and entropy, and one superfluid having zero viscosity and entropy. The densities of the two components ρ_n and ρ_s sum to the total density and vary with temperature such that at $T = o$, $\rho_s/(\rho_s + \rho_n) = 1$, and at $T = 2.17K$, $\rho_s/(\rho_s + \rho_n) = o$.

One can use this model to explain *Figure 1* Two reservoirs A and B containing superfluid helium are connected through a tube. If one applies heat to reservoir A, The normal component of the superfluid will flow to B carrying entropy (heat), while the superfluid component will backflow to A keeping the density constant. If one now interposes a porous medium in the connecting tube the following will take place. The superfluid component will still flow from B to A as before unimpeded by the small pores because of its zero viscosity. However, the porous medium will greatly impede the flow of the normal component from B to A. The pressure which drives the liquid from B to A is given by $P = s T$ where is the total density, s the specific entropy of the helium and ΔT the temperature difference between B and A. This pressure is called the thermomechanical or fountain effect pressure and can attain a value as high as half an atmosphere. If we allow reservoir B to deplete, we have the situation in Figure 1 (d). In this case, B represents a vent line to space and A a dewar.

The porous medium remains wet with superfluid helium despite the thermomechanical effect because surface tension forces give rise to capillary action. Under conditions of high heat flow, large ΔT's and hence large thermomechanical pressures are generated across the porous plug. In that situation, the thermomechanical force may overcome the surface tension force and the gas-liquid phase boundary would move from the outer surface into the plug. This would be observable as a sharply increasing

$T_A = T_B$

(a)

$2.17 K > T_A > T_B$

(b)

$\varrho g h = \varrho s (T_A - T_B)$

(c)

POROUS PLUG
ACTS AS
PHASE SEPARATOR

(d)
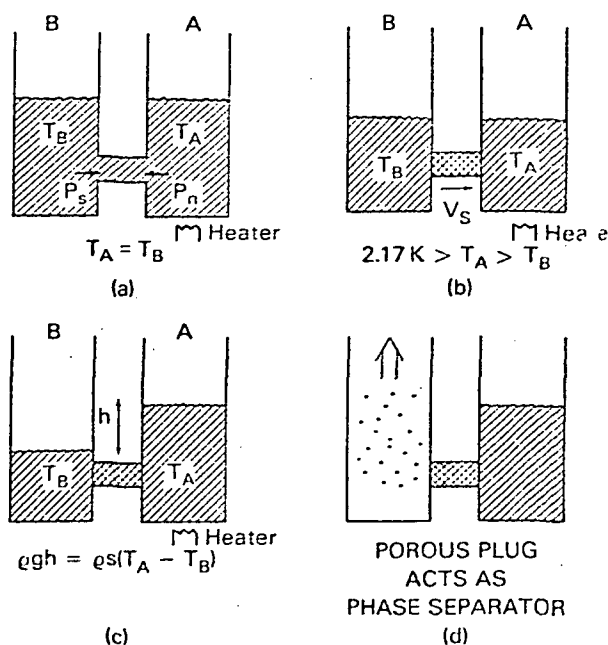
Contrasting histograms obtained with the ramp PD technique.

pressure and temperature drop across the plug, the gas being a less efficient mass transporter or thermal conductor than the superfluid helium. Based on room temperature flow measurements on the plug material, an effective pore diameter was obtained which along with the pore density and length was used to determine the points at which the phase separation boundary would retreat into the plug. Precision measurements made in our lab (schematic in Figure 2) verify these predictions to a remarkable degree considering there are no adjustable parameters in the calculation. We are also able to predict the temperature drop across the plug based on the two-fluid model in the region below this phase boundary retreat. Our calculations agree with the measured values within 10 percent.

We have also made measurements on a plug under minus one g conditions, to confirm that film flow out of the porous

plug in zero g will not be a problem. Our data show that an additional film flow of at most, only 4 percent of the nominal flow for COBE may be present.

An offshoot of the porous plug superfluid helium containment studies has been a proposal to use this effect to pump superfluid helium out of a supply dewar to refill a facility dewar in space. Electrically supplied heat on the outside of the porous plug would force the superfluid out. While the thermomechanical pump has been used in many laboratories for moving small amounts of superfluid helium, this would be the first large scale application of the effect.

Contact: M. DiPirro
Code 713

Sponsor: Office of Space Science and Applications
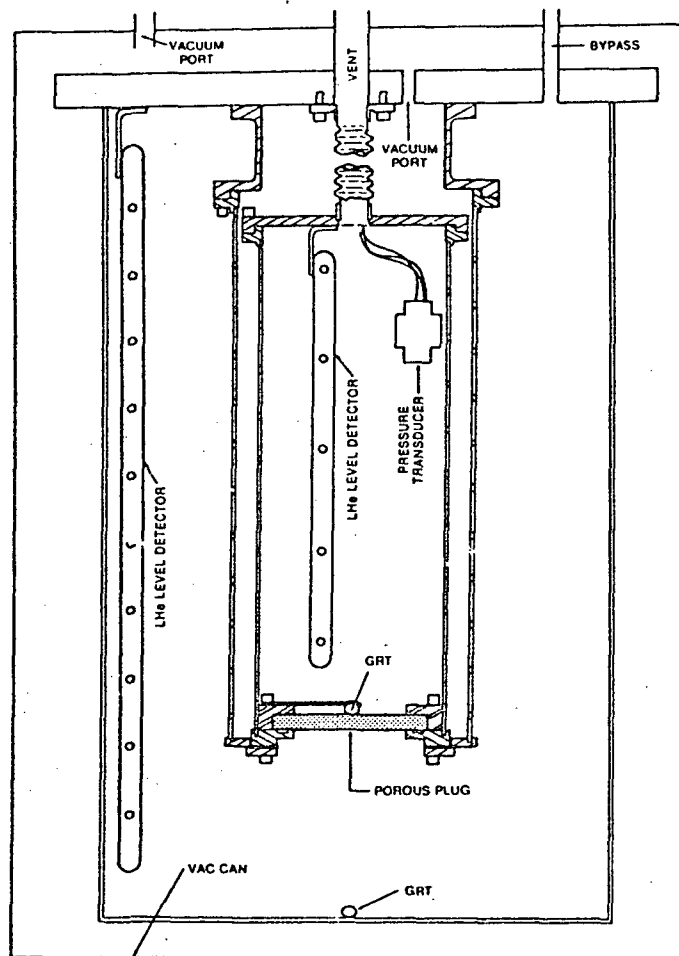
Schematic of porous plug test setup.

LONG-LIFETIME CRYOGENIC REFRIGERATOR

Many space instruments require ultralow temperature cooling to perform their measurements. Several Goddard Space Flight technology programs are underway to fulfill this need. Of particular importance is the development of an ultralow temperature (cryogenic) refrigerator that will operate in space for 3 to 5 years without maintenance.

The first unit of the new refrigerator, known as the Proof-of-Principle model Stirling Cycle Cryogenic Cooler, successfully completed 11,000 hours of operation on August 30, 1984. Running silently at an average speed of 25 cycles/sec., it generates 5w of cooling power at a temperature of 65 °K when its compression heat is rejected at 300 °K. Its reciprocating components work without conventional bearings, seals, or lubricants because they are levitated and centered by magnetic bearings. A closed-loop servo system controls the position of the free-floating pistons. Linear motion is provided by moving magnetic linear motors of a new design. Since there is no friction and wear, the operating performance of the cooler has not changed.

The second generation cooler known as the Technology Demonstration Model is being designed to meet shuttle mission requirements. The launch specifications necessitated improvements in: electromagnetic bearings, axial and radial position sensors, structural design of the moving elements, and the axial counterbalance. As in the first generation refrigerator, organic contamination has been eliminated by the use of all metal and ceramic construction. Reductions in system input power result from an integral magnetic displacer spring/motor and more efficient linear motors and drive electronics.

Ferrite variable reluctance position sensors provide improved temperature stability of the magnetic bearing control system. Additional bearing improvements are realized through increases in: gas film damping, AC/DC force capabilities, and structural resonant frequencies. Improved Linear Variable Differential Transformers (LVDT's) provide high frequency capabilities to the axial control systems. All clearance seal surfaces are specially treated to eliminate potential damage due to contact during launch and shipping. Transmitted vibrations are minimized by 6-degree of freedom spring mounts between the refrigerator and spacecraft. The counterbalance, a tuned spring mass system driven by a linear motor and supported radially by magnetic bearings, cancels the unbalanced axial force generated during operation.

Contact: Mr. Max Gasser
       Code 713.1

Sponsor: Office of Aeronautics and Space Technology
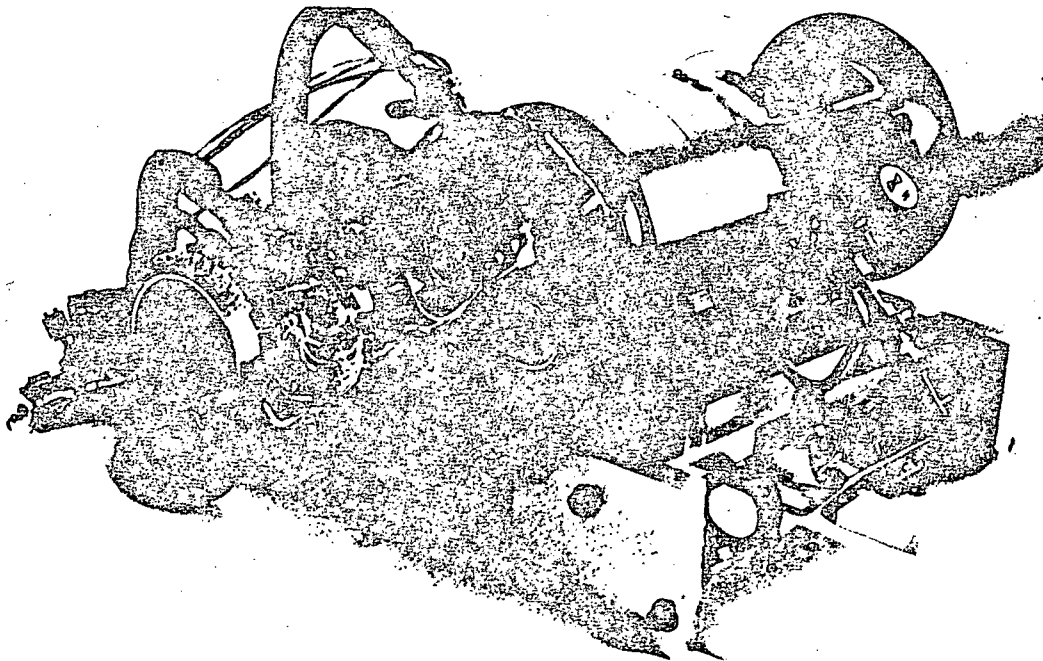
Proof-of-Principle. Model stirling cycle cryogenic cooler on a test stand with vacuum DEWAR removed.

HOPKINS ULTRAVIOLET TELESCOPE GRATING

The Hopkins Ultraviolet Telescope (HUT) is one of three spectroscopic flight instruments that will be flown on the ASTRO series of space shuttle missions. This telescope is designed to record far ultraviolet spectra from very faint cosmic sources. Included in the optical system of HUT is an ultraviolet spectrograph that has a 600 gr/mm grating which disperses the ultraviolet light into its respective wavelengths.

This grating is difficult to fabricate because of its size (20.5 cm diameter) and short 40 cm concave radius of curvature. There are, in general, 2 methods of fabricating diffraction gratings; conventional and holographic. The conventional method is achieved by using a diamond (of specified geometry) to burnish grooves into a material such as aluminum that has been evaporated on a substrate. For the holographic method, two intersecting beams from a single longitudinal mode laser are used to produce interference fringes that expose a photosensitive material (photoresist) deposited on a substrate, which, when processed produces grooves in relief. Several attempts by industry to rule this grating by the conventional diamond burnishing technique failed. This failure was attributed to the difficulties in moving the diamond tool and maintaining a proper groove profile (blaze angle) because the grating substrate had a very deep sag from a plane surface.

Since the conventional ruling method failed to produce a grating, HUT investigators from Johns Hopkins University came to the Goddard Space Flight Center and asked if we could fabricate the required grating. After a careful analysis of the grating parameters, we did successfully rule a high quality 600 gr/mm reflecting diffraction grating for the HUT Spectrograph.

Since this grating was difficult to fabricate even when using the holographic technique, production of a replica grating was attempted and successfully achieved by Bausch & Lomb Corporation from the master holographic grating. The replica grating was coated with osmium and evaluated at a near normal incident angle. The results of the evaluation showed a remarkable absolute efficiency of 6.0 percent in first order from 87 nm to 19 nm as measured by Johns Hopkins University personnel. The other remarkable feature of the grating was its near constant efficiency across the grating surface. For example, the efficiency did not change by more than 1.0 percent from one side to the other when measured at 1.8 cm increments through the center of the grating.

The production of this grating by holographic techniques represents a significant advance in the fabrication of large,

fast focal ratio diffraction gratings for use in the vacuum ultraviolet spectral region. At least 2 more replica gratings will be produced on stainless steel substrates from the master holographic grating. These replicas will be used as spares for HUT and the AIRES sounding rocket version of HUT.

Contact: Anthony J. Caruso
        Code 717

Sponsor: Office of Space Science and Applications

DIAMOND PROVIDES IMPROVED PERFORMANCE FOR 15-W S-BAND SEMICONDUCTORS

High reliability improved performance 5 cell 15 watt S-Band silicon bipolar semiconductors have been successfully developed utilizing type IIA diamond instead of beryllium oxide as the heat spreader. The need was brought about by continued difficulty in acquiring high rel, high power amplifiers such as previously used on ATS-6, GOES D, E, and F, and IUS, and now for GOES G and H satellites.

With the utilization of diamond as a heat spreader for high power S-Band silicon bipolar semiconductors, designers can now operate their non-derated transistors at a flange temperature (T_F) of 70°C without exceeding a junction temperature (T_J) of 125°C.

Type IIA diamond is one of the best electrical insulators with a thermal conductivity four times better than pure copper at 100°C as shown in Figure 1. Note the thermal conductivity of BeO which up to now has been the prevalent heat spreader material utilized. In terms of improvement with respect to electro-migration the device lifetime is improved by a *factor of four*.
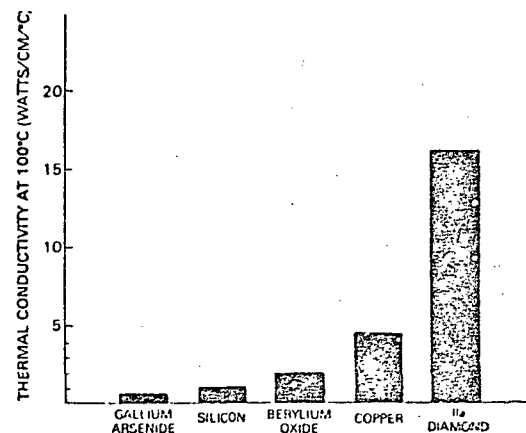
Comparison of thermal conductivity of solid state materials

Figure 2 illustrates T_j and O_j as a function of T_f for both types of semiconductors. The major goal was to be able to operate a non-derated improved transistor at a flange temperature of 70°C without exceeding the NASA/GSFC maximum T_j specification limit of 125°C. The thermal resistance (O_j) was calculated using the RF and DC data obtained at each test point of the T_j graph.

Graphs are available that compare the actual RF output power versus RF input power with T_f held at 43°C. The output was rematched at each input level for maximum Pout. Each curve represents the average of the three best devices of each type. Notice the standard devices are saturated at an input level of 3.5w, whereas the diamond devices appear to finally saturate at 5.7w, an overdrive condition of 2.0 dB. But even more important than the increased overdrive capability is that in the past it has been accepted that it was the *silicon* (in the die) that caused saturation to occur. This phenomenon appears to indicate that the thermal conductivity of the heat spreader plays a more important function than previously thought in determining how rapidly saturation occurs.

The improvement in the range of linear operation apparently due to the improved thermal control of the junction by the diamond heat spreader is certainly worth investigating for applications requiring linear amplifiers.

Another area which would likely benefit even more than silicon bipolar devices is the GaAs Power FETs. Their microwave reliability at this time is not near as well established as high power bi-polar are. Due to the smaller size of the higher frequency FETs the cost of the heat sinks would also be less. Programs are being formulated to include type IIA diamond investigations to FET's.

Contact: Larry Line
Code 727

Sponsor: Office of Space Science and Applications

MONOLITHIC 128 ELEMENT LEAD SULFIDE/MOS INTEGRATED CIRCUIT

Lead Sulfide (PbS) is a photoconductive material whose resistance changes in response to light in the 1 to 3 micrometer near infrared. It is one of the oldest and most reliable detectors in this wavelength region and has applications not only in space missions but many medical, commercial and defense oriented instruments. The general method of instrumenting these detectors is to deposit PbS on a substrate and physically bring the two terminals off of the device. Then by either hybridizing or by discreet solder methods, the electronic components are wired to the detector to form the sensor unit.
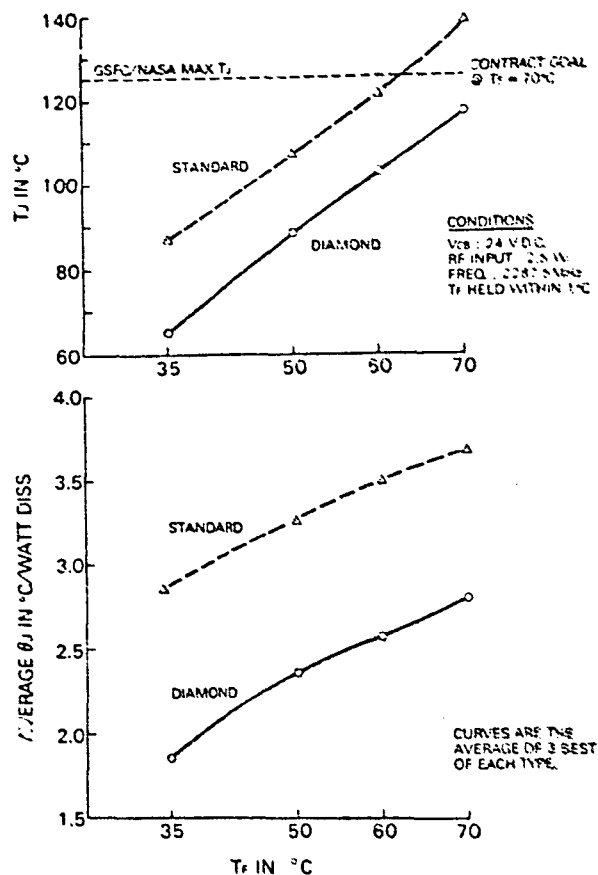
Figure 2. *Junction temperature (Tj) & thermal resistance (θJ) vs flange temperature (T_f)*

In order to improve the reliability, electronic signal processing and the pixel density a method for chemically depositing PbS directly on a P-Channel Metal Oxide Semiconductor (PMOS) integrated circuit has been developed. Initially one detector element was deposited on a single PMOS transistor forming a simple source-follower preamplifier circuit. The unit performed comparably to state-of-the-art detector assemblies that were available.

A second generation development consisted of an eight element array with sixteen transistors which when properly operated would sequentially multiplex the eight detector signals to a single output channel. This unit exceeded other lead sulfide assemblies by multiple integration of elements with active transistor devices.

A third and most recent development was the integration of 128 detector elements each with an approximate dimension of 18 micrometers by 25 micrometers. The electronics on the chip were based on the PMOS integrated circuit
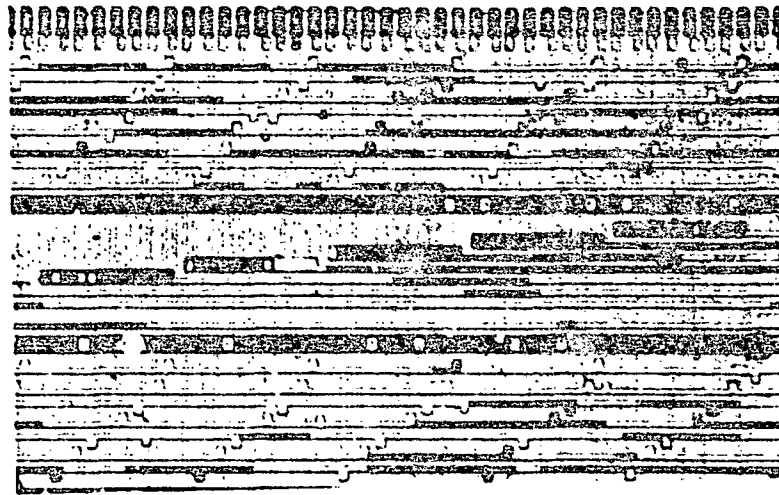
Photomicrograph of a segment of chip, showing the PbS elements and some electronics.

technology utilizing depletion mode resistors. The circuitry includes two 8 bit multiplexers, 16 commutators, 8 counters, and 3 decoders, approximately 1000 active devices, all on a 0.16 x 0.16 inch silicon ship. The on-chip electronics is operated with a ±8v supply and an external clock. Each detector element is sequentially connected to a single output channel and its signal is amplified. Due to the 300 microsecond time constant of PbS all 128 elements are interrogated in 4.0 milliseconds. A photomicrograph of a segment of the chip showing the PbS elements and some electronics is shown in figure. The metallization is gold rather than the conventional aluminum due to the strongly basic solution from which PbS is precipitated.

Other modifications to the standard PMOS technology were developed to ensure processing compatibility of the PbS deposition with MOS integrated circuitry. The ultimate application of this device will be for imaging in the near IR.

Contact: M. Jhabvala
            Code 724.1

Sponsor: Office of Space Science and Applications

ADVANCED THERMAL MANAGEMENT SYSTEMS DEVELOPMENT

New thermal transport systems are required for applications on a Space Station where high power sources can be remotely

located from their heat rejection surfaces. Conventional systems, such as those used on the Shuttle, utilize large energy consuming pumps to circulate a liquid for energy transport. As a replacement for these pumps, new devices are under development which use the surface tension forces established in a fine pored capillary wick to drive the liquid.

These devices called capillary pumps, require no power and have no moving parts that could wear out. By using common refrigerants with a high heat of vaporization, such as freon or ammonia, energy can be transferred at nearly a constant temperature. This allows a user of the system to place equipment anywhere in the loop without concern for temperature variation. An engineering model of a Capillary Pumped Loop (CPL) was assembled at GSFC. It consisted of a set of eight capillary pumps nested under a cold plate to simulate a user interface.

These pumps were connected through a transport loop to a condenser plate 10 meters away. The heat transport loop was operated over a variety of temperatures, power levels and sink temperatures to simulate space conditions. As can be seen from the accompanying figure, the evaporator temperature is constant while power is applied and the heat sink, representing the orbital environment, varied over a wide range. This system has been successfully tested with heat inputs totaling almost seven (7) kilowatts and heat sink temperature variations of +20°C to -20°C. The Capillary Pumped Loop represents the first evaporating/condensing system built by NASA for use on large orbiting spacecraft.
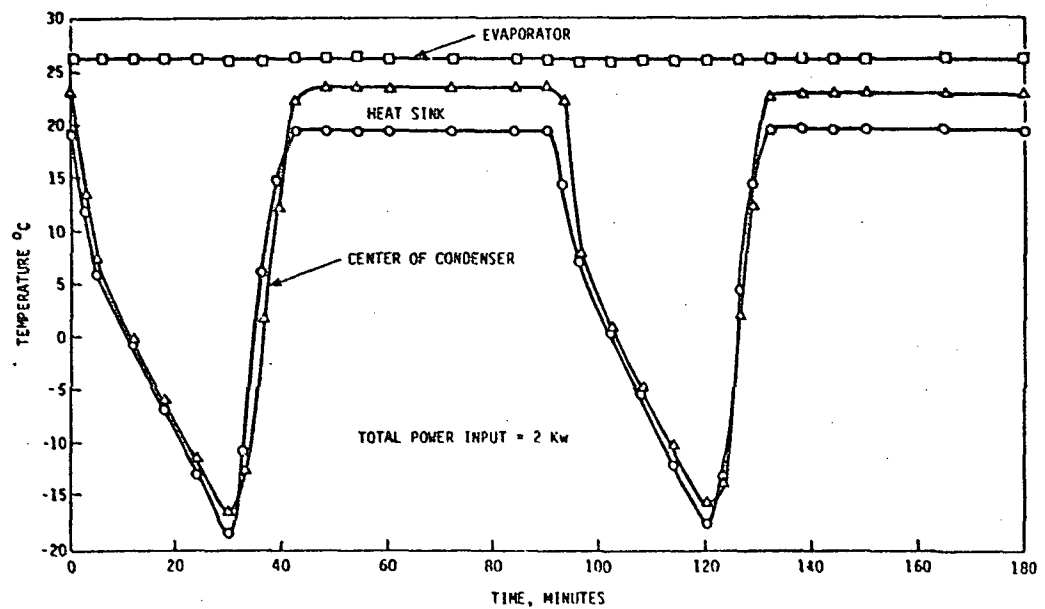
Temperature control with respect to heat sink temperature variations.

It is hoped that a prototype system will evolve which will be flight tested on Shuttle prior to incorporation into the design of the Space Station.

Contact: Stanford Ollendorf
Code 732

Sponsor: Office of Space Science and Applications

IUE TWO-GYRO CONTROL CAPABILITY

The International Ultraviolet Explorer spacecraft was joint-
ly developed by NASA, the European Space Agency ESA,
and the British Science and Engineering Research Council
SERC. IUE is an astronomical facility—a space telescope
which because of its geosynchronous orbit can be readily
operated by astronomers familiar with ground observatory
techniques. IUE is in its seventh year of successful opera-
tions and demand by the astronomical community for obser-
ving time on the telescope exceeds available time by a wide
margin.

The sub-arcsecond attitude reference needed to precisely
point and re-orient the spacecraft is provided by an iner-
tial reference assembly. This IRA consists of a set of six
state-of-the-art pulse-rebalanced gyroscopes with the at-
tendant control electronics, capable of sensing an angular
motion of as little as 0.01 arcseconds.

Between the launch date January 1978 and July 28, 1982
three of the six gyros of the IRA failed, each for a different
reason. The spacecraft requires a minimum of three operating
gyros to achieve its designed pointing capabilities. At the
present time, IUE is operating on its remaining three gyros
and obtaining slew accuracies of 2 arcminutes over large
angles and pointing accuracies of 0.25 arcseconds (exceeding
the design requirement of 1.0 arcsecond).

Because of the continuing demand for the spacecraft, NASA
intends to continue operating IUE even in the event of another
gyro failure. To this end, the Guidance and Control Branch
at the NASA Goddard Space Flight Center has designed,
developed and tested an IUE control system which will fly
the spacecraft using only two gyros and a Fine Sun Sensor.
This system effectively substitutes a 15-arcsecond sensor (the
FSS) for a 0.01-arcsecond sensor with little degradation of
performance. Spacecraft fine pointing for science observa-
tions and orbital velocity adjustments for station-keeping are
under the control of the NSSC-1 computer onboard IUE. Im-
plementation of the two-gyro control laws to support both
of these functions consisted of much assembly language
coding and optimization for speed and memory. The resulting
flight software was proven on the Bench Integration and Test
Facility at GSFC. The flight software system was delivered
to the Orbiting Satellites Project in January 1984 and is
available for uplink to IUE in the event of another failure.

Contact: M. Femiano
        Code 712

Sponsor: Office of Space Science and Applications

SOUNDING ROCKET PAYLOAD MAGNETIC ATTITUDE CONTROL SYSTEM

A newly-designed magnetic attitude control system for spin-
ning sounding rocket payloads has been developed at the
GSFC/WFF. This magnetic attitude control system (MACS)
permits the orientation of the payload spin-axis along the local
magnetic field lines and has wide application. This system
is an improvement of an earlier design, developed in 1981,
and allows effective operation over a wider range of spin
rates (0.5 to 3.0 cps). A magnetic test facility was establish-
ed at the WFF to test the MACS.

The newly-designed system uses a 2-axis magnetometer and
a lateral axis rate gyro to input the electronics. The elec-
tronics and nozzle-driver circuits were extensively redesigned
and have resulted in improved system performance; the
pneumatic design is unchanged from the earlier system. The
system uses two lateral cold-gas jets, oriented 180-degrees
apart in roll. Nitrogen and Argon gas have been utilized in
the system. The electronics, pneumatics manifold and
thruster nozzles were specifically designed for lightness and
compactness; the entire system, including gas tank, is pack-
aged into a volume roughly 10 inches high by 17 inches
diameter and weighs approximately 40 pounds. This new
control system was successfully flown in February 1984, on
simultaneously-launched rocket vehicles at two launch sites
near Fairbanks, Alaska and Fort Yukon, Alaska. The con-
trol systems successfully oriented and maintained both
payload's spin-axis to within one-half degree with respect
to the local magnetic field lines during flight. Spin rates for
the two systems were 1 and 2 cycles per second, respectively.

Contact: L. Warren Gurkin
        Code 1000

Sponsor: Office of Space Science and Applications

ELECTRICALLY CONDUCTIVE THERMAL CONTROL COATINGS

Development of a suitable coating for particle detector win-
dows required a closure that would cause little attenuation
of the incoming radiation, have an electrically conductive
outer surface to minimize charge build-up, and have suitable
optical properties to provide temperature control in space.
Starting with 0.1 mil Kapton or Mylar as the basic substrate,
trial vapor deposited coatings of low weight and low absorp-
tance/emittance ratios were investigated.

A successful procedure was developed for vapor depositing
thin coatings (100A to 200A) of Chromium or Titanium on

0.1 mil films of Kapton or Mylar which have an opaque (1000A) coating of Aluminum on the reverse side. The thin layer of Chromium causes an interference effect which raises the emittance of the coating from a low normal emittance value of En = 0.23 to a high value of En ≥ 0.62. This high emittance value is necessary for heat rejection purposes since the detectors are normally operated at cold temperatures. The Chromium or Titanium layer also has a low resistivity value of < 10K ohm/square which is sufficient to prevent electrical charge build-up that could damage the detectors.

These coatings have been qualified for flight use with respect to ultraviolet radiation. Samples were tested for an equivalent 1000 sun hours and found to be resistant to degradation both physically and electrically. Extrapolated results from thicker films suggest that these coatings will also be resistant to solar wind protons (3 keV) and high energy electrons (1 meV).

Contact: J. Henninger
         Code 754

SENSORS

LONG WAVELENGTH (15-30 μm) HETERODYNE COMPONENTS

Components are being developed for use in infrared heterodyne spectrometers for the study of electromagnetic radiation from remote sources at wavelengths between 15 and 30 μm. Infrared photomixers (HgCdTe photodiodes) and lead salt (PbSnSe) diode lasers are being developed.

Theoretical modeling of the optimum structure, composition and operation temperature regime for 30 μm HgCdTe photomixers was done. Using these results actual devices were fabricated with a sensitivity 4 times the ideal at 16 μm (NEP = 5×10^{-20} W/Hz) and 1 GHz bandwidth. Photomixers operating at wavelengths up to 30 μm have been fabricated with measured sensitivity 33 times ideal (NEP = 2.3×10^{-19}) and a flat heterodyne response to at least 500 MHz. Operating temperatures were 20 K.

Broad area PbSnSe diode lasers have been fabricated to operate up to 30 μm with total power output of several hundred W in a single mode. Individual lasers emitted many modes of radiation over a spectral range >100 cm^{-1} (depending on temperature) and each emitted mode could be continuously tuned over 1 cm^{-1}. Operating temperatures ranged from 13 to 40 K. Long term reliability of these devices has been demonstrated with reproducible device characteristics measured over a three year period. The first mesa-stripe geometry diode lasers operating between 25 and 30 μm have been developed. This device structure can permit higher temperature operation (several lasers operated above 70 K) and improved mode structure and tunability.

Most recent improvements consisted of a narrow mesa-stripe (20 μm wide) and short cavity length (120 μm long) geometry. This led to individual lasers emitting 500 W

of multimode power, 112 W in a true single mode and single mode operation over a greater laser tuning range above threshold than was previously achieved at these wavelengths.

The above photomixers and lasers have been tested in a 30 μm infrared heterodyne radiometer built for this purpose. Recently the first heterodyne measurements using several of the developed devices were made. A detector heterodyne quantum efficiency of 3 percent was measured at 28 μm on a 400°C black body with a resultant system NEP = 8×10^{-19} W/Hz. The system bandwidth was measured to be flat to 500 MHz. The system sensitivity was mainly limited by low diode laser local oscillator power and excess laser noise.

These first effort heterodyne components yielded a system performance 110 times ideal. This work is a first step in the ultimate development of coherent instruments for passive spectroscopy of remote molecular sources at 15 to 30 μm.

Contact: Dr. Theodor Kostiuk
         Code 693

Sponsor: Office of Aeronautics and Space Technology

MINIATURIZED ACOUSTO/OPTIC SPECTROMETERS

The development of very high frequency heterodyne receivers for use in astronomical research has created a need for wide bandwidth and high resolution intermediate frequency (IF) spectrometers. Often the receivers operate in the millimeter and submillimeter wavelength ranges in which high altitude platforms, such as aircraft, balloon, or spacecraft, are needed to escape from severe attenuation from telluric water vapor or other molecules. These receiver

packages have limited volume, weight and power to devote to backend processing. Conventional RF channelized filters, in which adjacently tuned discrete RC filters are used, cannot meet the severe weight, volume, and power requirements of a space-borne instrument.

Acousto-optic techniques offer an elegant way to provide wide bandwidth and high resolution in a small, lightweight, and low power package. An acousto-optic spectrometer (AOS) contains a small number of components; a coherent light source like a HeNe laser or a GaAs diode laser, collimating and focusing optics, a Bragg cell, and a linear array of photodetectors. The IF signal is fed into the Bragg cell where the RF power is converted to acoustic waves by a set of transducers. The sound waves modulate the index of refraction of the Bragg crystal so that a collimated coherent beam of light is diffracted at an angle which is dependent on the frequency of the RF signal. Also the amount of light diffracted is proportional to the amount of power at that particular frequency. When the diffracted beam is focussed on a linear array of detectors, the output of the array is the IF power spectrum we seek. The array output is often digitized and further digital integration is performed to increase receiver signal to noise. AOS's have been constructed both in-house at Goddard and by Litton ATI under contract to Goddard. The in-house effort has concentrated on obtaining first hand experience with the problem of stability and sensitivity of AOS as applied to astronomical applications and to develop high speed circuitry to use as digital processors for digital integration and Dicke switching. The GSFC AOS has 300 MHz bandwidth with 600 KHz resolution and is packaged in a 19 inch rack-mounted package. The GSFC contract to Litton ATI concentrated on obtaining wide bandwidth performance in a very small package. The Litton ATI's miniaturized AOS (mAOS) is housed in an 8 inch by 4 inch by 4 inch package and has 700 MHz bandwidth with 5 MHz spectral resolution. Even higher performance can be expected from future development from Litton ATI since a 1 GHz bandwidth 1 MHz resolution mAOS in the same size package as the 700 MHz system is now feasible.

Contact: Dr. Gordon Chin
        Code 693

Sponsor: Office of Aeronautics and Space Technology

THE IMAGING X-RAY SPECTROMETER

The Imaging X-ray Spectrometer is a solid-state silicon detector using "deep diodes" through the wafer formed by thermomigration of aluminum. Thermomigration is a method in which temperature gradient diffusion is used to drive aluminum posts through a silicon substrate with a lateral spread of a few percent (less than 5 percent) of the substrate thickness. The first such X-ray detectors were designed, fabricated, and tested at the Goddard Space Flight Center (GSFC). The detector array is unique because it offers both good energy and spatial resolution for the analysis of X-rays in the 1 to 20-keV range. Because the aluminum posts go completely through the detection substrate, the complete thickness of the wafer can be depleted, leading to high quantum efficiencies for X-rays in the 1 to 10-keV range. The quantum efficiency is a function of the silicon thickness. The thickness of the wafers to be used is only limited by the ability to drive posts because depletion voltages are now independent of substrate thickness. To date, good posts have been driven through 1300 micrometer wafers. Spatial resolution is attained by forming a grid structure surrounding individual thermomigrated aluminum posts. In the middle of each pixel is a post which forms the electron collection terminal for the individual pixel. An array of greater than 100 pixels, 1 mm^2 per pixel, is planned for the AXAF mission.

The critical parameter of interest is the noise level of the detector system. This noise level is measured by utilizing a Pulse Height Analyzer (PHA) spectrum of the 5.9 Kev Mn alpha line. The Full Width Half Maximum (FWHM) of the peak (in ev's) is considered the noise level for the detector system. Total noise has dropped from 2.25 keV in the early stages of research to our present value of about 250 ev. Of this 250 ev, about 190 ev was due to the detector while about 150 ev was due to the electronics. Improvements in on-chip integration of electronics and detector arrays should reduce system noise levels. Process and material changes are expected to further reduce the noise level of the detector. On chip integration of the electronics is being performed by CAD of amplifier systems in NMOS silicon gate technology to attack the electronics noise level.

An important factor is the available pixel size. Detector development using 7000 ohm-cm material has increased the pixel size so it is no longer a problem. The 700 micron pixel size described is readily obtained at voltages of 100 volts. Research is continuing to further reduce system noise levels and provide maximum integration.

Contact: George Alcorn
        Code 724

Sponsor: Office of Aeronautics and Space Technology

INFRARED ARRAY CAMERA DEVELOPMENT

Advanced spaceborne infrared scientific instruments implemented to date have used single element detectors or modest groups of single detectors. These instruments employ

the state-of-the-art in single element detectors and are represented by the IRAS and COBE survey spacecraft. The immense success of the IRAS survey has underscored the importance of the follow-on mission, Space Infrared Telescope Facility (SIRTF).

An advanced infrared array imaging camera system, applicable to the SIRTF observatory, has been under development at the GSFC. The system schematic representation is shown in Figure 1. An Aerojet Electrosystem extrinsic silicon array, accumulation mode charge transfer device, was used as the sensor. To minimize stray light and allow diffraction limited imaging, cold apertured reimaging optics were used in the dewar along with cold spectral filters covering the 8 to 13 micrometer wavelength atmospheric window. The camera electronic system includes an analog signal processor (to amplify, filter, and digitize the signals from the dewar), a digital signal processor (to preprocess the images) and a general purpose minicomputer (to control the data acquisition and storage). Extensive software has been developed for the array camera system. Digital preprocessing functions include snapshot, film clip, and co-add functions. Several engineering and science operating mode programs have been developed including observational programs such as a real time imager, a picture arithmetic program, a data acquisition program and a noise analysis program. Recently this instrument has been used to generate the highest resolution maps in the infrared of the Galactic Center. These observations and observations of many other objects has presented very convincing arguments for considering infrared array imagers for the next generation of spaceborne infrared instruments.

As a result of this effort a team of co-investigators including the Smithsonian Astrophysical Observatory, the Goddard Space Flight Center, the University of Arizona, the University of Rochester, and Ames Research Center has been selected to develop a Wide Field Imaging Camera for the SIRTF observatory.

Contact: G. Lamb
           Code 724

Sponsor: GSFC Director Discretionary Fund and
           Office of Aeronautics and Space Technology
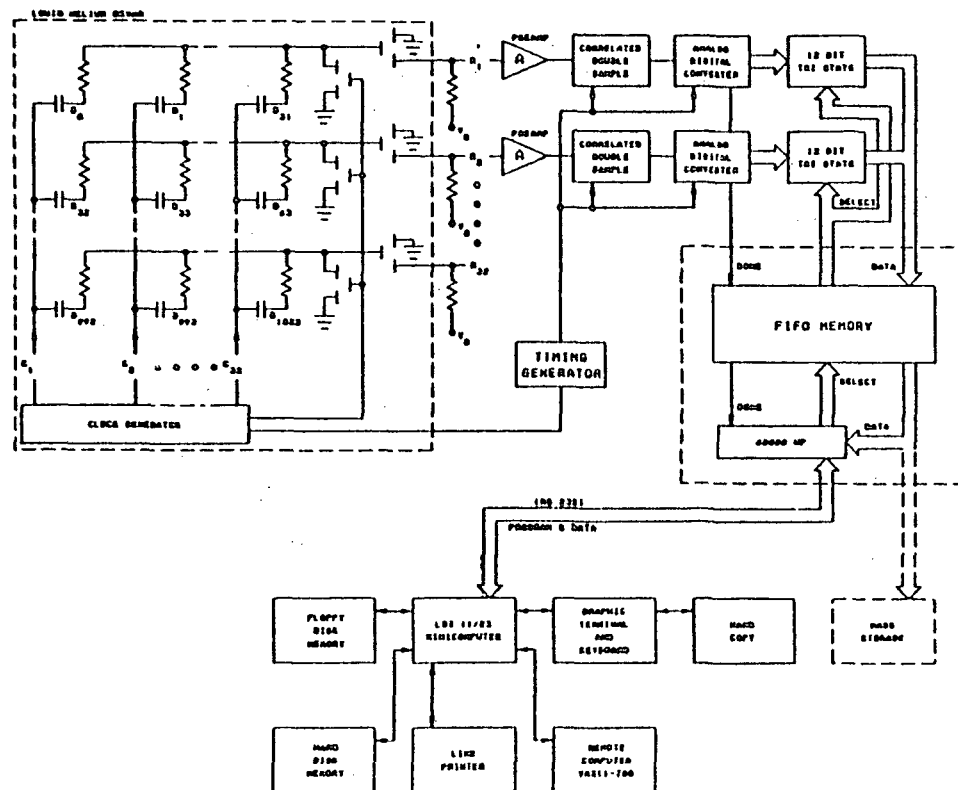
Infrared camera system diagram.

LIDAR MEASUREMENT OF THE ATMOSPHERIC PRESSURE PROFILE

Significant improvements in the measurement of the basic atmospheric parameters are required for improved weather forecasting, the prediction of climate change, and increased understanding of atmospheric processes. Measurement of the atmospheric pressure field is one of the basic requirements. Previously, there have been no current remote sensing techniques for measurement of the pressure field. Thus, important forecasting tools such as maps of surface pressure and 500 mb height contours must be produced either by *in situ* measurement or by indirect methods.

We have recently made the first accurate remote measurements of the atmospheric pressure profile. A differential absorption lidar system was used to make upward looking measurements of pressure as a function of altitude. The integrated absorption in the wings of lines in the O_2 A band provides a sensitive method for measuring the atmospheric pressure profile. Absorption troughs, regions of minimum absorption between two strongly absorbing lines, were used to make the measurements. This technique, which we developed, greatly desensitizes the measurements to the effect of laser frequency instabilities.

The pressure measurements were made with a ground based lidar system that uses a high resolution solid state Alexandrite laser and a high resolution dye laser to generate the pressure sensitive trough absorption and reference frequencies. An energy monitor measures the outgoing laser energy at each frequency to obtain the information needed for an integrated path absorption measurement of pressure. A high resolution etalon is used to periodically monitor the laser line shape, and a multipass oxygen absorption cell is used in conjunction with a relatively low resolution (0.1 cm^{-1}) spectrometer to set the laser frequency.

The energy backscattered from the atmosphere is collected with a 45-cm telescope and is detected with a high efficiency GaAs photomultiplier tube. Separation of the on-line and off-line laser pulses is accomplished by introducing a small time delay (100 μs) between the two laser pulses. A single detector channel is then used to observe both wavelengths.

The Alexandrite laser in our system is the highest resolution tunable pulsed solid-state laser ever employed for atmospheric measurements. It is continuously tunable from 720 to 790 nm with a bandwidth of 0.02 cm^{-1}. The laser has a frequency stability of 0.005 cm^{-1}, a pulse length of 130 ns, and an output energy of up to 100 mJ per pulse at a 10 Hz repetition rate.

An example of upward-viewing profiling measurements made with our ground-based lidar system is shown in Figure

1. The lidar system was set up to measure pressure with the on-line laser tuned to an absorption trough near 760 nm and with the reference laser tuned to a nonabsorbing frequency near 759 nm. The lidar signal returns were sampled with a 50 ns range gate (7.5 m vertical integration) and averaged over 100 shots. The figure shows a comparison of the lidar measured pressure profile above GSFC (latitude N 39.00°, longitude W 76.85°) to radiosonde data taken 1.5 hours earlier at Dulles Airport (latitude N 38.98°, longitude W 77.46°). Data were averaged to a 45 m vertical resolution to improve the signal-to-noise ratio. The average deviation of the lidar pressure data from the radiosonde data is 0.3 percent (3 mb).

Recently, we have incorporated a second Alexandrite laser into our system to produce the first all solid-state tunable lidar. The new laser system also has significantly greater capability because of a 30-fold increase in average output power. In addition to pressure measurements, our new system will be used to make temperature profile measurements.

Contact: C. Korb
Code 610

Sponsor: Office of Space Science and Applications

GALILEO PROBE MASS SPECTROMETER (JUPITER)

The Jovian atmosphere is comprised primarily of 90 percent hydrogen and 10 percent helium; it also includes minor amounts of the inert gases neon, argon, krypton, and xenon, and non-inert gases such as water, methane (CH_4), ammonia (NH_3), hydrogen sulfide (H_2S), acetylene (C_2H_2), and ethane (C_2H_6), and other trace constituents.

A mass spectrometer in the Galileo Probe will directly and repeatedly sample Jupiter's atmospheric gases at different altitudes as the Probe descends.

The instrument is being developed and built at NASA/Goddard Space Flight Center. It weights 13 kilograms and requires approximately 25 watts, about half of which is consumed in pumps and heaters in the sample inlet pumping system.

With its broad mass and sensitivity range, the instrument measures almost everything that enters it, making it ideal for this exploratory mission. The normal range of ion masses to be covered will be from 1 to 52 AMU (atomic mass units) with occasional sweeps from 1 to 150 AMU to search for heavier compounds.

Atmospheric gases will enter the mass spectrometer through two inlet ports at the apex of the Probe. These ports will be sealed by metal-ceramic devices and kept under vacuum until the Probe enters the Jovian atmosphere. Pyrotechnic devices will then release the covers, allowing atmospheric gases to enter the sensor and be pumped to the test cells.

The instrument will separate hydrogen from the gas samples to raise the relative abundances of the remaining gases in the sample. The instrument includes two "enrichment" cells which absorb trace gases such as hydrogen sulfide, phosphine, and complex hydrocarbons until only the noble (inert) gases remain. The noble gases are admitted to the ion source for analysis. The enrichment cell is then heated, the absorbed gases are desorbed, and the gases are admitted to the ionization region for analysis of the more complex compounds.

The Flight Unit instrument has been successfully installed and tested in the Galileo Probe and is now undergoing final checkout and calibration at GSFC.

Contact: Dr. Hasso B. Niemann
         Code 610

Sponsor: Office of Space Science and Applications

EARTH VIEWING IN THE SHORTWAVE INFRARED

Traditionally, the "infrared" portion of the electromagnetic spectrum is considered to extend from about 800 nm, the cut-off point of the human eye, to over 10,000 nm (10 microns). Scientists and engineers have found it necessary when speaking of the infrared to divide this large region of the electro,magnetic spectrum into more manageable portions. These portions generally correlate to the limits of the specific electronic means used to detect the radiation. One of these regions extends from about 1 micron to 3 microns and is called the shortwave infrared (SWIR).

A development milestone was achieved this past year in detecting SWIR radiation in a manner suitable for remote imaging from space. The first linear array of 512 contiguous detectors using Schottky barrier technology was demonstrated. Each detector is made from palladium silicide and is only 30 microns by 30 microns in size with the

capability of measuring SWIR radiation of only a few microwatts per square centimeter. These arrays must be cooled to approximately 120 K which is at least 30° warmer than most other detectors in this spectral region, a significant improvement from an engineering point of view.

These new arrays include unique features that will allow them to be used in satellite remote imaging systems. One of these is the layout of the array on an integrated circuit chip with detectors very close to the edge. The process of making these integrated circuit chips is such that numerous identical chips are cut out of a single large wafer which may be up to 6 inches in diameter. This allows for mass production and reduced cost, but can lead to rough edges on the chips and damage to any detectors deposited near the edges. However, processes for cutting and polishing these chips with little or no change are being developed so that several chips can be butted together to make linear arrays with thousands of detectors with gaps of only one or two elements at each of the butt joints.

Another unique feature is that the design consists of two closely spaced parallel linear arrays on the chip with a technique for attaching a different optical filter to each line of detectors. One set of butted chips can therefore sweep out a sequence of spectral lines using the pushbroom technique wherein the arrays are perpendicular to the line of travel of the spacecraft.

Development of linear detector arrays will continue as improvements are sought in areas such as sensitivity and spatial and spectral resolution. In the SWIR spectral region, transparent "windows" in the atmosphere allow radiation from the earth's surface to reach the spacecraft without being absorbed by water vapor. The information radiated by plants in the SWIR region is being studied at Goddard. Their spectral signatures are often unique and can be used to determine plant type, extent and health. In addition, these arrays would be used in geologic studies and other areas that are now waiting for this new technology.

Contact: Dr. James E. Kalshoven, Jr.
         Code 625

Sponsor: Office of Space Science and Applications

TECHNIQUES

SYSTEM MODEL FOR IMAGE REGISTRATION (SMIR)

The System Model for Image Registration (SMIR) system is an analytical simulation tool used to examine the geometric

aspects associated with image registration/rectification. A spacecraft flyby is simulated, including a variety of perturbations which affect the resulting image. SMIR has the capability to estimate the effects of various error sources on spacecraft imagery, to evaluate the ability of geometric cor-

rection techniques to improve image distortions, and to provide a measure of the registration/rectification errors associated with a linear array instrument on board a spacecraft. The SMIR software system is written in FORTRAN, runs on a VAX 11/780 computer, and makes use of a Grinnell graphics system to display images.

The design of the SMIR system allows the user to start with a given ideal scene, introduce geometric errors, correct the geometric errors, examine the distorted and corrected scene, and compare the ideal, distorted, and corrected scenes in various ways. SMIR produces the distorted scene by first computing the pointing vector coordinates of each detector at each sampling time, and then resamples the pixels of the ideal scene for the appropriate radiance values. In computing these coordinates, errors due to earth curvature and rotation are modeled and errors associated with spacecraft orbit control and attitude control can be simulated. Also, other errors that affect optical alignment such as thermal distortions, gravity release, gitter, assembly tolerances, and moisture effects can be simulated. SMIR has the capability to simulate nadir viewing, and off nadir viewing. Fore and aft views as well as side to side views can be simulated. The off nadir viewing capability together with a simple representation for terrain elevation provides a basis for which some stereo viewing can be examined. A model to represent the linear detector array geometric imperfections such as array length, butting, band to band parallelism, and band to band spatial separation is contained within the software.

The intent of the SMIR system is to provide a tool with which scientists and engineers can use and work together to help translate scientific requirements into engineering specifications.

Contact: W. Case
         Code 725

Sponsor: Office of Space Science and Applications

SYSTEMS ANALYSIS PROGRAM (SAPGM)

SAPGM encompasses a set of software modules designed to assist in the evaluation of advanced spaceborne sensing systems designs via simulation of their electro-optical data streams. It was originally developed by ITEK for the Goddard Space Flight Center (GSFC) in 1977 and is currently operational on VAX 11/780 computer systems in an enhanced form called SAPGM2. It has been used to analyze and simulate instruments such as the Landsat Thematic Mapper, the Cosmic Background Explorer (COBE) Diffuse Infrared Background Experiment (DIRBE), and the MLA (Multi-Linear Array) instrument.

SAPGM2 modules may be invoked in any order to transform simulated input into simulated output representative of what the instrument being modelled would actually produce (see figure). Each module accepts an input data set and produces an output data set that can be used by subsequently invoked modules. The primary modules available consist of the following:

Input Module—Reads input data from tape or disk and performs scaling or resolution reduction as required.

Optics Module—Simulates the blurring and distortions associated with optical system imperfections as well as allowing atmospheric attenuations to be included. Either spatial or frequency domain simulations may be performed.

Detector Module—The size, shape, and response contours of the detector elements are described and they are subsequently scanned over the input scene to produce the modulated output scene. Analog-to-digital conversion, frequency domain filtering, noise, gains/offsets, transfer efficiency, and other effects may be added by sub-modules as required.

Evaluation Module—Generates absolute value and difference value histograms and computes image entropy. Also computes power spectral density response curves and auto correlation functions for selected data sets. The results may be displayed on a Printronix line printer or on a Grinnell Image Display System.

SAPGM2 is an evolving program that is undergoing both in-house and contracted alterations to improve its simulation capabilities. These changes will support the off-nadir-viewing simulations required for linear array instruments and represent significant increases in the overall flexibility and utility of the SAPGM2 program.

Contact: C. Jackson
         Code 725

Sponsor: Office of Space Science and Applications

INTEGRATED ANALYSIS CAPABILITY (IAC)

The objective of the IAC has been to provide a highly effective, interactive analysis tool for integrated design of large space structures. IAC has focused on the technical disciplines of structures (both statics and dynamics), controls and thermodynamics. These disciplines are represented by state-of-the-art modules which existed at the start of the IAC development and are continuing to be maintained either by government laboratories or by private industry.

The IAC development started in June 1979 and the final delivery (Level 1) was made in July 1984. During this 5 year period, the IAC software has evolved through three phases: proof of concept, the first operational IAC called "Level O", and the final system. Phase III has extended the Level O code with significant enhancements to the executive/user interface and the general data management capabilities, extension of the database cataloging mechanism to include both structured and unstructured files, and incorporation of several additional controls modules. The extended IAC system is now referred to as "Level 1".

The architecture of the IAC system is shown in Figure 1. A significant portion of the code is the executive and data management software. Two key concepts driving the development of the IAC system are the user interface and code modularity. The executive is designed to be user friendly, providing extensive on-line assistance in the way of explanatory help and examples. Also, the executive and system software have provided for modular additions to the code. Every organization will have some unique modules which its users will want to interface with IAC, and the system has been developed to facilitate this kind of growth.

The IAC system architecture can be viewed as providing two products:

a. A specific interdisciplinary analysis capability having a set of interfaced technical modules (e.g., in Level 1, the coupling of thermal structures and controls disciplines).

b. A general framework product which serves as an "integrated base" whereby user groups can add desired modules and disciplines.

These two products are shown schematically in Figure 2. The diagram on the left exemplifies the specific capability of Level 1. The diagram at the right depicts the general integrating framework, into which "X-Y-Z" brand modules of a particular user group can be incorporated. Note that in either case, the core software is identical.

Contact: J. Young
        Code 731

Sponsor: Office of Space Science and Applications
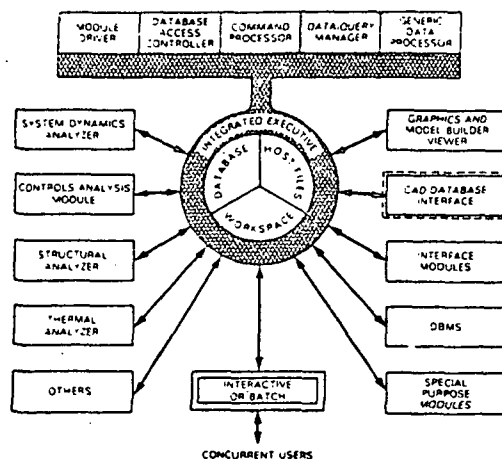
IAC architecture.
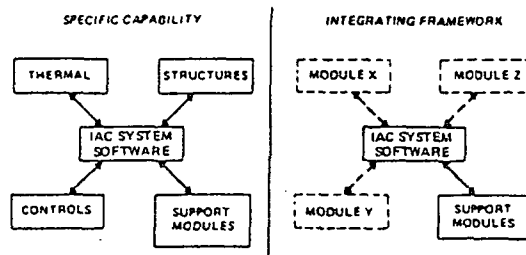
Two IAC products.

APPLICATIONS DEVELOPMENTAL DATA SYSTEM (ADDS)

The Landsat 2-3 image processing facilities have encountered significant difficulties in producing radiometrically and geodetically precise outputs at a satisfactory throughput rate. A major contributor to the problem is the volume of data associated with each image—approximately 30 megabytes for each Multispectral Scanner (MSS) image. The problem becomes more acute in the case of Landsat-4 with the advent of the Thematic Mapper (TM) which produces approximately 240 megabytes for each image. The Applications Developmental Data System (ADDS) was developed to demonstrate that the processing bottlenecks encountered in the previous Landsat image processing systems can be alleviated with a judicious application of state-of-the-art technology and a realization that only a minimal volume of data need be analyzed to produce Landsat images.

The ADDS approach utilizes high performance hardware for the majority of data exchanges, limits the volume of image data transferred to conventional hardware, and performs selected CPU intensive functions in hardware. The ADDS consists of: (1) two CSP, Inc. Macro Arithmetic Processors (MAP's) augmented with special peripherals that aid in the decommutation of TM image data, perform the radiometric and geodetic correction of the imagery, and a high speed interface to the mass storage device; (2) the Ampex Parallel Transfer Disks which are capable of sustained data transfers of 9.68 megabytes/second for image storage; (3) Floating Point System AP 180-V for computing radiometric and geodetic correction matrices; (4) a Digital Equipment Corporation VAX 11/780 to control the pro-

cessing pipeline; and (5) peripherals necessary to support the processing of raw TM data stored on high density tapes.

The ADDS system processes TM data as it flows through the system at 42.5 megabits/second. The majority of the data flows between the high density tapes, the MAP's, and the Ampex disks. Approximately 10 percent of the TM imagery is transferred to the VAX which computes the radiometric and geodetic correction matrices. The majority of these computations are performed by the FPS AP 180-V. The correction matrices are transferred to the MAP's, which apply the corrections as the image data are being transferred between the disks and high density tapes.

In this configuration, the system is able to radiometrically correct a TM image in 2 minutes and geodetically correct an image in 7 minutes for sustained periods. During its demonstration period, the system produced 325 radiometrically corrected images in 28 hours and geodetically corrected 256 images in 36 hours. By replicating the MAP string, it is possible to produce radiometrically and geodetically corrected images simultaneously at the rate of 8 minutes an image. The results of the demonstration clearly indicate that the architecture and processing philosophy employed by the ADDS can significantly reduce the Landsat image processing backlogs encountered by previous systems.

Contact: Mr. William L. Mocarsky
Code 734

Sponsor: Office of Space Science and Applications

USER SPACE DATA SYSTEMS

PILOT CLIMATE DATA SYSTEM

The Pilot Climate Data System (PCDS) is being developed by the Goddard Space Flight Center (GSFC) to manage a large collection of climate-related data of interest to the research community. The current capabilities of the PCDS include many tools for the survey of climate data. Utilities are available to browse, scan, study, select, filter, list, compress, perform statistics and display any data of interest. The PCDS now supports approximately twenty different data sets and is being used by several different in-house research groups. An experimental program in collaboration with Penn State University to remotely access these data for use in a graduate program in climatology has also been initiated.

The PCDS is designed to be an easy-to-use, generalized scientific information system. It efficiently provides uniform

data catalogs, inventories, and access methods, as well as manipulation and display tools for a large assortment of Earth, ocean, and atmospheric data for the climate-related research community. Programs conducted by NASA-sponsored investigators, such as climate, weather, and severe storm research (e.g., cloud and land-surface climatology), can be supported by the system.

Researchers can employ the PCDS to scan, manipulate, compare, display, and study climate parameters from diverse data sets. Data producers can use the system for validating and archiving data, or maintaining account records and data inventory. Information on data demands can be used by managers for planning data processing and analysis activities. In addition, academic researchers, who may be working with limited budgets, can obtain quick access to selected portions of larger data sets.

The highlights of the PCDS are outlined below:

● Effective Data Services:

  - Information on Availability of Data Sets

  - Rapid Output for the Desired Data Set Subsets

  - Easy and Convenient to Use

● Applications:

  - Climate Research Projects

    - Statistical Climatology
    - International Satellite Cloud Climatology Project
    - Global Ozone Distribution
    - Earth Radiation Budget Studies
    - Land-Surface Climatology
    - Solar-Flux

  - Other Research

    - Continental Vegetation Indices
    - Middle Atmospheric Electrodynamics
    - Distribution of Gravity/Magnetic Anomalies

● Key Software Features

  - Catalog of Available Climate-Related Data

  - Inventory of On-Line/Supported Data Available Through the PCDS

  - Sophisticated Retrieval/Archival Support for Actively Used Data Base Sets

  - Uniform User Interface

  - Utilities that Allow Data Manipulation

    - Statistical Evaluation
    - Subsetting of Large Volume Data Streams
    - Merging of Selected Data Sets
    - Data Independent Storage Structure

● State-of-the-Art Graphics

  - Multiple Two-Dimensional and Three-Dimensional Data Representations
  - High Performance Device-Independent Software
  - Publication/Presentation Quality Products

Typical graphic representation of PCDS data

There are several important innovations and accomplishments that have been achieved in the development of the PCDS to date. Some of these activities are:

● Development of the first self-describing, data-independent structure for any data that are oriented towards the user of the data rather than a computer programmer.

● Enhancement of graphics capabilities into a flexible, easy-to-use, integrated, data-independent system that supports many representation schemes of multidimensional data sets.

● Began support of the International Satellite Cloud Climatology Project (ISCCP) by developing a plan for the management of several of its data products. This work will continue into FY85 with the support of data within the PCDS.

● Addition of data-independent manipulation tools for subsetting, ungridding, averaging, algebraic combining and listing of data sets.

● Integration of data base management, computer graphics, network communication and data manipulation functions with data and information about data into a generalized, scientific information system.

A typical graphical representation of data available via the PCDS is shown below. It illustrates a geopotential height distribution over the north pole.

Contact: Lloyd A. Treinish
         Code 630.1

Sponsor: Office of Space Science and Applications

ON-LINE DATA CATALOG SYSTEM

Development of On-line Data Catalog System was begun
at the National Space Science Data Center (NSSDC) in
1984. This system is intended to enable scientists at GSFC
and elsewhere to quickly and easily find data relevant to
their current needs. The system is to consist of a Central
Directory plus a number of catalogs relevant to individual
data sets or data bases. Some of the catalogs may be held
at remote sites at which the data bases themselves are
held. Work has begun in the solar-terrestrial discipline.

The Directory addresses data sets in their entirety, and pro-
vides the scientist with information on the location, access
procedures, and other data set characteristics (e.g.,
parameters included quality, resolution, processing history,
data source characteristics). The Directory contains pointers
to catalogs when they exist. The catalogs address data set
parts, and enable a scientist to determine, for instance,
whether a particular type of in-situ data were being ac-
quired, in a desired location, at a particular time of
interest.

An initial Directory, with a limited data base, has been made
available to a segment of the external scientific community
for remote access and testing via the DECnet-based Space
Plasma Analysis Network (SPAN). This initial Directory is
structured as a relational data base, resides on the NSSDC
VAX, and is managed by the Oracle Data Base Management
System. The user interface is built around the Transportable
Applications Executive (TAE) package developed at GSFC.

A Steering Committee of predominantly university scientists
convened at GSFC in May 1984 to provide guidance to the
Directory development and to the more general Catalog
System development. This committee continues to be active.
The next stages are to finalize the Directory design, to build
an appropriate Directory data base concerning solar-
terrestrial data bases, and to extend the system into disciplines
other than solar terrestrial.

Contact: Joseph H. King
            Code 633

Sponsor: Office of Space Science and Applications

LASER VIDEODISC AND IMAGE RETRIEVAL

Laser videodisc hardware technology and data base manage-
ment software technology is being combined to yield an ef-
fective solution to the problems of 1) archiving very large
volume (greater than 10,000 images), non-digital image data
bases, and 2) retrieving that small subset of images needed
for any specific scientific study. The ability to visually scan

images may suffice for some studies, while for others, it may
enable the scientist to determine precisely which images he
must acquire and process digital data.

In order to perform its image archiving and retrieval ac-
tivity more effectively, the National Space Science Data
Center (NSSDC) has implemented a system which com-
bines videodisc and data base management technologies.
A planetary image data base has been received from the
Jet-Propulsion Laboratory (JPL) on one videodisc with
50,000 images on each side. Separately, Washington
University in St. Louis, supplied a PDP-11/34 compati-
ble data base management software package. Better Im-
age Retrieval Program (BIRP) and data bases of ancillary
parameters for each image contained in three major files
on the JPL videodisc (i.e., Viking Orbiter, Viking Lander,
and Voyager). These parameter sets include imaged area
coordinates, Sun and camera angles, and a number of
other parameters. By successively specifying values or
ranges for any subset of the available parameters in
response to system prompts, the user interactively nar-
rows the number of images to be retrieved and displayed
to just those most likely to be relevant to his current need.

NSSDC converted the BIRP package to run on its WICAT
microcomputer under the UNIX operating system. The
system consists of BIRP in the WICAT memory, the ancillary
parameter data bases on the WICAT's magnetic disc, the im-
ages on a videodisc player, and a display terminal for view-
ing retrieved images.

NSSDC is now prepared to host visiting scientists in retriev-
ing and viewing selected images from specific large image
data bases, disseminate the UNIX-compatible version of
BIRP and the JPL-created videodisc of 100,000 planetary
images, and apply its recent experience in the joint use of
videodisc and data base management technologies to the
management of Earth image data bases.

Contact: Joseph H. King
            Code 633

Sponsor: Office of Space Science and Applications

LARGE-SCALE COMPUTING SYSTEMS

The NASA Space and Earth Sciences Computing Center pro-
vides very high speed computational support for NASA-
sponsored scientific research, both to internal GSFC scien-
tists and to the general NASA/university community. This
support is provided through two major computing facilities,
with plans to merge physically these two over the next 18
months.
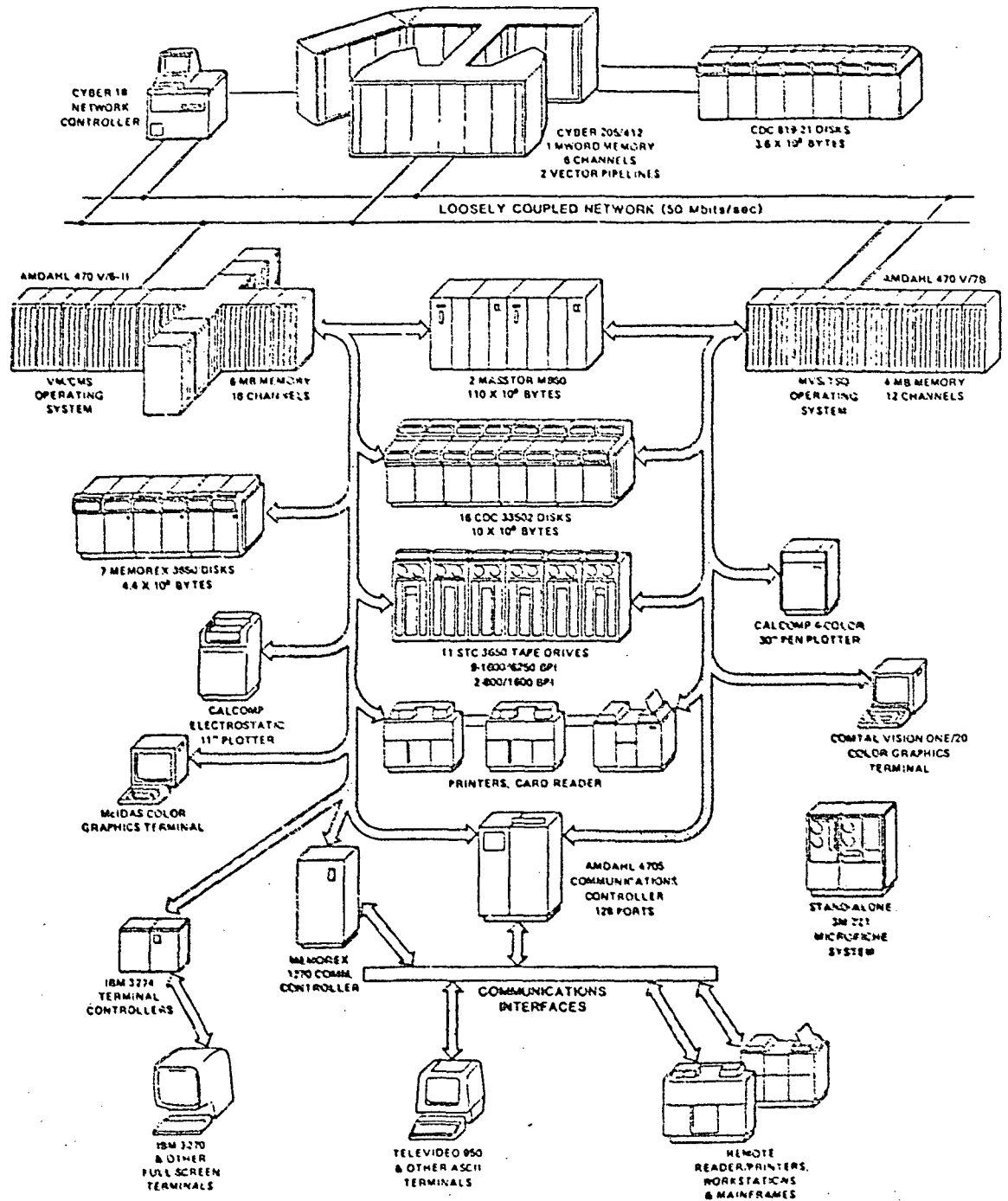
Vector processing facility

Scientific Computing Facility (SCF)

The SCF utilizes an IBM 3081 as its central processor. The 3081 is IBM's most advanced mainframe processor and utilizes highly integrated circuit technology packaged in Thermal Conduction Modules (TCM's). The TCM is a helium filled, encapsulated module, measuring 125 x 134 x 35 millimeters, and contains tens of thousands of logic circuits. Benefits of the new technology include significant reductions in space, power, and cooling requirements.

A technologically innovative development during FY84 involved installation of a tape accelerator provided by the Storage Technology Corporation. This device provides intelligence in the tape subsystem for buffering data and then streaming it over the I/O channel at full rated capacity of 3 Mbps. The increased channel efficiency allows reconfiguration of all data paths to improve overall interactive response time.

Another FY84 technology improvement involved installation of an IBM 3800 printing subsystem. The 3800 uses a laser and an electrophotographic process to produce very high quality printed output at speeds of up to 20,000 lines a minute. Users of the system may select from 60 type fonts for their output. By 1985 IBM will make available software to produce graphic output with a resolution of 240 pixels per inch.

A new SCF research thrust is in the area of graphics technology. The purpose of this effort is to design and develop a scientist-friendly system for graphical display of data. The system will be transportable over a wide class of computers and usable with many graphics devices. More specifically, the system will satisfy all general purpose graphics requirements in the user community.

Significant FY84 accomplishments include the development of functional specifications for the scientist-friendly interface to the commercially installed TEMPLATE package as well as the high level graphics routines to be used by the interface program. These specifications include a wide range of plotting options such as the display of contours, surfaces, and various world map projections, that are essential in the scientific environment.

FY85 plans call for the implementation and test of this interface on the IBM 3081, the VAX 11/780 and the IBM PC/XT.
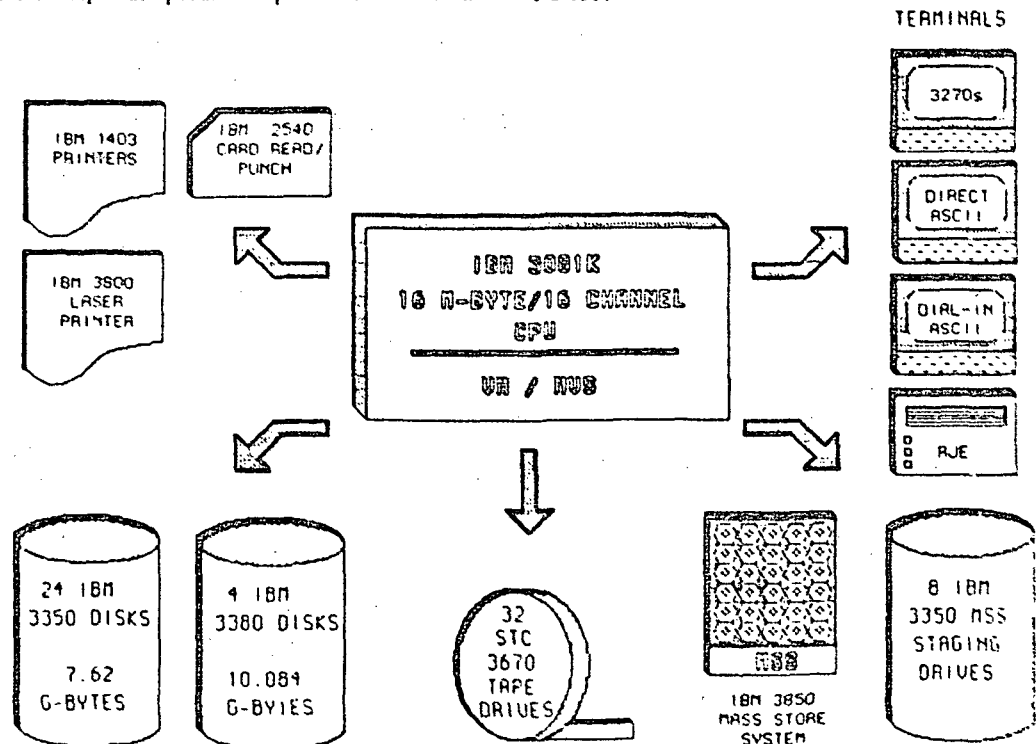
Scientific computing facility configuration.

Vector Processing Facility (VPF)

The VPF is an integrated set of computational tools and services centered around a Control Data Corporation (CDC) Cyber 205 supercomputer. The facility provides an order of magnitude improvement in numerical processing capability over conventional systems necessary to support finer scale and more complex meteorological, climatological, oceanographic, and geodynamic models.

The Cyber 205 is configured with 1 million 64-bit words of main memory and 2 concurrent vector pipeline processors, and is capable of performing up to 400 million floating point operations per second for optimized instruction sequences involving linked vectors. A multiprogramming operating system allows for virtual addressing of up to 2 trillion words.

Other capabilities available within the facility include two front-end Amdahl processors and a 110 gigabyte mass storage device. All of these are interconnected via a special purpose Loosely Coupled Network product provided by CDC.

A major initiative in FY85 calls for an additional million words of main memory. This, along with additional memory on the Amdahl front-ends, will significantly enhance the accuracy and granularity achievable with current models, in addition to enabling a new set of scientific problems to be addressed.

The future strategy for overall large-scale computing calls for a highly adaptable environment for revolutionary growth, exploiting advances in technology as they are available and appropriate. As discussed above, a major thrust during FY85 will be the physical consolidation of the two major facilities to further improve scientist access to these unique computational tools. In addition, a new technology initiative will be undertaken to establish the feasibility of integrating optical disc technology as a mass data storage component. A testbed activity will be initiated in FY85 with the view to incorporating this into the mainline system in the FY86/87 timeframe, or as the technology matures.

Contact: Joseph H. Bredekamp
Code 630

Sponsor: Office of Space Science and Applications

TRANSPORTABLE APPLICATIONS EXECUTIVE

The Transportable Applications Executive (TAE), a portable program for the management of interactive applications systems, serves three major groups: end users, applications programmers, and system designers. For the end user, TAE

provides a consistent user-computer interface, with both menu and command mode and easily accessed user-assistance in the form of online help, system messages, and program tutoring. For the applications programmer, TAE provides simplified but powerful user dialog and data access functions through a library of service subroutines. For the system designer, TAE provides a reusable framework and set of tools for flexibility in developing and ease in reconfiguring a system. TAE lowers the cost of system development, maintenance, and upgrade by providing software and structures for commonly recurring user requirements, by encouraging consistency in software development and documentation, and by allowing for experimentation in system design.

FY84 saw four major accomplishments in TAE development:

1. The implementation of a device-independent software package for image display and manipulation on raster devices;

2. The successful installation of TAE under UNIX;

3. The public release of the operational version of TAE; and

4. The establishment of a memorandum of understanding for cooperative software development and exchange with the USGS EROS Data Center.

The Display Management Subsystem (DMS) to TAE extends the TAE portability concept by allowing programs to be portable among raster imaging devices. DMS abstracts the generic features of raster display devices and treats display functions in a device-independent manner. The primary goal of DMS is to permit both programs and end users to access imaging devices without having to understand the hardware or particular configuration of a device.

TAE has been installed under Berkeley UNIX on three systems: a Digital Equipment Corporation VAX, a SUN Microsystems workstation, and a Gould SEL computer. These installations are facilitating the spread of TAE to the wide variety of computers on which UNIX has been implemented, particularly microcomputers. TAE/UNIX makes distributed systems with a common, user-oriented interface an exciting and real possibility.

The operational TAE underwent field testing in FY83 and had two operational releases in FY84, with a third scheduled for early FY85. It features a powerful procedural command language, integrated with menu and tutoring features for locating and executing functions. Users have the choice of synchronous, asynchronous or batch modes of operation. An in-line editor assists in repeating commands or entering

values. Other useful features include session logging, global variables, hierarchy searches for functions and unified error reporting.

The memorandum of understanding with the EROS Data Center calls for cooperative software development in both systems, including a VAX, SEL, and SUN workstation all under UNIX.

Twenty-five different sites—in government, academia and private industry—are actively using TAE. A successful user's conference, attended by more than 100 people, 70 from outside GSFC, was held May 1-2, 1984.

Contact: Dorothy Perkins, Martha Sczcur
         Code 630

Sponsor: Office of Space Science and Applications

SELF-DOCUMENTING/DESCRIBING DATA MODEL

Data sets evolve over time creating, for example, the need for costly updates and data structure modifications, and performance penalties for awkward data searches. To encourage increased data utilization, these inefficiencies must be overcome. The approach described here is to model this evolution using a Self-Documenting Model (SDM) technique. An SDM automatically captures the descriptions of the derived data sets into its catalog (directory). The catalog itself is a data set description management system that can be accessed, distributed to various places and users, and, in general, be managed like a data base.

A data model is self-describing or autological if it models both data and the description about data. This property is especially important for the catalog of a data model. Self-describing models allow users with some basic knowledge about the model to browse and find out all the information needed to use the data base. The basic required knowledge is minimal, dependent on the model itself, and independent of the data base content.

In order to experiment with the concepts of self-description and self-documentation, an experimental relational data base management system called ADMS was developed in conjunction with GSFC by the University of Maryland. It is an experimental vehicle to test advanced concepts for managing information evolution and information exchange.

ADMS is a friendly and simple relational data base system with very advanced features. It has a simple data manipulation language based on the relational algebra and a very simple transaction mechanism. It has a security subsystem based on the notion of views which allows tailored security control based on groups and capabilities. The relational operators are designed to take advantage of secondary indexes defined on attributes which speeds up the execution. An SQL+ interface has been designed using the transaction mechanism. (SQL + is the IBM System R language.) The SQL+ interface is a translator which accepts queries in SQL+ and translates them into sequences of basic ADMS commands. Similar interfaces can also be built for other languages such as QUEL of the INGRES system.

ADMS maintains a very sophisticated self-describing and self-documenting catalog for managing the relations and views defined in the data base. The catalog keeps track of all created relations and views derived from relations or other views. The catalog consists of several relations which are accessed by the same ADMS command language used to access the data base. One of these relations is called "derivations" which keeps track of all the views created by the users of ADMS. It also maintains the operations that were used in the derivation of each view in order to support rapid view updates necessitated by data base changes. Another important relation is "lapschema" which keeps statistical information on the accessing and updating activities on each relation and view. This information is used for self-organizing indexing techniques for very high performance.

Although the optimization of the ADMS system is not yet done, preliminary tests have shown exceptionally high system performance. The speed of execution stems from exploiting the concept of a relational view index which defines an access path, a matching algorithm which recognizes pieces of pre-existing access paths useful for answering the query on hand, and an algorithm which updates paths at a fraction of the cost of recreating from scratch. The principle behind this very fast view access is based on the fact that, in most ordinary data bases, the portion of an outdated access path between two consecutive requests of the same path is only a small fraction of the complete access path. Therefore, by recognizing and updating the small portion of the access path, the system saves a tremendous amount of disk I/O. This principle is termed "match and cache" and is very effective in many other computations provided the "matching" is less costly than redoing the whole computation in order to benefit from "caching." In the access path case this is true because the trade-off is between matching in main memory versus expensive disk I/O.

Current plans for this experimental system include gathering performance statistics on updates and queries using a Space Telescope-related catalogue.

Contact: Walter Truszkowski
         Code 522.1

Sponsor: Office of Space Tracking and Data Systems

COMPUTER SCIENCE RESEARCH

Computer Science Research in the area of Data Base Management is being conducted to develop methodologies, technologies and systems required to handle very large (10^{12} to 10^{15} bits) multisource data bases at distributed locations.

Fundamental research has been conducted on the data base uniformization problem to enable NASA's space data users to access any data base independent of its physical distribution and specific organization, and to provide a single common view of these data bases. The research has been led by the University of Maryland with the collaboration of Towson State University, the Catholic University of America, and Stevens Institute of Technology. This research has produced a number of research reports and Prentice-Hall will publish a two volume series which defines the data uniformization problem and describes a detailed solution to it. The books are entitled "Applied Data Base Logic I: Fundamental Issues" and "Applied Data Base Logic II: Heterogeneous Distributed Access View Integrated Data Base (DAVID)" system (see figure below) proposed as a solution to the data uniformization problem.

The DAVID system can overlay various distributed heterogeneous data bases (i.e., relational, hierarchical, or network) and interpret these to the user in a common external view as a generalized relational data base. This research is unique in several ways:

- It provides a uniform framework, namely data base logic, for many of the issues that must be dealt with in heterogeneous distributed query processing.

- This is the first study of multiple query processing and data base conversion over distributed, heterogeneous data bases.

- In addition to access through an interactive terminal, the system will also support host language interfaces through many popular programming languages (e.g., C, ADA, FORTRAN, LISP, etc).

Testing of the DAVID system concepts using sample data sets has begun and planning for its implementation as part of a complex land data system is being studied.

Contact: John H. Berbert
           Code 630

Sponsor: Office of Aeronautics and Space Technology
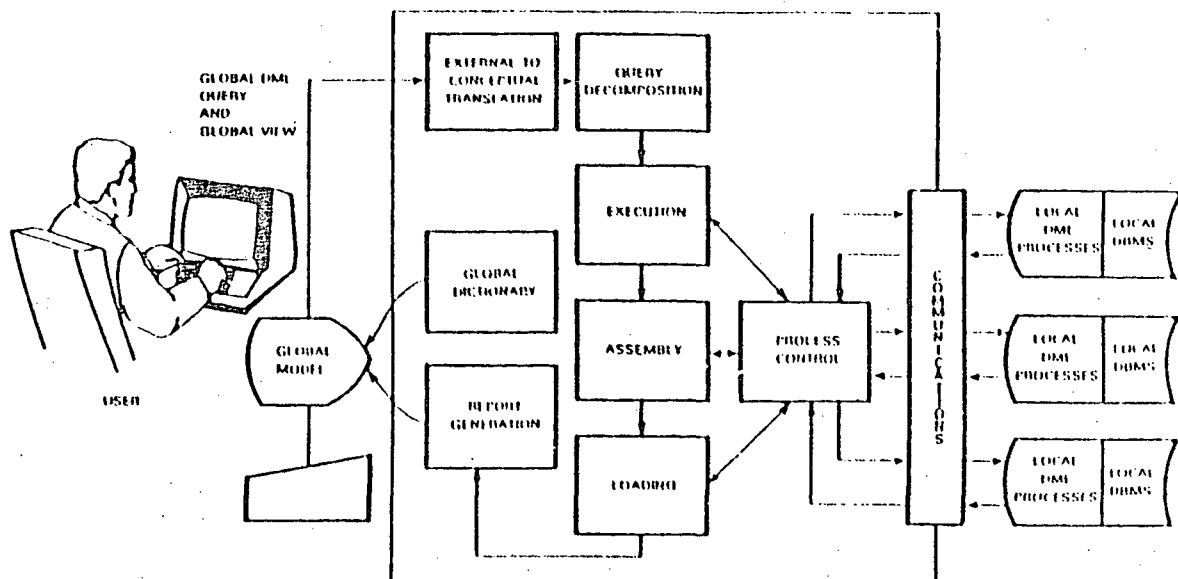
Distributed access view integrated data base (DAVID) system

SPACE COMMUNICATIONS AND NAVIGATION

85-MBPS MODEM FOR 34-MHz SATELLITE TRANSPONDER

A study was conducted to define a modem and codec combination which will provide throughput transmission of 85 Mbps in a 34 MHz DOMSAT transponder at a bit rate performance of 1×10^{-7} or better. By computer simulation, the study showed that this performance can be achieved with a predicted margin of 3.7 dB, using a technique proposed by Motorola, called serial minimum shift keying divided by two (SMSK/2), also known in the literature as duo-binary linear phase (DBLP) continuous phase modulation, and using 7/8-rate convolutional coding and threshold decoding. The specific DOMSAT and Earth station characteristics used in the simulation are those of the RCA Americom facilities presently providing 50 Mbps service between the White Sands TDRSS ground station and the GSFC.

The SMSK/2 technique is more tolerant to realistic hardware constraints than other techniques studied, and the principal implementation risk is in building filters in the modulator which can yield the required performance. Since the intended use of this equipment was for transmission of Landsat 84.903 Mbps thematic mapper data from the White Sands TDRSS ground station to the GSFC, implementation will be dependent upon the outcome of Landsat policy issues. The next step in the implementation process would be to develop and test prototype equipment, and communications carrier, which has the transponder and ground station facilities available for testing.

Contact: Donald D. Wilson
           Code 540

Sponsor: Office of Tracking and Data Systems

AUTONOMOUS INTEGRATED RECEIVE SYSTEM (AIRS)

The Autonomous Integrated Receive System (AIRS) will be used in the TDRSS and TDAS ground stations to provide improved S—band Single Access (SSA) performance. The autonomous feature will allow the AIRS to react spontaneously to changes in the link conditions and to provide self-diagnostic status information. The integrated feature will allow tasks such as Doppler correction, demodulation, detection, and decoding to share pertinent information so that the tasks will be performed in an integrated manner to optimize performance.

Phase 1 of the AIRS project, completed in August 1984, involved a study to define the functional requirements, provide a technology and cost assessment, and perform a computer simulation of hardware and software algorithms to predict AIRS performance. Future phases, beginning in FY 86, will involve design, development, and demonstration of the AIRS.

The results of the Phase 1 study show that improved performance and operational advantages over the current system can be obtained with today's technology, with relatively small risk, and at a competitive cost. Computer simulations show total time for acquisition and reacquisition of the PN code and the carrier frequency and phase about 20 times better than current performance, with bit error rate within 2.5 dB of theoretical optimum. The AIRS will utilize microprocessor and distributed processing technology for internal control and autonomous operation. It will accept commands from *external Automatic Data Processing Equipment (ADPE)* or from an operator console, and will then operate in one of three modes: the normal mode, the flexible data format mode, or the test mode.

In the normal mode the AIRS accepts setup commands defining user characteristics and the Doppler correction information for the initial acquisition, after which the AIRS selects the configuration best suited to the particular user characteristics. The AIRS updates its Doppler corrector and performs its own Doppler compensation in a stand-alone manner without any further intervention from *the ADPE*. The AIRS monitors its operational status continuously and provides this information externally. The normal mode assumes that the user data characteristics remain unchanged during the service period so that the carrier loop and bit synchronizer may be coupled to attain the best performance.

In the flexible data mode some performance is sacrificed because the carrier loop and bit synchronizer are decoupled to accommodate changes in data format and data rate during a service period. The AIRS will then maintain PN code lock and carrier lock independent of the setting of the bit synchronizer and decoder, which are dependent on the data format and data rate.

In the test mode the AIRS can be configured manually for the purpose of testing or experimentation.

The digital hardware employed by the AIRS will allow duplication of performance in different units of equipment and will minimize periodic calibration and other maintenance procedures. The modular structure and self-test features will facilitate rapid repair. The firmware control will allow changes in operation procedures and receiver characteristics as requirements change.

Contact: John J. Schwartz
        Code 531

Sponsor: Office of Space Tracking and Data Systems

AUTOMATED ORBIT DETERMINATION SYSTEM

An Automated Orbit Determination System (AODS) has been designed and implemented into a computational system which has the capabilities to provide both definitive and predictive orbital computations for multiple NASA projects. This automated orbit computations system has been developed in order to aid in the support of the operational requirements set forth by the different NASA projects and the research and development effort required for computations enhancements for project support.

The AODS has the computational capability to perform orbit determination through the use of observational tracking data from both the GSTDN and TDRSS environments. The automated techniques available in AODS assist the mission planner in performing multiple orbital solutions for a specific spacecraft or a multiple of spacecraft. In addition to the orbit determination techniques, the computational system has the capability to generate ephemeris data, both definitive and predictive, for a set of spacecraft. The automated techniques which have been implemented in this computational system are to assist the mission planners in trajectory propagation and orbit determination. The trajectory modelling for spacecraft propagation or orbit determination includes the capability to compute the effects of Earth gravity, drag, solar radiation pressure, solar and lunar gravitation.

The automated aspects of AODS have been implemented with the concept that the computational software makes specific decisions based on the computational parameters made available after the completion of selected computations.

Contact: Clarence E. Doll
        Code 550

Sponsor: Office of Space Tracking and Data Systems

ESTIMATION OF ORBITS DURING LONG LOW THRUST MANEUVERS

A filter based algorithm has been developed and tested that allows the simultaneous determination of a spacecraft's orbit and thrusting parameters for long, continuous, low-thrust maneuvers being extensively tracked by two TDRS spacecraft. This algorithm is intended for the ERBS type of orbit transfer (i.e., multiple revolution maneuver from the Shuttle release orbit) to the final mission orbit and requires fairly continuous tracking as would be planned for such

maneuvers when two TDRS's are available. In maneuvers of this type, small but steady errors in the thrust vector may cause the accumulation of large orbital uncertainties after several hours. Such large errors affect the tracking acquisition schedules and antenna pointings must be updated during the maneuvers. Study results showed that an extended Kalman Filter can be used to estimate the orbit and thrust parameters as measurements are taken, which will allow longer maneuvers to be executed.

Contact: G. D. Mistretta
        Code 550

Sponsor: Office of Space Tracking and Data Systems

ORBITAL MANEUVERS OF THE ISEE-3 FOR THE FIRST COMET ENCOUNTER

The third NASA International Sun-Earth Explorer (ISEE-3) was launched on August 12, 1978, to be placed into a unique halo orbit around the L1 libration point. It was equipped with plasma physics experiments designed to investigate the solar wind before it reached the Earth's vicinity. The ISEE-3 was also outfitted with considerable fuel—enough for a delta V of 430 meters/second.

In its original configuration, ISEE-3 was part of a team of satellites, with two others in low-Earth orbit. The ISEE-3 was designed to detect changes in the solar wind so that the other two satellites could see the effects on the magnetosphere about 1 hour later.

When, however, NASA did not fund a U.S. mission to investigate Halley's comet, Dr. Robert Farquhar suggested using the ISEE-3 spacecraft to intercept another comet before the arrival of Halley's comet. The comet was Giacobini-Zinner, and in order to have the spacecraft intercept it, some complicated and previously untried maneuvers had to be made, including double lunar swingbys. In addition to the knowledge that would be gained from the detailed study of a comet at close range (approximately 10,000 km), there was another benefit from this mission, namely that the proposed swingbys involved extended excursions into the Earth's geomagnetic tail between 80 and 240 Earth radii—a region which had never been explored before.

The maneuvering began on June 10, 1982, when a small rocket burst (delta V = 5 m/s) was used to bring the ISEE out of halo orbit on a trajectory toward the orbit of the Moon. On October 16, 1982, the ISEE drifted back past the Moon's orbit out to a peak, from which it "fell" back toward the Earth and was whisked around into a figure-eight shaped orbit

in the geomagnetic tail, where it remained from December 20, 1982 until March 30, 1983, a period of 14 weeks (Figure 1).

The figure-eight orbit had been calculated such that it would bring the spacecraft back into the vicinity of the Moon on March 30, 1983. The spacecraft used the Moon's gravitational field to put it into a low, elliptical orbit, which would cross the Moon's orbit. The next time that the spacecraft was in the Moon's region, on April 24, 1983, it used the Moon to accelerate it back into the geomagnetic tail, this time for 22 weeks and 3 days (Figure 2).

Upon its return, a similar double lunar swingby put the spacecraft into another figure-eight orbit, but this time outside of the geo tail. On December 22, 1983 at the conclusion of this orbit, the ISEE was propelled on a remarkably accurate escape trajectory towards its encounter with Giacobini-Zinner (on September 11, 1985) by a pass of only 120 km (80 miles) above the surface of the Moon (Figure 3).

It is important to note the precision and skill required to plan and execute the intricate series of maneuvers, which, now complete, has placed the ISEE-3 (renamed International Cometary Explorer (ICE)) on its way toward its new target. The entire set of maneuvers was accomplished using very little fuel. In fact, after 6 years of operation, including the current expedition to Giacobini-Zinner, only about one half of the satellite's fuel has been expended. The lunar swingbys were executed with such precision that there was very little need to make in-flight course corrections. On April 23, 1984, the comet was sighted and found to be very close to where they had expected it, so there will not be occasion to use much more of the fuel.

After its encounter with Giacobini-Zinner, the ICE spacecraft will continue in its heliocentric orbit (Figure 4) until sometime in August of 2013, when it will return to the Earth's vicinity. At this point there should be enough fuel remaining on board to push the spacecraft into low-Earth orbit where it may either be retrieved for study, or replaced in its halo orbit where it may then continue its original mission.

Contact: Dr. Robert Farquhar
        Code 550

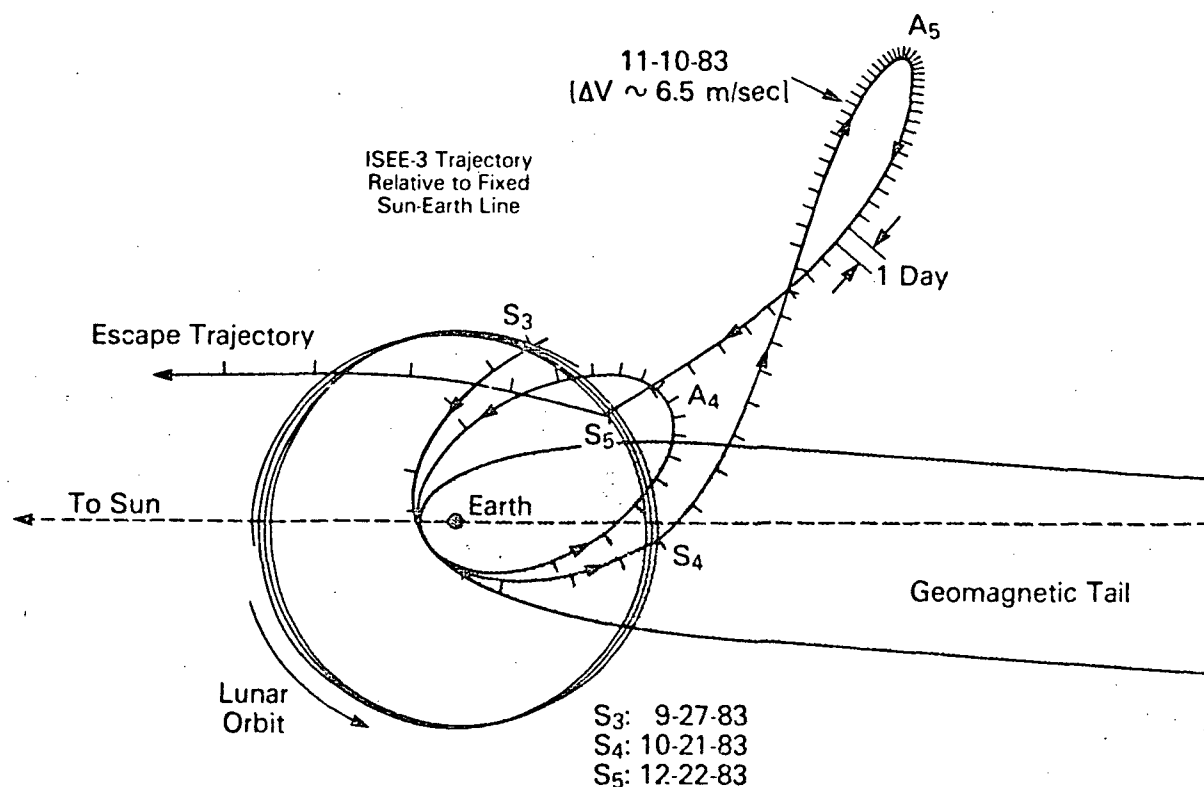Sponsor: Office of Space Science and Applications

Figure 1.   ISEE-3 brought out of halo orbit on a trajectory toward the orbit of the Moon.
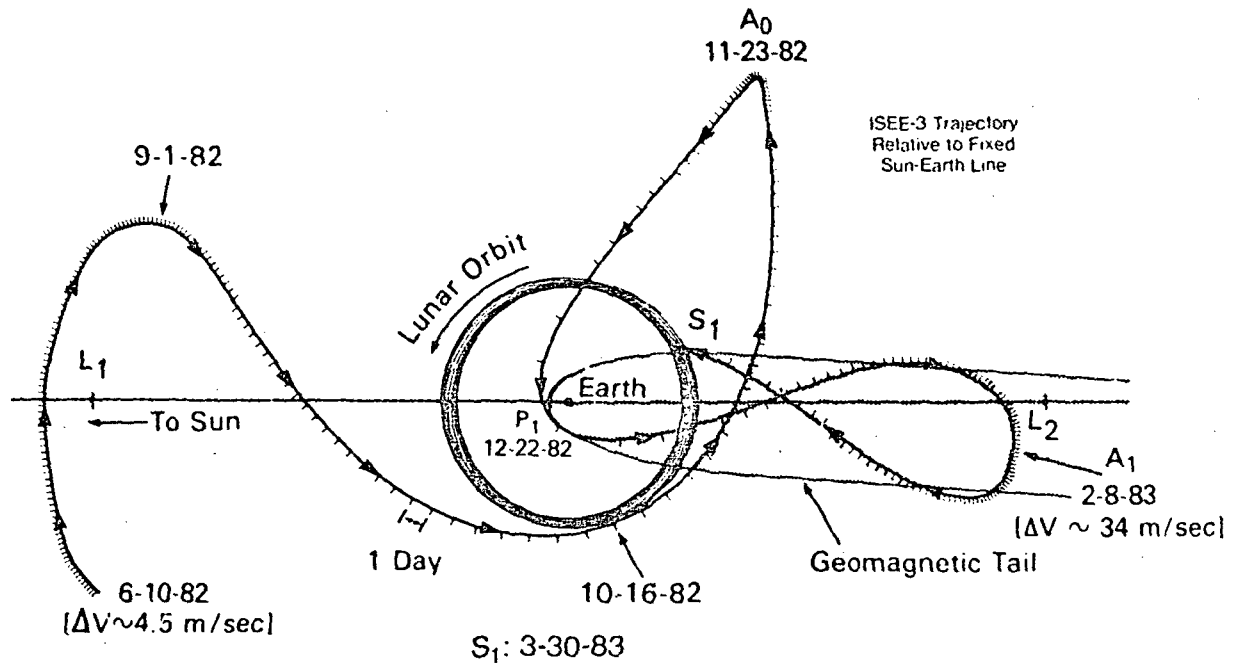
Figure 2.   ISEE-3 using Moon's gravitational field to be put into a low, elliptical orbit, which would cross the Moon's orbit.

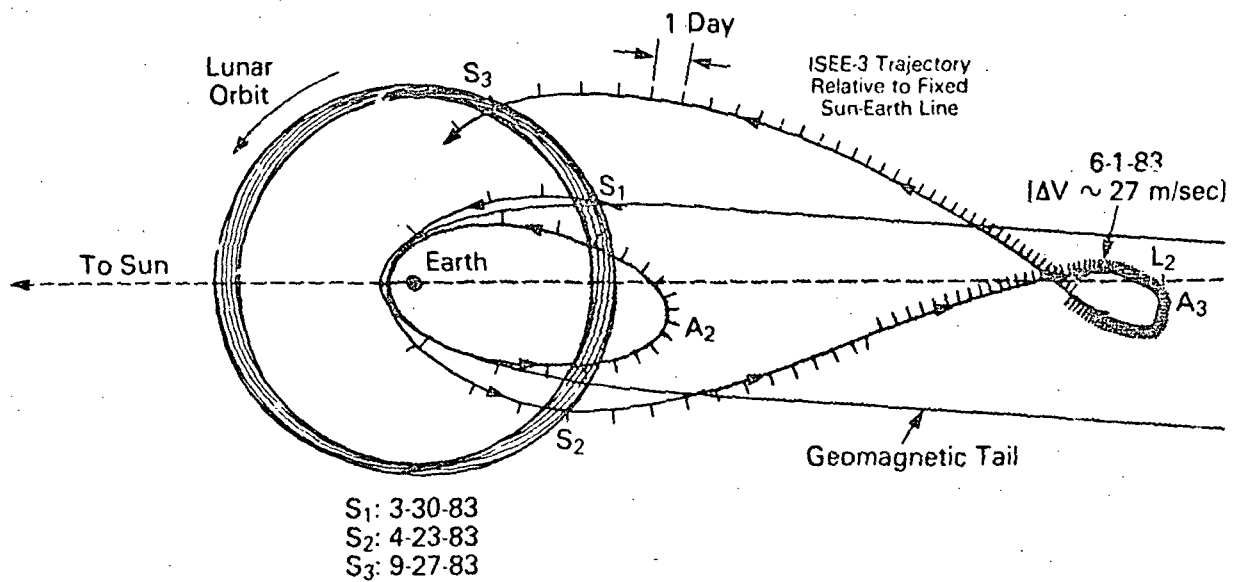*Figure 3.   ISEE-3 on an accurate escape trajectory towards its encounter with Giocobini-Zinner.*
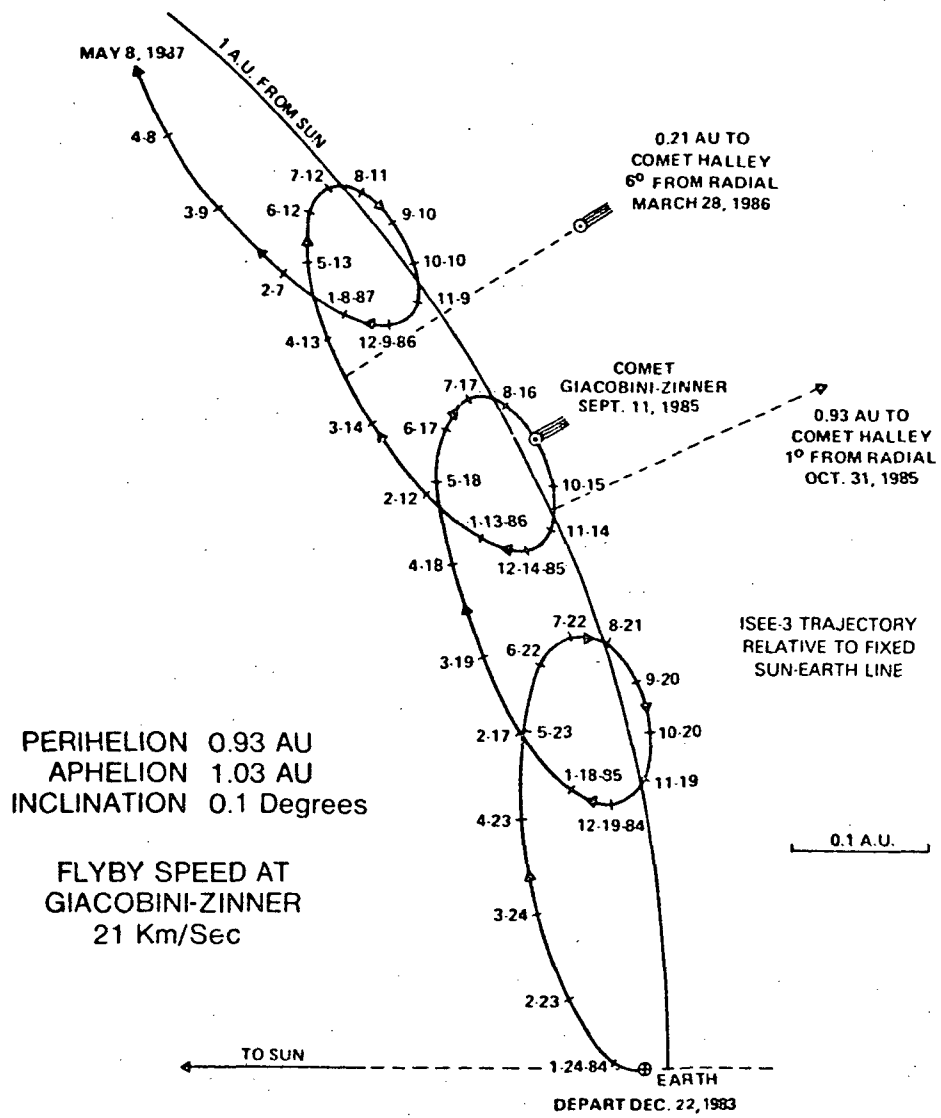
PERIHELION 0.93 AU
APHELION 1.03 AU
INCLINATION 0.1 Degrees

FLYBY SPEED AT
GIACOBINI-ZINNER
21 Km/Sec

Figure 4.   ICE spacecraft heliocentric orbit.

OBSERVABILITY OF DUST PARTICLE IMPACTS ON THE ICE SPACECRAFT

A study was undertaken to examine the feasibility of deriving comet tail dust density information from observations of spacecraft attitude dynamics during a comet flyby. Although the results of this study may find application for any comet explorer, it was specifically aimed toward the International Comet Explorer (ICE) currently scheduled to encounter the tail of the comet Giacobini-Zinner in September 1985.

This study became one of solving two general problems. The first was the modeling of expected spacecraft dynamics following impact by a comet dust particle. The second was to determine attitude knowledge accuracy and the sensitivity of ICE spacecraft attitude sensors to modeled particle impact. The relevant sensors for this study that are flown on ICE are an accelerometer and Fine Sun Sensor (FSS). The study approach was weighted toward producing numerical results from the Flexible spacecraft dynamics (FSD) simulator. Although the FSD simulator had been used in the past to support analysis of many Goddard spacecraft, some new simulation techniques had to first be determined. In particular, the physics of particle impact had to be investigated in order to understand energy transfer and to properly model impact duration. This effort relied on empirical results available in current literature. Following test simulations with hard verification, an extensive set of simulations were performed. Particle impact points, impact duration and appendage configuration were varied. A dust density model from the Jet Propulsion Laboratory (JPL) provided a range of particle masses which might be expected in the planned ICE flyby trajectory. The results of the FSD simulations, along with ICE attitude sensor performance analysis provided the basis for concluding the following:

1. The accelerometer frequency response is too low (30 cycles/second) and the sensitivity is too coarse (10^{-4} m/sec^2) to detect and measure any of the impacted particles on the ICE spacecraft.

2. The FSS (with an accuracy of 0.05 degrees) appears capable of measuring impacting particles only if their masses exceed 0.1 gram. JPL's modeled dust fluence for the encounter with Giacobini-Zinner indicates that the probability of such an impact is less than 0.1 percent.

3. The integrated effect of all particle impacts during the ICE encounter with Giacobini-Zinner should result in a small (less than 0.01 degree) cumulative attitude change for the spacecraft. This result tends to substantiate results from another independent study on this subject.

Although these study results could not justify additional analysis for the purpose of deriving dust information from ICE attitude dynamics, valuable information was provided to ICE mission planners. The spacecraft can now be targeted to the comet tail with added confidence that the spacecraft will survive the encounter with small attitude errors.

Contact: T. Stengle, D. Howell
             Code 550

Sponsor: Director's Discretionary Fund

SYSTEM AND SOFTWARE ENGINEERING

MULTISATELLITE OPERATIONS CONTROL CENTER (MSOCC) SOFTWARE DEVELOPMENT ENVIRONMENT

Two major products were completed during FY84 in the area of software productivity analysis, a "Realtime Design Check" methodology, and a comprehensive report on the software methodologies and tools utilized for developing software in MSOCC.

In evaluating the current MSOCC methodology, it became apparent there was a lack of performance analysis estimation early in the life cycle of system development. If such a performance analysis is not performed, the risk of producing a system which underperforms is significantly increased. A methodology was developed that can be used to predict the resulting performance of a system in the conceptual design phase. The methodology leads system developers through the completion of several forms (computerized spreadsheets) that facilitates:

- Development of a complete hardware diagram of the system.

- Development of the performance characteristics of all devices attached to the system.

- Development of input/output usage estimates.

- Development of central processing unit usage estimates.

- Development of total memory usage estimates.

- Development of a resource contention matrix.

This methodology, which is called the "Realtime Design Check," is documented in a report published in March 1984. The methodology has already been used successfully to identify potential performance problems with the Data Operations Control System.

The second product is a comprehensive report (and executive summary) on the current methodologies, their inherent problems, and the recommended changes to improve software development productivity in MSOCC.

The recommendations are grouped into the following categories:

- Changes to physical environment

- Changes to methodologies

- Recommendations on the purchase, or detailed evaluation (according to FIPS 99) of commercially available tools.

The report clearly identifies the primary software development problems in MSOCC, analyzes a large number of possible solutions to the problems, and recommends a specific set of the possible solutions to pursue further. Expected benefits, techniques to measure them, and an extensive bibliography are also given.

The results of the study were presented to contractors and to Code 510, who felt the problems were correctly identified and the solutions warranted action. As a result, a tools working group has been established to implement the recommendations of the study.

Contact: Gardiner Hall
                Code 511

Sponsor: Office of Space Tracking and Data Systems

SYSTEM COST ANALOGY TECHNIQUE

The purpose of the System Cost Analogy Technique (SCAT) is to provide an automated ability to obtain an end-to-end view of the ground system for both past and future missions in terms of resource needs (hardware, software, staff, and cost) over the life cycle of each mission in each facility within Mission and Data Operations. SCAT combines algorithms for comparing spacecraft ground data system architectures, functions, performance, and cost with a commercial spreadsheet package (Lotus 1-2-3) for data manipulation and display. SCAT is implemented in the Lotus 1-2-3 language on the IBM Personal Computer and is generally available through the Mission and Data Operations Office Automation Program.

SCAT encompasses a three-tiered hierarchy of spreadsheets. The highest level spreadsheet provides an integrated view of the entire ground system for any mission selected. The middle level provides several more detailed spreadsheets, one per functional area of the ground system. To date these encompass command, control, flight dynamics, data capture, processing, and distribution. The lowest level currently includes 31 spreadsheets, one for each mission-function combination (e.g., one for Space Telescope's control center and another for Space Telescope's data capture facility).

Each spreadsheet may be used either as an historical record of an existing mission or as a planning aid for a future mission. When used as a planning aid, SCAT helps the user select a "most similar" spreadsheet and then further helps the user make a variety of analogy adjustments by virtue of features embedded in the spreadsheets (e.g., automatic inflation to year of choice, built in complexity multipliers for disanalogy minimization, and ready manipulation of all resource values). All spreadsheets include automated tabular or graphical display of results.

In FY84 SCAT was implemented in four GSFC divisions within Mission and Data Operations for the purpose of providing a distributed decision support system capability. Each new mission using any of the functions or facilities of these divisions is expected to obtain a SCAT resource needs forecast during its Phase A study. In addition, a new spreadsheet will be created for that mission-function and subsequently updated at the end of each system engineering phase (B,C,D, and E). In FY 1985 SCAT will be extended to cover the remaining two divisions of Networks and Communications. In addition, a variety of SCAT evaluation and training sessions are planned.

Contact: Thomas J. Grenchik
                Code 522.2

Sponsor: Office of Space Tracking and Data Systems

SOFTWARE ENGINEERING TECHNOLOGY

During this past year, three major software reports were generated from the work performed in the software engineering technology studies. The three reports include:

- Managers Handbook to Software Development
- An Approach to Software Cost Estimation
- Recommended Approach to Software Development

These reports now provide the basis for the set of standards and the overall approach to the software development/management process within the flight dynamics area at

GSFC. They have also been adopted by several other organizations within NASA and will become a major contribution to the NASA-wide set of software standards and practices currently under development by the Office of the Chief Engineer.

The three reports are based on results of numerous software experiments and studies conducted at GSFC in an attempt to evaluate the impact of various software development processes and products. Flight dynamics projects, required to support GSFC missions, were used to measure proposed state-of-the-art techniques for the development process. By applying the techniques to these software projects and by closely monitoring the software process and product such measures as cost, reliability and overall complexity could be used to evaluate the techniques.

The software development techniques that have been studied in-depth include such technologies as independent verification and validation (IV&V), PSL/PSA, axiomatic design, Halstead metrics, structured analysis, structured programming, and numerous other software development methodologies and tools.

The reports that have been generated are designed to provide a general recommended framework for the overall software development/management process. The tools, techniques, measures and general approaches that are captured within these reports reflect the results of the studies and experiments that have thus far been completed.

Contact: Frank E. McCarry
Code 550

Sponsors: Office of Space Tracking and Data Systems and Office of Aeronautics and Space Technology

VISIPROG PROGRAM DEVELOPMENT ENVIRONMENT

VISIPROG is a program development environment with which to rapidly develop, test, and debug prototypes of soft - ware system components. The goal of this research is to gain insight into the very nature of prototypes and to develop experience in the use of prototyping approach for the development of spacecraft data systems. The VISIPROG system was developed as a joint program with the University of Maryland and the State University of New York. The simplistic model includes three physical windows displaying: (1) the input to the program, (2) the program itself, and (3) the output of the program.

In addition to these three windows, the system will support a simple mechanism for debugging via observation and control windows. Observation windows are essentially real time, interactive program checkpoints. Control windows permit direct, interactive manipulation of variable values. Observation and control windows may be "opened" at meaningful locations in the program.
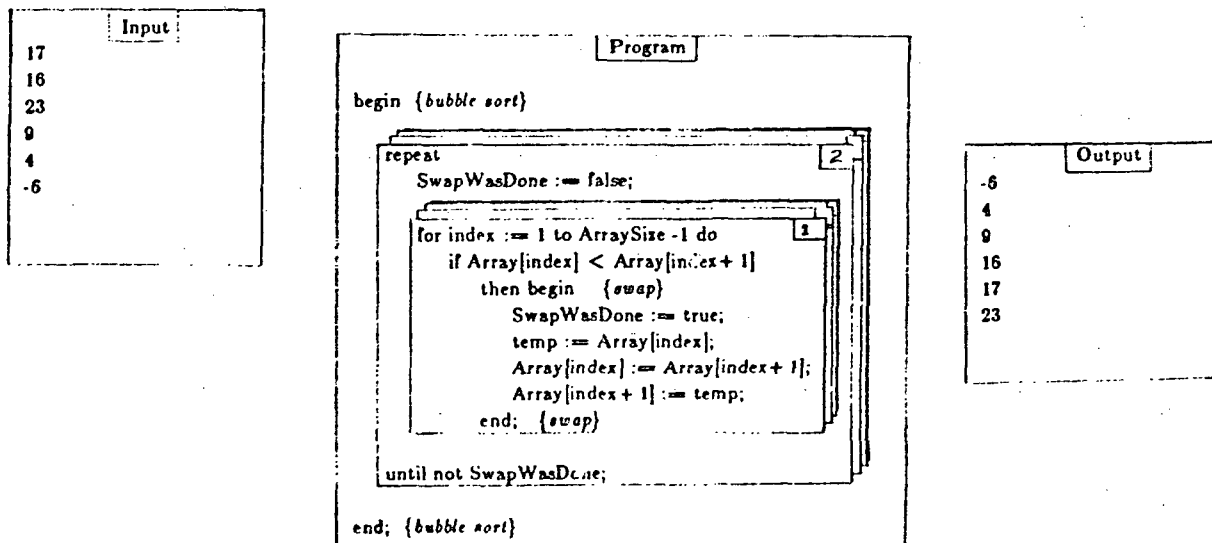
VISIPROG System Model

A language-knowledgeable editor is employed to ensure the syntactic correctness of the program at all times during program creation and updating. In addition, all static semantic errors (undefined variables, type conflicts, etc.) are automatically identified by the system.

VISIPROG uses a unique three dimensional display technique (see figure) for effectively illustrating the dynamics of program execution. In particular, each iteration control construct (e.g., while, repeat, for) is displayed using slightly skewed overlapping windows, one window for each execution iteration of the construct. This gives a unique three dimensional effect in which program execution is the third dimension, with "time" moving into the display. A mouse interaction device is used to "zoom in time" to select the window corresponding to a desired iteration. Observation and/or control windows may now be opened to observe and/or control data for this iteration. This feature provides an extremely powerful interactive debugging facility.

Editing of values in the input window directly and immediately influences the output window to ensure consistency between the input data and the data transformation defined by the program. The VISIPROG system also provides a mechanism for illustrating the correspondence between data fields in the input (output) window. Hence the association between input/output data and the corresponding input/output statement can always be established.

Current plans for the system include providing an Ada program prototyping capability and providing system access to GSFC program designers and developers for system performance evaluation.

Contact: Walter Truszkowski
          Code 522.1

Sponsor: Office of Space Tracking and Data Systems

GRAPHICAL USER INTERFACE DESIGN SYSTEM (GUIDES)

A major challenge for system engineers in the coming years is to develop systems which users can learn quickly and operate effectively. The user-computer interface is a major factor in determining whether a software system can be readily mastered by th user population. The GUIDES project was initiated to provide a tool for the rapid prototyping of dynamic user-computer interfaces.

Rapid prototyping is a software methodology that allows the interface designer to iteratively design and evaluate the learnability and effectiveness of several user interfaces with the intended users. This iterative approach to evaluation and modification of the user interface can be done early in the system development cycle, and, therefore, can be accomplished without costly software modifications to the application. A prototype, or model of the real system, permits a user to develop an understanding of the way the real system would work. This approach enables the developer to test and modify the user interface to optimize the interaction between the user and the system.

During FY84, research into the software market for such a rapid prototyping tool revealed a few user interface design systems, however, none provided facilities for evaluating the user interface and each had key limitations in the flexibility of the design capability provided to the interface developer. A functional requirements study was accomplished and supported by a detailed operational scenario depicting the steps for designing a user interface using GUIDES.

GUIDES enables the developer to interactively design and modify a user interface by using a sophisticated graphics editor and a User Interface Management System (UIMS). The GUIDES concept differs from many available graphics editors and computer-aided design packages because it incorporates a UIMS and also a built-in data collection and analysis capability. The UIMS enables a previously designed graphic display to become a dynamic user interface. The analysis capability assists in evaluating the alternative display designs which can be tested by actual users.

The completed design of GUIDES covers the four steps involved in creating a user interface:

- the graphics editor which allows one to create, edit, and save the layout of the screens (menus, messages, work spaces, graphic symbols, etc.) for a specific application;

- the mapper which maps interactively selected display items (e.g., touching a menu item) to an action routine in the application program;

- the interface execution which allows end-users to interact with the prototype interface, performing specific tasks and generating human performance data; and

- the data analyzer which assists the developer in detecting areas for improvement in the interface.

Contact: Karen Moe
          Code 522

Sponsor: Office of Space Tracking and Data Systems

MACHINE INTELLIGENCE

The objective of the Knowledge-Based English Enquiry Crew Activity Planner (KNEECAP) demonstration project is to explore the feasibility of using a knowledge-based expert system to support autonomous space station operations. The system is an adaptation of the existing Knowledge Based System (KNOBS), developed by the MITRE Corporation under sponsorship of the U.S. Air Force.

The operational capability goal is to allow the on-board crew to do their own activity timeline planning. The system will allow a crew member to define an activity and place it on the timeline. The system, in turn, will check three types of planning constraints.

- Whether there is time available on the crew member's timeline to accommodate the activity;

- Whether special constraints pertaining to the particular activity are satisfied (e.g., orbital position windows, sunlight/darkness conditions); and

- Whether overall timeline constraints are satisfied (e.g., required frequency of periodic activities, required order of sequential activities).

The system assists the crew not only in the initial formulation of activity timelines, but also in the replanning due to changed circumstances, while still maintaining the original constraints. The system also permits the crew to modify the constraints without reprogramming, in case the constraints prove insufficiently flexible or otherwise inappropriate. Finally, the system informs the crew of schedule impacts resulting from reported platform status changes, and responds to inquiries regarding acceptable planning alternatives.

The major accomplishment of FY84 is the completion of a working prototype demonstration system. This system runs on a DECsystem 20 mainframe computer and the INTERLISP programming environment. Currently the system makes use of four primary types of frames. (A frame is a collection of related data slots where specific values can be entered.) These frame types are:

- The mission frame, which has slots for items that are generally true for the entire Space Shuttle mission, (e.g., mission identifier, launch and landing sites, etc.);

- The payload frame, which has slots for details about each particular payload (e.g., payload name, length, weight,

and, if deployable, deployment window limitations in terms of latitude, longitude, and altitude values);

- The crew member frame, which acts as a coordination point for all activities scheduled for a particular crew member;

- The activity frame, which has slots for assigned crew member, activity type, related payload, begin time, and duration slots used for actual scheduling.

Using these frame types, the system can demonstrate capabilities such as:

- Single-slot constraints, e.g., checking that legitimate values are entered for launch site or landing site.

- Inter-slot constraints within one frame, e.g., checking that the launch site chosen is consistent with the orbital inclination chosen.

- Simple inter-frame constraints, e.g., checking that the lowest planned altitude in the Mission frame does not exceed the maximum permissable deployment altitude in an associated payload frame.

- Complex inter-frame constraints, e.g., checking that the ground track location computed from the start time in a deployment activity frame is within the latitude and longitude windows specified in the associated payload frame.

- Use of English-like queries, e.g., asking "WHEN ARE THE PALAPA-DEPLOY OPPORTUNITIES ON FLIGHT DAY 1?" to obtain a list of activity start times with acceptable corresponding ground track locations.

- Recently, the KNEECAP project has begun a new effort to move from a shared mainframe computer to a single-user LISP machine, specifically, the Symbolics 3600. This conversion which involves a software translation from INTERLISP to ZETALISP, will allow KNEECAP to achieve much faster response times than are possible on the shared mainframe. In addition, the move will allow KNEECAP to use a high-resolution bit-map graphics display, a window system, and a mouse-controlled pointer for the creation of a much more comfortable and efficient user interface.

Contact: J. Lundholm
Code 402

Sponsor: Office of Aeronautics and Space Technology

FLIGHT PROJECTS AND MISSION DEFINITION STUDIES

Highlights of FY84 in Flight Projects and Mission Definition Studies include the success-ful repair in space of the Solar Maximum spacecraft and the launches of Landsat-5, the Active Magnetosphere Particle Tracer Explorers, and the Earth Radiation Budget Experi-ment. In addition, planning and development continued for future free-flyers and Shut-tle payloads.

FLIGHT PROJECTS

THE SOLAR MAXIMUM REPAIR MISSION

On April 6, 1984, the Shuttle Orbiter Challenger lifted off with the STS-41C payload consisting of the Long Duration Exposure Facility (LDEF) and the Solar Maximum Repair Mission (SMRM) hardware and equipment flying a direct ascent to the Solar Maximum Observatory orbit. Upon achieving orbit, the cargo bay doors were opened and the Flight Support System (FSS) was checked out. The second flight day was devoted to the checkout of the Remote Mani-pulator System (RMS) and deployment of LDEF. At sunrise on the third day, the astronauts maneuvered the Orbiter to effect rendezvous with SMM. Astronaut James Crippen then brought the Orbiter within 200 feet of SMM and maintained station keeping while Astronaut George Nelson donned the Manned Maneuvering Unit (MMU) and prepared for the flight over to the satellite for capture. Astronaut James Van Hoften assisted Nelson in the MMU checkout and its outfit-ting with the Trunnion Pin Attachment Device (TPAD). The GSFC Payload Operations Control Center (POCC) also issued the final commands to the SMM to place it in a safe-to-capture configuration.

After POCC verification, Nelson flew the planned approach out of the cargo bay toward the SMM. Within the last few feet, he aligned the MMU between the gap in the arrays, and moved in for the trunnion capture. On the first impact of the TPAD with the spacecraft trunnion pin, the device failed to trigger and lock on to the pin. Twice more, Nelson backed away and unsuccessfully repeated the impact maneu-ver with increasing MMU velocity. Substantial spacecraft momentum had been imparted to the SMM resulting in rota-tion about all three spacecraft axes. To reduce these effects, it was decided that Nelson would grasp the starboard solar array and utilize the MMU propulsive capability to remove momentum. The crew felt that a contingency capture of SMM using the RMS could be effected if rates could be slowed. Because of the complex inertia imparted to the spacecraft, this technique was not effective. Due to low MMU fuel reserves, Nelson was called back to the Orbiter. An RMS capture was then attempted but SMM rates were too high and Sun angles incorrect. No capture was accomplished on Day 3 and the Orbiter was backed away for station keeping. The POCC then initiated actions to stabilize the now badly tumbling SMM. Because of high tumble rates, little solar power was available to charge batteries. The SMM was pro-gressively powered down while engineers were analyzing corrective actions.

It was decided to replace the existing magnetic unloading program, which contained both spacecraft steering and unloading capabilities, with a stronger magnetic unloading program called (B-Dot) which applies full energy to unloading spacecraft momentum. To accomplish this soft-ware change, 48,000 bytes of computer memory had to be dumped and reloaded prior to depletion of battery power.

While this program was eliminating spacecraft rates, power was being rapidly exhausted. Some 12 hours after initial cap-ture attempt, the spacecraft had been stabilized and, by good
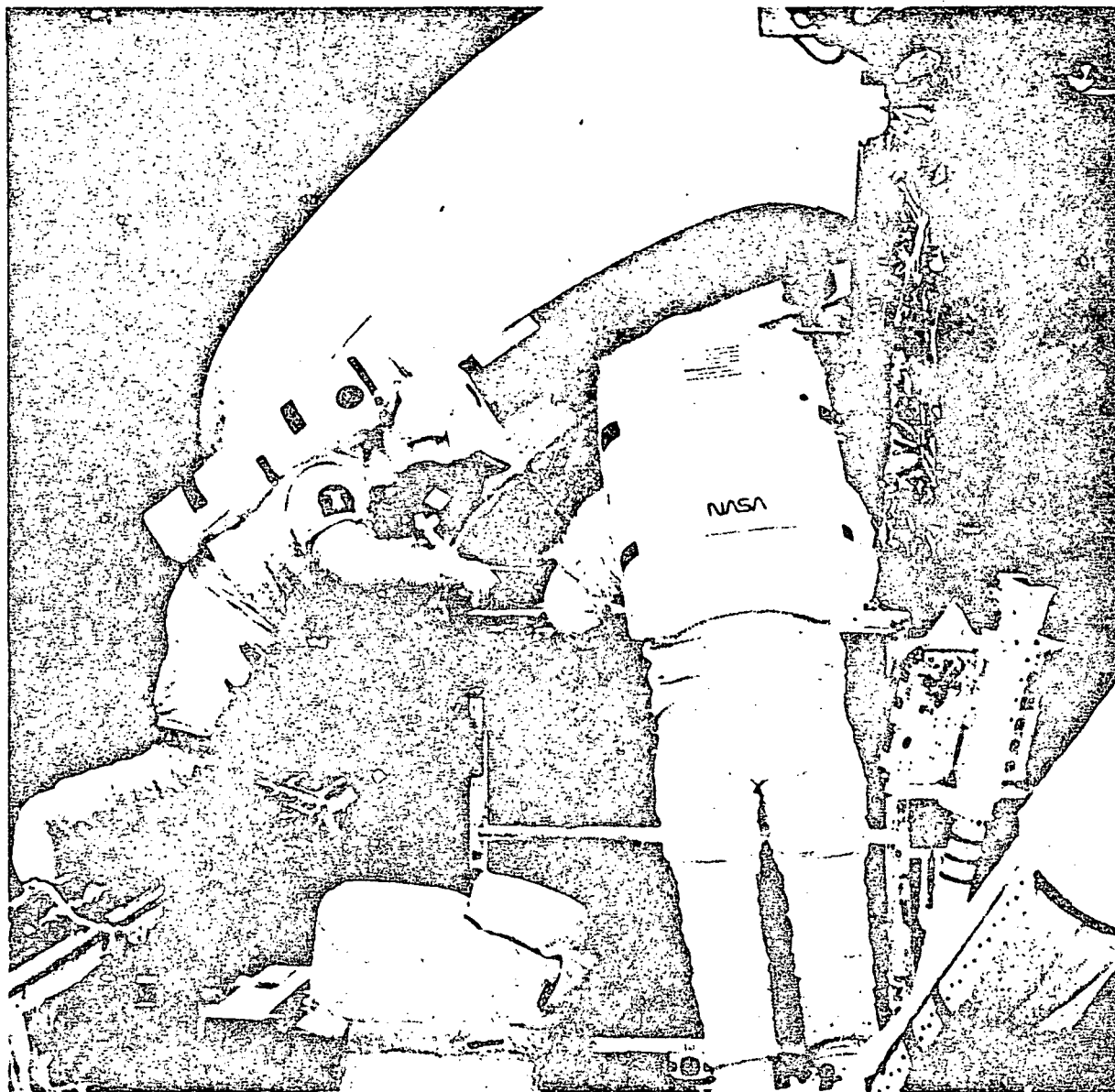
Following SMM berthing to ESS, Drs. Nelson and Van Hoften beginning MACS replacement.

fortune, was coarsely pointing at the Sun as it came out of eclipse. It was then necessary to offload the last program and reload the initial spacecraft program so as to maintain Sun pointing attitude.

The normal magnetic pointing program accomplishes Sun pointing by spinning the spacecraft about the roll axis at 0.9 degree per second through application of torque against the Earth's magnetic field in the pitch and yaw axes. Ground simulations indicated that a 0.5 degree per second spin rate

would be best for RMS capture. Unfortunately, as spacecraft spin rates are reduced, wobble about the pitch and yaw axes increases markedly. The spacecraft algorithm was modified to achieve this roll rate and through the next 24 hours the SMM was held Sun pointing and in full battery charge state.

Early on the fourth flight day, the second rendezvous was initiated. In order to conserve RCS propellant, the rendezvous and docking procedure was revised for this attempt.
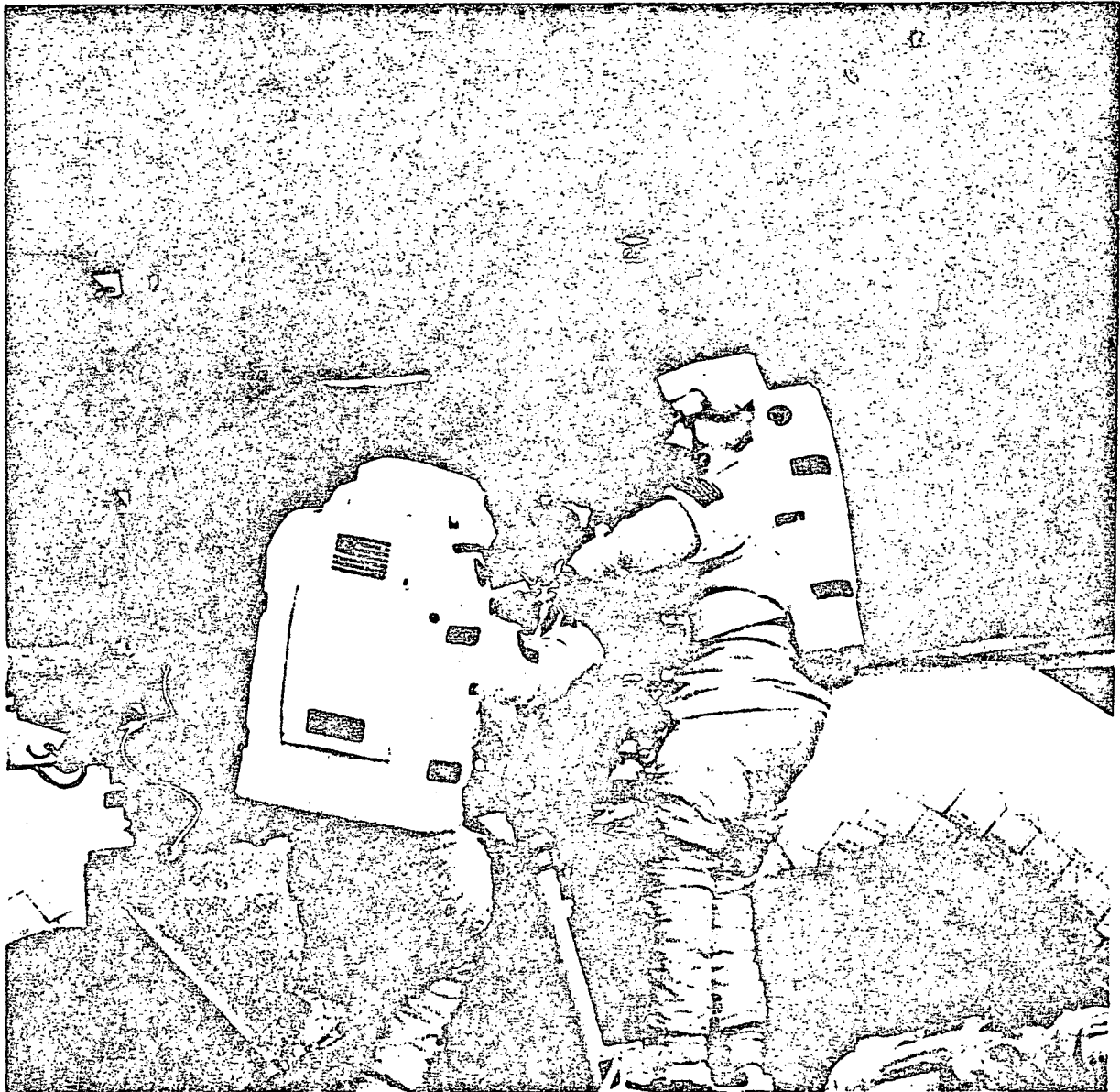
Astronauts completing the C/P MEB interchange.

The Orbiter was brought much closer to the SMM at the completion of the rendezvous maneuver and closure and capture initiated immediately. As Crippen flew the Orbiter up under the spacecraft, just above the cargo bay, Astronaut Terry Hart controlled the arm overhead. At the same time, SMM rotation and wobble angle rates were provided to Houston Mission Control from the POCC and relayed to the crew. Some 2 minutes after loss of voice contact over the Pacific, the SMM spacecraft was captured by the Orbiter RMS on

the first attempt. The satellite was then berthed on the FSS without difficulty.

The timeline was revised to accomplish the repairs in a single EVA. With the satellite under the control of the POCC, a baseline prerepair performance test was completed. On the morning of the fifth mission day, Astronauts Nelson and Van Hoften entered the cargo bay and initiated the repair with

the change-out of the Main Attitude Control System (MACS) module and installation of the X-ray Polychromator (XRP) Plasma Baffle. Following this activity, repair of the Main Electronics Box (MEB) was completed.

All repair activities were accomplished well ahead of the timeline. With the specialized tools provided, both astronauts found the repair tasks easier in space than in the neutral bouyancy facility. The relative ease with which the intricate MEB repair was accomplished indicates that with proper planning and training, much more difficult operations by EVA are possible.

After repair, a functional test was performed of the replacement ACS module. The spacecraft was then deployed on the RMS, the high-gain antenna extended, and a post-repair performance test accomplished by the POCC. The SMM was deployed in a fully operational condition on the sixth flight day of the mission. Although the planned reboost of SMM could not be accomplished due to shortage of propellant, an engineering test to confirm structure analysis was conducted using an RCS engine.

The failed hardware returned on the mission affords a unique opportunity to confirm failure analyses and to study the long-range effects of space environment on components and materials.

Initially, emphasis is being placed on confirming the postulated failure modes. Troubleshooting is being conducted to isolate the causes, components are to be replaced and system performance confirmed. Failed parts will be subjected to failure analysis to determine the failure mechanisms. After functional performance is reestablished, selected components will be removed and analyzed for parameter changes.

Materials are being studied to confirm postulated space degradation. Hardware is being inspected for evidence of micrometeorite damage.

Contact: Frank Cepollina
        Code 408

Sponsor: Office of Space Science and Applications

UPPER ATMOSPHERE RESEARCH SATELLITE MISSION

The objectives of the Upper Atmosphere Research Satellite (UARS) Mission are to understand the mechanisms that control upper atmosphere structure and variability, assess man's impact on the Earth's ozone layer, assess the potential effect of stratospheric change on weather and climate, and develop an effective strategy for stratospheric monitoring.

Meeting these objectives requires coordinated measurements on a global scale of atmospheric chemistry, winds, and energy input. These data will be acquired by a single observatory containing 11 scientific instruments and orbiting the Earth at an altitude of 600 km and an inclination of 57°. The UARS observatory will be a 3-axis stabilized, Earth-oriented satellite and will use the Multimission Modular Spacecraft (MMS) for attitude control, communications, and power storage. Since analysis of coordinated measurements is essential to the mission, a Central Data Handling Facility (CDHF) will be implemented at the GSFC for data processing and storage. Computer-based remote terminals will be located at each of the Principal Investigators facilities for communication with the CDHF and for performing data analysis.

During FY84, execution phase contracts and institutional agreements were signed for the flight instruments and conceptual reviews were conducted. The procurement process for the observatory was initiated and General Electric was selected as the observatory contractor. This contract is scheduled to start in April 1985. Also during this period, development of ground system requirements continued and preparation of the preliminary specification and statement of work for the CDHF was completed.

Current project planning is based on launch of the observatory in the fall of 1989 and 18 months of flight operations and 12 additional months of data processing and analysis.

Contact: Peter T. Burr
        Code 430

Sponsor: Office of Space Science and Applications
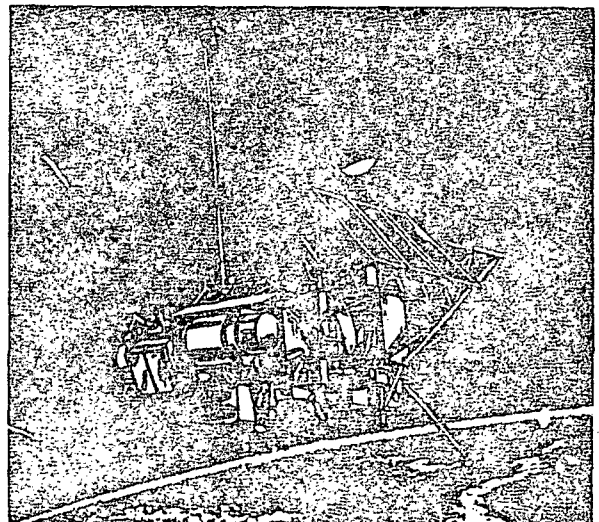
Upper Atmosphere Research Satellite.

ACTIVE MAGNETOSPHERIC PARTICLE TRACER EXPLORERS (AMPTE)

AMPTE stands for a group of three satellites that will work together to increase our understanding of Earth's magnetic fields. The three spacecraft in this international venture are the Ion Release Module (IRM), supplied by the Federal Republic of West Germany; and the United Kingdom Sub-satellite (UKS), supplied by the United States. All three were launched in early August 1984 by a single Delta vehicle with the Charge Composition Explorer (CCE) on top, the UKS in the center, and IRM on bottom (see figure).

The broad scientific objectives of the AMPTE program are to: 1) investigate the transfer of mass and energy from the solar wind to the magnetosphere that surrounds and protects the Earth, and its further transport and accelera-tion within the magnetosphere; 2) study the interaction between artificially injected and natural space plasmas; 3) study the dynamics of the charged-particle population in the magnetosphere; and 4) explore further the struc-ture and dynamics of ambient plasmas in the magnetosphere, particularly in the boundary regions.

The Delta vehicle placed all three satellites in an elliptical orbit, with an inclination to the equator of 28.8 degrees. The IRM and UKS were locked together in a single framework which had a solid rocket motor attached. This motor was fired at perigee to raise the IRM/UKS apogee. The CCE spacecraft also had a small solid rocket motor attached. It was fired at apogee in order to change its direction, so that the spacecraft orbit was aligned with the equator (within 5 degrees), while retaining the original apogee and slightly raising the perigee. The two higher spacecraft, which separated on a later orbit and operate independent-ly, retained their original equatorial inclination. The pur-pose of the differing orbits is to initially place the higher satellites outside the Earth's magnetic fields at apogee, while the lower one operates within the magnetopause, the outer boundary of Earth's magnetic field.

The IRM, by far the heaviest spacecraft at about 705 kilograms (1,554 pounds), has eight releasable canisters, each filled with 5.8 kilograms (12.8 pounds) of a lithium-copper oxide mixture, and eight similar ones filled with 13.5 kilograms (29.8 pounds) each of barium-copper oxide. The IRM also contains a plasma wave spectrometer, magnetometer, and other scientific instruments.

The UKS, which weighs 78 kilograms (172 pounds), con-tains a comprehensive set of plasma measuring instruments.

It has a cold-gas nitrogen propulsion system which can move the spacecraft from its minimum operating distance of 100 kilometers (62 miles) to 6,000 kilometers (3,728 miles) away from the IRM, as needed to measure the results of specific experiments.

The CCE weighs 240 kilograms (529 pounds). It has spec-trometers and magnetometers similar to those on the other two spacecraft. It differs from them in that its position below the upper magnetic field boundary provides a very different environment for its instruments to study the results of the active experiments of the IRM.

One of the most challenging unknowns in solar terrestrial physics today is how the energy and mass in the particles of the solar wind constantly emitted by the Sun are transfer-red to the magnetic fields of the Earth.

Early in the mission, scientists will release lithium canisters while the IRM is at apogee, above the magnetopause and the bowshock—the turbulence caused by the constant impact of the solar wind on the magnetopause. When an ion cloud is formed from the lithium gas, the solar wind will sweep it along through the bowshock until it reaches the magnetopause. There the scientists expect most of the vast stream of ions to spread out on all sides, entering the Earth's magnetic field at the north and south poles and going around the Earth to the rear, following the comet-shaped structure of the magnetopause. But some of these ions will penetrate the Earth's magnetopause, moving in toward the inner magnetic fields. With the CCE studying this activity from below, while the IRM and UKS study it from above, scien-tists expect to acquire valuable new data on exactly how the solar wind interacts with the bowshock and Earth's magnetic fields.

In December 1984, 4 months after the first lithium re-leases, normal precession processes will have moved the IRM and UKS satellites to where they will reach apogee directly ahead of the Earth as it moves along its orbital path. At apogee barium canisters will be released which will form an artificial comet, one with a diameter of as much as 600 kilometers (373 miles). Due to the way the bowshock widens and curves as it moves around the Earth, this comet will form above the magnetopause but below the bowshock, in an area called the magnetosheath. The results will be quite different from those where the ion cloud from the lithium releases was pushed toward the Earth by the solar wind, providing scientists some valuable new data.

The third set of lithium and barium releases will occur 3 or 4 months into 1985, when precession will have moved the two upper spacecraft to where they will reach apogee
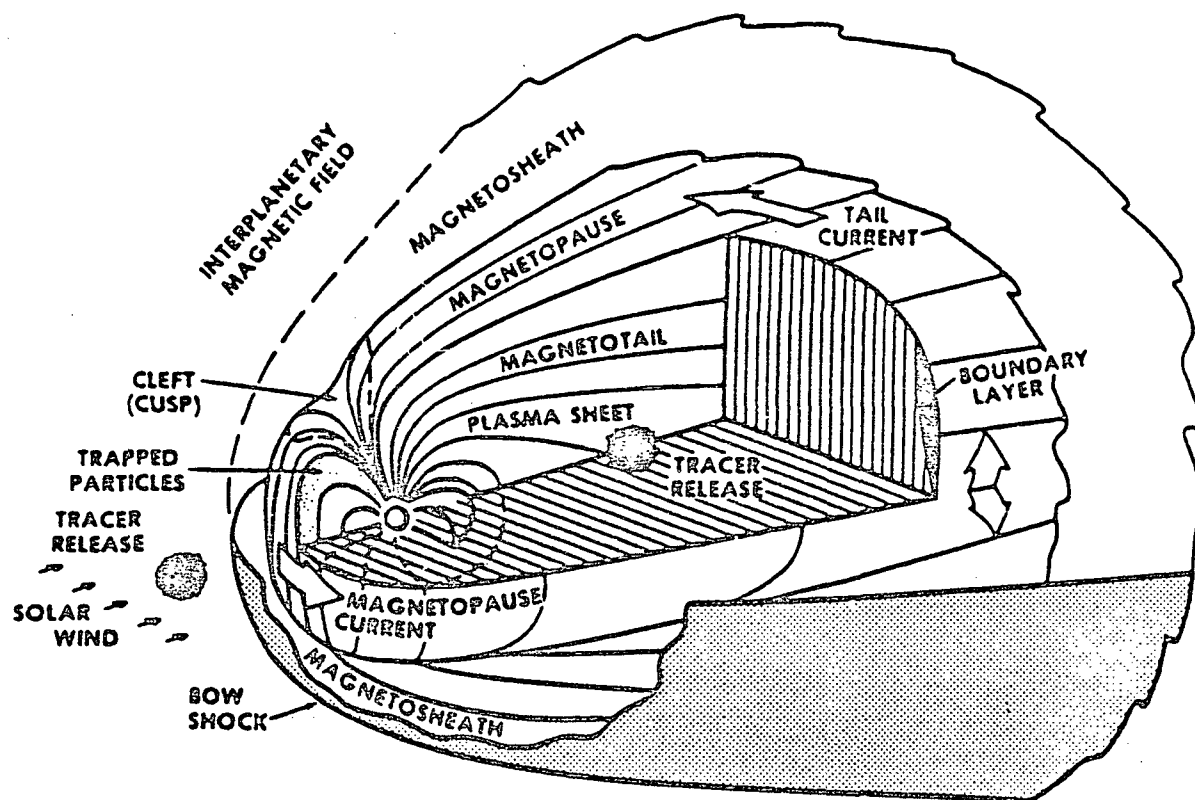
Region of AMPTE study.

behind the Earth in relation to the Sun. This area is called the magnetotail, the area where the magnetic field begins to taper off as the solar wind starts coming together again behind the moving Earth. The IRM will create barium and lithium clouds here at about 57,454 kilometers (35,700 miles) above the Earth's surface. This area is inside both the magnetopause and the bowshock, allowing all the cloud particles to flow directly to the Earth's inner magnetic fields. There, they are expected to flow around the irregular sphere formed by the magnetic fields, and also penetrate inside them.

With one spacecraft releasing chemical clouds at great distances from the Earth, another observing the effects from nearby, and a third watching from below the boundaries of the bowshock and magnetopause. AMPTE is one of the most complex scientific missions ever con-

ducted to gain a better understanding of the Earth's magnetic fields.

The GSFC represents the United States in the AMPTE program and the Applied Physics Laboratory/Johns Hopkins University was the prime contractor for the American Spacecraft (CCE). The Max Planck Institute for Physics and Astrophysics in West Germany, and the Rutherford Appleton Laboratory and Mullard Space Science Laboratory of Great Britain were responsible for the design and construction of their respective spacecraft (IRM and UKS).

Contact: Gilbert W. Ousley, Sr.
          Code 404

Sponsor: Office of Space Science and Applications

CCE

UKS

IRM
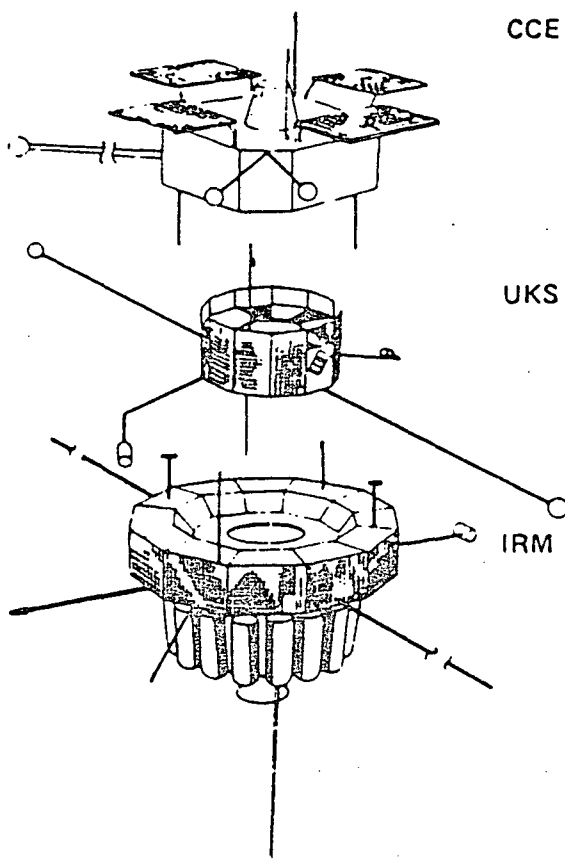
Charge Composition Explorer (CCE), United Kingdom Subsatellite (UKS), and Ion Release Module (IRM).

- A search for evidence of nucleosyn thesis—the fundamental building process in nature—particularly in the environment of supernova.

- Study of gamma-ray emitting objects whose nature is not yet understood.

- Exploration of our galaxy in the gamma-ray range, especially with regard to regions difficult to observe at other wavelengths; the orgin and dynamic pressure effects of the cosmic rays; and structural features, particularly related to high energy particles.

- Study of the nature of other galaxies in the energetic realm of gamma-ray, especially radio galaxies, Seyfert galaxies, BL Lacertae objects and quasars.

- Study of cosmological effects through the detailed examination of the search for primordial black hole emission.

- Study of intense gamma-ray bursts whose origins remain a mystery.

The mission contractor, TRW, has been under contract since February 1983. TRW is responsible for assuring that the overall mission of GRO is successful. TRW will build the spacecraft, integrate the science instruments, test, launch, and operate the observatory in orbit. The Fairchild Space Company (FSC) will furnish the communications and data handling module and the McDonnell Douglas Astronautics Company (MDAC) will furnish the two power modules.

Four large instruments are to be flown. The Burst and Transient Source Experiment (BATSE) is being built by the Marshall Space Flight Center (MSFC), the Oriented Scintillation Spectrometer Experiment (OSSE) is being built by the
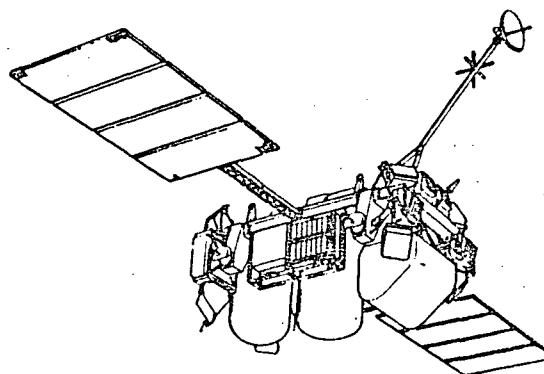
GAMMA-RAY OBSERVATORY (GRO)

The Gamma Ray Observatory (GRO) is one of the first large observatories to use the capabilities of the Space Transportation System (STS). This 35,000-lb observatory is designed to make gamma-ray observations over the energy range from about 0.06 to 3×10^4 MeV. In its 2-year mission the GRO will map the gamma-ray sources in the celestial sphere. The scientific instruments on GRO have sufficient sensitivity, resolution, and dynamic range to address the following crucial topics in astrophysics:

- Study of the dynamic evolutionary forces in compact objects such as neutron stars and black holes.

Gamma Ray Observatory

Naval Research Laboratory (NRL), the Energetic Gamma-Ray Experiment Telescope (EGRET) is being built by the Goddard Space Flight Center (GSFC), and the Imaging Compton Telescope (COMPTEL) is being built by the Max-Planck Institute (MPI). In 1984 all four instruments were in the final stages of design, and flight parts were in fabrication.

The GRO is planned to be flown in the latter part of 1988. The observatory will be placed in a 400-km circular orbit at 28.5° inclination. Data from the observatory will be transmitted via TDRS to the GSFC. The telemetered data are autonomous and will be distributed to the instrumenters for analysis.

Contact: Jerry Madden
         Code 400

Sponsor: Office of Space Science and Applications

SEARCH AND RESCUE SATELLITE-AIDED TRACKING MISSION

During FY84, the Search and Rescue (SAR) Satellite-Aided Tracking (SARSAT) Mission of the Metsat Project worked to improve the experimental 121.5/243 MHz ground system, raising it to an operational support state; continued the demonstration of successful operational use of the 121.5/243 MHz distress data, providing locations used in saving more than 280 people as of September 1984; completed the initial phase of Demonstration and Evaluation, showing that the system met or exceeded expectations; developed a coordinated COSPAS/SARSAT report to be distributed internationally during FY85; and began concentrating on the development of the 406 MHz system to overcome the system deficiencies inherent in the present 121.5/243 MHz system which uses a beacon system designed before satellite detection was a consideration.

The SAR Mission of the Metsat Project at the GSFC is responsible for the U.S. portion of the SARSAT Project, an international cooperative project involving the U.S., Canada, and France. NASA is the system manager of the U.S. participation which includes NOAA, DOT, and DOD. Canada provides the spaceborne repeater for relay of the 121.5 and 243 MHz signals from ELT's carried by approximately 200,000 U.S. aircraft and Emergency Position Indicating Radio Beacons (EPIRB) carried by more than 2000 ships. Canada also provides a repeater for experimental beacons operating at 406 MHz. France provides a spaceborne processor for the 406 MHz experiment beacons. The U.S. integrates these two instruments on board the Tiros Series of NOAA environmental satellites. Each country provides its own ground system. The location of the ELT's and EPIRB's

is accomplished with the same Doppler location principal demonstrated by satellite data collection systems such as the Nimbus RAMS and the ARGOS system. The Soviet Union cooperates with the SARSAT partners by making its own SAR satellite system, COSPAS, interoperable with the SARSAT system. The SARSAT equipment will also be carried by NOAA-F, -G, -H, -I, and -J to be launched during the remainder of this decade. GOES-G and -H will perform 406 MHz SARSAT experiments from geosynchronous altitude.

The first spacecraft capability, the Soviet COSPAS-1 satellite, was launched in June 1982 and made available to the SARSAT Project in September 1982. The second Soviet satellite, COSPAS-2 and the U.S., Canada, France SARSAT systems were launched on board NOAA's NOAA-8 operational environmental satellite. COSPAS-3 was launched in June 1984. It will be made available to the SARSAT Project after completion of check-out by the Soviets. NOAA-8 failed in June 1984. A new NOAA launch (NOAA-F) is planned for November 1984. The satellites are being used by the U.S. Air Force and the U.S. Coast Guard to assist in real world rescue operations using the 121.5/243 MHz Emergency Locator Transmitters (ELT's) employed by the aeronautical community and the EPIRB's employed in the maritime community.

The 121.5/243 MHz beacons have no requirement for a stable frequency component and no unique identification. Therefore satellite detection and location of these beacons presents many problems, such as: not all beacons are satellite detectable; poor locations and poor image rejection occur in some cases; lack of unique identification causes inability of rescue personnel to relate detections to specific beacons; and coverage is restricted to regions in which the satellite can view a ground station and beacon simultaneously. These problems will be eliminated after sufficient research and development on the experimental 406 MHz system allow it to become operational. During FY84, experimentation with the 406 MHz system has allowed the development of the detailed planning necessary to bring the system to operational status. Both beacon and ground system developments for the 406 MHz system will be conducted during FY85 and beyond.

Contact: Fred Flatow
         Code 480

Sponsor: Office of Space Science and Applications

EARTH RADIATION BUDGET EXPERIMENT (ERBE)

The Earth Radiation Budget Experiment (ERBE) Research Program will begin its extensive, long-range monitoring in October 1984 when NASA and the National Oceanic and Atmospheric Administration (NOAA) orbit the first satellite
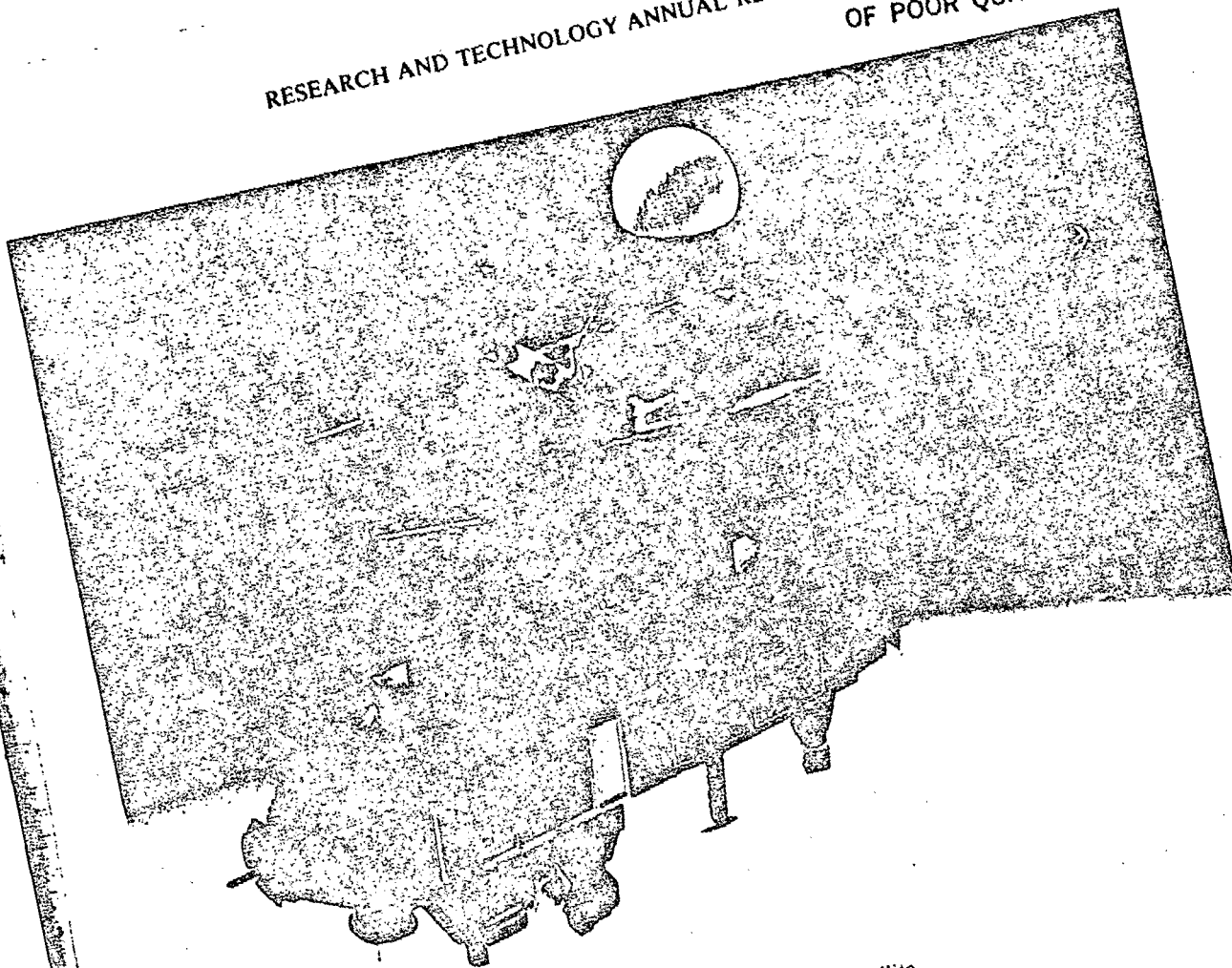
Earth Radiation Budget Satellite.

series for these studies. The system includes the satellite series for these studies, the mid-inclination satellite ERBS, and two Tiros-class satellites in near-polar, Sun-synchronous orbit (NOAA-F and NOAA-G). All three satellites will carry an identical, two-instrument package, called the ERBE. The ERBE will also carry an instrument for monitoring the vertical distribution of stratospheric aerosols, ozone and nitrogen dioxide, called the Stratospheric Aerosol and Gas Experiment-II (SAGE-II). Additional atmospheric physics and weather instruments will be flown on the NOAA satellites. This first satellite series will be analyzed and archived as the data base for all users.

The ERBE Research Program is managed by GSFC, Langley Research Center (LaRC) was given system responsibility for instrument development and science management. The Ball Aerospace Systems Division (BASD) of the Ball Corporation, under contract to the GSFC, designed and built the ERBE spacecraft bus, integrated the scientific instruments,

tested the satellite, and will support launch operations of the Space Shuttle Orbiter. BASD will also support the satellite for its orbital lifetime from the Project Control Center located at GSFC.

BASD also designed and built for the LaRC the SAGE-II instrument carried on ERBE. TRW designed and built for the LaRC the ERBE scanner and non-scanner instruments carried on all three spacecraft.

The ERBE observatory was integrated and tested at BASD, received an acoustics environment at GSFC, was placed on the Shuttle (STS-41G) during FY84, and is scheduled to be launched October 1, 1984.

The other ERBE instruments were also completed by TRW and integrated on the Tiros-class spacecraft at RCA in FY84. NOAA-F is scheduled for launch in early November 1984,

while NOAA-G will be launched in late 1985 or early 1986. Concurrent data are expected to be collected from all three spacecraft.

Contact: Carl L. Wagner, Jr.
Code 406

Sponsor: Office of Space Science and Applications

HUBBLE SPACE TELESCOPE

The objective of the Hubble Space Telescope (HST) Program is to establish and operate an astronomical facility consisting of an orbiting observatory and a ground system which will greatly exceed the capability of even the best ground-based observatory, and to make it available for research in optical astronomy.

The Goddard Space Flight Center (GSFC) is responsible for the science and operations aspects of the HST. Specifically, the HST Project at the GSFC is responsible for managing the following:

- Design and development of the five Scientific Instruments (SI's) for use on the first launch of the HST;

- Design and development of the SI Control and Data Handling (SI C&DH) system;

- Verification and Acceptance Program (VAP) to integrate and test the SI's and the SI C&DH;

- System engineering of the total ground systems;

- Design and development of the Science Operations Ground System (SOGS);

- Establishment and operation of the ST Science Institute (ST ScI), located on the Johns Hopkins University campus in Baltimore, Maryland, which will conduct the science operations; and

- Operation of the total observatory.

In addition, the GSFC Mission and Data Operations Directorate is responsible for the design, development, and maintenance of the Data Capture Facility, the Payload Operations Control Center, and other institutional support.

The European Space Agency (ESA) is providing the HST solar array, one scientific instrument, and participation in science operations.

During FY84, progress has been made in developing and integrating the flight instruments for the HST. The following were delivered to the GSFC and integrated with the VAP ground equipment to ensure readiness for delivery:

- Faint Object Spectrograph (FOS) designed and developed by Martin Marietta Aerospace, Denver Division for the University of California, San Diego;

- High Resolution Spectrograph (HRS) designed and developed for the GSFC by Ball Aerospace Systems Division;

- High Speed Photometer (HSP) designed and developed by the University of Wisconsin;

- Wide Field/Planetary Camera (WF/PC) designed and developed by Jet Propulsion Laboratory for the California Institute of Technology;

- Faint Object Camera (FOC) designed and developed by the ESA;

- SI C&DH designed and developed by IBM and Fairchild of Gaithersburg, Maryland.

The VAP was completed on March 21, 1984, 1 week ahead of schedule. Following the successful completion of VAP, which provided for electrical and performance testing of instruments along with testing for the acceptance of the SI C&DH flight software (which controls instrument status and provides some on-board data processing), the instruments entered a post-VAP rework period. This rework period enabled each of the instrument contractors to adjust and correct those deficiencies that surfaced during or, in some cases, just prior to the VAP.

Subsequent to the completion of this rework period, the instruments are scheduled for delivery to the Lockheed Missiles and Space Company (LMSC), Sunnyvale, California, for pre-Assembly and Verification testing. The first of these delivered was the SI C&DH which was delivered ready for use on July 20, 1984. The WF/PC was delivered and determined ready for use on July 27, 1984. The remaining instruments are completing the final stages of their rework period and will be delivered to the LMSC and be ready for use according to schedule. The last instrument to be delivered and ready for use is now scheduled for November 1984.

The HST Operations Control Center (STOCC) is the facility used for controlling the HST when it is placed into Earth orbit in 1986. The STOCC is located at GSFC and is operated by the LMSC.

The ST ScI has been created to administer the HST science research program for NASA and to plan and conduct the actual HST science observations. It is operated by the Association of Universities for Research in Astronomy under contract to NASA.

The SOGS. a complex network of computers and image processing terminals, is now being developed by TRW under contract to NASA. This system will schedule observations to be made by HST and to process the resulting data and provide products which are useful to astronomers. The hardware parts of the system are being assembled, and computer programs are being written that will enable the system to perform its needed functions. The SOGS will be delivered to the ST ScI beginning in FY85 and will then be subjected to extensive operational testing prior to the launch of HST.

Contact: Frank A. Carr
Code 400

Sponsor: Office of Space Science and Applications

LANDSAT-D

Landsat-D (5) was launched from the Western Space and Missile Center (WSMC) on March 1, 1984 into a 705 km altitude, 9:45 a.m., descending node Sun-synchronous orbit. Performance to date of the flight segment and the Multi-Spectral Scanner (MSS) and Thematic Mapper (TM) instruments has been excellent. About 75 percent of the instrument data taken on Landsat-5 have been successfully transmitted to the GSFC Transportable Ground Station (TGS) and to foreign users. Two minor anomalies have occurred; one of the orbit adjust thrusters has become inoperative, and one of the two narrowband tape recorders used for telemetry shows occasional difficulty in playback. Several successful orbit adjusts have taken place and the Landsat-5 is "on station" with the specified 16-day repeat cycle.

Landsat-4 continues to operate with two of four solar array panels fully functional. Its communication has S-band (both telemetry and MSS direct access) and Ku-band (TDRSS) operative. The command system is fully functional even though a redundant Central Unit (CU) on the On-Board Computer (OBC) has failed. The TM and MSS are operative, and all required subsystems to support Landsat-4 TM and MSS data acquisition are functional. In fact, a unique situation occurred several weeks after the launch of Landsat-5 and before its final "on station" orbit adjust. For several days, both 4 and 5 were in a position to image portions of the same scene simultaneously. Over 100 TM scenes were transmitted; Landsat-4 through TDRSS, and Landsat-5 via direct access X-band to the GSFC TGS. Performances of the TM's were

compared and provided valuable information on their radiometric and geometric calibration.

An inclination adjustment was successfully completed on Landsat-4 in late July 1984. This was the first inclination burn required since the launch of Landsat-4 in July 1982. The flight segment was restored to routine mission operations 1 day later.

An inclination adjustment was successfully completed on Landsat-4 in late July 1984. This was the first inclination burn required since the launch of Landsat-4 in July 1982. The flight segment was restored to routine mission operations 1 day later. The ground segment TM Image Processing System (TIPS) was completed and by the end of July 1984 was operating at specifications with 100 scenes per day of archival tapes, 50 scenes per day of product tapes, and 50 scenes per day of 241 mm film. Portions of the ground segment, devoted to the command and control of the flight segment, the flight segment itself, and the MSS processing operations have been transferred to NOAA in January 1983, on schedule. Landsat-5 and its control and MSS operations were turned over to NOAA in April 1984. TIPS was transferred to NOAA on September 1, 1984, 5 months ahead of schedule. At that time, the Landsat system will become fully operational.

Contact: L. Gonzales
Code 435

Sponsor: Office of Space Science and Applications

HITCHHIKER-G

The objectives of the Hitchhiker-G Program are to provide reduced lead time to flight opportunity, provide increased flight opportunities, reduce space flight costs, and maximize Shuttle load factors.

The Hitchhiker-G will allow exceptionally short preparation time requirements and still provide a full line of Space Transportation System (STS) features that were only available to long-term development programs in the past.

The Hitchhiker-G is based on use of the Shuttle Payload of Opportunity Carrier (SPOC) and applies a concept of filling the Shuttle manifest on an "as-available" basis. The system maximizes use of existing STS interface hardware to allow ease of integration for the customer. Since most Shuttle flights are not manifested to 100 percent capacity, the Hitchhiker-G stands ready to increase the Shuttle load factor in a way analogous to the familiar roadside hitchhiker. Basic capabilities are as follows:

Payload Weight: 750 lbs.
Mounting: Side of Orbiter Cargo Bay
Power: 1.4 kilowatts
Telemetry: 1.4 Megabytes/second to be shared among users
Maximum Number of Users: 6

There is no definite way of predicting the availability of Hitchhiker-G flights, it is expected that an adequate number of opportunities will be made available to supply the needs of interested customers on a timely basis. The most frequent opportunities seem to be for flights at 28 degrees inclination orbit and 160 nm altitude, although other orbit parameters are possible.

The Hitchhiker-G concept will provide the customer with a fairly routine method to obtain space flight opportunity.

During FY84, the System Design and Critical Design Reviews were completed. First flight is scheduled for the spring of 1985.

Contact: T. Goldsmith
         Code 730

Sponsor: Office of Space Flight

SPARTAN

The Spartan Program has developed carriers that replace the sounding rockets as carriers for instruments into the upper atmosphere and nearby space.

The Space Shuttle will transport Spartan to space, with the carrier attached within the payload bay. While in orbit, Spartan is an autonomous subsatellite, free from the constraints of the Space Shuttle. This autonomy allows the scientist to operate his instrument as precisely as he desires without placing any requirements on the Shuttle crew or the Shuttle attitude. The scientist can preplan a pointing sequence for an extensive selection of celestial objects or a particular area of the solar surface, which is executed by Spartan to arcmin precision. The observations are automatically stored on board the carrier on a tape recorder.

After a flight duration of up to 40 hours, Spartan will be retrieved by the Shuttle and returned to Earth. The tape-recorded data will be copied and sent to the scientist for analysis. The scientific analysis of the data is then carried out by the science team.

Three Spartan Missions are currently being developed. Spartan-1, the High-Energy Astrophysics Spartan will provide a structure with an optical bench to accommodate a variety of rectangular array detectors. It is designed to point

at stellar objects. Spartan-2, the Solar Physics Spartan will accommodate a 17-in. diameter telescope. It will use a solar fine-pointing capability to allow it to view selected points on the surface of the Sun. Spartan-3, the Ultraviolet Astronomy Spartan, will use concepts and hardware developed for the first two Spartans. It will accommodate a 22-inch stellar telescope, which is externally similar to the telescope of Spartan-2 and will use a stellar fine-pointing system similar to the one developed for Spartan-1.

Ultimately seven Spartan carriers will be available for flights. During FY84 Spartan-1 development was completed; environmental testing was accomplished; the Spartan Flight Support System completed and tested; and the spacecraft was delivered to Kennedy Space Center. Due to rescheduling of orbiter flights resulting from the first Discovery flight abort, manifesting has not been defined.

Contact: D. Shrewsberry
         Code 745

Sponsor: Office of Space Science and Applications

GET AWAY SPECIAL

The Get Away Special (GAS) payloads are small self-contained, closed or open cylinder-shaped containers housing experiments. These containers are mounted in the bay of the Shuttle.

The main objective of the GAS program is to encourage the use of space by all researchers, private individuals and organizations by providing an easy and comparatively inexpensive method to get a flight opportunity for a GAS experiment. At present, about fifty experiments are planned each year.

Since the beginning of the program, twenty-one payloads have flown to date. During FY84, thirteen payloads have been loaded and ready for flight. Five payloads have flown with eight scheduled for October 1, 1984.

The standard GAS containers are provided in two volumes: 5 cubic feet and 2½ cubic feet. Payloads of 100 and 200 lbs will be housed in 2½ cubic feet containers while 200-lb payloads will be in the 5 cubic feet containers.

To provide a fair opportunity to everyone wishing to participate in GAS programs, each experimenter is limited to two containers in every twenty flight assignments.

Two technological advancements to the GAS carrier system were accomplished over the past year. A Motorized Door Assembly (MDA) for providing a view out of the container

was developed and flown. Also, the preliminary design of a system for ejecting small satellites out of the GAS container was completed.

Contact: J. Barrowman
       Code 742.2

Sponsor: Office of Space Flight

OSS-2

The OSS-2 Program consists of a series of flights whose objectives are to investigate high energy astrophysics. The payload will be evolutionary in nature with a phased development of candidate instruments. As these instruments are developed they will be folded into the mission flight program. The program will baseline the Shuttle Payload of Opportunity Carrier (SPOC) for its interface avionics and in some cases for the instrument structural interface to the orbiter. The first flight of the University of Wisconsin Diffuse X-Ray Spectrometer (DXS) is a prime example of SPOC hardware utilization. The follow-on flights will also include a two-axis pointing system to be used to provide more accurate pointing than possible with the orbiter alone. The pointing system is feasible for use with numerous instruments provided they meet the performance and interface requirements of the pointer.

The first flight OSS-2/DXS objective is to determine the wavelength and intensity of the strongest X-ray lines that are emitted by the hot gas believed to occupy most of the interstellar volume.

The DXS instrument consists of two Bragg spectrometers using lead stearate crystals to cover the wavelength range 44 to 84 A on the first mission. Two more Bragg spectrometers using thalium acid phthalate crystals are added for the second mission to cover the wavelength range 11 to 24 A.

To meet mission objectives, a minimum of 60 orbits are required with continuous nighttime operation of the instrument with the orbiter -Z axis pointed to within 15 degrees of a selected celestial point near the midnight zenith. Additionally, the X-axis must be within 5 degrees of the orbital plane.

During FY84, the development phase of the DXS was started and is presently in the design phase.

Contact: Frank Volpe
       Code 420

Sponsor: Office of Space Science and Applications

THE X-RAY TIMING EXPLORER

The X-ray Timing Explorer (XTE), initiated as a study in 1980, is an Explorer mission dedicated to the observation of galactic sources in the energy range of 2 to 200 keV. Emphasizing measurements of transient phenomena with periods of milliseconds to years, the XTE will carry three major instruments: a Large Area Proportional Counter (LAPC), a Spinning Shadow Camera (SSC) and a High Energy X-ray Timing Experiment (HEXTE). The LAPC has an effective area of one square meter, twice the size of any similar contemporary instrument. The SSC provides a continuous monitor of the global field, providing both a continuous observation of all brighter sources and an alarm function for short-term transient phenomena. HEXTE extends the 60 keV limit of the LAPC to 200 keV. LAPC and HEXTE are narrow-field (1 degree FOV) instruments that will be pointed to targets for extended periods of time.

XTE will be launched by the Shuttle, tentatively in FY91, into a 28.5 degree orbit. It will continue to observe for 2 years at an altitude of 400 km. There will be two Guest Investigator facilities, at GSFC and the Massachusetts Institute of Technology.

The flight experiments were selected through an Announcement of Opportunity in November 1982. During the intervening 2 years, the science team, consisting of three Principal Investigators, has performed preliminary conceptual studies to define the mission requirements and plan the development of the XTE system. The anticipated starting date for the Execution Phase is in FY88.

Contact: William D. Hibbard
       Code 402

Sponsor: Office of Space Science and Applications

ADPE	Automatic Data Processing Equipment
AIRS	Autonomous Integrated Receive System
AMCID	Accumulation Mode Charge Injection Device
AMPTE	Active Magnetospheric Particle Tracer Explorers
AOIPS	Atmospheric Ocean Image Processing System
AOL	Air-Borne Oceanographic Lidar
AU	Angstrom Unit
AVHRR	Advanced Very High Resolution Radiometer
BUV	Backscattered Ultraviolet
COBE	Cosmic Background Explorer
CZCS	Coastal Zone Color Scanner
DE	Dynamics Explorer
DIRBE	Diffuse Infrared Background Explorer
DWS	Directional Wave Spectrum
EGRET	Energetic Gamma-Ray Experiment Telescope
ENSO	El Nino/Southern Oscillation
ERB	Earth Radiation Budget
ESA	European Space Agency
ESMR	Electrical Scanning Microwave Radiometer
EVA	Extra Vehicular Activity
FOC	Faint Object Camera
FSD	Flexible Spacecraft Dynamics
FSS	Fine Sun Sensor
FSS	Flight Support System
FWHM	Full Width Half Maximum
GARP	Global Atmospheric Research Program
GOES	Geostationary Operational Environmental Satellite
GRIS	Gamma Ray Imaging Spectrometer
GRO	Gamma-Ray Observatory
GSFC	Goddard Space Flight Center
HEAO	High Energy Astronomical Observatory
HIRS	High Resolution Infrared Radiometer Spectrometer
HUT	Hopkins Ultraviolet Telescope
HXRBS	Hard X-Ray Burst Spectrometer

ICE	International Cometary Explorer
IRAS	Infrared Astronomy Satellite
IRM	Ion Release Module
IRTF	Infrared Telescope Facility
ISCCP	International Satellite Cloud Climatology Project
ISEE	International Sun-Earth Explorer
IUE	International Ultraviolet Satellite
JON-SWAP	Joint North Sea Wave Project
KNEECAP	Knowledge-Based English Enquiry Crew Activity Planner
LAGEOS	Laser Geodynamics Satellite
LDEF	Long Duration Exposure Facility
LIF	Laser Induced Fluoroscence
LIMS	Limb Infrared Monitor of the Stratosphere
LOD	Length-of-Day
LVDT	Linear Variable Differential Transformers
MACS	Magnetic Attitude Control System
MASS	Mesoscale Atmospheric Simulation System
MHD	Magnetohydrodynamic
MIZEX	Marginal Ice Zone Experiment
MLEBM	Multi-Layer Energy Balance Model
MSOCC	Multisatellite Operations Control Center
MSS	Multi-Spectral Scanner
MSU	Microwave Sounding Unit
NMC	National Meteorological Center
NOAA	National Oceanic and Atmospheric Administration
NSSDC	National Space Science Data Center
PBL	Planetary Boundary Layer
PHA	Pulse Height Analyzer
POCC	Payload Operations Control Center
POCS	Passive Ocean Color Subsystem
POGO	Polar Orbiting Geophysical Observatory
PRB	Pitch and Roll Bouys
RMS	Remote Manipulator System
SARSAT	Search and Rescue Satellite
SBUV	Solar Backscattered Ultraviolet
SCR	Surface Control Radar
SDM	Self Documenting Model

SEEP	Shelf Edge Exchange Processes
SIRTF	Space Infrared Telescope Facility
SLR	Satellite Laser Ranging
SMIR	System Model for Image Registration
SMM	Solar Maximum Mission
SMMR	Scanning Multichannel Microwave Radiometer
SMRM	Solar Maximum Repair Mission
SO	Southern Oscillation
SOI	Southern Oscillation Index
SWIR	Shortwave Infrared
TID's	Travelling Ionospheric Disturbances
TM	Thematic Mapper
TOMS	Total Ozone Mapping Spectrometer
TOPEX	Topography Experiment
TOVS	TIROS Operational Vertical Sounder
TRM	Thermo Remenant Magnetization
UARS	Upper Atmopshere Research Satellite
UIMS	User Interface Management System
VAS	VISSR Atmospheric Sounder
VISSR	Visible Infrared Spin Scan Radiometer
VRM	Viscous Remenant Magnetization
XTE	X-Ray Timing Explorer